7 Single wires

The transport properties of small samples can be classified by using a number of length scales. First, in the presence of disorder, electron states may be localized in space, i. e. the wave function amplitude decays according to $e^{-x/\xi}$, where ξ is the *localization length*. If the *sample length* L is much larger than ξ, $L \gg \xi$, the sample is called *insulating* and the conductance $G \ll e^2/h$. In the opposite limit, $\xi \gg L$, the sample is called *metallic*, indicating that $G > e^2/h$, not referring to the chemical composition of the sample (see for example [85L1, 86W1, 88K1, 91W2, 92W1, 93K, 98T2] and references therein). Second, in a metallic sample, the carriers can travel freely for some distance l before they collide with an impurity. This distance $l = v_F\tau$ is the *mean free path length*, where v_F is the Fermi velocity of the carriers and τ is the mean free time between collisions with impurities (see for example [91W2, 92W1] and references therein). Third, the average distance an electron can travel before losing phase memory due to inelastic scattering is the temperature–dependent *phase coherence length* $l_\varphi = \sqrt{D\tau_\varphi}$ (see Section 7.3.4 on page 138 and Section 7.5.1 on page 157). Fourth, the *thermal diffusion length* $L_T = \sqrt{(\hbar D)/(k_B T)}$ denotes the distance two initially phase–coherent electrons whose energies differ by $k_B T$ can travel before their wavefunctions are significantly out of phase (see Section 7.3.4).

The thickness of a sample be t, its width w, and its length L. Its *effective dimensionality* then depends on the relevant length scale of the physical quantity under investigation. When examining interference corrections to the conductance, the relevant length scale is the phase coherence length l_φ. With respect to interference effects, a system is 3D for $l_\varphi < t, w, L$. It is 2D when $t < l_\varphi < w, L$ and 1D when $t, w < l_\varphi < L$ (see for example [92W1] and references therein). In the case of electron–electron interactions, the thermal diffusion length L_T is the relevant length scale to be compared with the sample dimensions. The name *quantum wire* is not a statement concerning the effective dimensionality of a sample. It refers to systems in which electron states are geometrically confined in two directions (and can move freely along the third direction) and only a few of the 1D energy levels are occupied. In conventional wires, the number of occupied subbands is of the order of $\approx 10^8$, in semiconductor quantum wires it is of the order of ≈ 1 (see for example [94G5] and references therein).

In wires prepared from a 2DEG in a semiconductor heterostructure one typically has $t < w$. When $l < w, L$ and $L < \xi$, the sample is in the *diffusive* regime. The electrons suffer many scattering events from impurities before they collide once with the sample boundary. When $w < l$, $l < L < \xi$, the wire is called *quasi–ballistic*. Scattering at the boundaries is more frequent than scattering at impurities. Finally, for $w, L < l$ and $L < \xi$, the device is *ballistic*. Carriers do not encounter impurity scattering at all on their paths through the device (see for example [92W1] and references therein).

One can conclude that in order to properly describe transport in small devices one has to know if it is an insulator or a metal and in the latter case, if it is in the diffusive, the quasi–ballistic or the ballistic regime. The effective dimensionality of the sample has to be inferred from the comparison of t, w, and L with the relevant length scale of the effect to be studied. But, even further, details of the measurement procedure have to be taken into account in order to choose an appropriate theoretical model. On the one hand, a measurement may be performed using two probes, i. e. the voltage is measured across the same probes the current is flowing through. The two–terminal resistance is defined as $R \equiv (V_1 - V_2)/I_{1\to 2}$. On the other hand, four probes may be used, namely two for current injection and two for voltage measurements. The four–terminal resistance is $R_{mn,kl} \equiv (V_k - V_l)/I_{m\to n}$. In the four–probe configuration, the carriers can propagate into the voltage probes and back (only the net current through the voltage probes has to be zero) or along the wire beyond the voltage probes and back. These contributions appear as part of the resistance of the wire of length L, which is in a four–probe measurement the distance between the voltage probes (see for example [86W1, 91W2, 92W1] and references therein).

7.1 Geometrical quantization

In a quantum wire, the carriers are confined along two directions. The energy bands of such a system can in principle by calculated by solving the Schrödinger equation. To find a form of the confinement potential appropriate for the sample at hand is a central problem in a quantitative theory, as the potential in general depends on the fabrication process of the wire. In order to obtain qualitative insight, assuming a square well potential or a parabolic potential is often sufficient. Both are exactly solvable (see for example [91R2, 94T, 96J3, 96S2, 97F, 98D] and references therein). The corresponding quantized energy spectrum is directly observable experimentally via *magnetic depopulation* or *quantized conductance*.

7.1.1 Magnetic depopulation

For an introduction into the phenomenon of magnetic depopulation of 1D subbands see Section 7.7.4 on page 194.

Berggren et al [86B2] (page 194) studied MC in samples similar to those in [86T] (page 178). Oscillations in the MC arose from successive magnetic depopulation of 1D subbands.

Van Houten et al [87vH] (page 195) fabricated GaAs channels and measured the low and high–field MR. At large fields, SdH oscillations were observed. In narrow samples, the Landau level index as a function of B^{-1} (Fig. 197) showed deviations from a linear behaviour, indicating depopulation of 1D subbands.

Menschig et al [90M1, 90M2, 91F2] patterned $In_{0.53}Ga_{0.47}As$/InP wires with widths down to 80 nm by EBL and deep RIE from a modulation–doped heterostructure. They studied the resistivity vs. wire width at zero magnetic field for $T = 330$ K, 77 K and 40 mK and observed a finite resistance for all temperatures and wire widths. The difference between geometrical and electrical width was small. SdH oscillations were periodic in a 310 nm wide wire and non–periodic in a 80 nm wide wire (Fig. 110), indicating a 1D energy spectrum. A negative MR due to WL which decreased with increasing wire width, and UCF were observed at low fields. A MR peak due to boundary scattering was found around ≈ 0.75 T, peak resistance and corresponding magnetic field increased as the wire width decreased (Fig. 111).

Bird et al [90B2] (page 140) observed 1D subband depopulation and SdH oscillations above 0.4 T in quasi–ballistic GaAs wires.

Bird et al [91B1, 92B2] (page 170) studied the four–terminal MR of a GaAs wire and found 1D subband depopulation.

Nakata et al [91N] (page 147) examined single GaAs wires and multiple wire structures. MR measurements on the single wires showed SdH oscillations, a deviation of $1/B$ vs. n_L from a straight line was attributed to magnetic depopulation of 1D subbands.

Wróbel et al [92W2] (page 118) prepared a two–terminal GaAs wire, measured SdH oscillations, and fitted the level index vs. $1/B$ by 1D theory.

Tang et al [92T2, 93T2] (page 118) performed four–terminal MR measurements on Si MOSFETs with a long narrow wire gate. They observed SdH oscillations, investigated the subband index vs. $1/B$ and found deviations from a linear behaviour at high $1/B$.

Yoh et al [92Y2] (page 197) fabricated wires on InAs/AlGaSb heterostructures, measured MR and observed SdH oscillations. The level index n_L vs. $1/B$ for a 350 nm wide wire deviated from linear behaviour in the low magnetic field region indicating geometrical quantization.

Nakata et al [93N, 94N2] (page 150) measured the MR of buried GaAs wires and observed SdH oscillations. The Landau level index vs. inverse magnetic field deviated from a linear behaviour

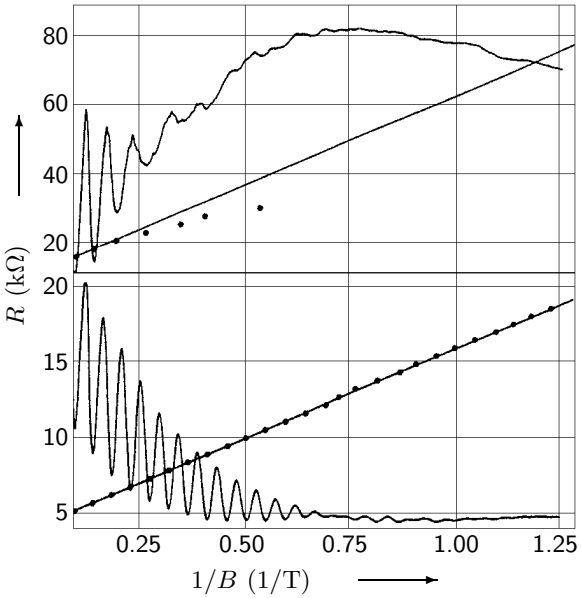

Fig. 110: MR curves at 40 mK for (top) an 80 nm and (bottom) a 310 nm wide InGaAs wire vs. $1/B$ (full lines) together with the dependence of the positions of the minima in the MR on $1/B$ (dots) [90M1].

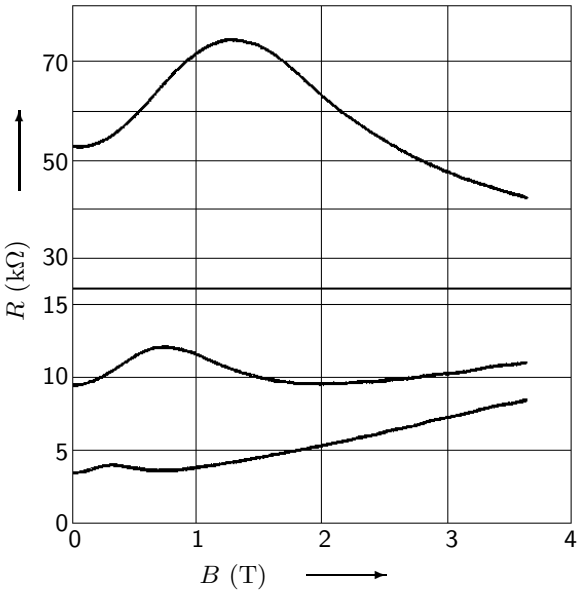

Fig. 111: Anomalous MR peak observed at low fields for (top) an 80 nm, a 190 nm, and a 420 nm (bottom) wide wire [90M1]. For this measurement, a high current (5 μA) was used in order to suppress the UCF.

for $w < 0.6\,\mu$m. From fits to the Landau plots, energy separations of 1.5 meV and 4.0 meV at the critical width were extracted.

Lettau et al [94L1] (page 173) investigated MR in GaAs wires. Above 1 T, R_L exhibited oscillations arising from magnetic depopulation of 1D subbands (subband spacings 0.4, 0.7, and 1.5 meV in 420, 274, and 133 nm wide wires).

Honda et al [95H3] (page 120) determined subband spacings in GaAs wires from magnetic depopulation measurements.

Okada et al [95O3] (page 122) fabricated in–plane gate GaAs wires. SdH oscillations were observed at $T = 4.2$ K for several values of V_g. Landau plots showed deviations from a linear behaviour for $V_g = -0.25$ V and $B^{-1} > 0.8\,\mathrm{T}^{-1}$.

Inoue et al [97I2] (page 175) investigated transport in InAs wires. From a Landau plot, a subband spacing of 6.9 meV was estimated.

Okada et al [97O] (page 150) measured MR of in–plane gate GaAs wires and wrap–gate InGaAs wires. Both showed SdH oscillations at $T = 4.2$ K and Landau plots deviated from a linear behaviour at low magnetic fields, indicating 1D transport.

Herfort et al [97H] (page 198) investigated undoped GaAs wires defined by a positively biased narrow top gate. SdH oscillations were observed and Landau plots deviated from a linear $1/B$ behaviour at weak magnetic fields, indicating 1D quantization.

Held et al [99H2] (page 175) fabricated GaAs wires by local oxidation using an atomic force microscope. MR traces showed SdH oscillations. The sublevel index vs. inverse magnetic field showed a non–linear behaviour indicating quantum confinement.

7.1.2 Quantized conductance

A consequence of geometrical quantization (see Section 7.1 on page 116) in a narrow ballistic wire is the *quantized conductance*. The conductance of a single clean 1D channel is $2 \cdot e^2/h$ (the factor 2 is due to spin degeneracy), independent of its filling because of a special relationship between the density of states and the Fermi velocity in one dimension [86L]. If transport is ballistics and the temperature is low, i. e. neither scattering nor thermal excitations mix the subband populations, and subband separation is large enough in order to be experimentally detectable, the conductance of a wire with N subbands occupied is quantized at values $N \cdot (2 \cdot e^2/h)$. As a subband is populated (depopulated), which can be controlled by increasing (decreasing) the Fermi energy (by changing the gate voltage), the conductance steps up (down) by $2 \cdot e^2/h$ and remains at this value until the next subband is populated (depopulated). Thus, the conductance as a function of Fermi energy is similar to a staircase with step height $2 \cdot e^2/h$. Spin degeneracy may be lifted by applying a parallel magnetic field. Then, additional conductance plateaux with heights e^2/h emerge (see for example [90D, 91O3, 92W1, 94T, 96S2, 97F, 98D, 98T2] and references therein). Quantized conductance was first observed experimentally in quantum point contacts in the year 1988 [88vW, 88W4] (see also Part II).

Kastner et al [88K2] (page 169) structured Si wires and measured the MR at several temperatures. The conductance at three different magnetic fields increased in a series of steps as V_g increased. Varying the temperature at $B = 8\,\mathrm{T}$ showed that each plateau disappeared at a different T. These observations were assumed to result from quasi 1D confinement.

Eugster et al [90E] (page 147) examined GaAs wires with three different lengths. Measuring the current through the two–terminal wires as a function of gate voltage, a $0.5\,\mu$m long wire showed conductance steps, indicating ballistic transport.

Nakata et al [91N] (page 147) fabricated GaAs wires, investigated G as a function of V_g, and observed resistance steps in a $0.2\,\mu$m wide wire.

Wróbel et al [92W2] prepared a two–terminal GaAs wire ($w = 0.4\,\mu$m, $L = 20\,\mu$m, $l = 12\,\mu$m) by EBL and deep etching which did not conduct electrically after cooling it down in the dark. After illumination, the wire was conducting and after switching off the light, the resistance increased with a time constant of the order of hours, providing a method of changing the Fermi energy. The conductance as a function of time showed five plateaux at $T = 4.2\,\mathrm{K}$ and $2.5\,\mathrm{K}$, while at $0.35\,\mathrm{K}$ they were obscured by UCF (fig 112). The step hight was $\Delta G \approx 0.25 \cdot (2 \cdot e^2/h)$. With an increasing magnetic field the number of visible steps was reduced and ΔG increased (Fig. 113). The MR was measured, SdH oscillations were observed, the level index vs. $1/B$ was fitted by 1D theory. The conductance steps were attributed to subband depopulation from $N = 12$ to 8.

Ismail et al [91I2, 91L1] (see page 270) reported AB oscillations in GaAs arrays of rings. Further, the conductance of the rings showed a step–like behaviour as a function of gate voltage at $4.2\,\mathrm{K}$. Similar steps were observed in $2 - 4\,\mu$m long single wires as well as in ten parallel wires. The step heights in the single wires were $2 \cdot e^2/h$ and $20 \cdot e^2/h$ in the parallel wires.

Chou et al [92C] (page 152) investigated split–gate GaAs wires with a barrier induced by a narrow metal gate. The current as a function of gate voltage showed quantized conductance in a $50\,\mathrm{nm}$ wide wire.

Tang et al [92T2, 93T2] performed four–terminal transport measurements on Si MOSFETs with a long narrow wire gate ($w = 70\,\mathrm{nm}$, $w_{\mathrm{eff}} \approx 82\,\mathrm{nm}$, $L = 1.5\,\mu$m) defined by EBL and RIE. In the gate–voltage dependence of the channel conductance and its derivative a steplike quantized conductance was observed with the first step at $\approx 0.6 \cdot e^2/h$ and a step size of about $0.3 \cdot e^2/h$ (Fig. 114). The discrepancy between the measured step hight and the theoretically expected step hight was explained by modelling the system as a quantum point contact in series with a large gate–

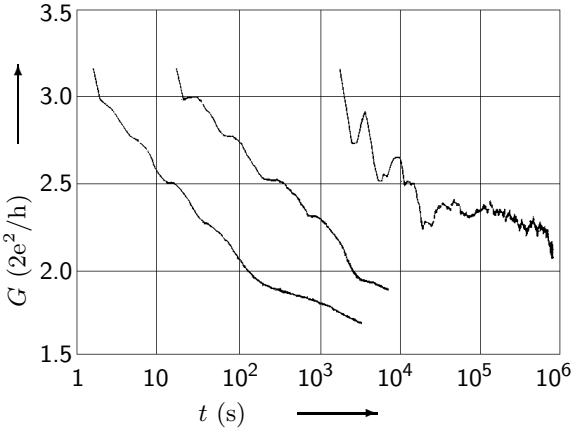

Fig. 112: Conductance as a function of time after switching off the LED for (left) $T = 4.2\,\mathrm{K}$, $2.5\,\mathrm{K}$, and $0.35\,\mathrm{K}$ (right) [92W2]. The traces for $2.5\,\mathrm{K}$ and $0.35\,\mathrm{K}$ were shifted to the right for clarity.

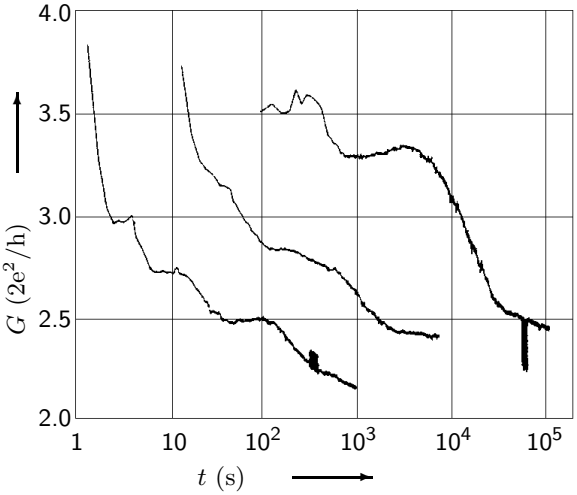

Fig. 113: Conductance as a function of time for (left) $B = 0\,\mathrm{T}$, $1\,\mathrm{T}$, and $2\,\mathrm{T}$ (right) [92W2]. The traces for $1\,\mathrm{T}$ and $2\,\mathrm{T}$ were shifted to the right for clarity. For $B = 0\,\mathrm{T}$ and $2\,\mathrm{T}$, telegraph noise–type fluctuations occured.

voltage dependent resistor. A nearly constant subband spacing of $0.92 \pm 0.005\,\mathrm{meV}$ was deduced from the data. Tang et al further applied a magnetic field, observed SdH oscillations, investigated the subband index vs. $1/B$ and found deviations from a linear behaviour at high $1/B$. Resonant tunneling through a single impurity state within the quantum point contact was also detected.

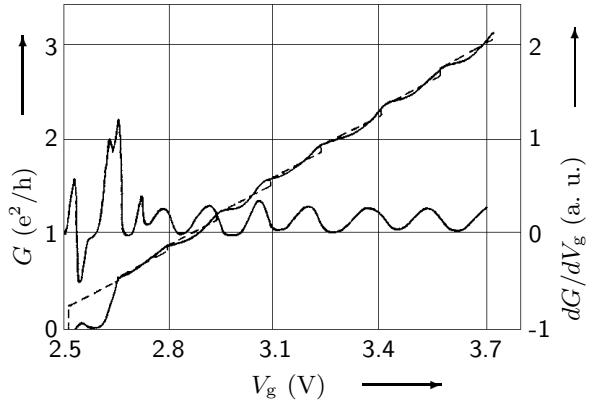

Fig. 114: Gate voltage dependence of the conductance (step–like curve, left axis) and its derivative (oscillating curve, right axis) for $T = 4.2\,\mathrm{K}$, $V_{\mathrm{SD}} = 0.1\,\mathrm{mV}$ and zero magnetic field [92T2].

Jin et al [92J2] studied wires (minimum width below 40nm) and rings fabricated from poly–crystalline Si by EBL and dry etching. The channel conductance showed a number of steps attributed to the population of 1D subbands. The first step was at $\approx 0.6 \cdot e^2/h$, the step size was about $0.3 \cdot e^2/h$.

Yamada et al [93Y] (page 153) studied the transport properties of a quasi–ballistic split–gate GaAs wire with a point contact in the centre of one side–boundary. The two–terminal resistance was measured as a function of the back–gate voltage for different voltages at the split gates. Plateaux were identified as peaks in the first derivative which moved as functions of the various gate voltages. The plateaux were classified into two groups probably due to different constriction origins. In the four–terminal resistance, the origin of the plateaux was the point contact itself.

Plateaux in the two–terminal resistance were assigned to unintentional, irregular constrictions in the wire.

Tang et al [93T1] studied the influence of the lateral wire width on the conductance of Si inversion wires ($w = 30 - 70$ nm, $L = 1\,\mu$m) defined by EBL and RIE. An increase in the conductance step size with decreasing lateral wire dimensions was observed. In a 30 nm wide wire, resonant tunneling features in the near–threshold regime and oscillatory conductance fluctuations superimposed on the quantized conductance steps were found. The observed features were attributed to geometric effects.

Chou et al [93C2] structured a GaAs double gate wire using a positively biased narrow wire gate ($w = 30$ nm) to create a 1D potential and a negatively biased split gate ($w = 0.3\,\mu$m, $L = 0.3\,\mu$m) to adjust the Fermi level. The current vs. split–gate voltage for various wire–gate voltages (at $T = 5$ K) showed plateaux at integer multiples of $\approx 2 \cdot e^2/h$. The current vs. wire–gate voltage for different split–gate voltages (at $T = 0.5$ K) also showed $2 \cdot e^2/h$ plateaux. Even though the 2DEG under the split gate started to populate for a split–gate voltage larger than -0.1 V, the $2 \cdot e^2/h$ plateaux were still distinguishable.

Hwang et al [94H1, 94H2] (page 172) reported systematic experimental study on transport in a low–disorder, low–density GaAs wire defined by a split gate. At $B = 0$ T, conductance steps were observed.

Nakajima et al [94N1, 95N1] reported fabrication of Si wires by SIMOX technology, EBL, anisotropic chemical etching and thermal oxidation. They performed conductance measurements at temperatures ranging from 25 K to room temperature. In a wire of dimensions $w = (20 \pm 2)$ nm, $t = (6 \pm 2)$ nm, $L = (95 \pm 10)$ nm they observed conductance quantization at temperatures up to 60 K (subband spacing 18-20 meV). In a wire of dimensions $w = (17 \pm 2)$ nm, $t = (5 \pm 2)$ nm, $L = (60 \pm 10)$ nm, conductance steps were found up to $T = 100$ K (subband spacing 30 meV) (Figs. 115 and 116).

Honda et al [95H3] observed quantized conductance in 2 to 30 μm long GaAs wires fabricated by EBL, plasma etching and subsequent wet etching ($l = 28\,\mu$m). To vary the width, Schottky gates were formed on the etched slopes adjacent to the wire. The dependence of G on the gate voltage (at $T = 105$ K) and on the wire length was studied (Fig. 117). The two–terminal conductance of 2 to 10 μm long wires showed conductance steps close to the values $N \cdot (2 \cdot e^2/h)$ at $T = 1.3$ K. For $N \geq 2$, a conductance dip near the threshold of the $(N + 1)$th subband due to scattering by a random potential was observed. In samples with a weaker lateral confinement, only the 2 μm long wires exhibited quantized conductance. Honda et al determined subband spacings of 2.6 meV for the first type of wire and of 1.6 meV for the second type of wire from magnetic depopulation measurements. The 20 and 30 μm long wires showed conductance steps with heights in the range of 0.6 to $0.7 \cdot (2 \cdot e^2/h)$.

Tarucha et al [95T] measured the two–terminal conductance of 2 to 10 μm long GaAs wires ($l = 28\,\mu$m) at various temperatures. To vary the wire width, Schottky gates were patterned on the chemically etched slopes adjacent to the wires. They found conductance steps close to the quantized values of $2 \cdot e^2/h$ as a function of gate voltage. With decreasing temperature a decrease of the conductance was observed. The temperature dependence of the conductance was stronger in the longer wires (Figs. 118 and 119). Tarucha et al interpreted their results in terms of mutual Coulomb interaction in the presence of a random potential. They also discussed the Luttinger model in order to explain their observations.

Inoue et al [94I2] observed quantized conductance in InAs wires ($w = 460$ nm (A) and $w = 365$ nm (B)) fabricated by a deep etch and a split gate. The two–terminal conductance of sample A vs. gate voltage showed quantized conductance at one– and two–fold multiples of $2 \cdot e^2/h$ for $T = 4.2$ K. Current and conductance of sample B as a function of source–drain voltage for different V_g was studied at 79 K. In G vs. V_g, two plateaux were observed for $T = 79$ K at three– and

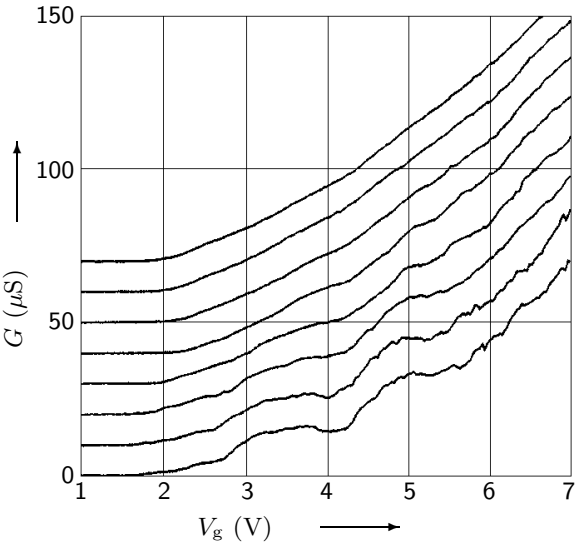

Fig. 115: Gate voltage dependence of the conductance of a 20 nm wide wire for (top) $T = 90\,\mathrm{K}$, 80 K, 70 K, 60 K, 50 k, 40 K, 30 K, and 26 K (bottom) at $V_{\mathrm{SD}} = 1\,\mathrm{mV}$ [94N1]. The curves have been vertically offset for clarity.

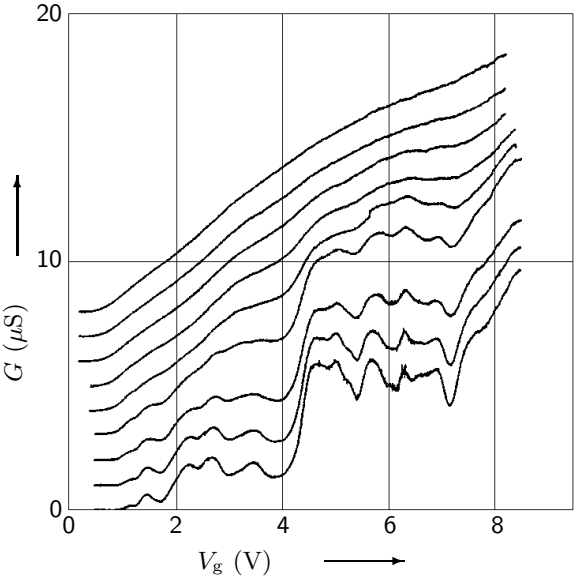

Fig. 116: Gate voltage dependence of the conductance of a wire smaller than the one in fig. 115 for (top) $T = 160\,\mathrm{K}$, 140 K, 120 K, 100 K, 80 K, 60 K, 45 K, 35 K, and 25 K (bottom) at $V_{\mathrm{SD}} = 1\,\mathrm{mV}$ [94N1]. The curves have been vertically offset for clarity.

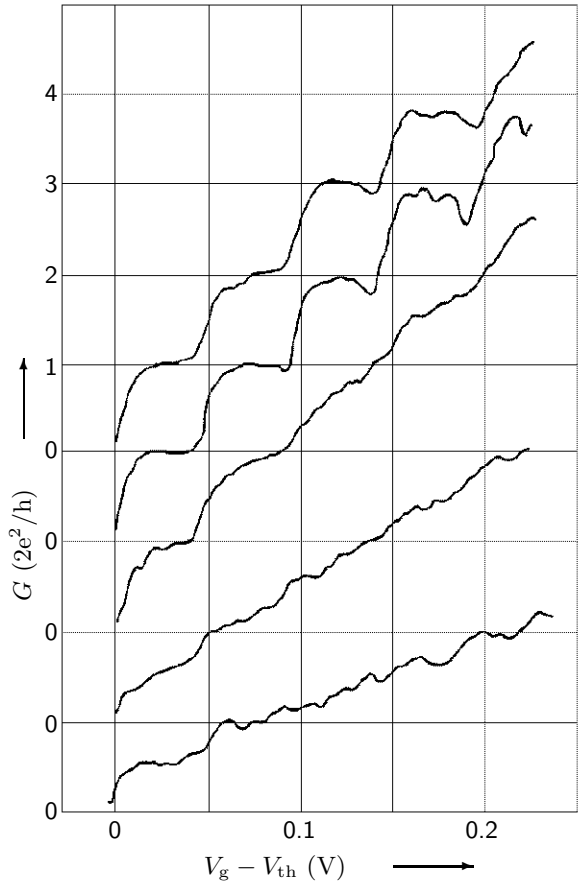

Fig. 117: Wire conductance as a function of effective gate voltage, $V_{\mathrm{g}} - V_{\mathrm{th}}$, at $T = 1.3\,\mathrm{K}$ for (top) $L = 2\,\mu\mathrm{m}$, $5\,\mu\mathrm{m}$, $10\,\mu\mathrm{m}$, $20\,\mu\mathrm{m}$, and $30\,\mu\mathrm{m}$ (bottom) [95H3]. The curves have been offset for clarity.

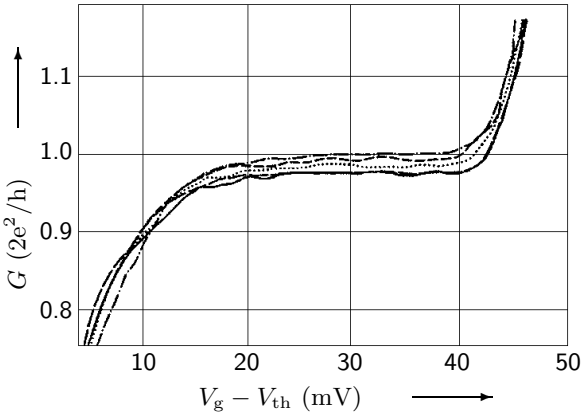

Fig. 118: Conductance vs. effective gate voltage at (top) $T = 1.17\,\mathrm{K}$, $0.97\,\mathrm{K}$, $0.73\,\mathrm{K}$, $0.49\,\mathrm{K}$, and $0.29\,\mathrm{K}$ (bottom) of the $2\,\mu$m long wire [95T].

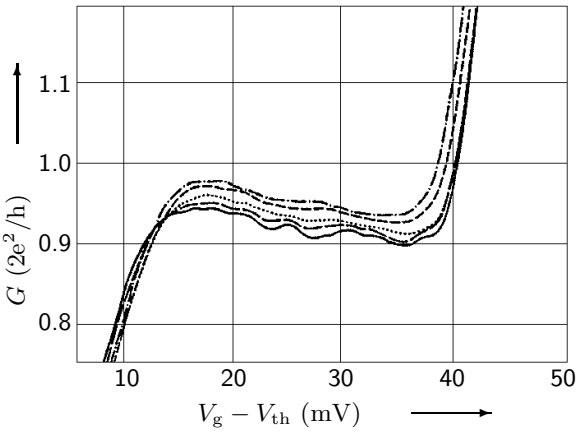

Fig. 119: Conductance vs. effective gate voltage at (top) $T = 1.13\,\mathrm{K}$, $0.95\,\mathrm{K}$, $0.73\,\mathrm{K}$, $0.50\,\mathrm{K}$, and $0.30\,\mathrm{K}$ (bottom) of the $5\,\mu$m long wire [95T].

four–fold multiples of $2 \cdot e^2/h$. The steps were still observable at 115 K, but were no longer at the quantized conductance values. Inoue et al finally investigated the current increment as a function of source–drain voltage.

Hashizume et al [95H1, 95H2] fabricated an in–plane gate GaAs wire ($w \approx 0.4\,\mu$m, $L \approx 1.6\,\mu$m) and measured I–V characteristics at $T = 3.8\,\mathrm{K}$. Conductance measurements vs. V_g performed near pinch–off revealed quantized conductance at temperatures up to 40 K. Oscillations were observed on the first plateau.

Namatsu et al [95N2] proposed a Si nanowire fabrication process allowing for a reduction of the thickness of nanowires without reducing the thickness of the source and drain regions. The gate–voltage dependence of the conductance at various temperatures showed a steplike structure up to $170 - 210\,\mathrm{K}$. The height of the steps was only $\approx 0.2 \cdot e^2/h$ (at 28 K) indicating the influence of some parasitic resistance. The steps became less distinct when the source–drain voltage was increased. A subband separation of 70 meV was estimated. Conductance oscillations observed at low gate voltages were attributed to the CB effect.

Yamada et al [96Y2] (page 154) fabricated GaAs wires with either a small mesa in the centre of the wire or a hole near the boundary of the wire, structured using a STM. The wire with the small mesa showed quantized conductance with step hight e^2/h for a conductance larger than e^2/h.The wire with a hole showed conductance quantization with step height $2e^2/h$.

Okada et al [95O3] fabricated in–plane gate GaAs wires ($w = 400 - 700\,\mathrm{nm}$, $L = 1600\,\mathrm{nm}$), measured I–V characteristics and found complete pinch–off and saturation at 3.8 K. The saturation current depended linearly on gate voltage. The narrow samples showed conductance quantization at zero field up to 40 K, while the 700 nm wide sample showed conductance quantization at $B = 5.0\,\mathrm{T}$. Oscillatory behaviour was present on the first plateau of a 400 nm wide sample. SdH oscillations were found at $T = 4.2\,\mathrm{K}$ for several values of V_g. Landau plots showed deviations from a linear behaviour for $V_g = -0.25\,\mathrm{V}$ and $B^{-1} > 0.8\,\mathrm{T}^{-1}$. Okada et al examined the influence of a magnetic field on quantized conductance at 2.9 K and found that a magnetic field increased the width of the plateaux.

Yacoby et al [96Y1, 97Y1] fabricated GaAs wires ($t = 14$, 25, and 40 nm, $L = 1 - 10\,\mu$m, $l = 10\,\mu$m) by cleaved edge overgrowth and observed quantized steps in the linear response conductance. The plateaux were flat to within 5% up to a wire length of $10\,\mu$m and their conductance values remained constant from $L = 1$ to $5\,\mu$m, but they deviated from $N \cdot (2 \cdot e^2/h)$. The non–

universal conductance values of the plateaux were reproducible to within 5% in all wires fabricated from the same quantum well material. With increasing temperature, the conductance values on the plateaux increased and approached $N \cdot (2 \cdot e^2/h)$ (Fig. 120). In the non–linear differential conductance, the plateaux rose with increasing dc bias, even exceeding $N(2 \cdot e^2/h)$. Yacoby et al discussed their observations in terms of different theoretical models, including the Luttinger model.

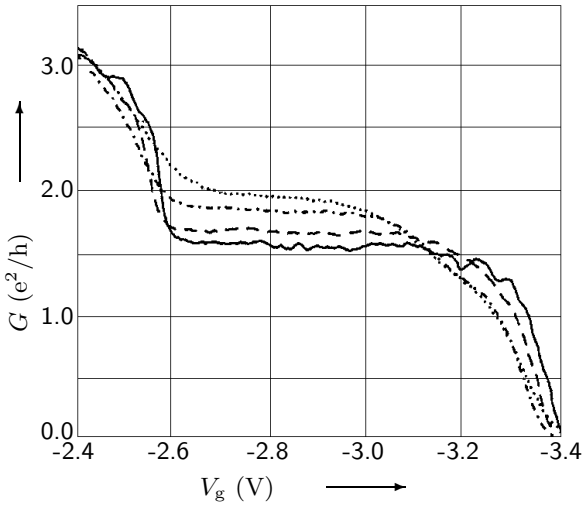

Fig. 120: Differential conductance of a 2 μm long GaAs wire in a 25 nm thick quantum well vs. top–gate voltage for (top) T = 25.3 K, 14.8 K, 4.7 K, and 1.0 K (bottom) [96Y1].

Okada et al [97O] (page 150) investigated in–plane gate GaAs wires and wrap–gate InGaAs wires. The conductance as a function of gate voltage showed steps.

Hashizume et al [96H1] fabricated in–plane gate GaAs wires (w = 1 μm, L = 1μm) and observed plateaux in the conductance vs. V_g up to a temperature of 100 K. They measured I-V characteristics at T = 2 K for different V_g and found a non–linear behaviour.

Yoh et al [97Y2] fabricated wires ($w \approx$ 10 nm, L = 50 μm) by self–organized lateral p-n-p doping on a patterned GaAs surface. At room temperature, small current steps with a period of $\approx$ 50 mV were observed in the current–voltage characteristic. At 77 K, conductance quantization was found.

Kane et al [98K1] used enhancement–mode FETs to structure GaAs wires (L = 5 μm, w = 250 nm or 500 nm and L = 2 μm, w = 250 nm) with a top gate and two side gates by EBL and a shallow wet etch. Conductance quantization as a function of top–gate and side–gate voltages was present in all wires. The conductance of the 2 μm long wire decreased at large top–gate voltage. With increasing temperature, conductance decreased. In the 5 μm long wire, the conductance steps as a function of side–gate voltage showed a deviation from $2e^2/h$. subband spacings of 1 meV and 2 meV were estimated for the 250 nm and 500 nm wide wires, respectively.

Park et al [98P1] (page 155) investigated transport through a corrugated GaAs wire. The periodically corrugated potential wall consisted of four notches whose width and separation were about 50 and 160 nm, respectively. The conductance of a device without corrugation varied smoothly as a function of gate voltage, exhibiting a plateau of height $\approx 2e^2/h$ at $V_g \approx$ 100 mV.

Kaufman et al [99K] measured conductance in V–grooved quantum wires. The GaAs quantum well layer of thickness t was positioned between two AlGaAs barriers. A negatively biased gate of length L allowed for the sequential depletion of the 2DEG and the wire. Conductance vs. gate voltage showed a step–like structure. For 2 μm< L <8 μm, transport was diffusive, while it was ballistic for $L <$ 1.5 μm ($l \approx$ 2 μm). The values of the conductance steps were lower than $2e^2/h$. The amount of the depletion depended on the wire thickness which in turn depended on the quantum well thickness. The depletion was larger in thinner wires. The suppression of the step values was

attributed to electron scattering at the interface between the 2DEG and the wire. Increasing the temperature led to a smearing of the step structure. The smearing occurred at lower temperatures in samples with a thicker quantum well. For $t = 26\,\text{nm}$ and $t = 12\,\text{nm}$, subband separations of $\approx 2.5\,\text{meV}$ and $\approx 5\,\text{meV}$, respectively, were deduced. Additional conductance features observed at fractional values of $2e^2/h$ were probably due to spin polarization effects.

Castleton et al [98C1] (page 156) studied two parallel ballistic wires formed in GaAs/AlGaAs DQW structures. Both channels exhibited conductance quantization with steps of height $2e^2/h$ and an additional structure at $0.7 \cdot 2e^2/h$.

Harrell et al [99H1] reported a technique to form 2D and 1D electron gases in undoped GaAs/AlGaAs heterostructures inducing the electron gas by use of a Schottky gate. A 1D wire showed quantized conductance at $T = 1.5\,\text{K}$ with plateaux at integer multiples $2e^2/h$.

Liang et al [99L] studied quantized conductance in GaAs split–gate ($w = 0.8\,\mu\text{m}$) wires of different lengths ($L = 3$, 5, and $6\,\mu\text{m}$, $l \approx 70\,\mu\text{m}$). The series resistance due to the bulk 2DEG was identical for all wires. The $3\,\mu\text{m}$ long wire showed 25 clean conductance steps, the plateau values were close to multiples of $2e^2/h$ after subtraction of the zero split-gate voltage bulk conductance. With increasing temperature, the conductance plateaux became less well defined but the midpoint of the plateaux remained close to multiples of $2e^2/h$. In the $5\,\mu\text{m}$ long wire, all conductance plateaux deviated from multiples of $2e^2/h$ by up to 8% at $T = 0.3\,\text{K}$. A resonant feature was observed which was attributed to resonant transmission due to a background impurity potential. As T increased, the plateau values increased, the first reached a value of $2e^2/h$ at $T = 1.58\,\text{K}$. In the $6\,\mu\text{m}$ long wire, the resonance structure was stronger than in the $5\,\mu\text{m}$ long wire. The plateaux were suppressed below $2e^2/h$, the first plateau deviated from $2e^2/h$ by 25% at $T = 0.3\,\text{K}$. The plateau values increased with increasing temperature but never reached $2e^2/h$ for $T < 1.39\,\text{K}$. At $T = 1.39\,\text{K}$ they were no longer well defined. It was assumed that reduction of the plateau values with increasing wire length was due to the introduction of elastic scattering.

Auslaender et al [00A] (page 165) fabricated GaAs wires by CEO. The conductance as a function of carrier density showed conductance plateaux which deviated from $2e^2/h$ due to the presence of disorder.

7.2 Fermi energy

The Fermi energy in a gated quantum wire can be varied by changing the voltage of the gate electrode. *Aperiodic conductance fluctuations* (AF) as a function of Fermi energy are observable experimentally, which may be of two different origins (see Section 7.2.1 on page 124). Further, *periodic conductance oscillations* due to the pinning of a *charge density wave* (CDW) or a *Wigner crystal* (WC) (see Section 7.2.2 on page 130) or due to the *Coulomb blockade* (see Section 7.6.1 on page 162) may emerge .

7.2.1 Aperiodic conductance fluctuations

The first possible origin of aperiodic fluctuations of conductance as a function of Fermi energy is the sparse population of the density of states of small localized samples. Each of the peaks in the density of states is the signature of one of the localized electron states. The conductance is proportional to the density of states and fluctuates as a function of gate voltage as the Fermi level is shifted through the sequence of peaks in the density of states (see for example [86W1, 88W2, 91W2] and references therein).

The second mechanism responsible for aperiodic conductance fluctuations is interference in diffusive samples. The electron trajectories within a conductor constitute a large number of loops and the trajectories may interfere coherently if half the circumference of such a loop is smaller than the phase coherence length. Whether interference is constructive or destructive depends

on the phase shift between the trajectories which depends on the exact impurity configuration. Each loop thus either gives a positive or a negative contribution to conductance, depending on the details of the paths. The sum of all of these random contributions, ΔG, does not vanish as $1/N$ with an increasing number of channels, N, because the channels are spatially correlated within a energy interval of width E_c. This *correlation energy* is the energy difference which, for carriers flowing along the same path across a distance l_φ, leads to a phase difference of the order 2π. The correlation of channels thus yields an effective number of independent channels which causes $\Delta G \approx e^2/h$. The fluctuations are characterized by the autocorrelation function, $K(\Delta E) \equiv \langle G(E)G(E+\Delta E)\rangle - \langle G(E)\rangle^2$, where $\langle \ldots \rangle$ refers to averaging over the impurity configurations. The characteristic width of the correlation function yields the correlation energy E_c.

Macroscopically identical wires have different conductances due to the interference contributions depending on the exact impurity configuration. The conductances differ by $\approx e^2/h$, independent of average conductance, material parameters, or sample length. In order to observe the random contribution to conductance one does not need to study an ensemble of wires. Changing the chemical potential by E_c in one sample generates a completely different interference pattern. Shifting the Fermi energy thus yields conductance fluctuations of average amplitude e^2/h. Further, in 2D and 1D, the interference pattern depends critically on the positions of the impurities. Moving a single impurity by approximately one de Broglie wavelength changes the conductance by $\approx e^2/h$.

The universal result for the fluctuation amplitude has led to the term *universal conductance fluctuations* (UCF). Nevertheless, ΔG is only universal in a two–terminal sample with $l \ll L \approx l_\varphi$. In a four–probe geometry, electrons can propagate into the voltage probes or beyond the probes along the main current path up to distances of the order l_φ and then return and contribute to the interference terms in the conductance. In samples $L \ll l_\varphi$, the effective sample area is the coherence area and hence, conductance fluctuations increase with decreasing sample length as the voltage fluctuations are length independent and $R \propto L$. When $L \gg l_\varphi$, the conductance includes the fluctuation patterns of L/l_φ independent blocks. As the fluctuation in G is of random sign, this effective ensemble average reduces ΔG. Averaging further occurs when the thermal energy, $k_B T$, is much greater than E_c. The fluctuation patterns of $k_B T/E_c$ energy intervals are superposed and ΔG is reduced by the factor $\sqrt{k_B T/E_c}$, thus $\Delta G \propto 1/\sqrt{T}$. When the voltage drop across the sample is larger than E_c/e, similar energy averaging occurs. In a non–local geometry, the conductance fluctuations decay exponentially with ΔL (where ΔL is the separation of the nearest voltage probe from the classical current path) as ΔG is proportional to the fraction of the electrons that retain phase coherence until they arrive at the probes which is $e^{-\Delta L/l_\varphi}$ (see for example [86W1, 87L2, 88K1, 89W1, 90D, 91A1, 91W2, 92W1, 97F, 97I1, 98D, 98J1] and references therein).

Fowler et al [82F, 83F, 86W2, 88F3] fabricated Si MOSFETs with two control electrodes and a metal gate allowing for a lateral confinement of the accumulation layer. A channel was about $10-100$ nm wide and $10\,\mu$m long. The conductance vs. gate voltage is shown in Fig. 121; the random noise–like structure varied from sample to sample, but was reproducible in a given sample. No qualitative change was observed for magnetic fields up to 5 T at 2 K. The temperature dependence of the conductance for different gate and control voltages was studied (Fig. 122). The data were fitted to a $e^{-(T_0/T)^n}$ dependence. The values of the exponent n vs. gate voltage exhibited a sharp transition from $n = 0.5$ to $n = 0.33$ which was interpreted as a transition from a 1D to a 2D behaviour as the channel broadened with increasing V_g. Further studies concerning temperature dependence and the possible origin of the structure in the conductance can be found in [84H].

Skocpol et al [84S] measured conductance and SdH oscillations in a narrow Si channel about $1\,\mu$m long and $40-200$ nm wide. The behaviour of the conductance vs. gate voltage of four devices varying in width from 55 to 120 nm is shown in Fig. 123. The two–terminal conductance scaled approximately with the width.

Kwasnick et al [84K2] studied Si MOSFETs with ≈ 70 nm wide inversion layers defined by a

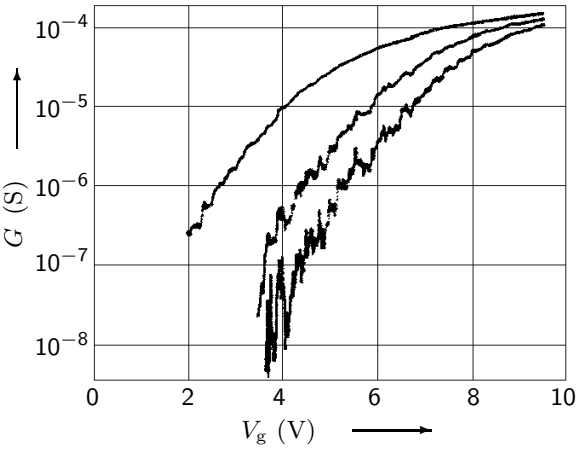

Fig. 121: Conductance vs. gate voltage for temperatures (top) T=1.99 K, 0.57 K, 0.25 K (bottom) [82F].

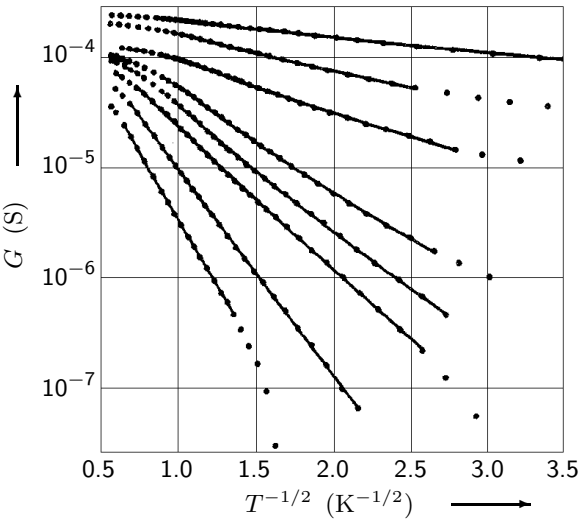

Fig. 122: Logarithm of conductance vs. $T^{-1/2}$ for (top) V_g = 9.0 V, 7.9 V, 7.3 V, 6.3 V, 5.9 V, 5.4 V, 4.9 V, 4.2 V (bottom) [82F]. Solid lines are the best fits to the data.

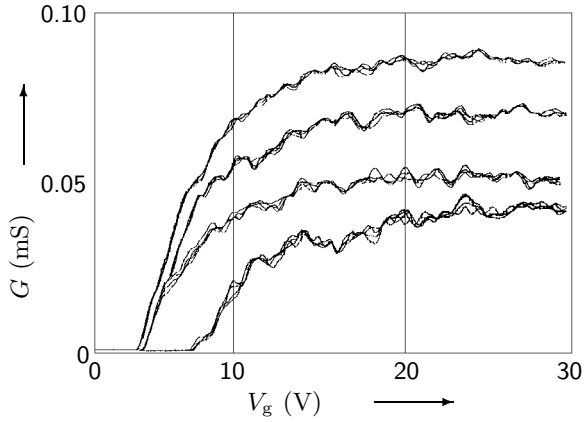

Fig. 123: Zero–field structure in four Si devices of widths (top) 120, 90, 75, 55 nm (bottom) [84S].

positively biased gate. For $T \geq 15\,\mathrm{K}$, the conductance increased almost linearly with V_g. Below 15 K, it showed a reproducible structure with large variations. This structure varied when T was temporarily raised to $T \geq 200\,\mathrm{K}$ or when V_g was temporarily raised by several volts above threshold. At the conductance maxima, the current decreased slowly with decreasing T; at the minima the current decreased rapidly (Fig. 124). The current increased exponentially with the driving voltage (Fig. 125).

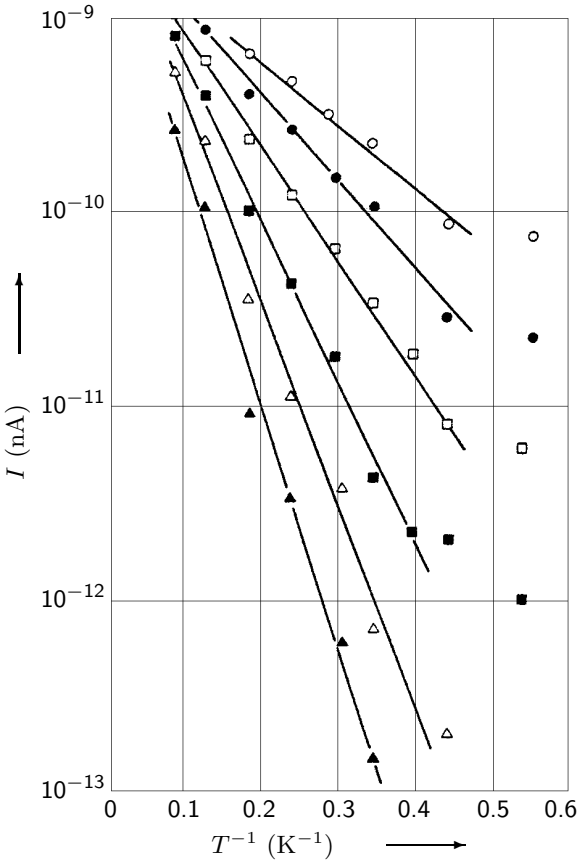

Fig. 124: Logarithm of the current vs. inverse temperature at $V_\mathrm{g} = 2.585\,\mathrm{V}$ for different values of the driving voltage: (top) 6 mV, 5 mV, 4 mV, 3 mV, 2 mV, 1 mV (bottom) [84K2]. The accuracy was $\pm 0.2\,\mathrm{pA}$.

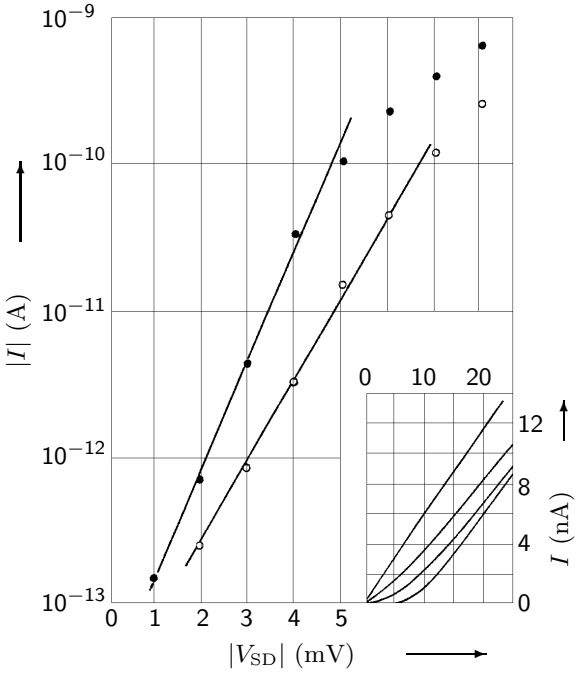

Fig. 125: Logarithm of the current vs. source–drain voltage at $T = 2.9\,\mathrm{K}$ and $V_\mathrm{g} = 2.585\,\mathrm{V}$ for both polarities of V_SD [84K2]. Inset: Linear plot of the current vs. V_SD at (top) $T = 24\,\mathrm{K}$, 11 K, 5 K, 2 K (bottom).

Webb et al [85W, 86W2, 88F3] studied Si MOSFETs with channel lengths of 10 μm and widths less than 30 nm. The conductance vs. gate voltage for several temperatures is shown in Fig. 126. The temperature dependence of the four largest peaks agreed with variable–range hopping above 200 mK (Fig. 127). The behaviour below 200 mK could be fitted equally well with either T^{-1} or $T^{-1/2}$, but the data displayed by the open circles deviated from this behaviour. The inset of Fig. 127 shows that the position of the peak at $V_\mathrm{g} = 4.5175\,\mathrm{V}$ shifted linearly with temperature. Fig. 128 gives an example of the I–V characteristics at the peak at $V_\mathrm{g} = 4.5175\,\mathrm{V}$ for several temperatures. A second harmonic signal was observed. Most of these observations were explained by a fluctuation model of hopping conductivity.

Skocpol et al [86S1] reported progress in fabricating and performing measurements on quasi 1D Si devices. They discussed the resistance of short narrow channels ($w \approx 30\,\mathrm{nm}$, $L = 100\,\mathrm{nm}$) as a function of gate voltage, which revealed AF, studied the influence of the width onto the threshold

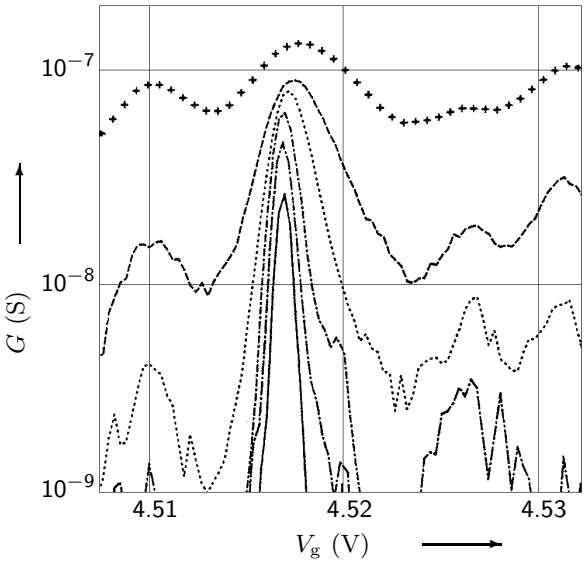

Fig. 126: Conductance vs gate voltage for (top) T = 221 mK, 151 mK, 103 mK, 65 mK, 51 mK, 36 mK) [85W]. Only the largest peaks are displayed for 65 mK and 36 mK.

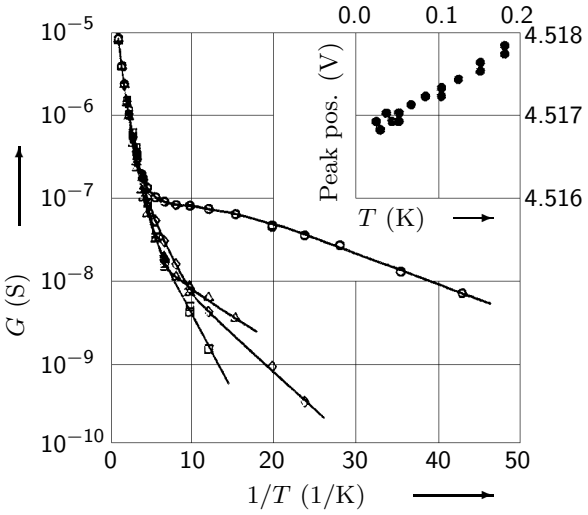

Fig. 127: Temperature dependence of four conductance peaks shown in Fig.126 at V_g = 4.5097 V (boxes), 4.5175 V (open circles), 4.5267 V (triangles), and 4.5321 V (diamonds). Solid lines are smooth curves through the data. Inset: Temperature dependence of the position of the peak at V_g = 4.5175 V in the temperature regime where it is isolated from the neighbouring ones.

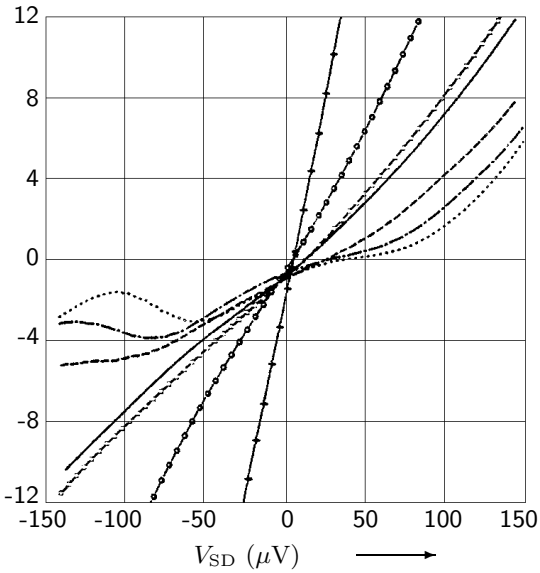

Fig. 128: Non–linear I–V curves obtained for an isolated peak (at V_g = 4.5175 V) for (from the top, right of the point of intersection at zero voltage): T = 330 mK, 221 mK, 102 mK, 67 mK, 46 mK, 33 mK, 23 mK [85W].

voltage and analysed SdH oscillations. Further, they examined the temperature dependence of the resistance structure and studied the MR structure (in the longitudinal and the Hall resistance) which also showed AF.

Kastner et al [87K1] studied the conductance of Si MOSFETs of width $\approx 100\,\text{nm}$ and observed reproducible conductance fluctuations as a function of gate voltage (Fig. 129). The temperature dependence at fixed V_{SD} for three values of V_g (two conductance minima and one maximum) and for a fixed V_g and different values of V_{SD} was studied. The activation energy decreased roughly linearly with V_{SD}, thus the current was expected to depend exponentially on V_{SD} (in the range where the corresponding energy is larger than k_BT) which was actually found in a certain range of V_{SD}. A crossover from exponential to linear behaviour was observed for small V_{SD}. When temperature was cycled above 200K or V_g was raised well above threshold, the conductance pattern changed. Kastner et al examined the amplitude of the conductance fluctuations vs. the average value of G (Fig. 130). The data indicated a transition from localized to extended states at $G = 10^{-6}\,\Omega^{-1}$.

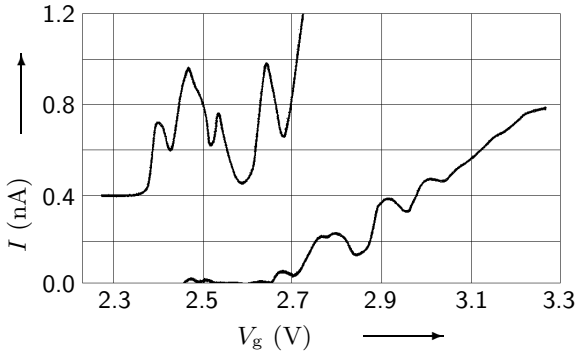

Fig. 129: Current vs. gate voltage near threshold for a $\approx$ 70 nm wide inversion layer [87K1]. The upper curve is an expanded view ($\times$10) of the lower one.

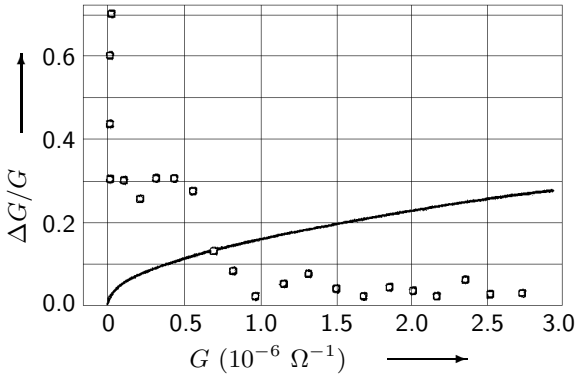

Fig. 130: Conductance fluctuations (boxes) and $[G/(e^2/h)]^{1/2}$ (solid line) at $T = 4.2\,\text{K}$ as a function of average conductance [87K1].

Wainer et al [88W1] measured MC fluctuations in narrow Si MOSFETs ($w \approx 40\,\text{nm}$, $L \approx 10\,\mu\text{m}$) in the strongly localized regime for a range of gate voltages. The peaks shifted for an increasing magnetic field to lower or higher V_g. At high fields, the density of peaks was reduced. The observed effects were attributed to Zeeman spin splitting of energy levels.

Wróbel et al [92W2] (page 118) examined a two–terminal GaAs wire which was conducting after illumination. After switching off the light, the resistance increased with a time constant of the order of hours, providing a method of changing the Fermi energy. The conductance as a function of time showed five plateaux at 4.2 K and 2.5 K, while at 0.35 K they were obscured by UCF (fig 112).

Ohata et al [92O2] (page 212) fabricated narrow Si channels and measured conductance vs. gate voltage at various temperatures. AF near the turn–on voltage were completely reproducible. As temperature was lowered, the fluctuations became gradually accentuated. The peak positions were insensitive to temperature or magnetic field but peak conductance and width showed strong temperature dependence. The observations were explained in terms of hopping conduction in the strongly localized regime.

Hughes et al [96H2] (page 213) examined variable range hopping conductance fluctuations in Si wires and GaAs wires. The temperature dependence of the fluctuation amplitude was studied.

7.2.2 Periodic conductance oscillations

Interacting electrons in quasi 1D systems show a tendency to form a *spin–* or *charge–density wave* or a *Wigner crystal*. The pinning of a CDW or a WC by impurities leads to a non–linear I–V characteristic as the current is suppressed until the voltage is large enough to depin the CDW (or WC). The pinning strength exhibits a maximum when the spacing between the pinning centres is an integral number of periods of the CDW (or WC). Changing the gate voltage affects the number of electrons in the system and thus influences the pinning energy, causing it to oscillate as a function of Fermi energy (see for example [79B, 79E, 79L1, 89M3, 90F2] and references therein). As a consequence, the current oscillates as a function of gate voltage. Another origin for periodic oscillations of conductance vs. gate voltage is the *Coulomb blockade* (see Section 7.6.1 on page 162).

Scott–Thomas et al [88S1] fabricated dual–gate Si wires defined by a split gate ($w_{\mathrm{eff}} = 27 \pm 7$ nm, $L = 1$, 2, and 10 μm) and measured conductance vs. gate voltage. Oscillations in G vs. V_{g} persisted to temperatures of 20 K and depended only weakly on T. The peak–to–valley change in G was independent of L. The oscillations were insensitive to magnetic fields as high as 8 T and to source–drain voltage. The MR increased at large B and reached a plateau at $2 \cdot e^2/h$ (for $B > 12$ T).

Scott–Thomas et al [89S2] created narrow Si inversion layers by a dual gate device with a 70 nm gap in the lower gate. Fig. 131 shows G vs. upper–gate voltage. Periodic oscillations were observed, the frequency was independent of magnetic field up to 8 T (Fig. 131). They examined the temperature dependence of one pair of periodic maxima and minima. Further, they studied the dependence of the differential conductance on V_{SD} and found an increase by orders of magnitude as V_{SD} changed from 0 meV to 0.2 meV. Above 0.2 meV, the differential conductance overshot and approached its high–temperature value. Scott–Thomas et al discussed a pinned charge density wave as possible origin for the observed effects. An alternative explanation based on a single–electron picture was proposed by Van Houten et al [89vH].

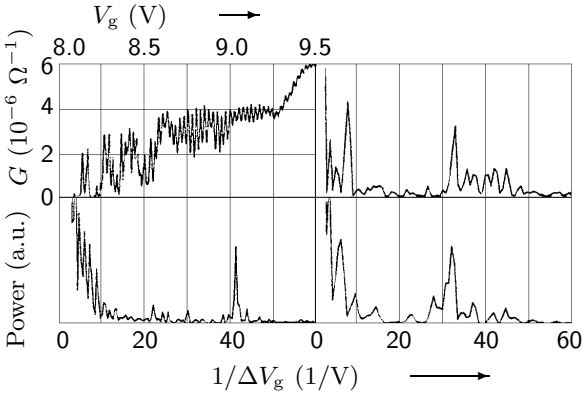

Fig. 131: Conductance G vs. V_{g} on upper gate for a 10 lμm long inversion layer at $T = 400$ lmK (top, left), corresponding Fourier spectrum (bottom, left), Fourier spectrum of the data of a 1 lμm long channel at zero magnetic field (top, right), and at $B = 6$ lT (bottom, right) [89S2].

Meirav et al [89M3] patterned 1.0 μm wide and 2 and 8 μm long GaAs channels in an inverted semiconductor–insulator–semiconductor structure which became conducting for a positive gate voltage $> 0.5 - 0.7$ V. For $T > 2$ K, the conductance rose smoothly with V_{g}, for $T < 1$ K it oscillated as a function of V_{g} (Fig. 132). The oscillations were periodic with a period of ≈ 1.7 mV. The structure was reproducible at low temperatures, but changed when warming the device to room temperature and cooling it down again. The oscillations persisted over a range of ≈ 30 mV above threshold and ceased abruptly beyond. Meirav et al deduced from numerical simulations that only one subband was occupied, second–subband occupation began around $25 - 30$ mV above threshold. They proposed the pinning of a Wigner crystal or a charge density wave by impurities to be responsible for the observed oscillations. In agreement with this model they found a non–linear dependence of G on an applied dc bias.

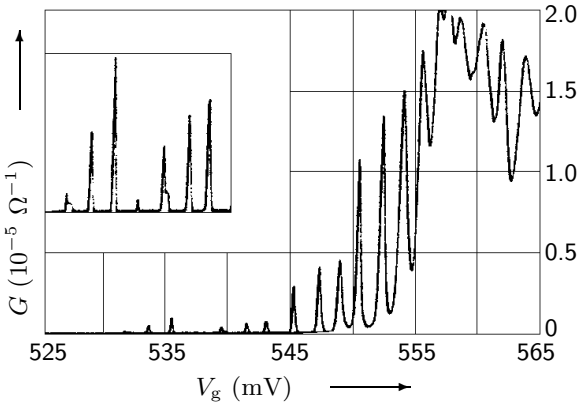

Fig. 132: Conductance vs. gate voltage of a narrow 2 μm long channel measured at 50 mK [89M3]. The inset shows an expansion of the first few oscillations.

Field et al [90F2] fabricated dual–gate Si MOSFETs with a split lower gate ($w_{\text{eff}} \leq 30$ nm) and narrow channels in GaAs/$Al_xGa_{1-x}As$ inverted heterostructures ($w_{\text{eff}} \approx 70$ nm) and studied in detail the behaviour of conductance vs. upper gate voltage. In Si devices, G varied periodically with V_g, the structures were reproducible. Similar features were observed in GaAs devices. All Si structures with $w_{\text{eff}} \leq 30$ nm showed the oscillations, but only 30% of the GaAs devices did. The period varied randomly from sample to sample and changed for a single device when it was cycled to room temperature and back again. Field et al proposed that the frequency was determined by the positions of charged defects or impurities. With increasing temperature the amplitude of the conductance oscillations decreased. The frequency of the oscillations was independent of temperature. A magnetic field reduced the random modulation of conductance but did not affect the period. For small V_{SD}, the current obeyed Ohm's law while the I–V characteristic was non–linear at higher V_{SD}. The phenomena were explained in terms of the CB and CDW models in which the Coulomb interaction between the electrons was responsible for the periodicity.

Staring et al [92S2] examined two sets of samples of narrow GaAs wires defined by a split–gate technique: in one set the channels were intentionally disordered by doping ($l = 0.7\,\mu$m); the other set was undoped, but disordered as well ($l = 3.9\,\mu$m). Two–terminal narrow–channel geometries ($w = 0.5\,\mu$m) and miniature Hall bars were studied. Near pinch off, the channels broke up into a small number of segments separated by potential barriers formed by scattering centres. Extensive studies of the conductance of the channels vs. gate voltage were performed at various temperatures and magnetic fields. Periodic conductance oscillations were observed in most of the channels, the period was not correlated with the length of the channels or the degree of disorder. At very low T, the regular oscillations were often replaced by an irregular pattern of sharp conductance peaks. The oscillation period was insensitive to a magnetic field, but the amplitude of oscillations and the average conductance were enhanced above the zero–field values in magnetic fields of intermediate strength and decreased in stronger fields. The height of the conductance peaks increased with decreasing temperature. The four–terminal longitudinal conductance in the Hall bar exhibited random structure as a function of magnetic field, but showed periodic oscillations as a function of gate voltage. In the Hall resistance, quasi–periodic oscillations as a function of magnetic field were observed in between the plateaux, below 2 T the Hall resistance showed random oscillations. The periodicity of the conductance oscillations was explained by the theory for Coulomb–blockade oscillations, the irregular conductance fluctuations at very low T were attributed to multiple segments in the wires.

Hwang et al [94H1, 94H2] (page 172) reported systematic experimental study on transport in a low–disorder, low–density GaAs wire defined by a split gate. As a function of the electron density, conductance oscillations were observed in a B–induced insulating phase. The oscillations became sharper and more developed as B increased. The average period of the conductance oscillations vs. V_g was examined and the behaviour of the oscillations with temperature was studied. The results were interpreted in terms of a pinned 1D Wigner solid.

Chandrasekhar et al [94C1] investigated In_2O_{3-x} wires and rings (see page 275). The conductance oscillated as a function of gate voltage. The I–V characteristic was non–linear.

7.3 Finite temperature

7.3.1 Conductance in general

In metallic samples, the resistance decreases with decreasing temperature as phonon scattering is frozen out. The resistance flattens when all temperature–dependent scattering processes have died out and impurity scattering dominates. As with decreasing temperature the phase coherence length becomes larger, the resistance may increase due to weak localization (see Section 7.7.2 on page 176). Taking electron–electron interactions into account also yields temperature–dependent contributions to the conductivity (see Section 7.6.1 on page 162). In localized samples, the resistance increases with decreasing temperature and scales to infinity as temperature drops to zero (see Section 7.10 on page 212).

Fowler et al [82F, 83F, 86W2, 88F3] (page 125) examined Si MOSFETs with two control electrodes and a metal gate allowing for a lateral confinement of the accumulation layer. The temperature dependence of the conductance for different gate and control voltages was studied (Fig. 122) and the data were fitted to a $e^{-(T_0/T)^n}$ dependence. The values of the exponent n vs. gate voltage exhibited a sharp transition from $n = 0.5$ to $n = 0.33$ which was interpreted as a transition from a 1D to a 2D behaviour as the channel broadened with increasing V_g.

Dean et al [82D] found typical 2D behaviour at $T = 1.4\,K$ in a Si channel about $1\mu m$ wide. The power–law temperature dependence of the conductance was, however, not consistent with 2D behaviour; Dean et al assumed a transition to 1D to take place as the temperature was reduced. The MC for low B was positive at $T = 1.2\,K$, as expected for a 2D system, and negative at $\approx 70\,mK$ (Fig. 133). For $B > 1\,T$, the magnetic length became shorter than the channel width and the conduction became 2D again. For narrower channels, $\approx 0.1\,\mu m$ wide, both power–law temperature dependence and negative MC persisted to higher temperatures.

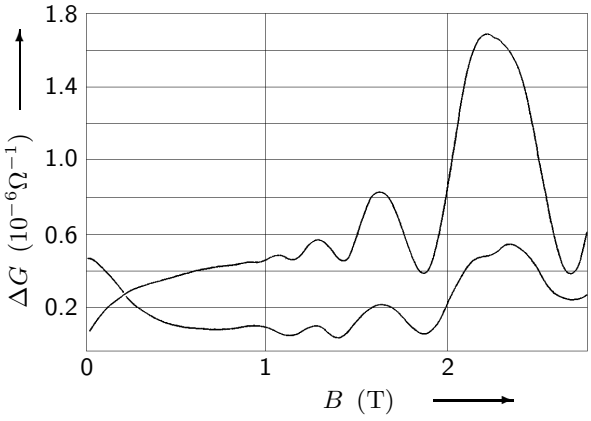

Fig. 133: MC for $V_g = 25$,V and a zero control voltage at 1.2 K (upper curve) and for a lattice temperature of 70 mK (lower curve) [82D].

Dean et al [84D] (page 212) examined Si MOSFETs in which the conductance as a function of temperature exhibited drastic changes, indicating 1D localization.

Thornton et al [86T] (page 178) studied narrow GaAs channels. The temperature dependence of the conductance for different gate voltages is shown in Fig. 174.

Haug et al [92H1] (page 180) investigated narrow channels fabricated on the cleaved surface of InAs quantum well structures. The edge resistance as a function of temperature behaved similarly to the bulk resistance down to 50 K, but became nearly independent of T at lower temperatures.

Iwano et al [93I] fabricated p–type Si wires ($L = 30 - 60\,\mu$m) using FIB doping with Ga ions. Two kinds of samples with different impurity concentrations (A: $N_{\mathrm{Ga}} \approx 5.1 \times 10^7\,\mathrm{cm}^{-1}$; B: $N_{\mathrm{Ga}} \approx 5.1 \times 10^9\,\mathrm{cm}^{-1}$) were prepared. The conductance of sample A had an activation–type temperature dependence while sample B showed a strong and a weak temperature–dependent region (Fig. 134) attributed to a competition between band conduction and 1D hopping conduction. With increasing substrate bias, the conductance in sample A was reduced to zero at 3.4 V and 77 K, while the conductance in sample B was hardly reduced at 4 V and 77 K, but decreased remarkably at 4.2 K. Fine structure was observed in the conductance of sample B vs. the substrate bias at 4.2 K. The MC of sample B was positive, which could not be explained by weak localization.

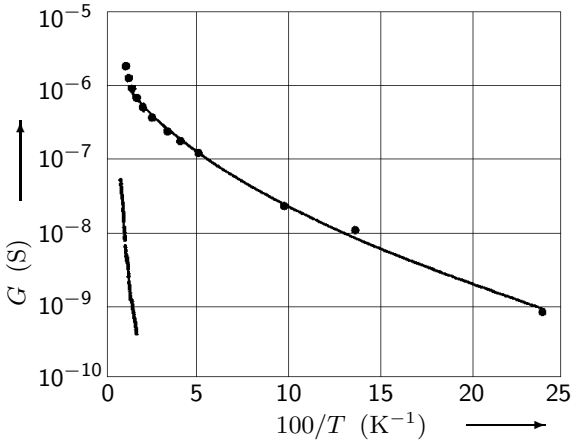

Fig. 134: Temperature dependence of the wire conductance for samples A (bottom) and B (top) [93I]. The substrate bias was 0 V. The electric field along the wire was 17 V/cm for sample A and 33 V/cm for sample B.

Hwang et al [94H1, 94H2] (page 172) investigated transport in a low–disorder, low–density GaAs wire defined by a split gate. The temperature dependence of the resistance at various B and V_{g} was studied.

Wada et al [94W] (page 211) studied transport phenomena in a poly–Si slit nanowire. The resistance of the slit nanowire increased with decreasing temperature ($4.2\,\mathrm{K} < T < 300\,\mathrm{K}$).

Wróbel et al [95W] (page 173) measured the two–terminal conductance of a GaAs wire as a function of magnetic field for different temperatures, $0.03\,\mathrm{K} \leq T \leq 0.6\,\mathrm{K}$ (Fig. 169). They found regions in which the conductance decreased as a power law for increasing temperature. Sharp peaks in the conductance for $3.0\,\mathrm{T} \leq B \leq 3.2\,\mathrm{T}$ were smeared by increasing temperature and were attributed to the presence of impurities. They also recorded the deviations of the conductance from the ideal plateau values as a function of temperature.

Iwano et al [94I3] fabricated Si wires ($w \approx 0.1\,\mu$m, $L = 50\,\mu$m) by FIB implantation of Ga^+ ions and studied the electrical conductance for different ion doses and annealing temperatures. The dependence of conductance on T showed three different regimes: (1) metallic conductance for a dose between 5.6×10^9 and $5.6 \times 10^{10}\,\mathrm{cm}^{-1}$ and an annealing temperature of 600 °C, (2) VRH conductance for a dose between 3.5 and $5.6 \times 10^9\,\mathrm{cm}^{-1}$ and annealing temperatures between 600 and 690 °C, and (3) NNH conductance for samples with a lower dose or a higher annealing temperature than in (2). The MR was also measured. A negative MR was attributed to WL, while a positive MR was interpreted as a reduction of the localization length.

Fukai et al [95F2] (page 167) fabricated InGaAs/InAlAs wires by Ga–FIB implantation and measured the temperature dependence of the two–terminal resistance which showed a maximum at $T = 1.6\,\mathrm{K}$.

Tarucha et al [95T] (page 120) measured the two–terminal conductance of 2 to 10 μm long GaAs wires. With decreasing temperature, a decrease of the conductance was observed. The temperature dependence of the conductance was stronger in the longer wires (Figs. 118 and 119).

Yoh et al [94Y] (page 143) fabricated free–standing InAs wires by EBL and wet etching and measured the resistance as a function of temperature.

Yano et al [95Y1] (page 163) measured the conductance of poly–crystalline Si wires at room temperature (Fig. 161). The temperature–dependence of the current was thermally activated.

Smith et al [97S3] (page 211) observed strongly non–ohmic behaviour of Si wires. With increasing temperature, the non–linearity became less pronounced. At 46 K, the wire had a linear I-V characteristic.

Yacoby et al [96Y1, 97Y1] (page 122) fabricated GaAs wires by cleaved edge overgrowth and observed quantized steps in the linear response conductance. With increasing temperature, the conductance values on the plateaux increased and approached $N(2 \cdot e^2/h)$ (Fig. 120).

Kane et al [98K1] (page 123) used enhancement–mode FETs to structure GaAs wires with a top gate and two side gates. Conductance quantization as a function of top gate and side gate voltages was observed. With increasing temperature, conductance decreased.

Iwano et al [98I2] (page 213) fabricated Si wires by FIB doping and investigated the localization length and the hopping distance in the 1D VRH regime. The temperature dependence of the conductivity showed an activation type behaviour for $T > 50\,\mathrm{K}$ and a VRH type behaviour for $T < 50\,\mathrm{K}$.

Park et al [98P1] (page 155) investigated transport through a corrugated GaAs wire. The periodically corrugated potential wall consisted of four notches whose width and separation were about 50 and 160 nm, respectively. They measured conductance vs. gate voltage for different source–drain voltages and observed oscillations for temperatures $17\,\mathrm{mK} < T < 106\,\mathrm{K}$. They studied the change of the oscillation intensity as a function of temperature.

Kaufman et al [99K] (page 123) measured conductance in V–grooved quantum wires. Conductance vs. gate voltage showed a step–like structure. Increasing the temperature led to a smearing of the step structure. The smearing occurred at lower temperatures in samples with a thicker quantum well.

Liang et al [99L] (page 124) studied quantized conductance in GaAs split–gate wires of different lengths (L = 3, 5, and 6 μm, $l \approx 70\,\mu$m). The 3 μm long wire showed conductance steps with plateau values close to multiples of $2e^2/h$. With increasing temperature, the conductance plateaux became less well defined but the midpoint of the plateaux remained close to multiples of $2e^2/h$. In the 5 μm long wire, all conductance plateaux deviated from multiples of $2e^2/h$ by up to 8% at $T = 0.3\,\mathrm{K}$. As T increased, the plateau values increased, the first reached a value of $2e^2/h$ at $T = 1.58\,\mathrm{K}$. Also in the 6 μm long wire, the plateaux were suppressed below $2e^2/h$, the first plateau deviated from $2e^2/h$ by 25% at $T = 0.3\,\mathrm{K}$. The plateau values increased with increasing temperature but never reached $2e^2/h$ for $T < 1.39\,\mathrm{K}$. At $T = 1.39\,\mathrm{K}$ they were no longer well defined.

Auslaender et al [00A] (page 165) reported evidence for Luttinger liquid behaviour in GaAs wires containing a single 1D island. The line shape of the RT peaks was measured for $0.25\mathrm{K} < T < 2.5\,\mathrm{K}$, it decreased with decreasing temperature. According to conventional CB theory, the line shape should have been independent of temperatur, while Luttinger liquid theory predicted $\Gamma \propto T^{1/g-1}$, where the parameter g (< 1) characterized the electron–electron interaction.

7.3.2 Conductance fluctuations and oscillations

Conductance fluctuations in localized samples (see Section 7.2.1 on page 124) are affected by temperature as the Fermi energy is smeared out. Conductance fluctuations due to interference effects (see Section 7.2.1 on page 124) decrease in amplitude with increasing temperature due to energy

averaging. Further, l_φ may change as a function of temperature (see Section 7.3.4 on page 138) which also affects ΔG. The periodic conductance oscillations caused by a pinned CDW or WC are influenced by temperature because thermal fluctuations destroy the long range order of the CDW or WC. Further, changes in the impurity configuration may be induced by temperature, shifting the positions of the pinning centres. Finally, the Coulomb blockade (see Section 7.6.1 on page 162) is only observable when the thermal energy is smaller than the charging energy.

Kwasnick et al [84K2] (page 125) measured conductance in Si MOSFETs. Below 15 K, it showed a structure with large variations. At the conductance maxima, the current decreased slowly with decreasing T; at the minima it decreased rapidly (Fig. 124).

Webb et al [85W, 86W2, 88F3] (page 127) studied the fluctuations of conductance vs. gate voltage for several temperatures in Si MOSFETs (Fig. 126). The temperature dependence of the four largest peaks agreed with VRH above 200 mK (Fig. 127). The behaviour below 200 mK could be fitted equally well with either T^{-1} or $T^{-1/2}$. The inset of Fig. 127 shows that the position of the peak at $V_g = 4.5175$ V shifted linearly with temperature.

Skocpol et al [86S1] (page 127) reported progress in fabricating and performing measurements on quasi 1D Si devices. The resistance of short narrow channels as a function of gate voltage revealed AF, they examined the temperature dependence of the structure.

Kastner et al [87K1] (page 129) examined the temperature dependence of conductance fluctuations as a function of gate voltage in narrow Si MOSFETs. The temperature dependence at fixed V_{SD} for three values of V_g and for a fixed V_g and different values of V_{SD} was studied.

Scott–Thomas et al [89S2] (page 130) observed periodic conductance oscillations as a function of gate voltage in narrow Si inversion layers. They examined the temperature dependence of one pair of periodic maxima and minima.

Field et al [90F2] (page 131) studied the of conductance vs. gate voltage in Si MOSFETs and narrow channels in GaAs/$Al_xGa_{1-x}As$. It varied periodically with V_g. With increasing temperature, the amplitude of the conductance oscillations decreased. The frequency of the oscillations was independent of temperature.

Ohata et al [92O2] (page 212) fabricated narrow Si channels and measured conductance vs. gate voltage at various temperatures. AF near the turn–on voltage were completely reproducible. The peak positions were insensitive to temperature or magnetic field. Peak conductance and peak width showed strong temperature dependence.

Staring et al [92S2] (page 131) examined narrow GaAs wires defined by a split–gate technique. Periodic oscillations of conductance vs. gate voltage were observed in most of the channels. The height of the conductance peaks increased with decreasing temperature.

Chou et al [92C] (page 152) investigated split–gate GaAs wires with a barrier induced by a narrow metal gate. The current as a function of gate voltage showed periodic oscillation peaks. The peak–to–valley ratio of the oscillations decreased with increasing temperature.

Yano et al [95Y1] (page 163) measured the conductance of poly–crystalline Si wires and observed quasi–periodic plateaux in the current vs. source–drain voltage (Fig. 161). The temperature dependence of the current was thermally activated. They interpreted their results in terms of the Coulomb blockade model.

Hughes et al [96H2] (page 213) examined VRH conductance fluctuations in Si and GaAs wires. In a two–terminal measurement, $\ln(G)$ was determined as a function of gate voltage at different temperatures. The temperature dependence of the fluctuation amplitude was studied.

7.3.3 Magneto resistance

This Section contains the description of experiments in which the influence of temperature on the magneto resistance was investigated. Aperiodic conductance fluctuations (see Section 7.7.3 on page 182) decay in amplitude with increasing temperature due to energy averaging. Further, corrections to the magneto resistance due to electron–electron interactions are temperature–dependent (see Section 7.6.1 on page 162). Third, SdH oscillations (see Section 7.7.4 on page 194) are affected by temperature because the Fermi energy is smeared out. Fourth, the temperature dependence of the bend resistance (see Section 7.7.6 on page 206) was investigated, etc.

Licini et al [85L2] (page 183) studied the MR of Si MOSFETs and found aperiodic oscillations as a function of magnetic field. The temperature dependence of the oscillation amplitude was consistent with e^{-L_0/L_T}, where L_0 was fixed and L_T varied as $T^{-1/2}$.

Choi et al [85C, 86C2] (page 168) investigated GaAs devices of different widths. In the narrow channels, the parabolic MR was independent of temperature at low magnetic fields and temperature dependent at higher fields. The temperature–dependent MR of a wide device followed 2D theory for electron–electron interactions, while the data of a narrow devices was described well by 1D theory below a certain critical temperature.

Zheng et al [86Z1] (page 200) structured four–terminal GaAs samples and measured the MR. Peaks in R_L in a narrow channel decreased in amplitude and became increasingly saw–toothed as temperature was lowered.

Skocpol et al [86S1] (page 127) examined the temperature dependence of the resistance structure as a function of magnetic field in quasi 1D Si devices.

Kaplan et al [86K2] (page 194) performed MC measurements in pinched Si MOSFETs and varied the temperature.

Whittington et al [86W3] (page 182) studied the MR of small n^+GaAs wires. The amplitude of the conductance fluctuations was independent of temperature below 10 K and decreased as $T^{-1/2}$ above 10 K.

Ishibashi et al [87I1] (page 182) fabricated narrow GaAs wires and measured the four–probe resistance. The magnitude of the AF was about $0.3{\cdot}e^2/h$ with only a weak dependence on temperature.

Thornton et al [87T2] (page 185) studied split–gate heterojunction GaAs field–effect transistors. They measured MC fluctuations at different temperatures and examined the variance of the fluctuations as a function of temperature (Fig. 185) and also investigated the magnetic correlation field as a function of temperature (Fig. 186).

Kastner et al [88K2] (page 169) structured Si wires and measured the MR at several temperatures. A transition to a state with a conductance about ten times higher than at $B = 0\,\mathrm{T}$ occurred at $B = 4\,\mathrm{T}$ (for $T = 100\,\mathrm{mK}$). This threshold field increased as T increased to 4.2 K. The magnitude of the conductance in the high–field state decreased with T (Fig. 165).

Chang et al [88C2] (page 187) reported MR measurements on ballistic GaAs/Al_xGa_{1-x}As heterostructure wires. The AF grew in amplitude ($> 30\%$) and shifted in frequency content as the temperature was lowered.

Chang et al [88C1] (page 201) examined narrow GaAs/AlGaAs heterostructures. They measured R_L and R_H, the AF in R_H increased with decreasing temperature (Fig. 204). The minimum in R_L at $\nu = 2$ showed a stronger T–dependence than the one at $\nu = 4$.

Mizuno et al [89M4, 90I1] (page 188) fabricated narrow GaAs wires and observed conductance fluctuations in MR curves. The amplitude of the fluctuations decreased nearly proportional to

$T^{-1/2}$ with increasing T above 0.5 K. Fourier spectra in the same field range for different temperatures were almost independent of T.

Takagaki et al [89T1] (page 207) measured a four–terminal negative resistance and studied the temperature dependence of the effect.

Gao et al [89G] (page 189) measured MR in narrow Si MOSFETs. Traces of UCF at various temperatures were studied. The amplitude of UCF and the magnetic correlation field, B_c, as functions of temperature were obtained from the data. For a wide device, the T–dependence of B_c deviated from the theoretical predictions.

Simmons et al [89S3, 91S1] (page 204) structured a narrow multi–terminal GaAs Hall bar, measured R_L and R_H around $\nu = 2$ and found high–frequency fluctuations on the shoulders of the minimum in R_L. As T was raised, the low–frequency resistance peaks remained relatively unchanged while the high–frequency peaks diminished rapidly.

Takagaki et al [90T1] (page 176) defined multi–terminal narrow GaAs channels and performed four–terminal non–local resistance measurements. At low fields, quasi–periodic fluctuations with a period of 20 mT were observed. The amplitude of the fluctuations grew as temperature decreased.

Takagaki et al [90T2] (page 208) fabricated narrow GaAs crossed wire junctions, observed a negative bend resistance at zero field and examined the temperature dependence of the amplitude of the negative bend resistance.

Bird et al [91B1, 92B2] (page 170) studied the four–terminal MR of a GaAs wire. UCF decayed with increasing temperature, comparison with theory implied a temperature–independent l_φ.

Nakata et al [91N] (page 147) fabricated GaAs wires and examined the temperature dependence of the MR.

Geim at al [91G, 92G2, 93G1, 93M2] (page 176) fabricated multi–terminal GaAs wires and measured the non–local MR for different temperatures (Fig. 170). For $T > 10$ K, the UCF were damped and a new type of oscillations was observed. The effect disappeared at both low and high temperatures.

Takaoka et al [91T1, 92T1] (page 199) measured the non–local MR of a macroscopic multi–terminal GaAs wire. The non–local SdH oscillations increased with decreasing temperature from 4.2 K to 1.7 K.

Taniguchi et al [91T2] (page 140) studied the phase breaking time τ_φ and the SO scattering time τ_{SO} in Si δ–doped GaAs wires. The temperature dependence of the amplitude of UCF in wires with strong SO scattering was examined.

Alphenaar et al [92A2] (page 204) investigated a narrow channel Hall bar. In the fractional quantum Hall regime ($\nu = 1/3$), a four–terminal conductance measurement as a function of gate voltage showed a series of conductance fluctuations. As temperature decreased, most peaks approached the conductance ($e^2/3h$). One peak, however, approached (e^2/h) at 45 mK. The height of this peak depended strongly on temperature and dropped below ($e^2/3h$) at $T \approx 120$ mK.

Gusev et al [92G4] (page 190) studied two types of GaAs samples: (1) wires fabricated by EBL and (2) wires fabricated by optical lithography. UCF were examined as a function of temperature.

Ochiai et al [93O1] (page 190) investigated UCF in GaAs wires. As a function of temperature, the fluctuation amplitude gradually increased with decreasing T, while there was no marked temperature dependence in B_c.

Main et al [94M2, 94G3] (page 172) studied MR in multi–terminal GaAs wires using local and non–local lead configurations. Strong resistance fluctuations were observed in the SdH oscillations at temperatures of 300 and 600 mK (Fig. 168). The temperature dependence of the fluctuations

was not monotonic.

Geim et al [94G4] (page 205) examined the quantum Hall effect in three types of GaAs multi–terminal devices: (A) $w \approx 1\,\mu$m, $L = 10 - 20\,\mu$m, exposed to bombardment by α particles; (B) $w \approx 1\,\mu$m, $L = 10 - 20\,\mu$m; (C) as sample B but with the width of the leads increasing rapidly from ≈ 1 to $10\,\mu$m. They measured R_L at different temperatures, in sample A the amplitudes of the SdH oscillations above 3 T decreased considerably as T decreased. In sample C, the high–field SdH peaks became narrower at low temperatures but their amplitudes remained nearly constant. Device B exhibited an intermediate behaviour. The plateaux in R_H in sample A were widest at 5 K and decreased at both higher and lower temperature. In sample C, the plateaux were always wider at lower T. Sample B exhibited a slight shrinking of the plateau at $\nu = 2$ at low T.

Wróbel et al [95W] (page 173) measured the two–terminal conductance of a GaAs wire as a function of magnetic field for different temperatures, $0.03\,\mathrm{K} \leq T \leq 0.6\,\mathrm{K}$ (Fig. 169). They found regions well below the upper edges of the plateaux (at $G = 2 \cdot e^2/h$ and $G = e^2/h$), in which the conductance decreased as a power law for increasing temperature. Sharp peaks in the conductance for $3.0\,\mathrm{T} \leq B \leq 3.2\,\mathrm{T}$ were smeared by increasing temperature.

Fukai et al [95F2] (page 167) studied InGaAs/InAlAs wires, measured UCF and investigated the temperature dependence of the fluctuation amplitude.

Bird et al [95B2] (page 192) investigated breakdown of UCF in quasi–ballistic GaAs wires. The temperature dependence of the average amplitude was independent of magnetic field.

Omling et al [95O5] (page 174) investigated the influence of the deposition of lead particles on the MR of a narrow GaAs channel. The resistance averaged over some MC fluctuations increased with temperature before particle deposition and it decreased afterwards.

Jaroszyński et al [95J, 96J2, 96D1] (page 181) investigated the MR of $Cd_{0.99}Mn_{0.01}Te$ and CdTe wires. At $\approx 3\,\mathrm{K}$, a temperature–induced crossover from a 3D to a 1D behaviour was observed. The amplitude of AF in $Cd_{0.99}Mn_{0.01}Te$ increased with decreasing temperature. The correlation field increased with temperature.

Noguchi et al [96N2] (page 142) measured the MC for $0.4\,\mathrm{K} < T < 30\,\mathrm{K}$ in GaAs wires and observed weak localization (Fig. 139). The weak–localization peak at $B < 0.04\,\mathrm{T}$ became steeper for fixed V_g as temperature decreased.

Jaroszyński et al [98J2] (page 192) studied $Cd_{1-x}M_xTe$ wires. The UCF amplitude in low magnetic fields was weakly temperature dependent at $T > 0.3\,\mathrm{K}$, but it increased abruptly below 0.3 K.

7.3.4 Phase coherence length

As temperature decreases, the density of thermal excitations decreases and hence the phase coherence length increases. At very small T, electron–electron interaction then is the dominant dephasing mechanism. In a conductor of dimensions $d \leq 2$, electron–electron interactions involving small energy transfers determine the phase coherent time τ_φ. It varies with temperature as $1/\tau_\varphi \propto T^{2/(4-d)}$. The phase coherence length is related to τ_φ via $l_\varphi = \sqrt{D\tau_\varphi}$ (see for example [84B2, 85A1, 85F, 86C1, 92W1, 97F, 97I1] and references therein). The effective dimensionality of a sample where electron–electron interactions are concerned is determined by the thermal diffusion length, $L_T = \sqrt{(\hbar D)/(k_B T)}$. It denotes the distance two initially phase–coherent electrons whose energies differ by $k_B T$ can travel before their wavefunctions are significantly out of phase (see for example [85A1, 92W1] and references therein).

Wheeler et al [82W, 84W] investigated Si MOSFETs with widths comparable to the inelastic scattering length. The MC of both a 2D system and a narrow channel were measured for different

temperatures. The inelastic scattering lengths were extracted from this data by fits to weak–localization theory (Fig. 135). For low temperatures, a $T^{-d/4}$ dependence (d dimensionality) was expected for impurity–mitigated scattering. The data thus indicated a 1D behaviour in the narrow channel.

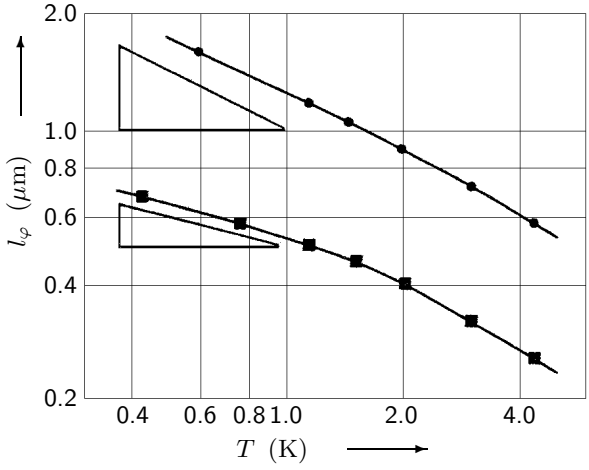

Fig. 135: Inelastic scattering length vs. temperature for a wide channel (upper curve) and a narrow channel (lower curve) [82W]. Triangles: guides to the eye with slopes $\propto T^{-1/2}$ (upper triangle) and $\propto T^{-1/4}$ (lower triangle).

Thornton et al [86T] (page 178) measured the MR of narrow GaAs channels. The data was fitted by weak–localization theory, and the temperature–dependent l_φ was extracted which varied approximately as $T^{-1/3}$ in agreement with 1D theory.

Choi et al [87C2] (page 179) examined the localization time scale in GaAs samples. The MR of a wide sample and a narrow sample was measured at different temperatures and fitted by 2D and 1D weak–localization theory, respectively (Fig. 175). The fitting parameter τ_φ is shown in Fig. 176. According to theory, it was fitted to a combination of T^2 and T dependences in the wide device and to a combination of T^2 and $T^{2/3}$ dependences in the narrow device.

Ishibashi et al [87I1] (page 182) fabricated narrow GaAs wires and measured the four–probe resistance. Via weak–localization measurements on a 2D film they obtained the inelastic scattering length ($l_\varphi \geq 0.2\,\mu$m below 4.2 K) as a function of temperature.

Thornton et al [87T2] (page 185) measured MR in split–gate heterojunction GaAs field–effect transistors. The temperature dependence of l_φ was deduced.

Taylor et al [88T2] (page 180) measured negative MR and UCF in GaAs structures. They extracted the phase breaking rate as a function of temperature.

Hiramoto et al [89H] studied the phase coherence length in GaAs wires of different widths (w = 30, 100, and 300 nm) fabricated by FIB implantation. MC measurements were performed, the data was compared with weak–localization theory, and $l_\varphi = 1.2\,\mu$m, $w_{\text{eff}} = 90$ nm (for the 100 nm wide wire) and $l_\varphi = 0.9\,\mu$m, $w_{\text{eff}} = 70$ nm (for the 30 nm wide wire) were extracted. With decreasing temperature, l_φ increased and became constant below 3 K (Fig. 136). Hiramoto et al concluded that some temperature–independent phase breaking mechanisms other than electron–electron scattering were present at low temperatures.

Pooke et al [89P] reported on measurements of weak–localization corrections to the conductivity in narrow accumulation layer Si MOSFETs ($w = 0.20 - 0.44\,\mu$m, $L = 100\,\mu$m). For $w = 0.44\,\mu$m and $T > 1$ K, the device was in the 2D localization regime. For $T < 1$ K, the MR was in agreement with 1D theory. The resulting values of l_φ were studied as a function of temperature, yielding $l_\varphi = (0.41 \pm 0.01)\,\mu\text{m}(T/\text{K})^{-0.39\pm0.03}$. For $w = 0.26\,\mu$m, it was $l_\varphi = (0.34 \pm 0.01)\,\mu\text{m}(T/\text{K})^{-0.36\pm0.03}$.

Taylor et al [89T4] (page 169) fabricated quasi–ballistic GaAs channels, measured the MR at various temperatures and extracted l_φ as a function of temperature.

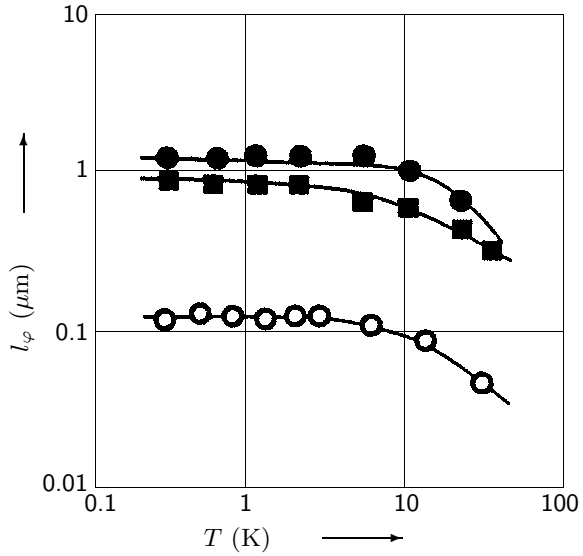

Fig. 136: Temperature dependence of the phase coherence length of two AlGaAs/GaAs wires (top) and a n-GaAs wire (bottom) [89H].

Gao et al [89G] (page 189) measured MR in narrow Si MOSFET's and extracted the inelastic diffusion length as a function of temperature.

Fukai et al [90F4] structured GaAs/AlGaAs on–facet wires ($w = 0.3\,\mu$m, $L = 1.7$ and $10\,\mu$m, $l = 0.7\,\mu$m) and determined the phase coherence length for temperatures down to 50 mK via the conductance fluctuation amplitude, the conductance fluctuation correlation field, and weak localization. From the amplitude of conductance fluctuations, $l_\varphi \propto T^{-0.28}$ for $T > 0.5$ K and l_φ constant for $T < 0.4$ K was found. A similar behaviour was obtained via the correlation field. The low–field MR was positive for $T \leq 0.08$ K, indicating the presence of SO interaction which is a temperature independent mechanism and was assumed to be responsible for the saturation of l_φ.

Bird et al [90B2] studied l_φ in quasi–ballistic GaAs wires ($w = 1.8\,\mu$m, $L = 30\,\mu$m) defined by wet etching. Above 0.4 T, 1D subband depopulation and SdH oscillations were observed. Below 0.15 T, aperiodic fluctuations in the MR were found and l_φ was extracted by comparison of the data with theory. For $T < 1$ K, the phase coherence length was almost independent of temperature, as was the correlation field. Bird et al suggested a breakdown of diffusive motion to be responsible for the saturation of l_φ.

Taniguchi et al [90T4] fabricated GaAs wires by EBL and two different ion–beam etching techniques: Ar ion–milling (IM) and RIE. The electron density in IM wires was 10% lower than in RIE wires. The MR of IM wires of different widths ($w = 10\,\mu$m, $L = 60\,\mu$m; $w = 3.0$ and $0.8\,\mu$m, $L = 20\,\mu$m) was studied and the phase coherence length as a function of temperature was extracted (Fig. 137). The narrow wires saturated below $1 - 2$ K with $l_\varphi = 0.33\,\mu$m, while above $1 - 2$ K $l_\varphi \propto T^{-1/2}$ was found. Taniguchi et al attributed the saturation of l_φ to electron scattering at the ion–damaged side walls. The contribution of electron–electron interactions to the conductivity was investigated by studying the MR vs. B^2 in the $w = 0.8\,\mu$m wide wire. In RIE wires the saturation of l_φ occurred in a similar manner as in IM wires. In RIE wires, l_φ was longer than in IM wires. The amplitudes of UCF in the wires were compared (Fig. 138), the difference was larger than expected from the difference in l_φ.

Bird et al [91B1, 92B2] (page 170) studied the four–terminal MR of a GaAs wire. The UCF decayed with increasing temperature, comparison with theory implied a temperature–independent l_φ. Bird et al discussed the possible origin for the saturation of the phase coherence length.

Taniguchi et al [91T2] studied the phase breaking time τ_φ and the SO scattering time τ_{SO} in Si δ–doped GaAs wires. They investigated the temperature dependence of τ_φ and τ_{SO} in wires

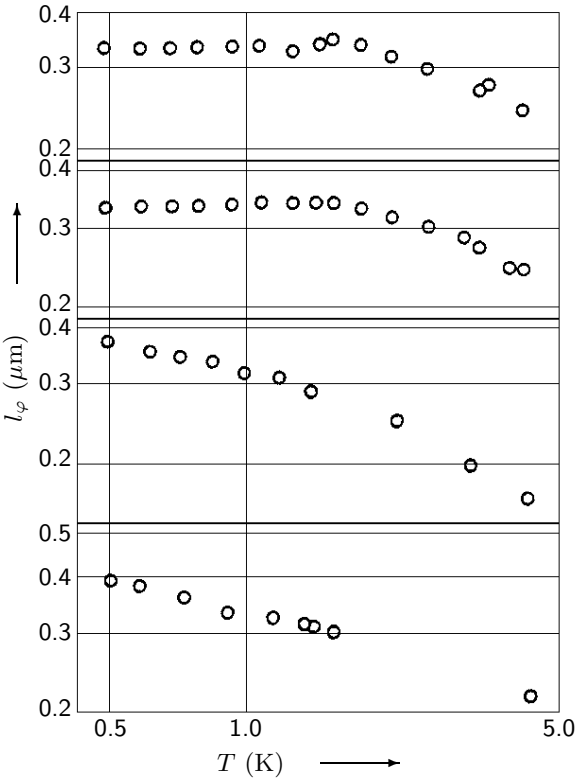

Fig. 137: Temperature dependence of l_φ in IM wires of widths (top) $w = 0.8\,\mu$m, $w = 3.0\,\mu$m, $w = 10\,\mu$m, and a film (bottom) [90T4].

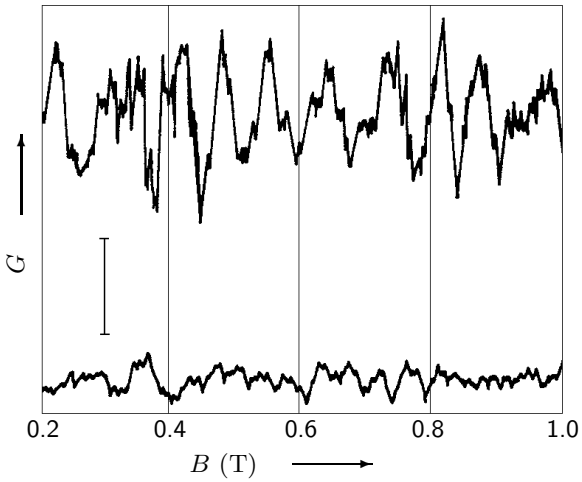

Fig. 138: UCF in $0.2\,\mu$m wide wires fabricated by RIE (top) and IM (bottom) [90T4]. The vertical bar denotes a conductance amplitude of $0.01 \cdot e^2/h$. The conductance has been vertically offset for clarity.

fabricated by ion milling or wet chemical etching and found saturation of τ_φ when τ_φ became comparable to τ_{SO}.

Ramon et al [93R] patterned narrow GaAs wires ($w = 0.15 - 1.0\,\mu$m, L is 5 or 10 times w; $w = 0.2 - 0.4\,\mu$m, $L = 2$ and $35\,\mu$m; $w = 0.6 - 1.0\,\mu$m, $L = 4\,\mu$m; $l = 70$ nm) by EBL and dry plasma etching and found a strong dependence of the total depletion width on the accelerating voltage used during the etching process. From low–field MR data, the phase coherence length as a function of temperature was extracted using weak–localization theory: l_φ saturated below 6 K. At higher fields, UCF were observed, l_φ was again deduced from the data. A quasi–periodic structure in the conductance fluctuations was attributed to AB interference in some closed loops.

Noguchi et al [96N2] investigated the phase breaking time of GaAs wires defined by (A) FIB implantation ($w = 0.08 - 0.38\,\mu$m, $L = 5$ or $10\,\mu$m) and (B) a split gate ($L = 40$ or $100\,\mu$m) as a function of temperature. They measured the MC for $0.4\,\mathrm{K} < T < 30\,\mathrm{K}$ and observed weak localization and AF (Fig. 139). From theoretical fits, τ_φ vs. T was obtained for various samples with different μ and E_F. Im samples with intermediate mobility, $\tau_\varphi \propto T^{-2}$ above 8 K, $\tau_\varphi \propto T^{-2/3}$ for $2\,\mathrm{K} < T < 8\,\mathrm{K}$, while τ_φ saturated below $1 - 2$ K. This behaviour was explained by electron–electron scattering. In samples with a low mobility, τ_φ saturated below 2 K (with values ranging from 0.3 to 2 ps) and $\tau_\varphi \propto T^{-2/3}$ for $2\,\mathrm{K} < T < 8\,\mathrm{K}$. In samples with a high mobility, τ_φ behaved consistent with electron–electron scattering above 1 K and did not saturate below 1 K, $\tau_\varphi \propto T^{-2/3}$ for $T < 1$ K. In these samples, a MR peak at $B \approx 0.1$ T was ascribed to boundary scattering. The weak–localization peak at $B < 0.04$ T became steeper for fixed V_g as temperature decreased. The saturation value of τ_φ increased with mobility as $\propto \mu^{0.8}$ in samples B and as $\propto \mu^{1.3}$ in samples A. With increasing E_F, the saturation value of τ_φ decreased in the lowest–mobility sample. In samples with intermediate mobility, the saturation value of τ_φ increased with E_F as $\propto E_F^{0-4.4}$. Noguchi et al ascribed the saturation of τ_φ to spin–flip scattering by paramagnetic impurities.

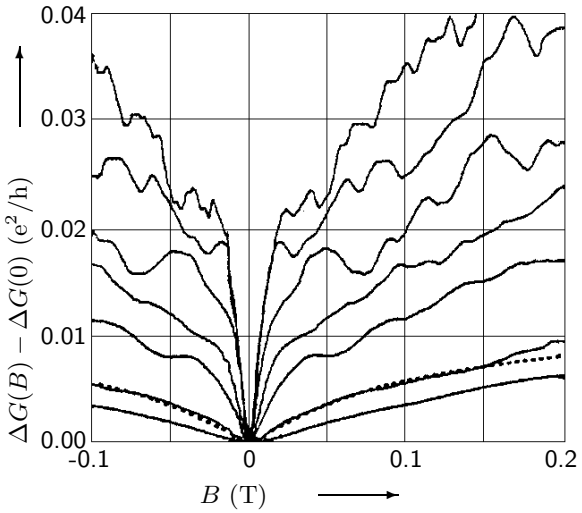

Fig. 139: MC curves of the τ_φ–saturated wire at $T = 0.7$ K for (right, top) $V_g = -0.9$ V, -1.3 V, -1.5 V, -1.7 V, -1.9 V, -2.1 V, and -2.3 V (right, bottom) [96N2]. The dotted line shows a weak–localization fit for a specular boundary condition for $V_g = -2.1$ V.

Linke et al [97L] (page 164) investigated the dephasing rate of electrons not in equilibrium in the diffusive regime. They used GaAs wires, measured the four–terminal MC and analysed the data in terms of weak localization. The phase breaking rate was determined as a function of temperature.

7.3.5 Current heating

Carriers inside a conductor which are accelerated by an electric field in such a way that their mean kinetic energy exceeds the mean lattice temperature are called *hot electrons*. They are out

of equilibrium with the lattice. Energy relaxation proceeds mainly via phonon scattering. The phenomenon is referred to as *current heating* (see for example [62S, 91R1] and references therein). Current heating may be used in order to establish large gradients in electron temperature along a wire. The thermoelectric coefficients then determine the electric current generated because of the temperature gradient. In mesoscopic metallic systems, these coefficients show large fluctuations when the chemical potential or the magnetic field are varied. These fluctuations are due to interference effects (see for example [87A1, 87E, 88S2, 90G1, 97F] and references therein).

Dean et al [84D] (page 212) examined Si MOSFETs with channel widths of $\approx 1\,\mu$m, performed electron heating measurements, and studied electron–phonon scattering.

Gallagher et al [90G1] measured the thermopower of multi–terminal n^+-type GaAs wires fabricated by EBL and dry etching. The two–terminal MR showed AF coexisting with SdH oscillations and an underlying negative MR due to weak localization. They applied an electric field along the wire and measured the thermoelectric voltage between the ends of the side arms (Fig. 140). Large fluctuations in the thermopower were formally in agreement with theory, but the absolute magnitude differed from the theoretical predictions by a factor of two.

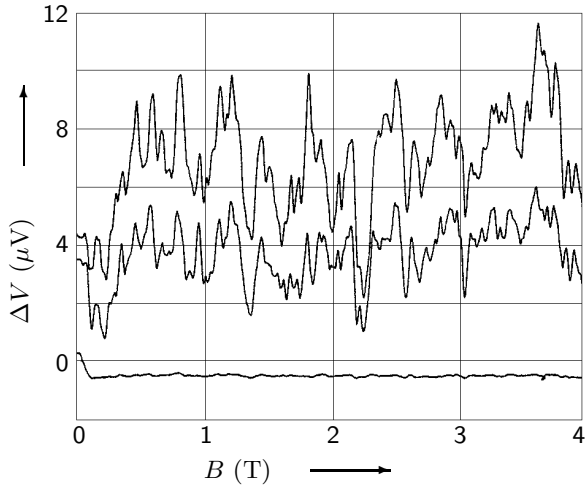

Fig. 140: dc thermoelectric voltage fluctuations due to an electron temperature gradient [90G1]. Heating ac voltage across the sample was (bottom) 0, 17 and 45 μV (top). Middle trace has been offset by 4 μV and top trace by 7 μV.

Molenkamp et al [94M3, 95dJ] measured the differential resistance in GaAs wires ((A) $w = 3.9\,\mu$m, $L = 20.2\,\mu$m, $l = 12.4\,\mu$m; (B) $w = 4.0\,\mu$m, $L = 63.7\,\mu$m, $l = 19.7\,\mu$m; (C) $w = 4.0\,\mu$m, $L = 127.3\,\mu$m, $l = 19.7\,\mu$m) and observed a non–monotonic current dependence of the differential resistance. Heating of the electron gas was achieved by passing a dc current through the wire. They studied the effect for various lattice temperatures. They discussed their results in terms of a transport theory which combined electron–electron scattering with partly diffusive boundary scattering.

Yoh et al [94Y] fabricated free–standing InAs wires by EBL and wet etching. They first measured the resistance as a function of temperature. Second, using this data as a thermometer, they investigated the dependence of the sample resistance on heating currents. The electron temperature increased from 4.2 to 10 K with a heating current of 100 nA (Fig. 141). The results were compared to the Wiedemann–Franz law. The experimental data deviated from the theoretical curves when the power consumption exceeded $\approx 3\,\mathrm{nJs}^{-1}$.

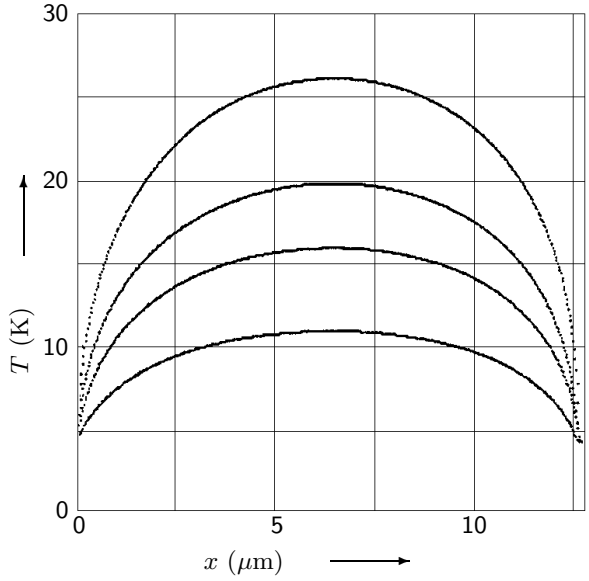

Fig. 141: Electron temperature profile along the wire for heating currents (top) $I = 500\,\mathrm{nA}$, 300 nA, 200 nA, and 100 nA (bottom) [94Y].

7.4 Sample geometry

7.4.1 Width and length

In metallic samples, the resistance scales approximately as $R \propto L$. In localized samples, the resistance increases exponentially with increasing sample length (see Section 7.10 on page 212). Further, wire width and length in comparison with sample–intrinsic length scales (such as l, l_φ, L_T, etc.) determine the effective dimensionality of the system. Changing w and L can thus affect transport properties due to dimensional crossovers.

Moreover, w naturally determines the width of the confinement potential in quantum wires. As a consequence, the subband spacing depends on w and so do the widths of the conductance steps in the quantized conductance with respect to gate voltage (see Section 7.1.2 on page 118).

Where conductance fluctuations due to interference effects are concerned (see Section 7.2.1 on page 124 and Section 7.7.3 on page 182), changing L affects the ratio L/l_φ and may thus either lead to effective ensemble averaging for $L \gg l_\varphi$ or to breakdown of universality and length–dependent fluctuations for $L \ll l_\varphi$.

Fowler et al [82F, 83F, 86W2, 88F3] (page 125) examined Si MOSFETs with two control electrodes and a metal gate allowing for a lateral confinement of the accumulation layer. They studied the temperature dependence of the conductance for different gate and control voltages (Fig. 122). A transition from a 1D to a 2D behaviour was observed as the channel broadened with increasing V_g.

Dean et al [82D] (page 132) found typical 2D behaviour at $T = 1.4\,\mathrm{K}$ in a Si channel about $1\,\mu\mathrm{m}$ wide. The power–law temperature dependence of the conductance was, however, not consistent with 2D behaviour. The MC for low B was positive at $T = 1.2\,\mathrm{K}$, and negative at $\approx 70\,\mathrm{mK}$ (Fig. 133). For narrower channels, $\approx 0.1\,\mu\mathrm{m}$ wide, both power–law temperature dependence and negative MC persisted to higher temperatures.

Skocpol et al [84S] (page 125) found that the two–terminal conductance scaled approximately with the channel width in narrow Si wires.

Choi et al [85C, 86C2] (page 168) examined GaAs devices of different widths. Four–terminal MR data for a wide sample and for three narrow samples are shown in Fig. 164. The temperature–insensitive MR was larger and the onset of SdH oscillations occurred at larger B for smaller w.

Zheng et al [86Z1] (page 200) structured four–terminal GaAs samples and measured the MR of wide, short narrow, and long narrow devices. Differences in the characteristic features of the QHE were observed. Zheng et al studied the development of the narrow–channel characteristics as a function of channel width. They found that the narrow–channel characteristics diminished when the probe spacing was reduced to several micrometers.

Skocpol et al [86S1] (page 127) studied the influence of the channel width onto the threshold voltage in quasi 1D Si devices.

Zheng et al [86Z2] realized a GaAs channel by a split gate. The narrowest conducting channel achieved was 0.37 μm wide at $V_g \approx -1.9$ V. The channel resistance as a function of gate voltage (controlling the channel width) and MR data are shown in Fig. 142. The increase in the oscillation period in the SdH oscillations with decreasing V_g indicated a decreasing electron density. Low field MR data were fitted by a 1D weak–localization theory (Fig. 143). The inelastic scattering length was extracted from the fits and its functional dependence on the channel conductivity was studied and compared with theory.

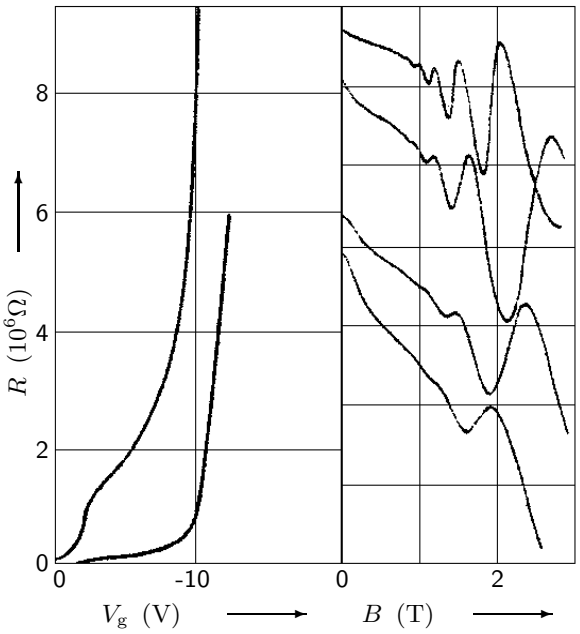

Fig. 142: Channel resistance vs. gate voltage at $T = 4.2$ K (left picture; left curve is right curve $\times 10$) and SdH oscillations for (top) $V_g = -0.3$ V (50 kΩ/div.), -1.0 V (125 kΩ/div.), -1.25 V (250 kΩ/div.), and -1.5 V (500 kΩ/div.) (bottom) at $T = 1.3$ K (right picture) [86Z2].

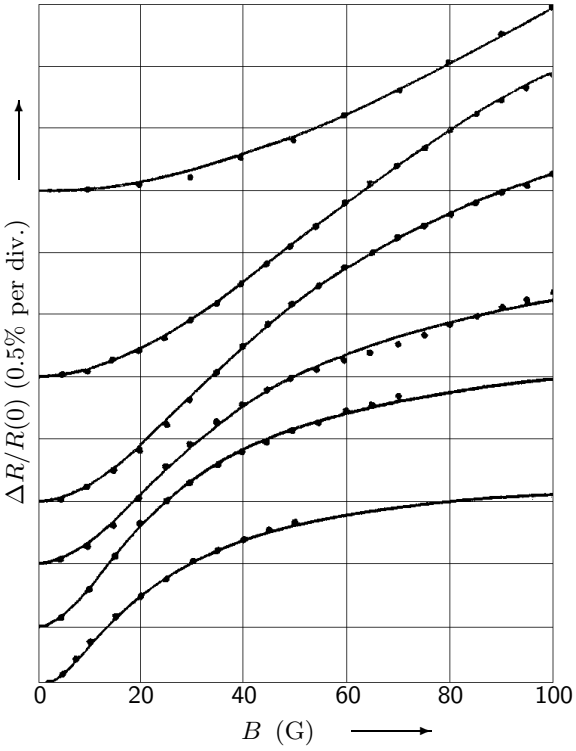

Fig. 143: MR for (top) $V_g = -1.5$ V, -1.25 V, -1.0 V, -0.75 V, -0.5 V, and -0.3 V (bottom) at $T = 1.3$ K [86Z2]. Solid curves are fits to 1D weak–localization theory.

Van Houten et al [86vH] used an electrostatic confinement of the electrons by a shallow mesa structure obtained via etching in GaAs. The narrowest structure fabricated was 40 nm wide. The resistivity was studied for different channel widths and SdH measurements were performed. Low–field MR data revealing weak localization are shown in Fig. 144. Reproducible AF were found for $B > 0.1$ T.

Choi et al [87C2] (page 179) examined the effect of L on localization in GaAs/$Al_xGa_{1-x}As$ samples of different geometries.

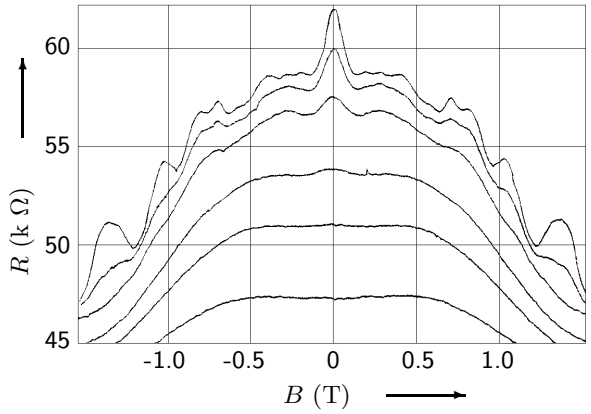

Fig. 144: MR for a 500 nm wide sample at temperatures (top) $T = 3.8$ K, 5.7 K, 10 K, 20 K, 30 K, and 50 K (bottom) [86vH].

Skocpol et al [87S2] (page 183) compared the behaviour of a Si device with a probe spacing of 150 nm with one of probe spacing of 5 μm. They studied fluctuations of the resistance in multi–probe devices and found that the amplitude of the fluctuations increased as the square root of the probe spacing for $L > l_\varphi$. At smaller probe spacings, the amplitude remained constant.

Thornton et al [87T2] (page 185) studied split–gate heterojunction GaAs field–effect transistors. They measured MC fluctuations and studied the variance of the fluctuations for different channel widths (Fig. 185).

Grassie et al [87G1] (page 195) studied SdH oscillations in GaAs wires. The amplitude of the oscillations was smaller in narrow wires than in wide regions.

Hiramoto et al [87H1, 88H2] fabricated GaAs wires by FIB implantation. The conductance of the channels decreased linearly with decreasing width and vanished for $w = 0.48\,\mu$m. The minimum effective channel width fabricated was 20 nm. The low–field MC of wires of different widths was measured and fitted by 1D weak–localization theory deducing l_φ. At higher fields, the MC showed AF, the amplitude of the fluctuations depended on the channel width (Fig. 145).

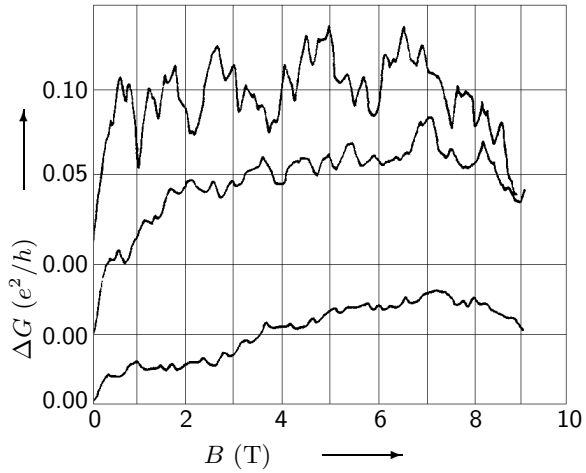

Fig. 145: MR of three wires with (top) $w_{\rm eff} = 0.12\,\mu$m, $0.053\,\mu$m, and $0.02\,\mu$m (bottom) at 1.3 K [87H1].

Roukes et al [87R] (page 201) reported the first quenching of the Hall effect in narrow GaAs channels. The width dependence of this effect was studied in numerous wires, quenching was observed for $w \leq 200$ nm.

Chang et al [88C2] (page 187) performed MR measurements on ballistic GaAs/$Al_xGa_{1-x}As$ wires. They varied the probe spacing by measuring between different leads.

Ford et al [88F2] (page 202) studied narrow GaAs Hall bars defined by a Schottky gate for $V_g \leq -0.6\,V$. They examined the Hall voltage as a function of channel width (Fig. 205) and found deviations from the classical behaviour for low B.

Thornton et al [89T5] (page 160) defined GaAs wires and measured the MR. They observed a positive zero–field MR showing an anomalous maximum. Amplitude and field position of the latter increased as the width of the wire decreased (Fig. 160). It scaled with the ratio of cyclotron length to wire width.

Menschig et al [90M1, 90M2, 91F2] (page 116) patterned $In_{0.53}Ga_{0.47}As/InP$ wires and studied the resistivity vs. wire width at zero magnetic field. A negative MR at low fields decreased with increasing wire width. A MR peak due to boundary scattering was found, peak resistance and corresponding magnetic field increased as the wire width decreased (Fig. 111).

Eugster et al [90E] defined GaAs wires with three different lengths ($L \approx 0.0\,\mu m$, $0.5\,\mu m$, $1.0\,\mu m$) via confining gates ($w \approx 0.2 - 0.3\,\mu m$) fabricated by EBL. Measuring the current through the two–terminal wires as a function of gate voltage, a broad temperature–independent plateau in the current was observed for the constriction. It indicated that tunneling was the main transport process. The $0.5\,\mu m$ long wire showed conductance steps, indicating ballistic transport. The I–V_g characteristic for the $1.0\,\mu m$ long wire was mostly featureless, indicating diffusive transport.

Nakata et al [91N] fabricated single GaAs wires using Ga FIB implantation. The structural widths ranged from 0.5 to $10\,\mu m$, the conduction widths from 0.2 to $9.7\,\mu m$. The voltage probes were $20\,\mu m$ apart. A Schottky gate was used to control carrier density. Multiple wire structures were patterned by FIB with periods ranging from $0.24\,\mu m$ to $0.60\,\mu m$. The conductance in the single wires decreased monotonically with decreasing width. Carrier density and mobility in the single wires were studied as a function of w; μ was almost constant for $w < 1\,\mu m$, possibly due to confinement to 1D states. MR measurements on the single wires showed SdH oscillations, deviations of $1/B$ vs. n_L from a straight line were attributed to magnetic depopulation of 1D subbands. An anomalous resistance peak observed in the low–field MR was attributed to diffusive sidewall scattering. The temperature dependence of the MR was examined, as was the relation between the peak amplitude and temperature. Measuring R as a function of V_g, resistance steps were observed in a $0.2\,\mu m$ wide single wire. Conductance vs. carrier density was studied. In the multiple wire structures, peaks in the conductance vs. gate voltage were observed. The peak interval of 0.09 V corresponded to a subband separation of 2.2 meV. The first conductance peak was enhanced in comparison to the other peaks.

Eugster et al [91E] (see also [90E], page 147) defined GaAs wires using split gates. The lengths were $0.0\,\mu m$ (constrictions), $0.5\,\mu m$, and $1.0\,\mu m$, the lithographic widths varied from 0.1 to $0.5\,\mu m$ for the constriction and from 0.1 to $0.3\,\mu m$ for the wires. The I–V_g characteristic of $1.0\,\mu m$ long wires was studied at $T = 300\,K$, a 1D regime was only found for widths above $0.2\,\mu m$. The longer devices were in general easier to pinch off as could be seen from I–V_g characteristics of samples of different lengths. Both, width and length influenced the onset of a 1D regime.

Feng et al [92F1, 92F2] fabricated wires (structural width $1.0\,\mu m$) from δ–doped GaAs, side–gated across deep trenches ($0.3\,\mu m$ deep, $0.5\,\mu m$ wide) defined by EBL and RIE. The channel resistance increased as the reverse bias on the gate increased (and the wire width decreased) and pinched off for gate voltages exceeding $\approx 8\,V$. MR at different V_g was measured, results were fitted by 1D weak–localization theory. The phase coherence length stayed constant ($l_\varphi \approx 0.13\,\mu m$) while the wire width decreased in a linear fashion as the reverse bias on the gates increased. The width at $V_g = 0\,V$ was estimated to be $1.05\,\mu m$. From SdH oscillations it was inferred that the electron density remained constant over the measured range of V_g and that the channel pinched off due to the reduction of its width.

Ishibashi et al [92I1] performed transport measurements in a GaAs wire defined by a split gate ($w = 0.6\,\mu m$, $L = 2\,\mu m$, $l \approx 1\,\mu m$ at 1.2 K). The resistance as a function of gate voltage at

$T = 1.2\,\mathrm{K}$ increased with decreasing V_g (i. e. decreasing wire width) and showed small fluctuations probably due to the presence of impurities. The MR showed SdH oscillations at zero gate voltage. As V_g became increasingly negative, the SdH oscillations decayed and AF became prominent. Ishibashi et al interpreted their observations in terms of a transition from metallic ($R < h/e^2$) to non–metallic ($R > h/e^2$) transport.

Ochiai et al [91O2, 92O1] (page 171) investigated MR in GaAs wires, an amplitude analysis of SdH oscillations revealed two different scattering times at high and low magnetic fields in etched wires. The boundary field between the two regimes depended on the wire width.

Haug et al [92H1] (page 180) fabricated narrow channels on the cleaved surface of InAs quantum well structures and measured the MR. Aperiodic fluctuations became weaker for an increasing width of the InAs well.

Blaikie et al [92B3] reported a fabrication technique in which the lateral confinement of a wire was provided by p–n junctions while the electron density could be varied by means of a surface Schottky gate. From a δ–doped GaAs/AlGaAs heterostructure, $10\,\mu$m long wires with different structural widths were fabricated. The channel resistance was studied as a function of surface gate bias and implanted gate bias. MR measurements were performed and SdH oscillations, the quantum Hall effect and an anomalous MR peak due to boundary scattering were observed. The electrical width was deduced from the data. It was possible to vary separately both the width and the electron density.

Hirayama et al [92H3] studied in–plane gated GaAs wires ($L = 5$ or $10\,\mu$m) fabricated by Ga FIB scanning with distances between the centres of the FIB scanned lines varying from 0.6 to $10\,\mu$m. The channel resistance of a $1.5\,\mu$m wide wire was measured as a function of the left and right gate voltages, $V_{g,l}$ and $V_{g,r}$, respectively (Fig. 146). For $V_{g,l} > 0$, a resistance jump occurred, the threshold of $V_{g,r}$ became independent of $V_{g,l}$. In a $0.6\,\mu$m wide wire, no resistance jump was observed, the threshold voltage decreased with the electron density n. In another $1.5\,\mu$m wide wire, no jump was found for $n \leq 1.8 \times 10^{11}\,\mathrm{cm}^{-2}$, but it appeared at $n = 1.9 \times 10^{11}\,\mathrm{cm}^{-2}$. With increasing wire width, the resistance jump became more prominent (Fig. 147), even a $10\,\mu$m wide channel could be pinched off. The resistance jump did not depend on magnetic field and occurred only at low T (at 1.5 and 4.2 K, but not at 77 K). The transport characteristics in the normal region (away from a resistance jump) were examined. It was deduced that the effective channel width could be changed within $0.6\,\mu$m. Almost all the change of the channel resistance with gate voltages could be explained by the change of the effective channel width, the change of the carrier density had only a small influence.

Ishibashi et al [92I2] (page 190) studied conductance fluctuations in the quasi–ballistic regime in split–gate GaAs wires. The amplitude of MR fluctuations was examined as a function of the wire width. It increased with the width in a $2\,\mu$m long sample and eventually approached e^2/h, while it was independent of width in a $6\,\mu$m long wire and smaller than e^2/h. The correlation field was studied as a function of the wire width.

Tarucha et al [93T3] investigated transport in 4 to $60\,\mu$m long ballistic GaAs channels ($w = 2 - 8\,\mu$m, $l = 67\,\mu$m). The I–V characteristic for a $2\,\mu$m wide wire was nearly identical for all channels with $L \leq 20\,\mu$m, the resistance increased for longer channels (Fig. 148). The resistance of $4\,\mu$m wide channels was independent of length for $L \leq 12\,\mu$m. The differential resistance vs. voltage for $2\,\mu$m wide channels showed a minimum at a voltage of several mV, which was more pronounced in the shorter channels (Fig. 149). In the presence of a magnetic field, the minimum in the differential resistance disappeared above $500 - 600\,\mathrm{G}$.

Block et al [93B1] (page 171) studied the MR of wires fabricated from $In_{0.53}Ga_{0.47}As/InP$ heterostructures. An anomalous MR peak was observed. The peak amplitude increased with decreasing wire width and the magnetic–field position of the maximum shifted to larger values (Fig. 167).

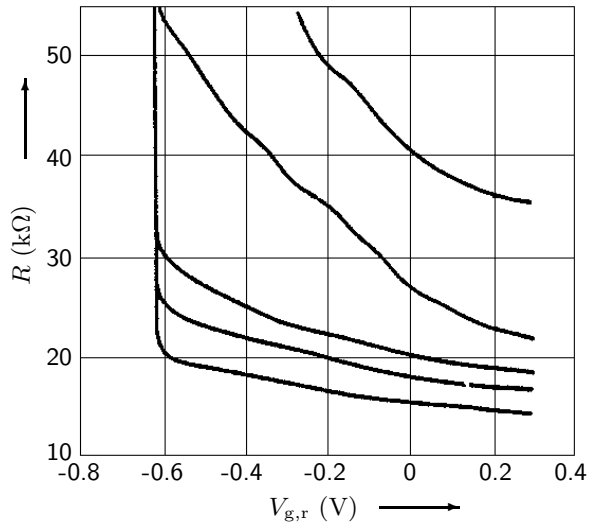

Fig. 146: Channel resistance characteristics as a function of right gate voltage of a 1.5 μm wide and 5 μm long wire at 1.5 K for left gate voltage (top) $V_{g,l} = -0.5$, -0.25, 0, 0.25, and 0.5 V (bottom)[92H3].

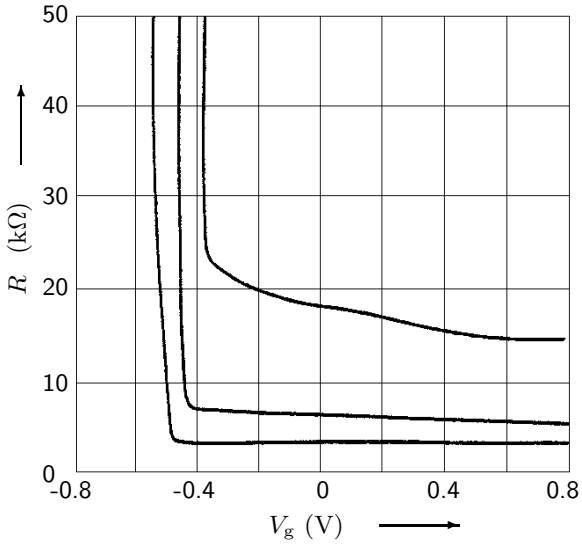

Fig. 147: Channel resistance as a function of $V_g = V_{g,r} = V_{g,l}$ for (top) $w = 2.5$, 3.5, and 4.9 μm (bottom) at 1.5 K [92H3].

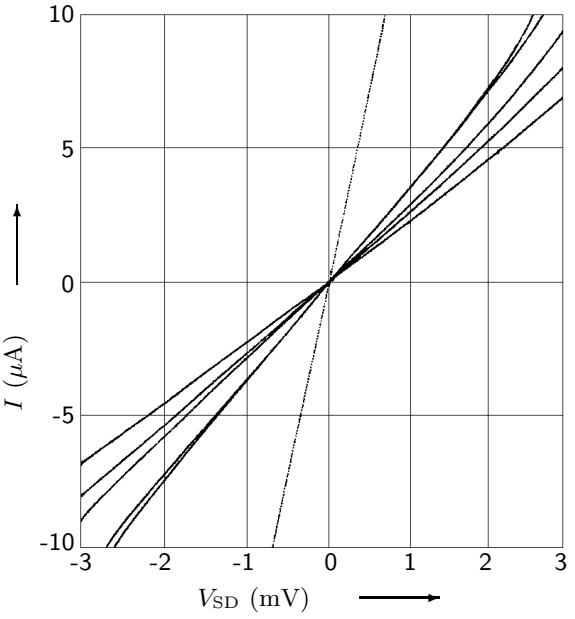

Fig. 148: Current–voltage characteristics for (right, top) $L = 4\,\mu$m, 16 μm, 30 μm, 40 μm, and 60 μm (right, bottom) [93T3].

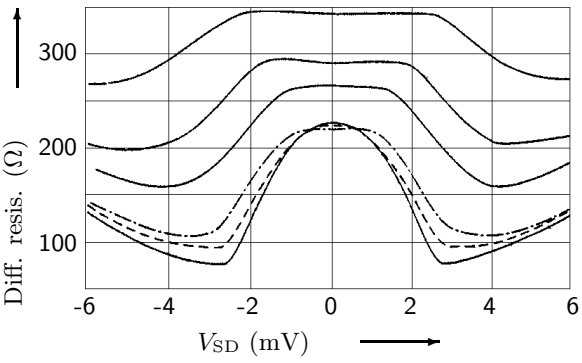

Fig. 149: Differential resistance as a function of source–drain voltage for (top) $L = 60\,\mu$m, 40 μm, 30 μm, 16 μm, 8 μm, and 4 μm (bottom) [93T3].

Tang et al [93T1] (page 120) studied the influence of the lateral width on the conductance of Si inversion wires. An increase in the conductance step size with decreasing lateral wire dimensions was observed.

Onishi et al [93O2, 93O3, 94O1] (page 191) studied MR in split–gate GaAs wires. The correlation field B_c of UCF was smaller in the shorter wires, it increased with decreasing w_{eff}.

Nakata et al [93N, 94N2] fabricated buried GaAs wires ($L = 2\,\mu$m) by EBL, wet chemical etching, and MOCVD regrowth. They studied two types of buried wires: for type 1 the buried thickness was 50 nm (partial burying of the sidewall), for type 2 it was 120 nm (sidewall completely buried). The conductance as a function of the structural width was examined and the critical width determined ($0.4\,\mu$m for type 1, $0.1 - 0.2\,\mu$m for type 2). In the MR, the number of SdH oscillations decreased with decreasing wire widths. The Landau level index vs. inverse magnetic field deviated from a linear behaviour for $w < 0.6\,\mu$m. From fits to the Landau plots, energy separations of 1.5 meV (type 1) and 4.0 meV (type 2) at the critical width were extracted.

Honda et al [95H3] (page 120) observed quantized conductance in 2 to 30 μm long GaAs wires and studied the dependence of G on the wire width and length (Fig. 117).

Tarucha et al [95T] (page 120) measured the two–terminal conductance of 2 to 10 μm long GaAs wires at various temperatures. The temperature–dependence of the conductance was stronger in the longer wires (Figs. 118 and 119).

Ochiai et al [95O1] (page 192) investigated UCF in split–gate GaAs wires. They examined the influence of the wire width on $B_c(B)$ and on the average amplitude.

Koester et al [96K3] (page 181) investigated weak localization in Si wires. The four–terminal conductance decreased linearly with the width.

Inoue et al [97I2] (page 175) investigated transport in InAs wires. They examined the charge velocity at 77 K as a function of channel width and length. The high–field velocity increased in the narrow wires.

Okada et al [97O] structured in–plane gate GaAs wires and wrap–gate InGaAs wires. Both showed SdH oscillations at $T = 4.2$ K. Landau plots deviated from a linear behaviour at low magnetic fields, indicating 1D transport. The wire width as a function of gate voltage was determined from the Landau plots. At zero field, the conductance as a function of gate voltage showed steps. Near pinch–off, conductance oscillations were observed.

Maemoto et al [97M] fabricated single and multiple InAs wires with a corrugated surface along the wire (period of corrugation $0.2\,\mu$m) and measured MR. Features due to boundary scattering were observed. The channel–length dependence of the I–V characteristic was studied. The high–field electron velocity was estimated from I–V characteristics and was found to increase with decreasing channel width. A transistor was fabricated from InAs wires and compared to 2D transistors.

Liang et al [99L] (page 124) studied quantized conductance in GaAs split–gate wires of different lengths ($L = 3$, 5, and $6\,\mu$m, $l \approx 70\,\mu$m). With increasing wire length, the plateau values were reduced.

7.4.2 Crossed–wire junctions

In the ballistic regime, transport through *crossed wire junctions* may lead to quenching of the Hall resistance (see Section 7.7.5 on page 200) and to negative bend resistances (see Section 7.7.6 on page 206).

Takagaki et al [88T1] (page 207) examined narrow multi–branched electron wave guides made

from GaAs/AlGaAs heterostructures. A crossed–wires shape was structured, the current flowed diffusively between adjacent probes. In a lead configuration, in which the current had to flow around a bend, the average resistance was negative (Fig. 213).

Takagaki et al [89T2] (page 193) observed non–local voltage fluctuations in a quasi–ballistic GaAs electron waveguide with two junctions and six leads. In a crossed–wire lead configuration they found a negative average resistance at low magnetic fields (Figs. 193 and 194).

Ford et al [89F2] fabricated ballistic GaAs samples with two cross regions 6 μm apart and joined by a straight narrow channel of constant width. One of the two cross regions was nominally perfect, the others were (1) a cross with tapered corners, (2) a cross as in (1) but with a diamond–shaped dot in the centre, and (3) a cross with voltage probes narrower than the current probes. The devices were covered with a gate, channels did not conduct at $V_g = 0$ V, but were turned on at $\approx +0.35$ V. The Hall resistance vs. B for device 1 is shown in Fig. 150. The quenching disappeared at $T \geq 10$ K, the negative R_H survived up to 20 K. The Hall resistances vs. B for devices 2 and 3 are displayed in Figs. 151 and 152. Ford et al attributed the observed effects to geometrical scattering of electrons entering the cross regions.

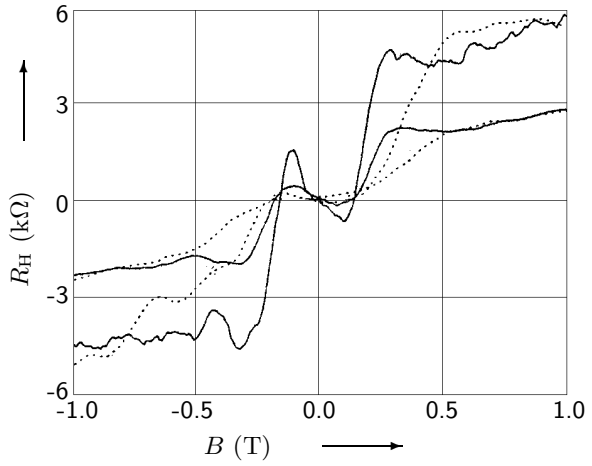

Fig. 150: Resistance R_H vs. B for device 1 for (top) $V_g = 0.55$ V and 0.43 V (bottom) at 4.2 K [89F2]. The solid and dotted lines are for the widened and normal crosses on the same sample.

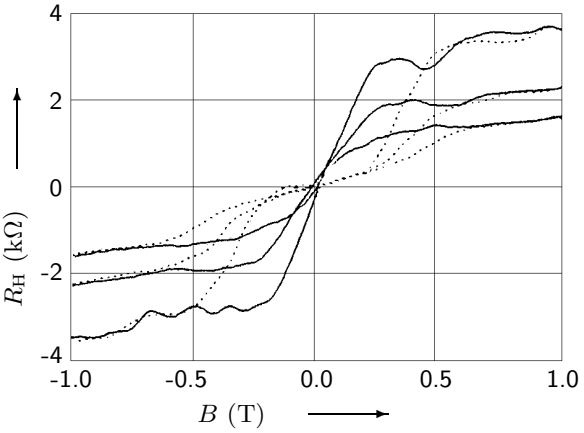

Fig. 151: Resistance R_H vs. B at (top) $V_g = 0.75$ V, 0.6 V, and 0.5 V (bottom) for device 2 [89F2]. The solid and dotted lines are for the widened cross with a central dot and the normal cross on the same sample.

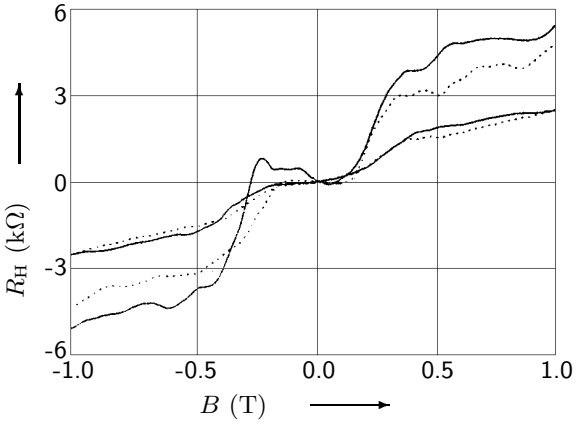

Fig. 152: Resistance R_H vs. B at (top) $V_g = 0.4$ V, and 0.26 V (bottom) for device 3 [89F2]. The solid and dotted lines are for the cross with narrow probes and the normal cross on the same sample.

Takagaki et al [89T1] (page 207) revisited the four–terminal negative resistance found previously (see [88T1] on page 207). In a crossed–wire junction, the resistance was negative at $B = 0\,\mathrm{T}$ and approached the classical value $R \approx 40\,\Omega$ with increasing field but showed a maximum around $B = 0.3\,\mathrm{T}$ (Fig. 214).

Takagaki et al [89T3] (page 208) fabricated multi–channel ballistic GaAs wires, performed MR measurements, found an increase in the resistance due to a bend in the current path and four–terminal negative resistance at a crossed–wire junction.

Ford et al [90F3] (page 208) extended previous studies ([89F2] on page 151) on how the geometry of a cross region affected the Hall resistance. They studied diagonal junctions and one with adjacent very wide probes.

Takagaki et al [90T2] (page 208) fabricated narrow crossed GaAs wire junctions and studied the bend resistance and the Hall resistance.

Kakuta et al [91K2, 92K2] (page 208) fabricated a cross–shaped GaAs junction with four side gates. The corners of each wire were rounded, the wires became wider over a distance of $0.7\,\mu\mathrm{m}$ towards the cross. The bend resistance was studied for several V_g.

7.4.3 Special geometries

Apart from the crossed–wire junctions (see Section 7.4.2 on page 150), other special geometries studied were a wire with an artificial barrier induced by a gate, two parallel wires coupled by a ballistic window, a Y–shaped wire, wires with voltage probes connected at angles $\neq 90°$, a wire with a point contact in one side boundary, a wire with an artificial impurity induced by a gate or structured using an STM, two parallel wires coupled by a window, wires with chains of anti–dots inside, a wire with a set of quantum dots in one side wall, a wire with a buried superconductor dot, a corrugated wire, a wire with an embedded ferromagnetic dot, a wire with Au nano dots, and two wires in a double quantum well structure.

Chou et al [92C] fabricated split–gate GaAs wires ($w = 50 - 100\,\mathrm{nm}$) with a barrier induced by a narrow metal gate ($w = 50\,\mathrm{nm}$). The current as a function of gate voltage showed nine periodic oscillation peaks (period 15 mV) before the onset of the first $2 \cdot e^2/h$ conductance plateau and quantized conductance in the 50 nm wide wire. Five oscillations (period 9 mV) were observed in a 100 nm wide wire (Fig. 153). The peak–to–valley ratio of the oscillations decreased with increasing source–drain voltage or temperature. Chou et al discussed their observations in terms of the Coulomb blockade.

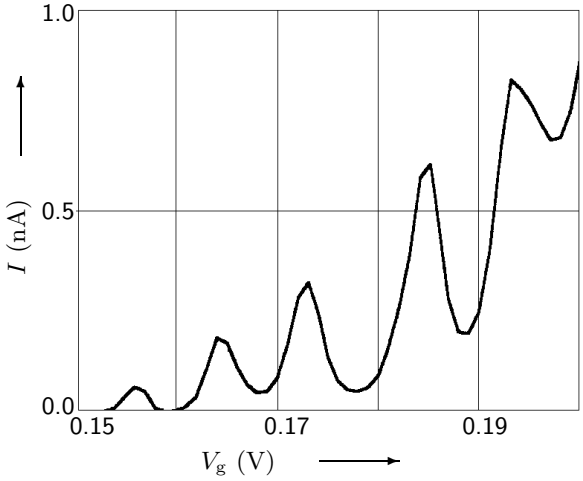

Fig. 153: The source–drain current vs. gate voltage (100 nm gate gap) before the onset of the first $2e^2/h$ conductance plateau for $T = 0.5\,\mathrm{K}$ and $V_\mathrm{SD} = 1\,\mathrm{mV}$ [92C].

Hirayama et al [92H2] examined four–terminal transport through two in–plane gated parallel GaAs wires ($w = 1.25\,\mu$m, $L = 5\,\mu$m) structured by FIB scanning and coupled by a ballistic window ($L = 1.25\,\mu$m). The longitudinal resistance as a function of magnetic field showed SdH oscillations and a negative peak at $B = 0\,$T, indicating the existence of a side–ways ballistic component (Figs. 154 and 155). The Hall resistance showed quantized plateaux. After the disappearance of the negative peak around $B = 0\,$T, $R_{\rm L}$ became almost zero, then the resistance minima again became negative in a intermediate–field region. For a longer window structure, $R_{\rm L}$ became positive. The longitudinal resistance as a function of gate voltage exhibited an oscillatory behaviour.

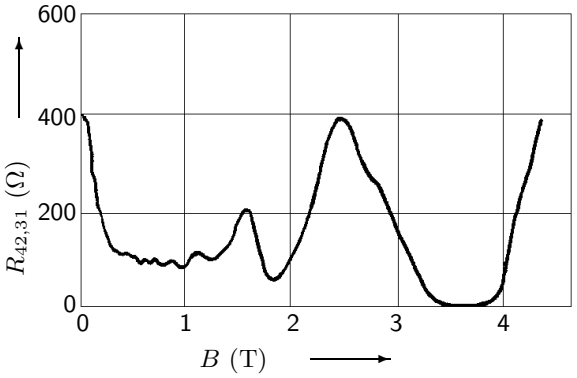

Fig. 154: Longitudinal resistance $R_{\rm L2} = R_{42,31}$ at $T = 1.5\,$K [92H2].

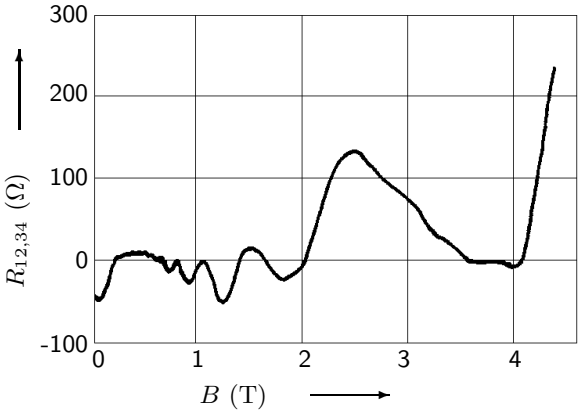

Fig. 155: Longitudinal resistance $R_{\rm L1} = R_{12,34}$ at $T = 1.5\,$K [92H2].

Aihara et al [92A1] studied Y–shaped GaAs wires ($w = 0.4\,\mu$m, $L = 1.2\,\mu$m, $l = 3.6\,\mu$m) with a stub fabricated in a split–gate configuration. The conductance as a function of gate voltage exhibited oscillations with a period of 25.6 mV at $T = 0.4\,$K and $I = 5$ and 50 nA. The amplitude of the peak in the Fourier transform of the data decreased with increasing current level. When the reflection wall in the stub was removed, the observed fluctuations were aperiodic. The periodic oscillations were thus attributed to quantum interference of electron waves in the stub.

Cumming et al [93C3] (page 208) fabricated a multi–terminal split–gate GaAs wire with voltage probes connected at angles of 45°. The voltage probes were shadowed from the adjacent current probes. The longitudinal resistance as a function of magnetic field and the bend resistance were examined (Fig. 215).

Yamada et al [93Y] studied the transport properties of a quasi–ballistic split–gate GaAs wire ($w = 1\,\mu$m, $L = 8\,\mu$m, $l = 2\,\mu$m) with a point contact (also defined by a split–gate) in the centre of one side–boundary. The two–terminal resistance was measured as a function of the back gate voltage for different voltages at the Schottky gates. Plateaux were identified as peaks in the first derivative which moved as functions of the various gate voltages. The plateaux were classified into two groups probably due to different constriction origins. In the four–terminal resistance, the origin of the plateaux was the point contact itself. Plateaux in the two–terminal resistance were assigned to unintentional, irregular constrictions in the wire. At a certain gate voltage, only one kind of plateaux was observed in the four–terminal resistance of the point contact and in the two–terminal resistance of the wire.

Feng et al [93F, 93T4] fabricated a GaAs device with an artificial impurity induced by a gate. The gates were defined by EBL, the radius of a centre gate was 150 nm, the inside radius of a surrounding dot was 450 nm. The centre gate could be controlled independently from the other gates, depletion occurred at $-0.42\,$V. Using a certain configuration of gate voltages, a quantum wire containing an artificial impurity could be defined. MR measurements were performed at

$T = 20\,\mathrm{mK}$ and AB oscillations were observed when the impurity was turned on. The period of the oscillations decreased for an increasingly negative voltage on the centre gate. When the gate voltages defining the wire were made more negative, the period increased. At ranges of magnetic field at which edge states formed and were partially reflected or transmitted due to the impurity, tunneling through the single–electron magnetically bound states of the impurity took place and an enhancement of conductance was observed which was periodic in magnetic field.

Hirayama et al [93H1] fabricated two parallel GaAs wires coupled by a ballistic window ($w = 1.25\,\mu\mathrm{m}$, $w_{\mathrm{eff}} = 250\,\mathrm{nm}$, length of the window $L_{\mathrm{w}} = 1.2\,\mu\mathrm{m}$, and $w = 0.65\,\mu\mathrm{m}$, $w_{\mathrm{eff}} = 150\,\mathrm{nm}$, $L_{\mathrm{w}} = 0.6\,\mu\mathrm{m}$) by FIB scanning. Three kinds of four–terminal resistances were studied as a function of magnetic field and in–plane gate voltage at $T = 50\,\mathrm{mK}$ and $1.5\,\mathrm{K}$. One of the longitudinal resistances was negative at $B = 0\,\mathrm{T}$. Fine structure appeared at 50 mK, which was more pronounced in the smaller structure. Oscillations in the longitudinal resistances at larger B were attributed to AB interference effects. The longitudinal resistance was also investigated as a function of gate voltage at $B = 0\,\mathrm{T}$, $0.25\,\mathrm{T}$, and $0.4\,\mathrm{T}$. A small–period oscillation ($\Delta V_{\mathrm{g}} = 0.04 - 0.05\,\mathrm{V}$) was superimposed on the background oscillation ($\Delta V_{\mathrm{g}} \approx 0.2\,\mathrm{V}$).

Kirczenow et al [94K2] (page 158) introduced an artificial impurity (by means of a 300 nm wide gate) into a 900 nm wide GaAs wire defined by gates. They studied the conductance of the system for various gate voltage configurations.

Blaikie et al [95B1] (page 173) performed MR measurements on quasi–ballistic multi–terminal GaAs wires defined by implanted gates. Samples with voltage probes joining the wire at angles $\neq 90°$ were structured and longitudinal, bend, and Hall resistances were investigated. A negative longitudinal resistance was found, the bend resistance was negative at $B \neq 0\,\mathrm{T}$, the Hall resistance was non–linear although quenching around $B = 0\,\mathrm{T}$ was not strong.

Yamada et al [96Y2] fabricated GaAs wires defined by a split gate ($w = 0.8\,\mu\mathrm{m}$, $L = 2.5\,\mu\mathrm{m}$, $l = 2.1\,\mu\mathrm{m}$) with either a small mesa in the centre of the wire or a hole near the boundary of the wire, structured using a STM. The wire with the small mesa showed quantized conductance with step hight e^2/h for a conductance larger than e^2/h and Coulomb oscillation–like features for a conductance smaller than e^2/h. In the current–voltage characteristics, a CB staircase was observed. The wire with a hole showed conductance quantization with step height $2e^2/h$ and a smaller pinch–off voltage than a wire without hole. The conductance of a wire with a larger hole showed switching due to electron traps on the hole cone interface.

Kikutani et al [96K2] fabricated a GaAs wire defined by a split gate ($w = 1.0\,\mu\mathrm{m}$, $L = 2.0\,\mu\mathrm{m}$) with a buried ferromagnetic QD. The resistance as a function of gate voltage at $T = 0.3\,\mathrm{K}$ showed a kink at $V_{\mathrm{g}} \approx -2.3\,\mathrm{V}$. For $V_{\mathrm{g}} > -2.3\,\mathrm{V}$, conductance steps with an amplitude larger than $2e^2/h$ were observed, while for $V_{\mathrm{g}} < -2.3\,\mathrm{V}$, the conductance steps were smaller than $2e^2/h$.

Bergmann et al [96B3] investigated magneto transport in periodically modulated InGaAs wires ($w = 340\,\mathrm{nm}$, $L = 30\,\mu\mathrm{m}$, $l = 2.4\,\mu\mathrm{m}$). Sample A was structured with a chain of antidots ($a = 200\,\mathrm{nm}$) along the central wire axis. The MR showed an anomalous peak at $B = 0.4\,\mathrm{T}$ due to diffusive boundary scattering. A peak at 1.56 T was associated with a pinched orbit of electrons around one antidot (Fig. 156). At higher magnetic fields, SdH oscillations were observed. In sample B, antidot chains were positioned at both sides of the wire sidewalls. A localized orbit between four antidots caused a peak in the MR at $B = 1.76\,\mathrm{T}$.

Widjaja et al [96W] measured MR in GaAs wires defined by a split–gate ($w = 1\,\mu\mathrm{m}$, $L = 3\,\mu\mathrm{m}$) in which one gate included a corrugation that produced a set of coupled quantum dots. A negative MR due to weak localization and SdH oscillations were observed. Small oscillations were superimposed upon the negative MR.

Aoki et al [97A2] fabricated a split–gate GaAs wire ($w = 1.2\,\mu\mathrm{m}$, $L = 2\,\mu\mathrm{m}$) with a buried superconductor dot. They performed low–temperature transport measurements, conductance steps

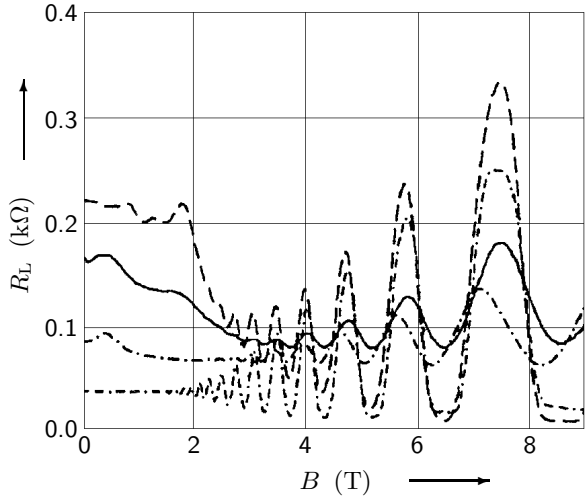

Fig. 156: MR traces of a 2DEG patterned with a square array of antidots with a period of 200 nm (top, dashes), a 340 nm wide periodically modulated wire with a chain of antidots of period 200 nm at the central axis (second, solid), an unpatterned 340 nm wide wire (third, dash–dot), and an unpatterned 2DEG (bottom, dash–dash–dot) [96B3].

as a function of V_g were observed. The wire was pinched off at $V_g \approx -2.5$ V. Periodic conductance oscillations were observed below the pinch–off voltage.

Geim et al [97G1] used multi–terminal GaAs Hall bars with widths of $0.2-1.0\,\mu$m with metallic discs of diameters $0.2-1.0\,\mu$m positioned at the cross junctions in order to measure the magnetization of the discs via measurements of the Hall resistance.

Park et al [98P1] investigated transport through a corrugated GaAs wire ($L = 4\,\mu$m, $w = 0.8\,\mu$m) fabricated by EBL and chemical etching. The periodically corrugated potential wall consisted of four notches whose width and separation were about 50 and 160 nm, respectively. Current and conductance were measured as a function of gate voltage. The conductance of a device without corrugation varied smoothly, exhibiting a plateau of height $\approx 2e^2/h$ at $V_g \approx 100$ mV. In the corrugated device, oscillatory features with an intensity of $\approx 40\%$ were observed. Distances between the major peaks were ≈ 80 mV in the negative gate–voltage range and ≈ 120 mV in the positive gate–voltage range, respectively. Park et al measured conductance for different source–drain voltages and observed oscillations below $100\,\mu$V and for temperatures $17\,\text{mK} < T < 106\,\text{K}$. They studied the change of the oscillation intensity as a function of source–drain voltage and temperature. They further calculated theoretically the gate voltages for resonant transmission and compared them with the positions of the measured conductance peaks.

Yamada et al [98Y, 98K2] investigated transpo—citert through a ferromagnetic Ni dot embedded in a GaAs wire defined by a split gate ($w = 1\,\mu$m, $L = 2\,\mu$m). From magnetic force microscopy data it was deduced that the dot comprised of mainly two domains before and one domain after the application of a magnetic field. Transport through the dot was measured at 0.3 K with and without a magnetic field. The CB–related conductance oscillations at zero field were aperiodic and not reproducible while the oscillations at ± 1600 G were periodic and reproducible. From current–voltage characteristics, the size of the Coulomb gap was deduced. A gap of $8-9$ mV at zero field reduced to $5-6$ mV at ± 5000 G, attributed to an expansion of the effective dot size. Yamada et al proposed that the domain wall in the absence of a magnetic field splits the dot into two effectively smaller subdots and acts as a resistive barrier.

Ford et al [98F1] fabricated Si wires ($L = 2\,\mu$m, $w = 10-50$ nm) by EBL and RIE and deposited Au nanodots between source and drain electrodes. The I–V characteristic at 4.2 K and 77 K showed Coulomb gaps of 0.8 V and 0.7 V, respectively. A measurement at 77 K before deposition of the nanodots did not show CB. The precise behaviour of the devices varied with the number and the size of tunnel junctions an islands in between the source and drain electrodes.

Thomas et al [99T] investigated the transport properties of two strongly coupled 1D channels

defined by a split–gate ($w = 1.2\,\mu$m, $L = 0.4\,\mu$m). Conductance steps were observed as long as only one channel was open. The in–plane MR was measured. The results were interpreted in terms of bonding and anti–bonding subbands of two coupled 1D wires.

Castleton et al [98C1] studied two parallel ballistic wires formed in GaAs/AlGaAs double quantum well (DQW) structures. The separation between the wires was 30 nm in sample 1 and 3.5 nm in sample 2. A split gate defined a 1D channel in each of the 2DEGs ((1) $w = 0.8\,\mu$m, $L = 0.5\,\mu$m; (2) $w = 1.2\,\mu$m, $L = 0.5\,\mu$m) and a mid gate controlled the electron density ((1) $w = 0.3\,\mu$m; (2) $w = 0.5\,\mu$m). A gate extending across the full width of the Hall bar was used to pinch–off the upper 2DEG. The conductance of sample 1 was measured as a function of split–gate voltage for a mid–gate voltage of 0.5 V for both, the two layers in parallel and the lower layer alone. For a split–gate voltage below -4.5 V, the lower wire was fully depleted, while the upper wire was conducting until -4.9 V. For a mid–gate voltage of -0.2 V, the upper wire was fully depleted for a split–gate voltage below -3.3 V, while the lower wire was conducting until -3.75 V. Both channels exhibited conductance quantization with steps of height $2e^2/h$ and an additional structure at $0.7{\cdot}2e^2/h$. In the weakly coupled sample, the single–wire regions were separated by the double–wire region, while in the strongly coupled sample, single–wire behaviour was observed for any mid–gate voltage between -0.48 V and 0.5 V for a two–channel conductance $\leq 4e^2/h$. When the upper channel was populated, it partially screened the lower channel from the mid–gate bias. For a constant conductance of the lower wire, mid–gate and split–gate voltage were swept showing an influence of the conductance of the upper wire.

Gompertz et al [98G2] performed MR measurements on quasi–ballistic GaAs wires in a DQW system ($w = 400$ nm and 800 nm, layers separated by 2.5 nm). For a magnetic field applied perpendicular to the layers at $T = 0.3$ K, a resonance at $B \approx 11$ T due to delocalization of electrons between the QWs was observed. An additional feature due to a distortion of the energy dispersion curve by the symmetric–antisymmetric splitting was enhanced in comparison to the 2D system. For a magnetic field applied in parallel, the resonance became broader, the additional feature was weakened. UCF with relative amplitudes close to e^2/h were observed, a phase coherence length of $0.6\,\mu$m at 0.3 K was estimated. The UCF were due to electrons tunneling between the layers and disappeared for $B > 10$ T.

Stoddart et al [98S1] investigated two parallel GaAs wires ($w = 800$ nm, $L = 0.5$, 1, and $3\,\mu$m) in a DQW (barrier thickness between 2.2 and 4.9 nm) defined by RIE. For $T < 4$ K and a magnetic field applied perpendicular to the layers, the MR showed conductance fluctuations at low fields followed by SdH oscillations at larger fields. A phase coherence length of $3.3\,\mu$m was estimated. A reduction of the resistance at small fields due to suppression of backscattering was observed. UCF were also found for $B < 8.6$ T when the field was applied parallel to the layers, due to coherent tunneling of electrons between the QWs. The amplitude of the conductance fluctuations decreased with increasing thickness of the barrier between the layers, the correlation field was 70 ± 10 mT for all samples.

Moon et al [99M] studied the in–plane MR of vertically coupled GaAs quantum wires. Split gates ($w = 0.4\,\mu$m, $L = 0.1$, 0.2, and $0.3\,\mu$m) on each side of a double quantum well heterostructure (width $0.8\,\mu$m) defined the wires. At a top slit–gate voltage of ≈ -0.8 V, two coupled wires formed. The first wire pinched–off at -2.35 V, both pinched off for $V < -3.9$ V. The behaviour as a function of the bottom split–gate voltage was similar. MR was measured for an in–plane field perpendicular to the current flow. A large broad peak in the MR was observed in the gate voltage regime corresponding to two open 1D channels. The effect was interpreted as an intrinsic Fermi–surface related property of a ballsitic coupled 1D–1D system.

Fujii et al [99F1] fabricated an air bridge silicon nanowire. The wire was maintained between two electrodes (distance $60\,\mu$m), its width decreased towards the middle of the interval, at the centre it was $20 - 100$ nm. The separation from the substrate was ≈ 300 nm. The I–V characteristic

showed three regimes: first an almost linear increase with bias voltage, then a decrease and an almost constant regime. A hysteresis was also observed in the I–V characteristic.

7.5 Impurities

7.5.1 General

One has to distinguish between collisions with static potentials such as lattice defects and collisions with time–varying potentials such as phonons or fluctuating spins. The average length an electron can travel before colliding with a static impurity is called the *mean free path length*, $l \equiv v_F \tau$, where v_F is the Fermi velocity and τ is the mean time between scattering events at static impurities. Static potentials shift the electron's phase in a deterministic way, such that an arbitrary path and its time–reversed path yield the same electron wavefunction. In contrast, the average length an electron can travel before colliding with a time–dependent potential is called *phase coherence length*, $l_\varphi \equiv \sqrt{D\tau_\varphi}$, where D is the diffusion constant and τ_φ is the mean time between scattering events at time–dependent impurities. Time–dependent potentials shift the electron's phase randomly and a certain path and its time–reversed path yield different electron wavefunctions. One refers to collisions with static potentials as *elastic* scattering and to collisions with time–dependent potentials as *inelastic* scattering (see for example [89W1] and references therein).

The transport properties of a conductor depend on the density of impurities and also on their positions. For example, the interference contributions to conductance responsible for UCF (see Section 7.2.1 on page 124 and Section 7.7.3 on page 182) depend on the exact impurity configuration. Shifting a single impurity by more than λ_F completely rewrites the interference pattern and changes the conductance by $\approx e^2/h$. Further, charge density waves or Wigner crystals may be pinned by impurities and lead to non–linear I–V characteristics and periodic oscillations of conductance vs. Fermi energy (see Section 7.2.2 on page 130).

Mailly et al [89M2] (page 187) applied a voltage pulse of 0.4 V amplitude and 15 ms duration to a GaAs wire. Resistance jumps due to the change of the impurity potential occurred.

Scott–Thomas et al [89S2] (page 130) observed periodic oscillations of conductance vs. gate voltage in narrow Si inversion layers (Fig. 131). They discussed a pinned charge density wave as possible origin for the observed effect.

Takagaki et al [89T2] (page 193) observed non–local voltage fluctuations in a quasi–ballistic GaAs electron waveguide. The fluctuations were reproducible under the same conditions, but changed after thermal cycles, suggesting that the fluctuations were sensitive to the microscopic configuration of elastic scatterers.

Scherer et al [89S1] monitored the electrical characteristics of GaAs submicron devices *in situ* during ion beam patterning. They studied how the resistance of narrow wires evolved with increasing exposure to a Ne beam and how it depended on the energy of the beam. They examined the resistivity vs. ion dose at two different temperatures, 300 K and 78 K. Finally, they explored the resolution limit inherent to the ion beam process.

Meirav et al [89M3] (page 130) examined GaAs channels. For $T < 1$ K, the conductance oscillated as V_g increased (Fig. 132). They proposed the pinning of a Wigner crystal or a charge density wave by impurities to be responsible for the oscillations.

Mailly et al [90M3] (page 188) patterned GaAs wires and applied voltage pulses to the samples causing the resistance to increase abruptly and then to decrease. The relaxation was followed by resistance jumps due to a redistribution of impurities.

Field et al [90F2] (page 131) measured conductance vs. gate voltage in Si MOSFETs and narrow channels in GaAs/$Al_xGa_{1-x}As$. It varied periodically with V_g. It was proposed that the

frequency was determined by the positions of charged defects or impurities.

Klepper et al [91K3] fabricated GaAs wires ($w = 3\,\mu$m, $L = 22\,\mu$m, $l = 0.4\,\mu$m) and studied the MC for different numbers of impurities. By IR illumination of the samples, donors in a Si-doped layer adjacent to the 2DEG were ionised, adding scatterers to the device. MC before and after illumination was measured (Fig. 157), the dependence of the conductance change ΔG_N on the number of added scatterers N was $(\Delta G_N/G)^2 \propto N^{(1.0\pm0.1)}$. Decorrelation of the conductance–fluctuation traces was achieved by addition of a sufficiently large number of scatterers, $N_c \approx 30000$ at $T = 2.5\,$K.

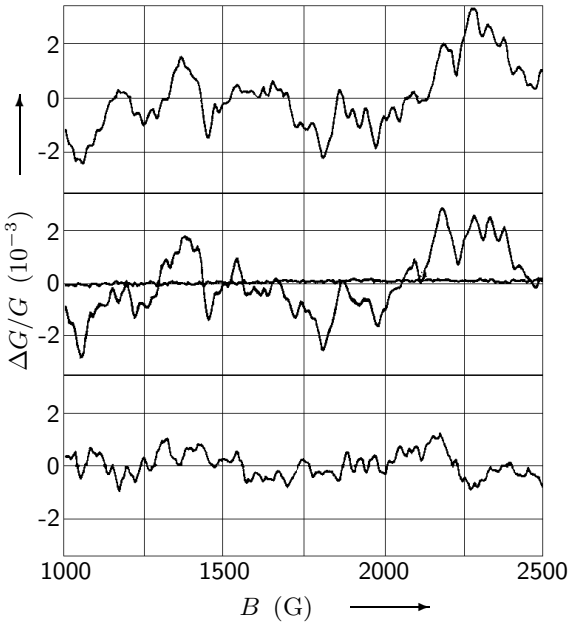

Fig. 157: MC traces at $T = 3\,$K, $\Delta G \equiv G(T) - G_{av}$ [91K3]. Top trace was taken before IR illumination. Middle oscillating trace was taken after a period of illumination which added $N \approx 25000$ scatterers (curve with small ripples is corresponding noise). Bottom trace is the difference between the MC traces obtained before and after illumination.

Ishibashi et al [92I1] (page 147) performed transport measurements in a GaAs wire defined by a split gate. The resistance as a function of gate voltage showed small fluctuations, probably due to the presence of impurities.

Feng et al [93F, 93T4] (page 153) examined a GaAs device with a centre gate. Using a certain configuration of gate voltages, a quantum wire containing an artificial impurity could be defined. MR measurements were performed at $T = 20\,$mK and AB oscillations were observed when the impurity was turned on.

Kirczenow et al [94K2] introduced an artificial impurity (by means of a 300 nm wide gate) into a 900 nm wide GaAs wire defined by gates. They studied the conductance of the system for various gate voltage configurations. In the MR, large oscillations together with beats were observed. The period of the oscillations was not constant but increased abruptly when B increased past certain values.

Honda et al [95H3] (page 120) observed quantized conductance in 2 to 30 μm long GaAs wires (Fig. 117). For $N \geq 2$, a conductance dip near the threshold of the $(N + 1)$th subband due to scattering by a random potential was observed.

Wróbel et al [95W] (page 173) measured the two–terminal conductance of a GaAs wire as a function of magnetic field for different temperatures (Fig. 169). Sharp peaks in the conductance were attributed to the presence of impurities.

Tarucha et al [95T] (page 120) measured the two–terminal conductance of 2 to 10 μm long GaAs wires at various temperatures. They found conductance steps close to the quantized values

of $2 \cdot e^2/h$ as a function of gate voltage (Figs. 118 and 119). They interpreted their results in terms of mutual Coulomb interaction in the presence of a random potential.

Yamada et al [96Y2] (page 154) fabricated GaAs wires defined by a split gate with either a small mesa in the centre of the wire or a hole near the boundary of the wire, structured using a STM, acting as an artificial impurity.

Ng et al [98N1] (page 164) investigated transport in amorphous Si wires partly recristallized. In the I–V characteristics of a 150 nm long and 50 nm wide wire they found conductance oscillations due to CB. They proposed hopping conduction between a limited number of trapping sites in amorphous regions or grain boundaries as an explanation of their results.

Liang et al [99L] (page 124) studied quantized conductance in GaAs split–gate wires of different lengths (L = 3, 5, and 6 μm, $l \approx 70\,\mu$m). The 3 μm long wire showed 25 clean conductance steps, the plateau values were close to multiples of $2e^2/h$. In the 5 μm long wire, all conductance plateaux deviated from multiples of $2e^2/h$ by up to 8% at $T = 0.3$ K. In the 6 μm long wire, the plateaux were suppressed below $2e^2/h$ by up to 25% at $T = 0.3$ K. It was assumed that reduction of the plateau values with increasing wire length was due to the introduction of elastic scattering.

Auslaender et al [00A] (page 165) fabricated GaAs wires by CEO. The conductance as a function of carrier density showed disorder–induced deviations from the conductance plateaux. For a density below the onset of the first plateau, the wire split into two parts as the highest barrier crossed the Fermi energy. Decreasing the density further, a single 1D island formed and resonant tunneling was observed.

7.5.2 Boundary scattering

In quasi–ballistic and ballistic samples, the carriers scatter several times from the boundaries before they suffer a collision with an impurity. Specular boundary scattering does not change the component of the momentum in forward direction (parallel to the side walls). However, when some fraction of the boundary scattering is diffusive, this will lead to a reduction of the conductance. The nature of the boundary scattering is characterized by the parameter p, which is zero for complete diffusive scattering and one for complete specular scattering. In a wire with $p < 1$, electrons with a large component of momentum parallel to the wire interact only seldom with the edges at zero magnetic field and contribute significantly to the conductivity. At finite magnetic field, the Lorentz force increases the perpendicular component of momentum, increasing the scattering rate with the diffusive boundaries and thus increasing the resistivity. When the cyclotron radius r_c is related to the wire width as $w/r_c \approx 0.5$, the carriers either perform loops inside the wire without contributing to transport, or they are confined to the edges where backscattering is suppressed (see Section 7.7.1 on page 167). At this stage, the bulk resistivity for $B = 0$ T is recovered. At intermediate magnetic fields, the magneto resistance exhibits a maximum. The position of the maximum depends on w and p (see for example [98T2] and references therein).

Choi et al [85C, 86C2] (page 168) measured the MR of GaAs devices of different widths. The temperature–insensitive MR was larger and the onset of SdH oscillations occurred at larger B for smaller w, which Choi et al attributed to the influence of boundary scattering.

Van Houten et al [88vH] performed MR measurements at temperatures 100 mK − 14.3 K on a 100 μm long and nominally 0.5 μm wide channel fabricated from a GaAs/AlGaAs heterostructure [86vH]. The elastic mean free path was larger than the channel width. In the magnetic–field dependence of the conductance, 1D weak localization was observed (Fig. 158). Boundary scattering effects were included into weak–localization theory in order to analyse the data (Fig. 159). Sidewall scattering was found to be specular rather than diffusive.

Simmons et al [88S3] (page 168) performed MR measurements on doubly connected rings and

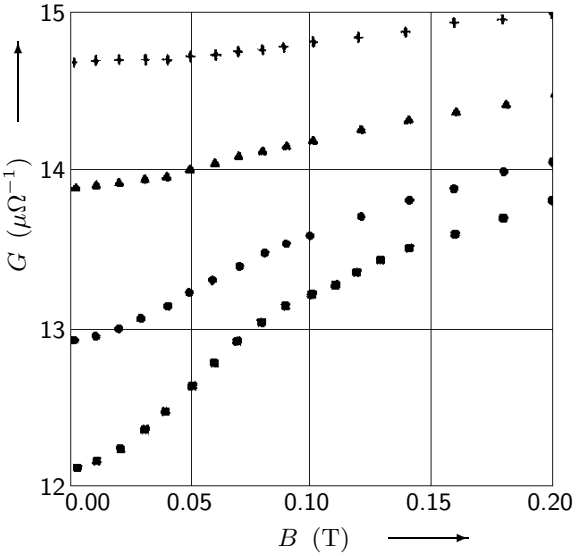

Fig. 158: Perpendicular field MC at (top) T = 14.3 K, 10.1 K, 5.9 K, and 4.0 K (bottom) [88vH].

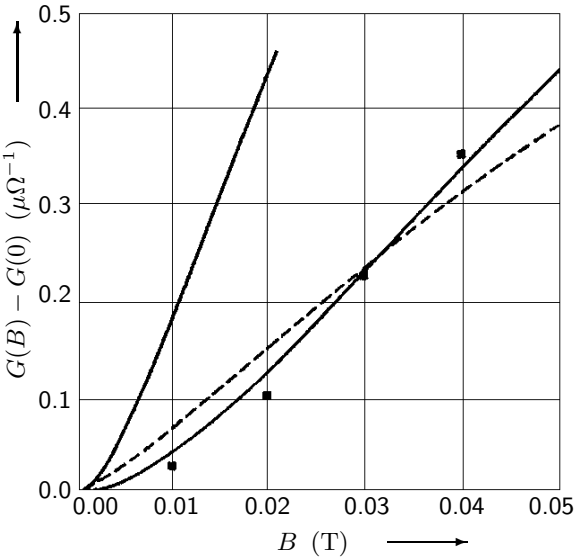

Fig. 159: Analysis of the T = 4.0 K MC data (fig.158) [88vH]. Solid lines are best fits for diffusive (upper solid line) and specular (lower solid line) boundary conditions with l smaller than the bulk value of 1 μm. Dashed line is for diffusive scattering with unrealistically high l = 7 μm.

standard Hall bridges made from GaAs/Al_xGa_{1-x}As heterostructures. They observed a large MR peak at $B = 0$ T which they attributed to diffusive boundary scattering. They extracted values for the inelastic diffusion length and attributed a reduction for $B < 0.5$ kG to diffusive boundary scattering.

Grassie et al [87G1] (page 195) studied SdH oscillations in GaAs wires. By comparison with theory, the scattering rate was extracted, it was insensitive to temperature in the narrow wires. Grassie et al attributed this to the influence of the sample walls.

Taylor et al [89T4] (page 169) fabricated quasi–ballistic GaAs channels, measured the MR at various temperatures and discussed specular side wall scattering.

Thornton et al [89T5] defined GaAs wires by either low–energy ion exposure or confinement between split gates and measured MR. In the ion exposed wires, they observed a positive zero–field MR showing an anomalous maximum. Amplitude and field position of the latter increased as the width of the wire decreased. Similar features were observed in split–gate wires (Fig. 160). Thornton et al attributed the resistance maximum to diffusive scattering of electrons from the wire edges. The maxima scaled with the ratio of cyclotron length to wire width. With decreasing carrier concentration, the relative amplitude of the resistance maximum decreased. The data suggested a qualitative difference in the nature of scattering at electrostatic and ion–exposed boundaries.

Menschig et al [90M1, 90M2, 91F2] (page 116) measured MR in $In_{0.53}Ga_{0.47}As$/InP wires. A peak due to boundary scattering was found around ≈ 0.75 T, peak resistance and corresponding magnetic field increased as the wire width decreased (Fig. 111).

Taniguchi et al [90T4] (page 140) measured MR in GaAs wires of different widths and extracted the phase coherence length as a function of temperature (Fig. 137). The narrow wires saturated below $1 - 2$ K with $l_\varphi = 0.33\,\mu$m. Taniguchi et al attributed the saturation of l_φ to electron scattering at the ion–damaged side walls.

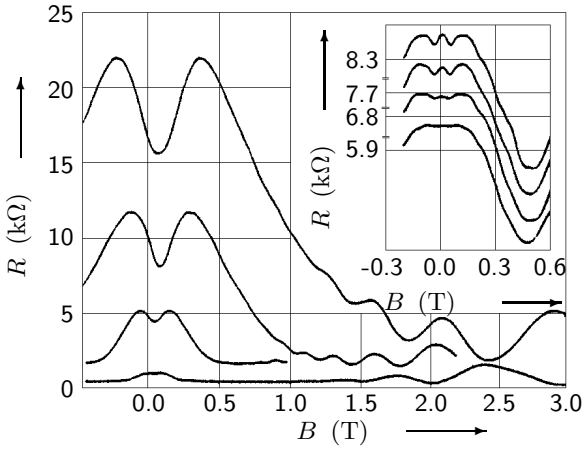

Fig. 160: MR of 12μm long ion–exposed wires of widths (top) 0.13 μm, 0.26 μm, 0.51 μm, and 1.15 μm (bottom) at $T = 4.2$ K [89T5]. Inset: Low–field data from a 12 μm long split–gate wire for (top) $V_g = -0.78$ V, -0.83 V, -0.86 V, and -0.98 V (bottom).

Bird et al [91B1, 92B2] (page 170) studied the four–terminal MR of a GaAs wire. A negative background in the MR resulted from a combination of boundary scattering and electron–electron interaction effects.

Nakata et al [91N] (page 147) fabricated GaAs wires and observed an anomalous resistance peak in the low–field MR due to diffusive side wall scattering.

Yamada et al [92Y1] structured two types of GaAs wires by locally destroying the conductivity of the 2DEG by FIB using Be: (1) one with a pair of in–plane gates, allowing to vary both, w and n; (2) the other with a planar Schottky gate, allowing to vary n without affecting w. From MR data, n, w_{eff} and the specularity factor p of the boundary were derived. For a sample of type 1, p decreased with increasing n and w_{eff}. For a sample of type 2, p was almost independent of n. It was concluded that the most important diffusive scatterers near the boundary were point defects generated during ion implantation.

Ochiai et al [91O2, 92O1] (page 171) studied MR in four–terminal GaAs wires fabricated by EBL and dry etching and in two–terminal split–gate wires. An amplitude analysis of SdH oscillations revealed two different scattering times at high and low magnetic fields in the etched wires. In the split–gate system, the relative change between the different relaxation times was much smaller than for the etched wires, probably due to the different nature of the boundary scattering in the two systems.

Blaikie et al [92B3] (page 148) reported a fabrication technique in which the lateral confinement of a wire was provided by p–n junctions while the electron density could be varied by means of a surface Schottky gate. They measured the MR of GaAs wires and observed an anomalous MR peak due to boundary scattering.

Block et al [93B1] (page 171) studied the MR of wires fabricated from $In_{0.53}Ga_{0.47}As$/InP heterostructures. An anomalous MR peak due to boundary scattering was observed. The peak amplitude increased with decreasing wire width and the magnetic–field position of the maximum shifted to larger values (Fig. 167).

Molenkamp et al [94M3, 95dJ] (page 143) measured the differential resistance in GaAs wires and observed a non–monotonic behaviour. They discussed their results in terms of a transport theory which combined electron–electron scattering with partly diffusive boundary scattering.

Lettau et al [94L1] (page 173) investigated MR in GaAs wires. In the longitudinal MR, a maximum for $B < 1$ T reflected diffusive boundary scattering.

Blaikie et al [95B1] (page 173) performed MR measurements on quasi–ballistic multi–terminal GaAs wires defined by implanted gates. A peak in the longitudinal resistance due to diffusive

boundary scattering was observed.

Iwano et al [94I3] (page 133) fabricated Si wires by FIB implantation of Ga^+ ions and studied the electrical conductance for different ion doses and annealing temperatures. The MR was measured. A negative MR was attributed to WL, while a positive MR was interpreted as a reduction of the localization length.

Omling et al [95O5] (page 174) observed a MR maximum at $B = 0.22\,\mathrm{T}$ due to boundary scattering in a GaAs wire.

Bergmann et al [96B3] (page 154) investigated magneto transport in periodically modulated InGaAs wires. The MR showed an anomalous peak at $B = 0.4\,\mathrm{T}$ due to diffusive boundary scattering.

Noguchi et al [96N2] (page 142) observed a MR peak at $B \approx 0.1\,\mathrm{T}$ in GaAs wires which was ascribed to boundary scattering.

Maemoto et al [97M] (page 150) fabricated single and multiple InAs wires with a corrugated surface along the wire and measured MR. Features due to boundary scattering were observed.

Held et al [99H2] (page 175) fabricated GaAs wires by local oxidation using an atomic force microscope. From an anomalous MR peak at low fields due to boundary scattering a specularity ≥ 0.95 was deduced.

7.6 Interactions

7.6.1 Electron–electron interaction

When electron–electron interactions are taken into account, corrections to the conductivity occur. In the diffusive regime, the temperature dependence of these corrections is of the form $\Delta\sigma \propto \ln(k_\mathrm{B}T\tau/\hbar)$ in two dimensions and $\Delta\sigma \propto T^{-1/2}$ in one dimension. A correction to the resistivity in a magnetic field is proportional to B^2. Interaction effects are effectively one–dimensional when the sample width is smaller than the thermal diffusion length. At small temperatures, when the density of thermal excitations is low, electron–electron interaction is the main dephasing process determining $l_\varphi(T)$ (see for example [82H, 84A1, 84K1, 85A1, 85E, 85G, 85P, 85C, 86C1, 97F] and references therein).

Another phenomenon due to electron–electron interactions is the *Coulomb blockade* (CB), i. e. the conductance of a small island inside a wire, separated from the rest of the wire by tunnel barriers, oscillates as a function of electron density. The island may be modelled as a small capacitor with charging energy $Q^2/2C$, where Q is the charge on and C is the capacity of the island. An electron can only traverse the island when the energy levels for N and $N+1$ electrons on the island are degenerate. This situation may be achieved by tuning the electron density via a gate voltage. As transport is possible when the energy levels are degenerate and is blocked due to Coulomb interaction when they are not degenerate, the conductance of such a system oscillates periodically as a function of gate voltage (see for example [91A2, 92G3, 92K3, 94T, 95M1, 97F, 98D] and references therein).

Finally, a 1D system of interacting electrons may be described by the Luttinger model. The eigenvalue problem is exactly solvable based upon a few approximations. The model allows for the exact calculation of a number of transport properties in the presence of interactions which may be tested experimentally (see for example [79E, 79S, 95V, 96S3, 98D]).

Dean et al [84D] (page 212) examined Si MOSFETs and observed a drop in the conductivity with increasing magnetic field which they attributed to electron–electron interaction effects.

Choi et al [85C, 86C2] (page 168) investigated GaAs devices of different widths. The temperature–dependent MR of a wide device followed 2D theory for electron–electron interactions.

Thornton et al [86T] (page 178) studied interaction corrections to the conductance of narrow GaAs channels. The phase coherence length was extracted from MR data and the corrections to conductivity due to electron–electron interaction were calculated using this l_φ and were compared with the data.

Taylor et al [89T4] (page 169) fabricated quasi–ballistic GaAs channels, measured the MR at various temperatures and discussed electron–electron interaction effects.

Field et al [90F2] (page 131) measured conductance vs. gate voltage in Si MOSFETs and narrow channels in GaAs/$Al_xGa_{1-x}As$. It varied periodically with V_g and the phenomenon was explained in terms of the CB and CDW models.

Taniguchi et al [90T4] (page 140) investigated the contribution of electron–electron interactions to the conductivity in GaAs wires by studying the MR vs. B^2.

Bird et al [91B1, 92B2] (page 170) studied the four–terminal MR of a GaAs wire. A negative background in the MR resulted from a combination of boundary scattering and electron–electron interaction effects. An unexpected saturation of the interaction component was found around 1 K, indicating a saturation of the thermal diffusion length.

Staring et al [92S2] (page 131) examined narrow GaAs wires defined by a split–gate technique. Periodic oscillations of conductance vs. gate voltage were observed in most of the channels. The periodicity of the conductance oscillations was explained by the theory for Coulomb–blockade oscillations.

Chou et al [92C] (page 152) investigated split–gate GaAs wires with a barrier induced by a narrow metal gate. The current as a function of gate voltage showed periodic oscillation. Chou et al discussed their observations in terms of the Coulomb blockade.

Hwang et al [94H1, 94H2] (page 172) reported on systematic experimental study of transport in a low–disorder, low–density GaAs wire defined by a split gate. As a function of the electron density, conductance oscillations were observed in a B–induced insulating phase. Hwang et al interpreted their results in terms of the 1D Wigner solid and also discussed the Coulomb Blockade.

Molenkamp et al [94M3, 95dJ] (page 143) measured the differential resistance in GaAs wires and observed a non–monotonic current dependence of the differential resistance. They studied the effect for various lattice temperatures. They discussed their results in terms of a transport theory which combined electron–electron scattering with partly diffusive boundary scattering.

Tarucha et al [95T] (page 120) measured the two–terminal conductance of 2 to 10 μm long GaAs wires at various temperatures and found conductance steps close to the quantized values of $2 \cdot e^2/h$ (Figs. 118 and 119). They interpreted their results in terms of mutual Coulomb interaction in the presence of a random potential and also discussed the Luttinger model in order to explain their observations.

Yano et al [95Y1] measured the conductance of poly–crystalline Si wires and observed quasi–periodic plateaux in the current vs. source–drain voltage at room temperature (Fig. 161).The temperature dependence of the current was thermally activated. They interpreted their results in terms of the Coulomb blockade model.

Namatsu et al [95N2] (page 122) proposed a Si nanowire fabrication process allowing for a reduction of the thickness of nanowires without reducing the thickness of the source and drain regions. Conductance oscillations observed at low gate voltages were attributed to the CB effect.

Yamada et al [96Y2] (page 154) fabricated GaAs wires with either a small mesa in the centre of the wire or a hole near the boundary of the wire, structured using a STM. The wire with the small mesa showed Coulomb oscillation–like features for a conductance smaller than e^2/h. In the current–voltage characteristics, a CB staircase was observed.

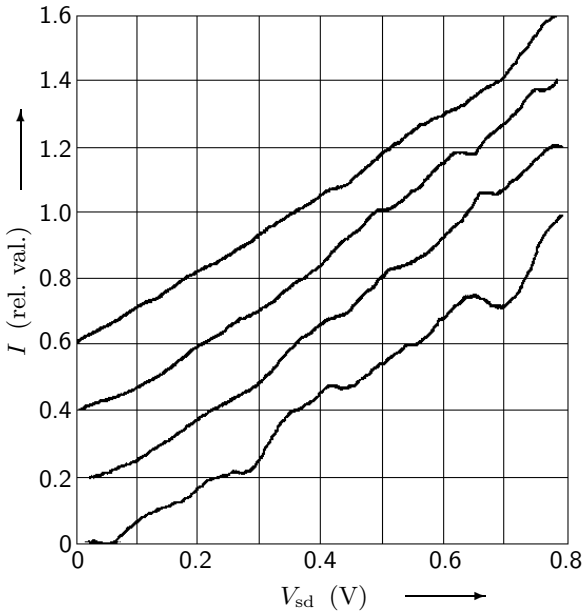

Fig. 161: Current vs. source–drain voltage at room temperature for (top) $V_g = -1.5\,V$, $-2\,V$, $-2,5\,V$, and $-3\,V$ (bottom) [95Y1]. The vertical axis is the relative value, which is measured current divided by the current at 0.8 V.

Noguchi et al [96N2] (page 142) investigated the phase breaking time of GaAs wires, the behaviour of $\tau_\varphi(T)$ was explained by electron–electron scattering.

Smith et al [97S3] (page 211) observed strongly non–ohmic behaviour in Si wires defined by side gates and several equally spaced peaks were observed in the conductance. They discussed their results in terms of the CB effect.

Yacoby et al [96Y1, 97Y1] (page 122) fabricated GaAs wires by cleaved edge overgrowth and observed quantized steps in the linear response conductance. The plateaux deviated from $N \cdot (2 \cdot e^2/h)$. Yacoby et al discussed their observations in terms of different theoretical models, including the Luttinger model.

Linke et al [97L] investigated the dephasing rate of electrons not in equilibrium in the diffusive regime. They used GaAs wires ($w = 0.5\,\mu m$, $w_{eff} = 354\,nm$, $L = 5 - 15\,\mu m$, $l = 0.9\,\mu m$) defined by EBL and shallow wet etching. The four–terminal MC was measured and the data analysed in terms of weak localization. The phase breaking rate was determined as a function of temperature. The relevant phase breaking mechanism was Nyquist phase breaking. For zero magnetic field, the conductance as a function of dc bias showed a pronounced minimum with a half–width of 1 mV, symmetric around zero bias voltage. The amplitude of this minimum was studied as a function of magnetic field. Linke et al assumed that the injected electrons were not in equilibrium with the electron gas inside the wire and suggested that the conductance minimum was due to quenching of weak localization caused by inelastic electron–electron interaction of non–equilibrium electrons.

Ng et al [98N1] investigated transport in amorphous Si wires partly recristallized. In the I–V characteristics of a 150 nm long and 50 nm wide wire they found conductance oscillations due to CB with a period of 1.4 mV corresponding to a capacity of 56 aF. An oscillation period of 10 mV was attributed to the combined effects from multiple tunnel junctions. The asymmetry of the I–V characteristics was ascribed to parallel or different conduction paths or to resonant tunneling effects. The authors proposed hopping conduction between a limited number of trapping sites in amorphous regions or grain boundaries as an explanation of their results.

Yamada et al [98Y, 98K2] (page 155) investigated transport through a ferromagnetic Ni dot embedded in a GaAs wire. They found CB–related conductance oscillations. From current–voltage characteristics, the size of the Coulomb gap was deduced. A gap of $8 - 9\,mV$ at zero field reduced to $5 - 6\,mV$ at $\pm 5000\,G$.

Irvine et al [98I1] observed CB in polycrystalline Si wires ($w = 20 - 30$ nm, $t = 30$ nm) with grain sizes of ≈ 20 nm. A Coulomb staircase in the I–V characteristic at 4.2 K showed steps with a period of ≈ 43 mV, implying a capacity of 1.86 aF. The staircase persisted up to a temperature of 30 K. Reproducible oscillations were observed in the current as a function of side–gate voltage. Their period decreased from 230 mV sharply to 50 mV at a side gate voltage of 0.5 V. The effective capacities were 0.7 and 3.2 aF, respectively. Irvine et al speculated that the changes in period might be due to electrostatic screening effects caused by grain–boundary defect states.

Ford et al [98F1] (page 155) fabricated Si wires and deposited Au nanodots between source and drain electrodes. The I–V characteristics at 4.2 K and 77 K showed CB.

Auslaender et al [00A] reported evidence for Luttinger liquid behaviour in GaAs wires ($L = 5\,\mu$m, $t = 25$ nm, $w = 10$ nm) fabricated by CEO. The conductance as a function of carrier density showed disorder–induced deviations from the conductance plateaux. For a density below the onset of the first plateau, the wire split into two parts as the highest barrier crossed the Fermi energy. Decreasing the density further, a single 1D island formed and resonant tunneling was observed. From the charging energy, the length of the island was estimated to be $100-200$ nm. The line shape of the resonance was measured for $0.25\text{K} < T < 2.5$ K, it decreased with decreasing temperature, see Fig. 162. According to conventional CB theory, the line shape should have been independent of temperatur, while Luttinger liquid theory predicted $\Gamma \propto T^{1/g-1}$, where the parameter g (< 1) characterized the electron–electron interaction. Fitting the measured data to Luttinger liquid theory yielded $g = 0.82$ for one CB peak and $g = 0.74$ for another CB peak. The change in carrier density in between the two CB peaks was responsible for the change in g. Similar power law behaviour was observed in three different wires. The parameter g estimated from the charging energy was ≈ 0.4 and deviated significantly from the value of g deduced from $\Gamma(T)$. When in addition to the ground state also an excited state contributed to the RT, the behaviour of $\Gamma(T)$ deviated from a simple power law. Also this behaviour was in perfect agreement with theoretical predictions, Fig. 163.

7.6.2 Electron–phonon interaction

Electron–phonon scattering is the main mechanism for energy relaxation of carriers, but becomes less important at low temperatures where thermal excitations are frozen out. At finite temperatures, electron–phonon scattering limits the phase coherence length (see for example [82A, 86C1, 91R1, 93L1, 95W, 97F, 98D] and references therein).

Dean et al [84D] (page 212) studied electron–phonon scattering in Si MOSFETs.

Wróbel et al [95W] (page 173) measured the two–terminal conductance of a GaAs wire as a function of magnetic field for different temperatures (Fig. 169). The data were found to be consistent with results from model calculations of the inelastic rate for electron–phonon scattering.

Naylor et al [96N1] performed phononconductivity measurements in a GaAs wire defined by a split gate ($w = 0.4\,\mu$m, $L = 10\,\mu$m). They measured resistance vs. gate voltage. A CuNi heater was used as the phonon source. A phonon pulse caused a transient increase in the conductance of the channel. Naylor et al discussed their observations in terms of electron–phonon interaction.

Inoue et al [97I2] (page 175) investigated transport in InAs wires. They examined the charge velocity at 77 K as a function of channel width and length. The high–field velocity increased in the narrow wires, indicating a reduction of the 1D electron–phonon interaction.

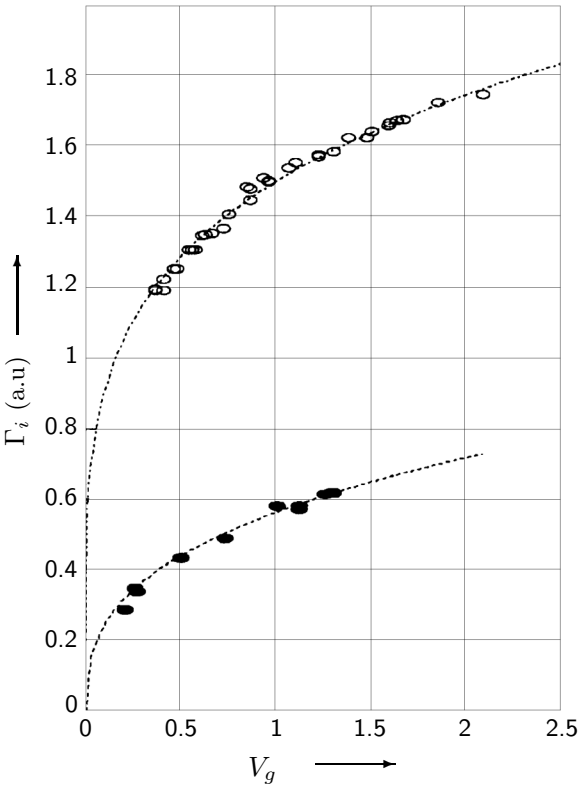

Fig. 162: Intrinsic linewidth of the resonance peak, Γ_i (arbitrary units), for two different RT peaks denoted by open circles and closed circles, respectively, as a function of temperature (in units of gate voltage) [00A]. The power law fits are $T^{0.22}$ corresponding to an interaction parameter of $g = 0.82$ (upper curve) and $T^{0.35}$ corresponding to $g = 0.74$ (lower curve).

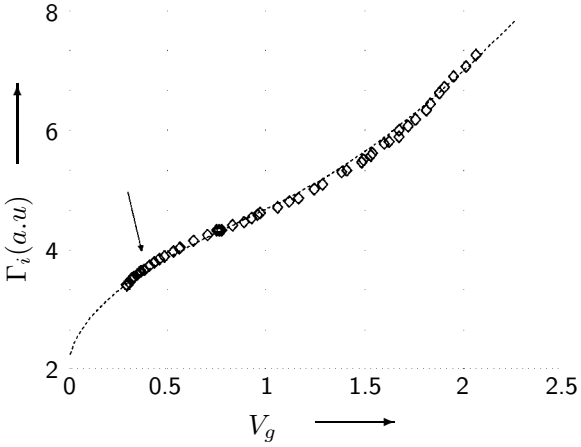

Fig. 163: Intrinsic linewidth of the resonance peak, Γ_i (arbitrary units), when also an excited state contributes to the RT as a function of temperature (in units of gate voltage) [00A]. The dashed line is a fit according to theory. The low–temperature behaviour is $T^{0.5}$ corresponding to $g = 0.66$.

7.6.3 Spin–orbit interaction

According to the theory of weak localization (see Section 7.7.2 on page 176), the presence of spin–orbit (SO) scattering changes the sign of the correction to conductivity at zero magnetic field. It thus transforms weak localization into *weak anti–localization* (see for example [84B2, 85F, 86C1, 98D] and references therein).

Fukai et al [90F4] (page 140) structured GaAs/AlGaAs on–facet wires and determined the phase coherence length from weak localization. The MR was positive at low field for $T \leq 0.08\,\mathrm{K}$, indicating the presence of SO interaction.

Taniguchi et al [91T2] (page 140) studied the phase breaking time τ_φ and the SO scattering time τ_{SO} in Si δ–doped GaAs wires. They investigated the temperature dependence of τ_φ and τ_{SO} and found saturation of τ_φ when τ_φ became comparable to τ_{SO}. The temperature dependence of the amplitude of UCF in wires with strong SO scattering was examined.

Fukai et al [95F2] fabricated InGaAs/InAlAs wires ($w = 0.4\,\mu\mathrm{m}$, $L = 1.0\,\mu\mathrm{m}$, $l = 0.056\,\mu\mathrm{m}$) by Ga FIB implantation. The temperature dependence of the two–terminal resistance showed a maximum at $T = 1.6\,\mathrm{K}$. The decrease of resistance below 1.6 K was interpreted as anti–localization in the presence of strong SO scattering. Fukai et al measured UCF and investigated the temperature dependence of the fluctuation amplitude. Finally, they studied various characteristic scattering times as functions of temperature.

7.7 Magnetic field

7.7.1 General

In this Section, experiments are described in which miscellaneous magnetic–field dependent phenomena like for example anomalous MR peaks due to diffusive boundary scattering, corrections to conductivity due to electron–electron interactions, or consequences of edge transport were examined. Experiments in which special phenomena like *weak localization* (see Section 7.7.2 on page 176), *aperiodic conductance fluctuations* (see Section 7.7.3 on page 182), *Shubnikov–de–Haas oscillations* (see Section 7.7.4 on page 194), the *quantum Hall effect* (see Section 7.7.5 on page 200), or the *bend resistance* (see Section 7.7.6 on page 206) have been investigated, will be described in the following sub–sections. Before starting the descriptions of the experiments, the difference between *two–* and *four–terminal measurements*, the meaning of the words *local* and *non–local* and the transport along *edge states* shall shortly be discussed.

In a *two–terminal measurement*, the resistance is symmetric with respect to reversal of magnetic field, $R(B) = R(-B)$. In a *four–terminal measurement*, this is not the case. One can, however, retain symmetry by interchanging current with voltage leads, $R_{ij,nm}(-B) = R_{mn,ij}(B)$. Further, combinations of four–terminal resistances may be chosen which are symmetric or anti–symmetric with respect to reversal of magnetic field: $R_{\mathrm{S}} = [R_{mn,ij}(B) + R_{mn,ij}(-B)]/2$ and $R_{\mathrm{A}} = [R_{mn,ij}(B) - R_{mn,ij}(-B)]/2$. The anti–symmetric resistance R_{A} is nearly independent of the separation of the voltage probes as it is generated in the regions within distance l_φ from the probes. The symmetric resistance R_{S} is accumulated along the whole distance L and up to l_φ into the voltage probes. In multi–terminal devices, various lead configurations may be chosen. A geometry is called *local* when the voltage is measured along the classical current path. It is called *non–local*, when the voltage probes are spatially separated from and do not intersect with the classical current path (see for example [86W1, 88B2, 90D, 91T3, 91W2, 92W1, 93B3] and references therein).

In a magnetic field which is strong enough that the cyclotron radius r_{c} is smaller than $w/2$, electrons are flowing along the edges of a device. From the classical point of view, electrons inside the wire move on circular orbits due to the Lorentz force. Electrons at the edges are scattered

towards the centre of the wire, bend back due to the Lorentz force, are scattered again, and finally move along so–called *skipping orbits* along the edges. In the quantum–mechanical picture, transport in the bulk is not possible for a Fermi energy in between two Landau levels, as all available states within the Landau bands are occupied and thus scattering of electrons is forbidden by the Pauli principle. At the edges however, the Landau levels are bent upwards and small excitations are possible as the Landau levels cross the Fermi energy. Transport along these so–called *edge states* can only flow in one direction at one side of the sample and in the other direction at the other side of the sample. Consequently, backscattering is suppressed (see for example [90D, 91T3, 96S2, 97F, 98D]).

7.7.1.1 Local geometry

Dean et al [84D] (page 212) examined Si MOSFETs and observed a drop in the conductivity with increasing magnetic field which was attributed to electron–electron interaction effects.

Choi et al [85C, 86C2] fabricated devices of different widths from GaAs/$Al_xGa_{1-x}As$ heterostructures by photolithographic techniques. Four–terminal MR data for a wide sample and for three narrow samples are shown in Fig. 164. In the narrow channels, the parabolic MR was independent of temperature at low magnetic fields and temperature dependent at higher fields. The temperature–dependent MR of the wide device followed 2D theory for electron–electron interactions, while the data of the narrow devices was described well by 1D theory below a certain critical temperature. The temperature–insensitive MR was larger and the onset of SdH oscillations occurred at larger B for smaller w, which Choi et al attributed to the influence of boundary scattering. For very narrow channels, aperiodic and temperature independent oscillations consistent with UCF theory occurred in addition to the SdH oscillations [86C2].

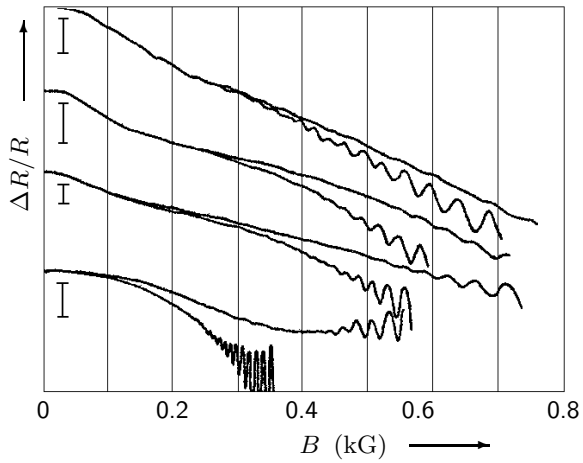

Fig. 164: Change of resistance vs. magnetic field for (top) w=1.1 μm, T = 4.2 K; 1.1 μm, 1.6 K; 3.0 μm, 4.2 K; 3.0 μm, 1.6 K; 6.2 μm, 4.2 K; 6.2 μm 1.6 K; 156 μm, 4.2 K; 156 μm, 1.6 K (bottom) [86C2]. The vertical bars denote an amplitude of (top) 5%, 5%, 2%, and 1% (bottom).

Wainer et al [88W1] (page 129) measured MC fluctuations in narrow Si MOSFETs for a range of gate voltages. The peaks shifted for an increasing magnetic field to lower or higher V_g. At high fields, the density of peaks was reduced. The observed effects were attributed to Zeeman spin splitting of energy levels.

Simmons et al [88S3] performed MR measurements (at T = 0.3 K) on doubly connected rings ($w \approx 1\,\mu$m, $L = 25\,\mu$m) and standard Hall bridges ($w \approx 1\,\mu$m, $L = 2\,\mu$m) made from GaAs/$Al_xGa_{1-x}As$ heterostructures. They observed h/e AB oscillations in the rings, and a large MR peak at B = 0 T and an anomalous step in the Hall resistance at $B \approx 1$ kG in the Hall bridges. They suggested the peak at $B = 0$ T to be due to diffusive boundary scattering. Samples of both geometries showed resistance fluctuations. Simmons et al extracted values for the inelastic diffusion length and attributed a reduction for $B < 0.5$ kG to diffusive boundary scattering.

Kastner et al [88K2] structured Si wires ($w \approx 100\,\mathrm{nm}$, $L = 7\,\mu\mathrm{m}$) and measured the MR at several temperatures. A small negative MR and UCF were observed at low fields. A transition to a state with a conductance about ten times higher than at $B = 0\,\mathrm{T}$ occurred at $B = 4\,\mathrm{T}$ for $T = 100\,\mathrm{mK}$. The threshold field increased as T increased to 4.2 K. The magnitude of the conductance in the high–field state decreased with T (Fig. 165). The conductance at three different magnetic fields increased in a series of steps as V_g increased. Varying the temperature at $B = 8\,\mathrm{T}$ showed that each plateau disappeared at a different T. These observations were assumed to result from quasi 1D confinement. Kastner et al further studied the current as a function of source–drain voltage and observed a small negative differential resistance (Fig. 166).

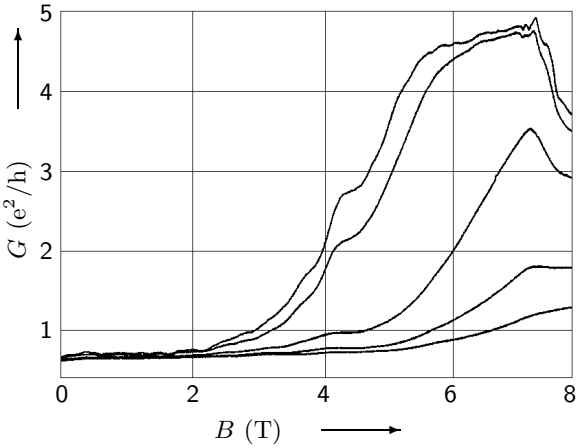

Fig. 165: Magnetic field dependence of the two–terminal conductance of a narrow inversion layer at a fixed carrier density ($V_\mathrm{g} = 6.5\,\mathrm{V}$) for (top) $T = 100\,\mathrm{mK}$, 800 mK, 2 K, 3 K, and 4.2 K (bottom) [88K2].

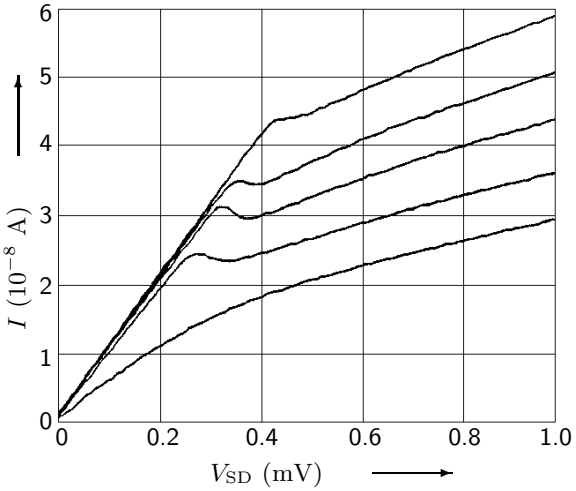

Fig. 166: Current as a function of source–drain voltage at $T = 100\,\mathrm{mK}$, $B = 6.7\,\mathrm{T}$, and (top) $V_\mathrm{g} = 5.2\,\mathrm{V}$, 4.8 V, 4.6 V, 4.4 V, and 4.2 V (bottom) [88K2]. The slope at high source–drain voltage approaches the zero–field conductance.

Scott–Thomas et al [88S1] (page 130) fabricated dual–gate Si wires defined by a split gate and measured conductance vs. gate voltage. The MR increased at large B and reached a plateau at $2 \cdot e^2/h$ for $B > 12\,\mathrm{T}$.

Cheeks et al [88C3] reported a new technique for patterning small GaAs wires using helium ion beam exposure. No change in carrier density occurred. By thermal annealing at 500°C for 20 s or at 300°C for longer times the damage created by the He ion beam could be removed. Cheeks et al performed MR measurements.

Yamada et al [89Y] (see page 230) investigated arrays of buried on–facet channels and short single mesa–shaped bar samples. They performed MR measurements.

Taylor et al [89T4] fabricated quasi–ballistic GaAs channels ($w = 0.16 - 0.54\,\mu\mathrm{m}$, $L = 10\,\mu\mathrm{m}$) via EBL and shallow etching. They measured the MR at various temperatures (from 2 K to 300 K) and found a negative MR below 0.1 T due to weak localization and UCF. They extracted l_φ as a function of temperature. They discussed electron–electron interaction effects, specular side wall scattering, a $\propto B^2$ behaviour of the MR above 48 K and the formation of skipping orbits. From comparisons with theory they found that conducting and nominal channel widths were comparable. They examined MR for different angles between B and the sample normal. Finally, they found that the channels were unstable at helium temperatures: carrier density, channel width and mobility decreased with time, the instability was greater for the narrower channels.

Thornton et al [89T5] (page 160) defined GaAs wires by either low–energy ion exposure or confinement between split gates and measured MR. In the ion exposed wires they observed a positive zero–field MR showing an anomalous maximum. Similar features were observed in split–gate wires (Fig. 160). Thornton et al attributed the resistance maximum to diffusive scattering of electrons from the wire edges.

Pfeiffer et al [90P1] reported the fabrication of a GaAs 2DEG at a cleaved interface overgrown via MBE. Two–probe MR measurements were performed.

Ochiai et al [90O1, 91I1] structured GaAs wires ($w = 0.7\,\mu$m, $L = 2\,\mu$m, $l = 430\,$nm) by EBL and dry etching and measured the longitudinal and the Hall resistance. Up to a magnetic field of 2 T, UCF were observed in $R_{\rm L}$ and above 2 T, SdH oscillations occurred. The Hall resistance did not show perfect plateaux. The Landau level index vs. $1/B$ deviated from a straight line for $B^{-1} < 0.4\,{\rm T}^{-1}$. The inflection point was almost independent of temperature. Ochiai et al examined the single–particle relaxation time and the total relaxation time and found two different values for the latter for high and low fields, the crossover being near $0.4\,{\rm T}^{-1}$. The total relaxation time was almost independent of temperature for $0.3\,{\rm K} < T < 4.2\,{\rm K}$. Ochiai et al argued that for magnetic fields higher than 2.5 T, diffusive propagation of electron waves was suppressed and edge channels formed, affecting the Fan diagram and the relaxation times.

Menschig et al [90M1, 90M2, 91F2] (page 116) examined $In_{0.53}Ga_{0.47}As/InP$ wires. MR traces showed depopulation of magnetic subbands and SdH oscillations (Fig. 110). A negative MR which decreased with increasing wire width and UCF were observed at low fields. A MR peak due to boundary scattering was found, peak resistance and corresponding magnetic field increased as the wire width decreased (Fig. 111).

Field et al [90F2] (page 131) measured conductance vs. gate voltage in Si MOSFETs and narrow channels in $GaAs/Al_xGa_{1-x}As$. The conductance varied periodically with $V_{\rm g}$. A magnetic field reduced the random modulation of conductance, but did not affect the period.

Taniguchi et al [90T4] (page 140) fabricated GaAs wires and investigated the contribution of electron–electron interactions to the conductivity by studying the MR vs. B^2 in a $w = 0.8\,\mu$m wide wire.

Bird et al [91B1, 92B2] studied the four–terminal MR of a GaAs wire structured by deep wet etching ($w = 1.8\,\mu$m, $L = 30\,\mu$m). UCF and SdH were observed. The UCF decayed with increasing temperature, comparison with theory implied a temperature–independent l_φ. A negative background in the MR resulted from a combination of boundary scattering and electron–electron interaction effects. A saturation of the interaction component was found around 1 K, indicating a saturation of the thermal diffusion length. At large magnetic fields ($r_c < w$) and high T, smooth SdH oscillations were observed. 1D subband depopulation was found. At low T, a rapid decay in the high–frequency component of the UCF was found, the noise–like structure at higher fields was quasi–periodic. Bird et al discussed the possible origin for the saturation of the phase coherence and the thermal diffusion lengths.

Nakata et al [91N] (page 147) examined GaAs wires, measured MR, observed SdH oscillations, and attributed a deviation of $1/B$ vs. $n_{\rm L}$ from a straight line to magnetic depopulation of 1D subbands. An anomalous resistance peak observed in the low–field MR was attributed to diffusive boundary scattering. The temperature dependence of the MR was examined, as was the relation between the peak amplitude and temperature.

Yamada et al [92Y1] (page 161) measured the MR of two types of GaAs wires. From the data, n, $w_{\rm eff}$ and the specularity factor p of the boundary were derived.

Wróbel et al [92W2] (page 118) studied a two–terminal GaAs wire. The conductance as a function of time showed five plateaux. With an increasing magnetic field, the number of visible steps was reduced and ΔG increased (fig 113).

Ochiai et al [91O2, 92O1] studied MR in four–terminal GaAs wires (varying width, $L = 2\,\mu$m) fabricated by EBL and dry etching and in two–terminal split–gate wires ($w \approx 1.2\,\mu$m, $L = 2\,\mu$m). The resistance of the split–gate wire varied with gate voltage, conductance quantization was not observed. An amplitude analysis of SdH oscillations revealed two different scattering times at high and low magnetic fields in the etched wires. The boundary field between the two regimes depended on the wire width. Ochiai et al attributed the observed effect to the formation of edge channels. In the split–gate system, SdH oscillations became weaker with increasing V_g, only one relaxation time was observed at zero gate voltage, while at $V_g = -1.0\,$V again two relaxation times were found. The relative change between the different relaxation times in the split–gate wires was much smaller than in the etched wires, probably due to the different nature of the boundary scattering in the two systems (diffusive in the etched wire, specular in the split–gate wire).

Ohata et al [92O2] (page 212) fabricated narrow Si channels and measured conductance vs. gate voltage at various temperatures. AF near the turn–on voltage were completely reproducible and the peak positions were insensitive to magnetic field. Ohata et al also measured the MC at different gate voltages. A large positive MC was observed in the hopping regime around 3 T using a perpendicular field. The MC changed for a variation of V_g. For a parallel magnetic field, the MC was negative.

Staring et al [92S2] (page 131) examined narrow GaAs wires defined by a split–gate technique. Periodic oscillations of conductance vs. gate voltage were observed in most of the channels. The oscillation period was insensitive to a magnetic field, but the amplitude of oscillations and the average conductance were enhanced above the zero–field values in magnetic fields of intermediate strength and decreased in stronger fields. The four–terminal longitudinal conductance in the Hall bar exhibited random structure as a function of magnetic field.

Blaikie et al [92B3] (page 148) reported a fabrication technique in which the lateral confinement of a wire was provided by p–n junctions while the electron density could be varied by means of a surface Schottky gate. They measured the MR of GaAs wires and observed an anomalous MR peak due to boundary scattering.

Hirayama et al [92H2] (page 153) examined four–terminal transport through two in–plane gated parallel GaAs wires coupled by a ballistic window. The longitudinal resistance as a function of magnetic field showed SdH oscillations and a negative peak at $B = 0\,$T, indicating the existence of a side–ways ballistic component (Figs. 154 and 155). The Hall resistance showed quantized plateaux. For a longer window structure, R_L became positive.

Iwano et al [93I] (page 133) measured the conductance of p–type Si wires. Two kinds of samples with different impurity concentrations were prepared. The MC of one sample was positive, which could not be explained by weak localization.

Tarucha et al [93T3] (page 148) investigated transport in ballistic GaAs channels. The differential resistance vs. source–drain voltage for $2\,\mu$m wide channels showed a minimum at a voltage of several mV (Fig. 149). In the presence of a magnetic field, the minimum in the differential resistance disappeared above $500 - 600\,$G.

Block et al [93B1] studied the MR of wires ($w = 70{-}240\,$nm) fabricated from $In_{0.53}Ga_{0.47}As$/InP heterostructures by EBL and RIE. At weak magnetic fields, a negative MR due to weak localization was found, which was most pronounced for the smallest widths. At larger magnetic fields, an anomalous MR peak (due to boundary scattering) was observed, followed by SdH oscillations. The peak amplitude increased with decreasing wire width and the magnetic–field position of the maximum shifted to larger values (Fig. 167). Block et al presented an extensive comparison of the data to theoretical calculations.

Feng et al [93F, 93T4] (page 153) examined a wire containing an artificial impurity. MR measurements were performed at $T = 20\,$mK and AB oscillations were observed when the impurity

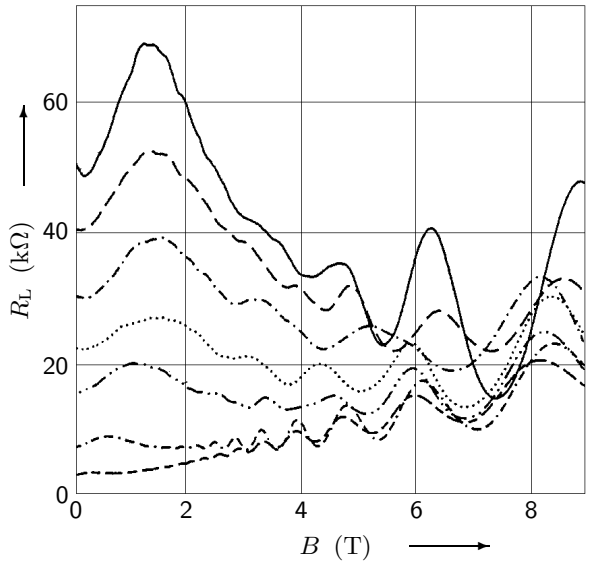

Fig. 167: MR traces of $In_xGa_{1-x}As/InP$ wires with geometrical widths of (left, top) 70 nm, 80 nm, 100 nm, 120 nm, 140 nm, 220 nm, and 420 nm (bottom) at $T = 4.2$ K [93B1].

was turned on. At ranges of magnetic field at which edge states formed and were partially reflected or transmitted due to the impurity, tunneling through the single–electron magnetically bound states of the impurity took place and an enhancement of conductance was observed which was periodic in magnetic field.

Hirayama et al [93H1] (page 154) fabricated two parallel GaAs wires coupled by a ballistic window and studied four–terminal resistances as a function of magnetic field. Oscillations in the longitudinal resistances at large B were observed and attributed to AB interference effects.

Hwang et al [94H1, 94H2] reported systematic experimental study on transport in a low–disorder, low–density GaAs wire ($w = 1\,\mu$m, $w_{\rm eff} \approx 0.1 - 1.0\,\mu$m, $L = 1.2\,\mu$m) defined by a split gate. At $B = 0$ T, conductance steps were observed. The conductance did not depend on temperature for $-2.2\,{\rm V} < V_{\rm g} < 0\,{\rm V}$, but for $V_{\rm g} < -2.2\,{\rm V}$ ($G < e^2/h$) the conductance changed by more than an order of magnitude in the range $25\,{\rm mK} < T < 300\,{\rm mK}$. For $V_{\rm g} > -2.2\,{\rm V}$, the IQHE was found. The FQHE was observed for $V_{\rm g} > -1.9\,{\rm V}$, the development of the 1/3 FQHE state was investigated as a function of $V_{\rm g}$. As B increased beyond the 1/3 FQHE state, the channel became an insulator. The temperature dependence of the resistance at various B and $V_{\rm g}$ was studied. As a function of the electron density (varied via a back gate), conductance oscillations were observed in the B–induced insulating phase. The oscillations became sharper and more developed as B increased. The observation of conductance oscillations depended also on $V_{\rm g}$. Hwang et al examined the average period of the conductance oscillations vs. $V_{\rm g}$. The behaviour of the oscillations with changing temperature was also studied. The I–V characteristics at a maximum and a minimum of the conductance oscillations were non–linear. Hwang et al interpreted their results in terms of the 1D Wigner solid and also discussed the Coulomb Blockade.

Main et al [94M2, 94G3] studied MR in multi–terminal GaAs wires ($w_{\rm eff} \approx 1\,\mu$m, $L = 10\,\mu$m and $20\,\mu$m) using local and non–local lead configurations. Strong resistance fluctuations were observed in the SdH oscillations at temperatures of 300 and 600 mK (Fig. 168). The relative peak amplitude increased with increasing magnetic field. Different configurations of probes gave similar but not identical resistance fluctuations. The temperature dependence of the fluctuations was not monotonic. Main et al attributed the sharp, isolated peaks to resonant tunneling through localized states in the wires.

Kirczenow et al [94K2] (page 158) introduced an artificial impurity into a GaAs wire defined by gates. They measured the MR and observed large oscillations together with beats. The period

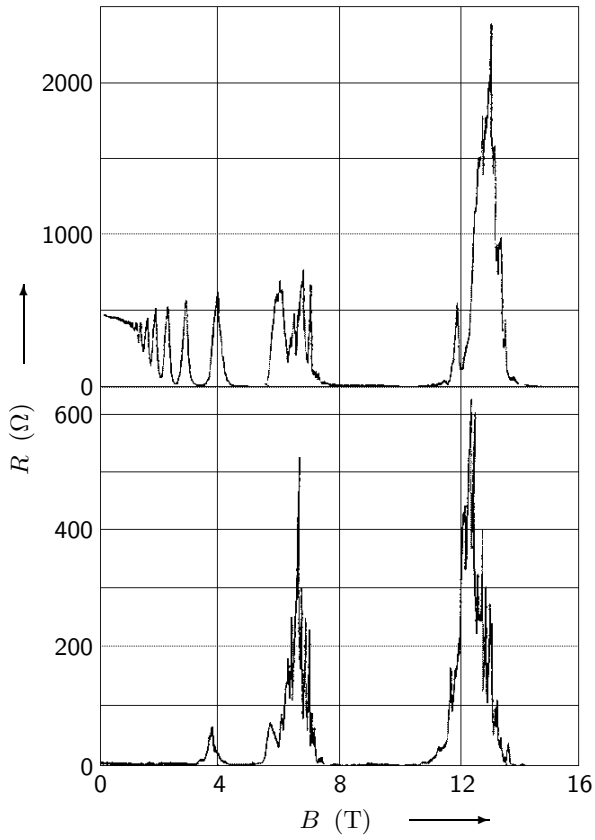

Fig. 168: MR at $T = 300\,\mathrm{mK}$ of a wire in the usual longitudinal configuration (top) and a non–local configuration (bottom) [94M2].

of the oscillations was not constant but increased abruptly when B increased past certain values.

Lettau et al [94L1] investigated MR in single GaAs wires ($w = 133 - 433\,\mathrm{nm}$, $L = 7.5\,\mu\mathrm{m}$) and performed FIR spectroscopy on wire arrays. In the longitudinal MR, a maximum for $B < 1\,\mathrm{T}$ (at $T = 4.2\,\mathrm{K}$) reflected diffusive boundary scattering. The position of the maximum was independent of temperature. Above 1 T, R_L exhibited oscillations arising from magnetic depopulation of 1D subbands. A Landau plot deviated from a linear $1/B$ behaviour (subband spacings 0.4, 0.7, and 1.5 meV in 420, 274, and 133 nm wide wires). At sufficiently high B, the period of the SdH oscillations was consistent with a 2D theory. For $B \leq 50\,\mathrm{mT}$, a negative MR due to weak localization was observed. Reproducible AF were also found. As a consequence of the ballistic motion of the electrons, the low–field ($B < 1\,\mathrm{T}$) Hall resistance was quenched. In addition, it exhibited a series of plateau–like features which were independent of temperature.

Blaikie et al [95B1] performed MR measurements on quasi–ballistic multi–terminal GaAs wires defined by implanted p–type gates ($w = 0.6\,\mu\mathrm{m}$, $w_\mathrm{eff} = 0 - 0.2\,\mu\mathrm{m}$, $L = 10\,\mu\mathrm{m}$, $l = 4.3\,\mu\mathrm{m}$). Quenching of the Hall resistance, negative bend resistance at $B = 0\,\mathrm{T}$, a peak in the longitudinal resistance due to diffusive boundary scattering and a junction–scattering peak were observed. The results were extensively discussed in terms of a semiclassical billiard–ball model. In order to test the predictions of a negative longitudinal resistance, samples with voltage probes joining the wire at angles $\neq 90°$ were structured and longitudinal, bend, and Hall resistances were investigated. A negative longitudinal resistance was confirmed, the bend resistance was negative at $B \neq 0\,\mathrm{T}$, the Hall resistance was non–linear although quenching around $B = 0\,\mathrm{T}$ was not strong.

Wróbel et al [95W] measured the two–terminal conductance of a GaAs wire ($w = 0.8\,\mu\mathrm{m}$, $w_\mathrm{eff} = 0.35 \pm 0.05\,\mu\mathrm{m}$, $L = 20\,\mu\mathrm{m}$) as a function of magnetic field (perpendicular to the wire) for different temperatures, $0.03\,\mathrm{K} \leq T \leq 0.6\,\mathrm{K}$ (Fig. 169). They found regions well below the upper edges of the plateaux (at $G = 2 \cdot e^2/h$ and $G = e^2/h$), in which the conductance decreased as

a power law for increasing temperature. Sharp peaks in the conductance for $3.0\,\mathrm{T} \leq B \leq 3.2\,\mathrm{T}$ were smeared by increasing temperature and were attributed to the presence of impurities. They also recorded the deviations of the conductance from the ideal plateau values as a function of temperature. The data were found to be consistent with results from model calculations of the inelastic rate for electron–phonon scattering.

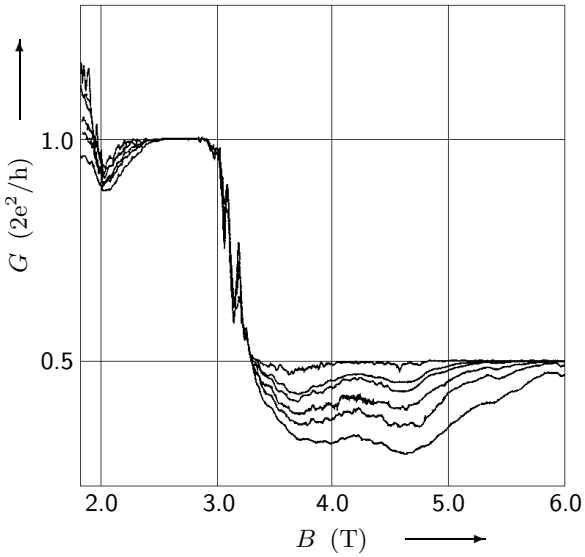

Fig. 169: Conductance vs. magnetic field for (right, top) $T = 0.03\,\mathrm{K}$, $0.10\,\mathrm{K}$, $0.20\,\mathrm{K}$, $0.30\,\mathrm{K}$, $0.40\,\mathrm{K}$, and $0.60\,\mathrm{K}$ (right, bottom) [95W].

Omling et al [95O5] investigated the influence of the deposition of lead particles on the MR of a narrow channel ($w = 400\,\mathrm{nm}$, $w_{\mathrm{eff}} = 250\,\mathrm{nm}$, $L = 5\,\mu\mathrm{m}$, $l = 3\,\mu\mathrm{m}$) defined by shallow wet etching in a GaAs/AlGaAs wafer. They observed reproducible aperiodic conductance fluctuations and an underlying MR with a maximum at $B = 0.22\,\mathrm{T}$ due to boundary scattering before the deposition of the lead particles. Then, lead particles with a size distribution between 80 and 250 nm were randomly distributed on the structure. The zero–field resistance increased by 50% and the maximum at 0.22 T disappeared. The resistance averaged over some conductance fluctuations increased with temperature before particle deposition and it decreased afterwards.

Okada et al [95O3] (page 122) fabricated in–plane gate GaAs wires. The 700 nm wide sample showed conductance quantization only at $B = 5.0\,\mathrm{T}$ and not at $B = 0\,\mathrm{T}$. Okada et al examined the influence of magnetic field on quantized conductance at 2.9 K and found that a magnetic field increased the width of the plateaux.

Bergmann et al [96B3] (page 154) investigated magneto transport in periodically modulated InGaAs wires. Sample A was structured with a chain of antidots along the central wire axis. The MR showed an anomalous peak at $B = 0.4\,\mathrm{T}$ due to diffusive boundary scattering. A peak at 1.56 T was associated with a pinched orbit of electrons around one antidot (Fig. 156). In sample B, antidot chains were positioned at both sides of the wire sidewalls. A localized orbit between four antidots caused a peak in the MR at $B = 1.76\,\mathrm{T}$.

Hughes et al [96H2] (page 213) examined variable range hopping conductance fluctuations in Si and GaAs wires and investigated the influence of a magnetic field.

Gusev et al [98G3] measured MR in a non–uniform magnetic field. The samples were fabricated by overgrowth of GaAs and AlGaAs materials on pre–patterned GaAs wires with trapezoidal cross–sections ($w = 0.5 - 1\,\mu\mathrm{m}$, $L = 10\,\mu\mathrm{m}$). For $T = 1.5\,\mathrm{K}$, fields up to 10 T, and different angles ϕ between the field an the normal substrate plane, they found a large positive MR and SdH oscillations. As the field was tilted away from the normal direction, the SdH oscillations shifted to higher fields, their period was not constant on a $1/B$ scale. Gusev et al determined a critical

angle ϕ_c at which the SdH oscillations changed their behaviour. Their amplitude decreased when ϕ approached ϕ_c and increased again for $\phi > \phi_c$.

Inoue et al [97I2] investigated transport in InAs/AlGaSb wires ($w = 0.1 - 0.7\,\mu$m, $L = 1 - 10\,\mu$m). A large negative MR was observed at 4.2 K. From a Landau plot, a subband spacing of 6.9 meV was estimated. Inoue et al examined the charge velocity at 77 K as a function of channel width and length. The high–field velocity increased in the narrow wires, indicating a reduction of the 1D electron–phonon interaction.

Linke et al [97L] (page 164) investigated the dephasing rate of electrons not in equilibrium in the diffusive regime. The conductance as a function of dc bias showed a pronounced minimum with a half–width of 1 mV, symmetric around zero bias voltage. The amplitude of this minimum was studied as a function of magnetic field.

Maemoto et al [97M] (page 150) fabricated single and multiple InAs wires with a corrugated surface along the wire and measured MR. Features due to boundary scattering were observed.

Iwano et al [98I2] (page 213) fabricated Si wires by FIB doping and investigated the localization length and the hopping distance in the 1D VRH regime. They measured MR and found both, negative and positive MR at low fields in different samples. They extracted $a = 2$ nm, a hopping distance $r = 8 - 9$ nm, and $\rho_F = 10^9\,\mathrm{cm}^{-1}\mathrm{eV}^{-1}$ from the data.

Yamada et al [98Y, 98K2] (page 155) investigated transport through a ferromagnetic Ni dot embedded in a GaAs wire. From magnetic force microscopy data it was deduced that the dot comprised of mainly two domains before and one domain after the application of a magnetic field. CB–related conductance oscillations at zero field were aperiodic and not reproducible while the oscillations at ± 1600 G were periodic and reproducible. The Coulomb gap of $8 - 9$ mV at zero field reduced to $5 - 6$ mV at ± 5000 G. Yamada et al proposed that the domain wall in the absence of a magnetic field splits the dot into two effectively smaller subdots and acts as a resistive barrier.

Thomas et al [99T] (155) investigated the transport properties of two strongly coupled 1D channels defined by a split–gate and measured the in–plane MR.

Gompertz et al [98G2] (page 156) performed MR measurements on quasi–ballistic GaAs wires in a DQW system. For a magnetic field applied perpendicular to the layers, a resonance at $B \approx 11$ T due to delocalization of electrons between the QWs was observed. An additional feature due to a distortion of the energy dispersion curve by the symmetric–antisymmetric splitting was enhanced in comparison to the 2D system. For a magnetic field applied in parallel, the resonance became broader, the additional feature was weakened. UCF with relative amplitudes close to e^2/h were observed.

Stoddart et al [98S1] (page 156) investigated two parallel GaAs wires in a DQW. A reduction of the resistance at small fields due to suppression of backscattering was observed.

Moon et al [99M] (page 156) studied the in–plane MR of vertically coupled GaAs quantum wires defined by split gates. A large broad peak in the MR was observed in the gate voltage regime corresponding to two open 1D channels.

Held et al [99H2] fabricated GaAs wires by local oxidation using an atomic force microscope. The oxide lines had a width of 100 nm and a height of 10 nm. The length of the wires was $L = 40\,\mu$m and the lithographic width varied between 35 nm and 150 nm. Wires with widths below 40 nm, however, were insulating. MR traces were measured at 100 mK. UCF at low fields and SdH oscillations at higher fields were observed. The sublevel index vs. inverse magnetic field showed a non–linear behaviour indicating quantum confinement. A depletion length of (15 ± 5) nm was estimated from the data. From an anomalous MR peak at low fields due to boundary scattering a specularity ≥ 0.95 was deduced. After the deposition of a gate on top of the wire, the width of the wires could be tuned by both, top gate and in–plane gates.

7.7.1.2 Non–local geometry

Behringer et al [89B2] structured multi–probe GaAs electron waveguides ($w = 0.5\,\mu$m) by shallow RIE and performed MR measurements for various different lead configurations. They found that the path of the current outside the region between the voltage probes influenced the resistance.

Takagaki et al [90T1] defined multi–terminal GaAs channels by EBL and shallow ion etching ($w \approx 0.5 - 0.6\,\mu$m, $w_{\rm eff} \approx 0.1 - 0.2\,\mu$m, $l = 2.5\,\mu$m) with lead distances L from 0.4 to 1.35 μm and performed four–terminal resistance measurements. Probes were chosen such that the classical current path did not intersect with the voltage probes. The MR exhibited a peak at zero field. At low fields, quasi–periodic fluctuations with a period of 20 mT were observed which disappeared at $B \approx 0.3 - 0.4$ T. The amplitude of the oscillations was studied as a function of L, a phase coherence length of 0.8 μm was deduced. The amplitude of the fluctuations grew as temperature decreased. Takagaki et al attributed the quasi–periodic fluctuations to interference effects.

Geim at al [91G, 92G2, 93G1, 93M2] fabricated multi–terminal GaAs wires (w = 150, 250, 350, and 450 nm; distances between adjacent probes 1 μm; $l_\varphi = 0.3\,\mu$m at 4.2 K). They measured the non–local MR $R_{\rm ab,cd}$ (current between contacts a and b, voltage difference between contacts c and d, see inset of Fig. 170) for different temperatures and w = 150 nm (Fig. 170). For $T > 10$ K, the UCF were damped and a new type of oscillations was observed. Local SdH oscillations, $R_{\rm ac,bd}$, are shown in Fig. 171. An investigation of the amplitudes of peaks at 8.7 T and 11 T of a $L = 2\,\mu$m configuration, $R_{\rm ab,ef}$, as a function of temperature (Fig. 172) showed that the effect disappeared at both low and high temperatures. Geim et al attributed the observed effect to the coexistence of ballistic transport along the edges and diffusive and dissipative conduction in the bulk.

Tsukagoshi et al [91T4, 92T1] investigated the non–local resistance in mesoscopic multi–terminal GaAs wires ($w = 0.48\,\mu$m, 0.57 μm, and 0.67 μm). The amplitude of non–local SdH oscillations decreased with increasing ΔL (distance between current and voltage probes), it decreased greatly when extra probes were contained between current and voltage probes. In a wide sample, non–local SdH oscillations were observed up to $\Delta L = 1.5$ mm. The experimental results agreed well with a theory based upon the coexistence of edge and bulk states.

Main et al [94M2, 94G3] (page 172) studied MR in multi–terminal GaAs wires using local and non–local lead configurations.

Park et al [95P1, 95P2] measured the non–local MR of AlGaAs/GaAs wires ($w = 2\,\mu$m, $L = 4\,\mu$m). In local probe configurations, they observed typical quantum Hall plateaux and SdH oscillations which contained small oscillations between the plateaux for $B > 3$ T. In non–local probe configurations, they found fine oscillations superimposed on non–local SdH oscillations. The period of the fine oscillations decreased with increasing magnetic field. Park et al analysed their data in terms of mixing of edge states.

7.7.2 Weak localization

In diffusive or quasi–ballistic samples for $l \ll l_\varphi$, an electron may return to its origin after multiple scattering. A time–reversed path belongs to each path the electron may choose and the two time–reversed paths arrive in phase at the origin and thus interfere constructively if phase memory is retained along the paths. As a consequence, the probability to return to the origin is enhanced and the probability to traverse the sample is reduced in comparison to the classical picture. As the temperature decreases, l_φ increases (see Section 7.3.4 on page 138) and ever larger loops contribute to the constructive interference at the origin and hence the resistance of the sample increases. This mechanism is referred to as *weak localization* and the time–reversed pairs of paths are sometimes called *Cooperons*. The constructive interference at the origin is critically dependent on time–reversal symmetry. A perpendicular magnetic field changes the phase along these paths, advancing it on one path and retarding it on the other. A magnetic flux of $\Phi = h/2e$ dephases the paths

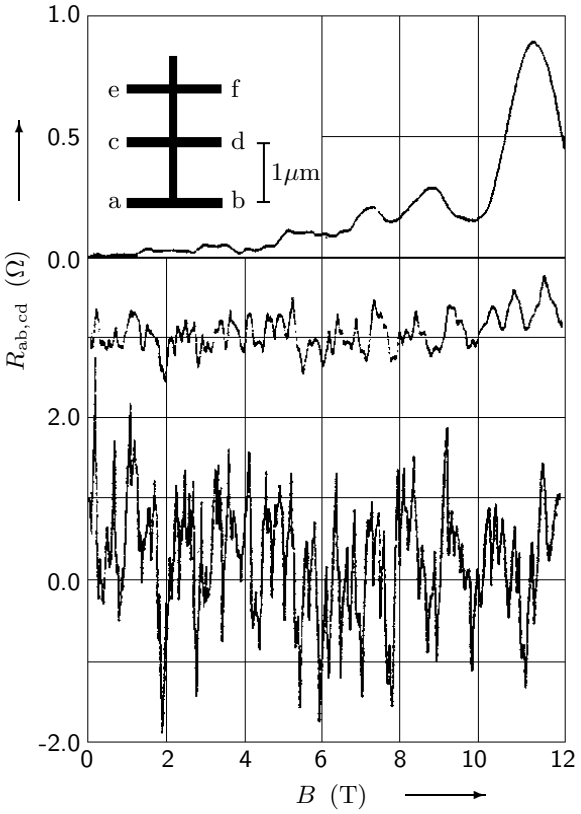

Fig. 170: The non–local MR traces for $L = 1\,\mu$m, $w = 150\,$nm at (top) $T = 30\,$K, 9 K, and 4 K (bottom). The 9 K trace is offset upwards by $3\,\Omega$ for clarity. The 30 K trace has threefold magnification. Inset: The sample geometry.

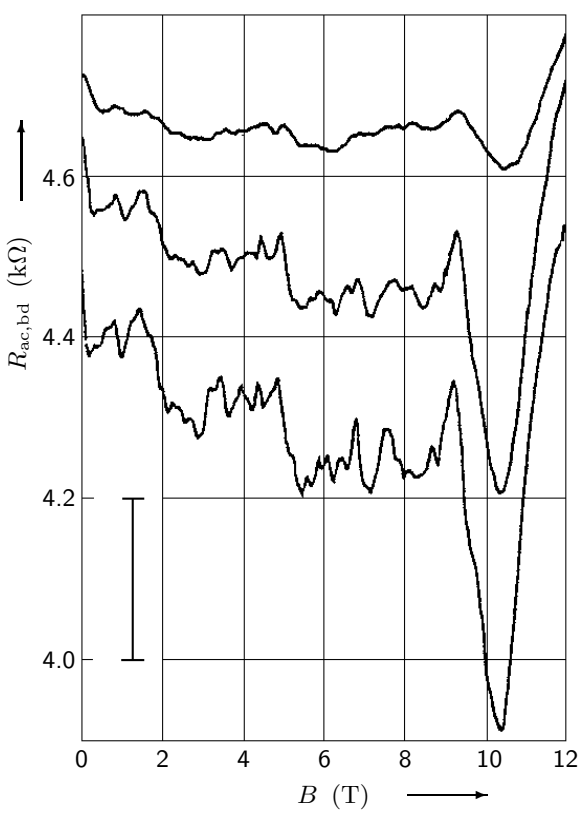

Fig. 171: Local MR at (top) $T = 30\,$K, 9 K, and 4 K (bottom). The 9 K and 30 K traces are offset upwards by 0.2 and $0.4\,$kΩ, respectively, for clarity. The vertical bar denotes a magnitude of 5%.

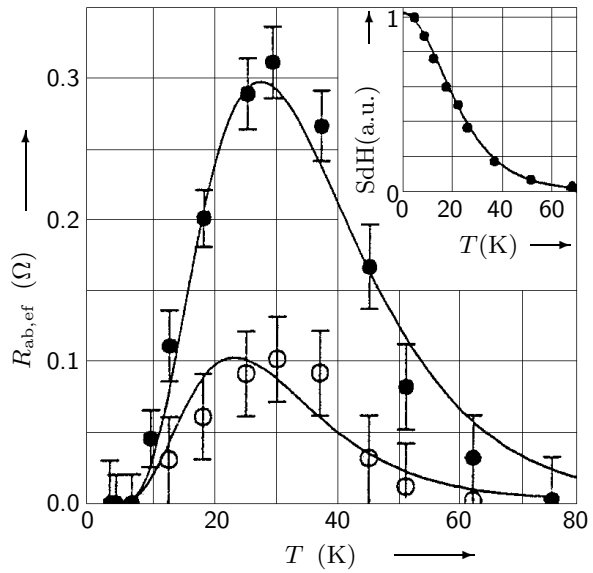

Fig. 172: The temperature dependence of $R_{ab,ef}$ for the two peaks of a $L = 2\,\mu$m sample at 8.7 and 11 T. Solid lines are the best fits to the temperature dependence using theory, circles are the experimental data. Inset: The temperature dependence of the relative amplitude of local SdH oscillations (the solid line represents theory).

sufficiently in order to turn off weak localization. A negative magneto resistance is the consequence. In the presence of spin–orbit scattering (see Section 7.6.3 on page 167), the magneto resistance is positive (see for example [84B2, 85F, 88K1, 90D, 92W1, 97F, 98D, 98J1] and references therein).

Wheeler et al [82W, 84W] (page 138) measured the MC of Si MOSFETs and extracted the inelastic scattering length from the data by comparison to weak–localization theory.

Dean et al [82D] (page 132) measured low–field MC in a Si channel and found a positive MC at $T = 1.2\,\mathrm{K}$ and a negative MC at 70 mK (Fig. 133).

Thornton et al [86T] studied interference and interaction corrections to the conductance of narrow channels in GaAs/AlGaAs heterojunctions. The samples had the shape of Hall bars, channels were formed by gates with gaps $15\,\mu$m long and $0.6\,\mu$m wide. The increase in conductance with magnetic field at $V_\mathrm{g} = -1.2\,\mathrm{V}$ is illustrated in Fig. 173. The data was fitted by 1D weak–localization theory, and a width of the conducting channel of 45 nm ±10% and the temperature–dependent l_φ were extracted. The phase coherence length varied approximately as $T^{-1/3}$ in agreement with 1D theory. The quantum interference correction and the correction due to electron–electron interaction were calculated using this l_φ and were compared with the data. The temperature dependence of the conductance for different gate voltages is shown in Fig. 174.

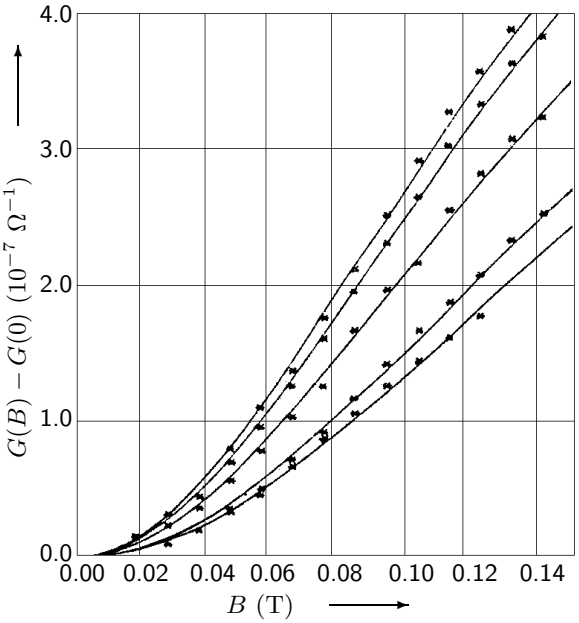

Fig. 173: Conductance vs. magnetic field for (top) $T = 0.41\,\mathrm{K}$, 0.46 K, 0.56 K, 0.6 K, and 1.0 K (bottom) [86T]. The lines indicate the best fits at each T according to 1D weak–localization theory.

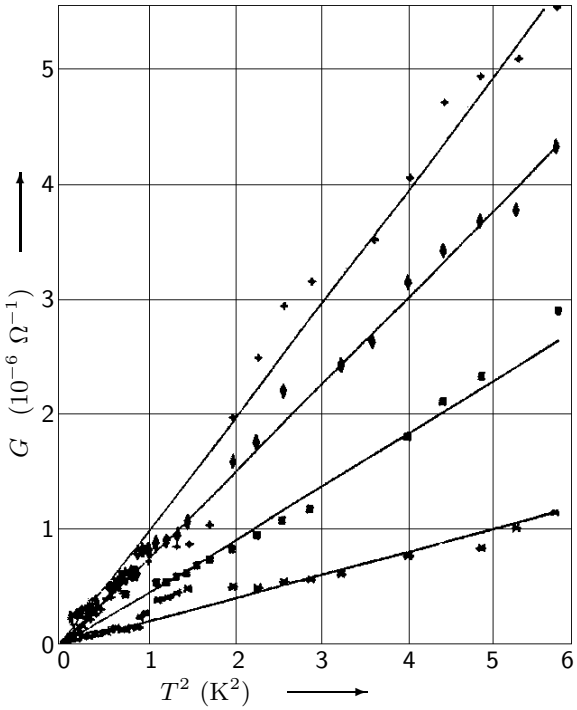

Fig. 174: Conductance vs. T^2 for (top) $V_\mathrm{g} = -1.210\,\mathrm{V}$, $-1.215\,\mathrm{V}$, $-1.220\,\mathrm{V}$, and $-1.225\,\mathrm{V}$ (bottom) [86T].

Kaplan et al [86K3] (page 182) studied the MC in narrow Si channels. They extracted the inelastic scattering length from comparison of the low–field MC with weak–localization theory.

Zheng et al [86Z2] (page 145) realized a GaAs channel by a split gate and fitted low field MR data by 1D weak–localization theory (Fig. 143). The inelastic scattering length was extracted from the fits.

Van Houten et al [86vH] (page 145) studied GaAs wires, low–field MR data revealing weak localization are shown in Fig. 144.

Choi et al [87C2] examined the localization time scale in GaAs/$Al_xGa_{1-x}As$ samples of different geometries structured by photolithographic techniques. The MR of a wide sample ($w = 300\,\mu$m, $L = 2100\,\mu$m) and a narrow sample ($w = 0.21\,\mu$m, $L = 62\,\mu$m) was measured at different temperatures and fitted by 2D and 1D weak–localization theory, respectively (Fig. 175). The fitting parameter τ_φ is shown in Fig. 176. According to theory, τ_φ was fitted to a combination of T^2 and T dependences in the wide device and to a combination of T^2 and $T^{2/3}$ dependences in the narrow device. Choi et al further studied the effect of L on localization. They also found AF in the MR of a short channel sample.

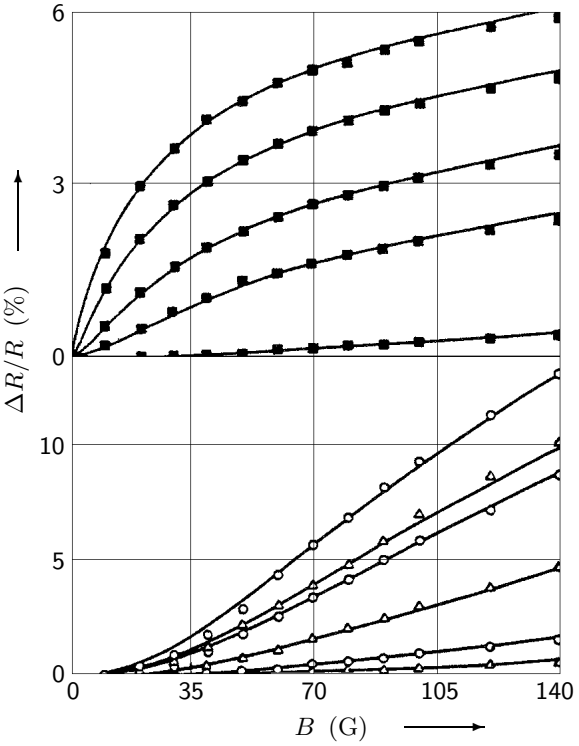

Fig. 175: Magnitude of the negative MR for a wide channel (top) and a narrow channel (bottom) at (upper picture, top) $T = 0.30$ K, 0.49 K, 0.88 K, 1.39 K, 4.20 K (bottom), and (lower picture, top) $T = 0.35$ K, 0.57 K, 0.73 K, 1.20 K, 2.00 K, 3.60 K (bottom) [87C2]. The solid curves are theoretical fits.

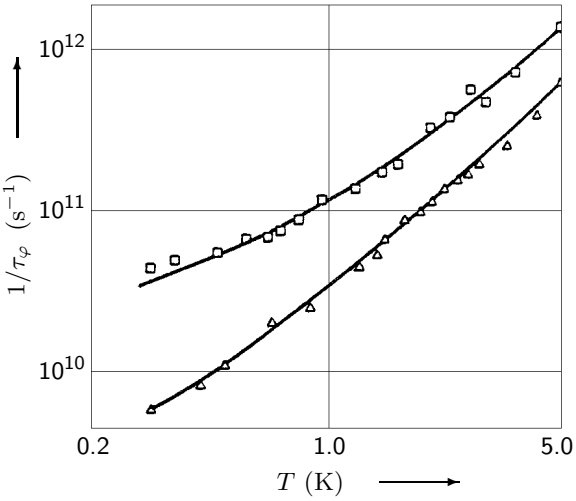

Fig. 176: The phase breaking rate for the wide channel (triangles) and the narrow channel (boxes) as obtained from the fits in Fig. 175 vs. temperature. The solid curves are theoretical fits.

Ishibashi et al [87I1] (page 182) fabricated narrow GaAs wires and measured the four–probe resistance. Via weak–localization measurements on the 2D film, they obtained the inelastic scattering length ($l_\varphi \geq 0.2\,\mu$m below 4.2 K) as a function of temperature.

Choi et al [87C1] determined the effective widths of narrow GaAs channels ($w = 0.8 - 2.4\,\mu$m) fabricated by photolithographic techniques and chemical etching via 1D localization theory. They measured the four–terminal MR and deduced w_{eff} and l_φ. For a sample with $w = 1.0\,\mu$m, a conducting width of $0.31\,\mu$m was found. The depletion width in different samples ranged from 0.3 to $0.8\,\mu$m with an uncertainty of about $\pm 20\%$.

Van Houten et al [88vH] (page 159) performed MR measurements at temperatures 100 mK – 14.3 K on a channel fabricated from a GaAs/AlGaAs heterostructure [86vH]. In the magnetic field dependence of the conductance, 1D weak localization was observed (Fig. 158). Boundary scattering effects were included into weak–localization theory in order to analyse the data (Fig. 159).

Taylor et al [88T2] measured negative MR and UCF in two different types of structures: GaAs wires with (A) a length of 10 μm and widths of 90 – 300 nm, and (B) with widths of 180 – 540 nm. They analysed the data of samples A with a model based on Fourier transforms and found evidence that negative MR and UCF were manifestations of the same phenomenon. They extracted the phase breaking rate as a function of temperature. In samples B, Taylor et al observed SdH oscillations at high fields. Both, the UCF and the negative MR at low fields varied with the angle between magnetic field and sample–normal.

Hiramoto et al [87H1, 88H2] (page 146) measured the low–field MC of GaAs wires and fitted the data by 1D weak–localization theory, deducing l_φ.

Kastner et al [88K2] (page 169) structured Si wires and measured the MR at several temperatures. A small negative MR due to weak localization was observed at low fields.

Hiramoto et al [89H] (page 139) studied the phase coherence length in GaAs wires of different widths. MC measurements were performed, the data was compared with weak–localization theory, and $l_\varphi = 1.2\,\mu$m, $w_{\text{eff}} = 90$ nm (for a 100 nm wide wire) and $l_\varphi = 0.9\,\mu$m, $w_{\text{eff}} = 70$ nm (for a 30 nm wide wire) were extracted (Fig. 136).

Pooke et al [89P] (page 139) reported on measurements of the weak–localization correction to the conductivity in narrow accumulation layer Si MOSFETs. For $w = 0.44\,\mu$m and $T > 1$ K, the device was in the 2D regime. For $T < 1$ K, the MR was in agreement with 1D theory.

Taylor et al [89T4] (page 169) fabricated quasi–ballistic GaAs channels, measured the MR at various temperatures and found a negative MR below 0.1 T due to weak localization. They extracted l_φ as a function of temperature.

Gallagher et al [90G1] (page 143) studied multi–terminal n^+–type GaAs wires. The two–terminal MR was negative due to weak localization.

Fukai et al [90F4] (page 140) structured GaAs/AlGaAs on–facet wires and determined the phase coherence length at temperatures down to 50 mK via weak localization. The low–field MR was positive for $T \leq 0.08$ K, indicating the presence of SO interaction.

Menschig et al [90M1, 90M2, 91F2] (page 116) patterned $In_{0.53}Ga_{0.47}As$/InP wires and observed a negative MR due to weak localization which decreased with increasing wire width.

Galloway et al [90G2] (page 189) investigated a n^+–GaAs wire and observed a negative MR.

Taniguchi et al [90T4] (page 140) fabricated GaAs wires, measured the MR of wires of different widths and extracted the phase coherence length as a function of temperature by comparison of the data to weak–localization theory (Fig. 137).

Feng et al [92F2, 92F1] (page 147) studied wires made from δ–doped GaAs, side gated across deep trenches. MR at different V_g was measured, results were fitted by 1D weak–localization theory.

Haug et al [92H1] fabricated narrow channels on the cleaved surface of InAs quantum well structures. The widths of the channels were defined by the thickness of the InAs wells. The edge resistance as a function of temperature behaved similarly to the bulk resistance down to 50 K, but became nearly independent of T at lower temperatures, indicating a partly metallic edge. MR was measured in a four–probe configuration ($L = 0.1$ mm). A strong negative MR up to 2 T and reproducible AF at higher fields were observed. From a comparison of the low–field data with weak–localization theory, $l_\varphi = 0.5\,\mu$m was deduced for $w = 20$ nm (assuming $l = 0.2\,\mu$m). The

fluctuations at high fields were consistent with 1D theory. The oscillations became weaker for an increasing width of the InAs well. In a 80 nm wide channel, SdH oscillations became noticeable at $B > 5$ T. In 10 nm wide InAs wells, metallic edge conduction was not found. At low T, some samples showed telegraph noise.

Ishibashi et al [92I2] (page 190) studied MR fluctuations superimposed on a negative background due to weak localization in the quasi–ballistic regime in split–gate GaAs wires.

Block et al [93B1] (page 171) studied the MR of wires fabricated from $In_{0.53}Ga_{0.47}As/InP$ heterostructures. At weak magnetic fields, a negative MR due to weak localization was found, which was most pronounced for the smallest widths (Fig. 167).

Brown et al [93B2, 93M2] (page 191) studied diffusive GaAs wires and observed negative MR due to weak localization at low fields.

Onishi et al [93O2, 93O3, 94O1] (page 191) studied split–gate GaAs wires and observed a negative MR consistent with weak–localization theory. The phase coherence length was extracted from the data.

Ramon et al [93R] (page 142) patterned narrow GaAs wires and extracted the phase coherence length as a function of temperature from low–field MR data using weak–localization theory.

Dietl et al [93D] (page 191) reported on n-$Pb_{0.98}Mn_{0.02}Te$ wires with a positive low field MR.

Lettau et al [94L1] (page 173) investigated MR in GaAs wires. For $B \leq 50$ mT, a negative MR due to weak localization was observed.

Shitara et al [95S] prepared GaAs wires ($w = 250$ nm, $L = 50\,\mu$m) by overgrowth on patterned GaAs substrates using MBE. They carried out four–terminal MR measurements and observed weak localization, reproducible resistance fluctuations and SdH oscillations.

Jaroszyński et al [95J, 96D1, 96J2] investigated the MR of $Cd_{0.99}Mn_{0.01}Te$ and CdTe wires ($w \approx 0.3\,\mu$m, $L = 5\,\mu$m) fabricated by EBL and wet etching. The negative low–field MR in CdTe was due to weak localization. At ≈ 3 K, a temperature–induced crossover from a 3D to a 1D behaviour was observed. The positive low–field MR in n^+–$Cd_{0.99}Mn_{0.01}Te$ was attributed to the effect of the giant exchange spin splitting upon electron–electron interaction. No dimensional crossover was observed. The amplitude of AF was independent of magnetic field and increased with decreasing temperature. The correlation field increased with either temperature or magnetic field, a behaviour not observed in non–magnetic wires.

Noguchi et al [96N2] (page 142) measured the MC for $0.4\,\text{K} < T < 30\,\text{K}$ in GaAs wires and observed weak localization (Fig. 139). The weak–localization peak at $B < 0.04$ T became steeper for fixed V_g as temperature decreased.

Koester et al [96K3] investigated weak localization in Si wires ($w = 0.04 - 1.0\,\mu$m, $L = 10\,\mu$m) fabricated by EBL and RIE. The carrier density could be varied by the help of a back gate. The four–terminal conductance decreased linearly with the width (at $T = 4.2$ K). In the MR at $T = 1.3$ K, SdH oscillations were observed for $|B| > 1$ T, while a negative MR attributed to weak localization was observed at $|B| < 0.3$ T. The data was fitted to theory, l_φ and τ_φ were extracted. The weak–localization correction to the conductance increased with more positive values of V_g, but for $V_g > 2$ V, the weak localization disappeared in some samples. The phase coherence length increased with the electron concentration.

Widjaja et al [96W] (page 154) measured MR in wires defined by a split–gate in which one gate included a corrugation that produced a set of coupled quantum dots. A negative MR due to weak localization was observed.

Gusev et al [98G3] (page 174) measured MR in a non–uniform magnetic field. For $T = 1.5$ K, fields up to 10 T, and different angles between the field an the normal substrate plane, they found

a large positive MR.

Linke et al [97L] (page 164) investigated the dephasing rate of electrons not in equilibrium in the diffusive regime. They used GaAs wires, measured the four–terminal MC and analysed the data in terms of weak localization.

7.7.3 Aperiodic conductance fluctuations

Aperiodic conductance fluctuations due to interference between electron paths (see Section 7.2.1 on page 124) are observable as a function of magnetic field. If the change in magnetic field is greater than the characteristic correlation field, the sample conductance changes by $\approx e^2/h$. The correlation field B_c is the field necessary to cause some significant relative phase shift among the paths. The correlation function $K(\Delta B) \equiv \langle G(B)G(B+\Delta B)\rangle - \langle G(B)\rangle^2$, where $\langle \ldots \rangle$ denotes an average over impurity configurations, decays on the scale of B_c . The theoretical model leading to UCF breaks down for magnetic fields with $\omega_c\tau > 1$, where ω_c is the cyclotron frequency and τ is the mean elastic scattering time. In a non–local geometry, the conductance fluctuations decay exponentially with ΔL (here ΔL is the separation of the nearest voltage probe from the classical current path) as ΔG is proportional to the fraction of the electrons that retain phase coherence until they arrive at the probes, which is $e^{-\Delta L/l_\varphi}$. As the flux depends only on the component of the magnetic field perpendicular to the plane of the loops of the electron paths, the aperiodic conductance fluctuations depend not only on the magnitude of B but also on the angle between the magnetic field and the plane of the loops (see for example [86W1, 88K1, 89W1, 91W2, 92W1, 98D] and references therein).

7.7.3.1 Angle dependence

Kaplan et al [86K3] studied the MC of narrow Si channels for different angles between the field and the sample–normal in devices similar to those fabricated by Fowler et al ([82F], page 125), see Figs. 177 and 178. The features at large fields were SdH oscillations. Kaplan et al extracted the inelastic scattering length and the channel width from comparison of the low–field MC with weak–localization theory. Further, the AF were measured as a function of gate voltage in order to estimate the correlation energy.

Whittington et al [86W3] studied the MR of small n^+GaAs wires 10 μm long and 0.09 to 0.3 μm wide, fabricated by EBL and dry etching. MR data for various angles θ between the magnetic field and the normal to the plane of the substrate is shown in Fig. 179. Each curve was reproducible when T was kept constant. The MR for larger fields is displayed in Fig. 180. SdH oscillations were observed for $B > 5$ T only for traces close to $\theta = 0°$. The amplitude of the conductance fluctuations was independent of temperature below 10 K and decreased as $T^{-1/2}$ above 10 K.

Ishibashi et al [87I1] fabricated narrow doped GaAs wires and measured the four–probe resistance. Via weak–localization measurements on the 2D film, they obtained the inelastic scattering length ($l_\varphi \geq 0.2\,\mu$m below 4.2 K) as a function of temperature and compared it with the thermal diffusion length. The MC of a narrow wire normalized by e^2/h is shown in Fig. 181. The magnitude of the AF was about $0.3 \cdot e^2/h$ with only a weak dependence on temperature. By examining the MR at various orientations of the magnetic field, Ishibashi et al showed that the structure depended mainly on the perpendicular component of the field.

Taylor et al [88T2] (page 180) measured negative MR and UCF in GaAs structures. Both, the UCF and the negative MR at low fields varied with the angle between magnetic field and sample–normal.

Taylor et al [89T4] (page 169) fabricated quasi–ballistic GaAs channels, measured the MR at various temperatures and found UCF. They examined the MR for different angles between B and

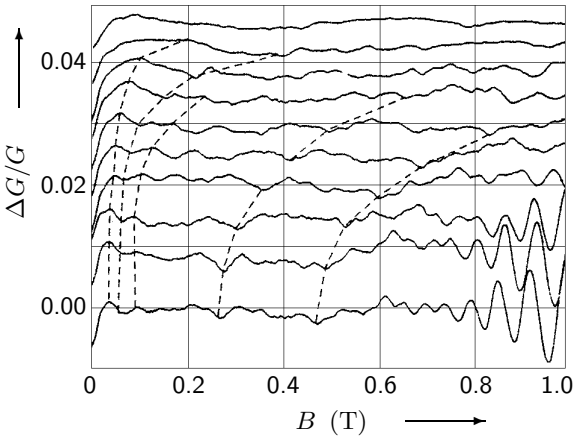

Fig. 177: Fractional change in the MC for (top) $\theta = 94°$, $84°$, $74°$, $64°$, $53.5°$, $44.5°$, $35°$, $24°$, $10°$, $0°$ (bottom) at $V_g = 11\,V$ and $T = 0.47 \pm 0.02\,K$ [86K3]. The slowly varying background has been substracted. The dashed lines track several structures from curve to curve as θ is varied.

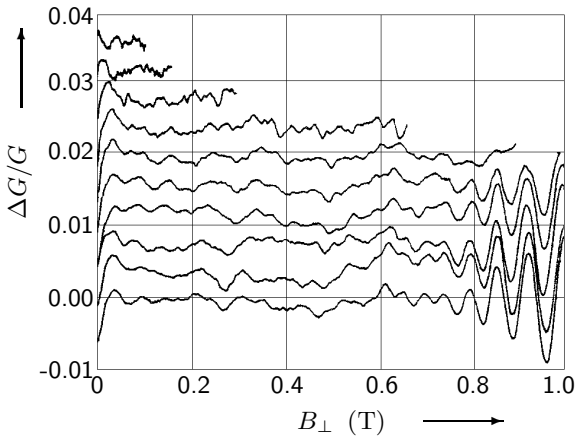

Fig. 178: Same data as in Fig. 177 plotted vs. the perpendicular component of the magnetic field, (top) $\theta = 94°$, $84°$, $74°$, $64°$, $53.5°$, $44.5°$, $35°$, $24°$, $10°$, $0°$ (bottom).

the sample normal.

7.7.3.2 Local geometry

Licini et al [85L2] studied Si MOSFETs similar to those in [84K2] (see page 125), at gate voltages well above threshold. MR measurements showed aperiodic oscillations of the resistance as a function of magnetic field perpendicular to the Si surface (Fig. 182). The structure was reproducible for fixed V_g. As there was no gradual shift of the oscillations with V_g, the MR oscillations were assumed not to result from energy shifts of the eigenstates (Fig. 183). The temperature dependence of the oscillation amplitude was consistent with e^{-L_0/L_T}, where L_0 was fixed and L_T varied as $T^{-1/2}$. MR oscillations were assumed to be a direct consequence of quantum interference.

Choi et al [85C, 86C2] (page 168) measured the MR of GaAs devices of different widths. For very narrow channels, aperiodic and temperature independent oscillations occurred [86C2].

Skocpol et al [86S1] (page 127) studied MR the longitudinal and the Hall resistance in quasi 1D Si devices and found AF.

Skocpol et al [86S2] fabricated narrow Si MOSFETs with multiple contacts and widths in the range $0.04 - 1.0\,\mu m$. They observed AF as a function of magnetic field, the pattern changed with V_g. From a set of data they extracted $\langle G \rangle = 11.7 \cdot e^2/h$, $\Delta G = 0.65 \cdot e^2/h$, the correlation field $B_c = 0.48\,T$, and the correlation gate voltage $V_{gc} = 0.22\,V$. A comparison between the amplitude of the AF and the theoretical prediction for UCF is shown in Fig. 184. For segments in which the inelastic scattering length was longer than the distance between the voltage probes, the effective quantum area deduced from the measured B_c systematically exceeded the area between the voltage probes and the measured ΔG exceeded e^2/h.

Van Houten et al [86vH] (page 145) observed reproducible AF in GaAs wires for $B > 0.1\,T$.

Choi et al [87C2] (page 179) examined GaAs/$Al_xGa_{1-x}As$ samples and found AF in the MR of a short channel sample.

Skocpol et al [87S2] compared the behaviour of a Si device with a probe spacing of 150 nm with one of probe spacing of $5\,\mu m$. The channels were 250 nm wide. Data was taken at $T \approx 0.4\,K$

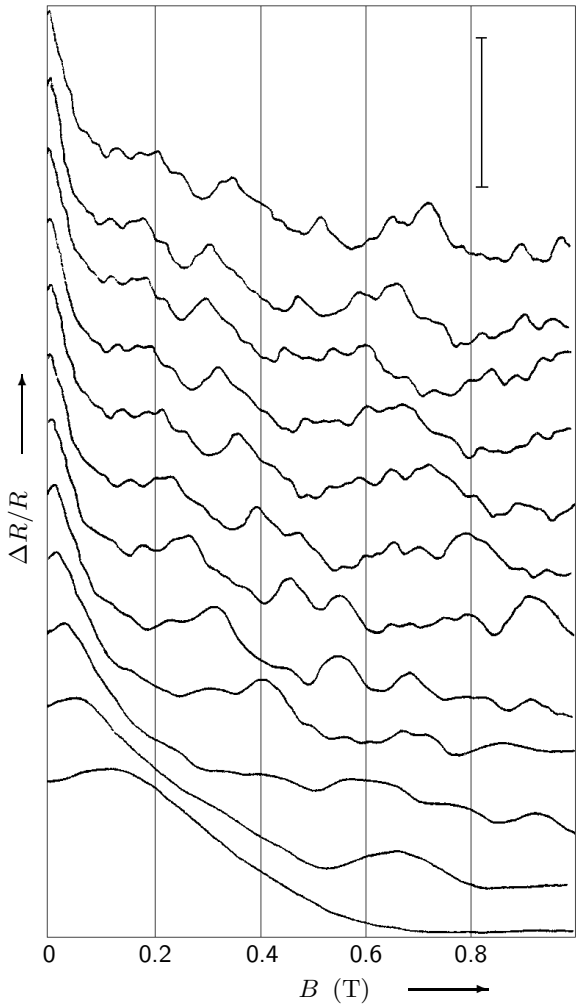

Fig. 179: Transverse MR of a 0.26 μm wide wire for (top) $\theta = -20°$, $-10°$, $0°$, $10°$, $20°$, $30°$, $40°$, $50°$, $60°$, $70°$, $80°$, and $90°$ (bottom) at T =4.2 K [86W3]. The vertical bar denotes an amplitude of 5%.

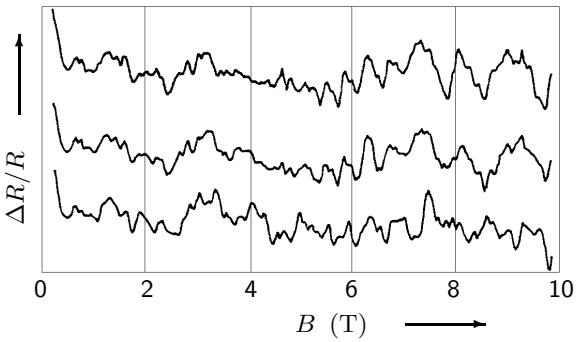

Fig. 180: Transverse MR at 4.2 K of a 0.26 μm wide wire for three different values of θ [86W3]. Top curves are within $1°$ of $\theta = 0°$; bottom curve is for $\theta = 5°$. SdH oscillations are only present in the two top curves.

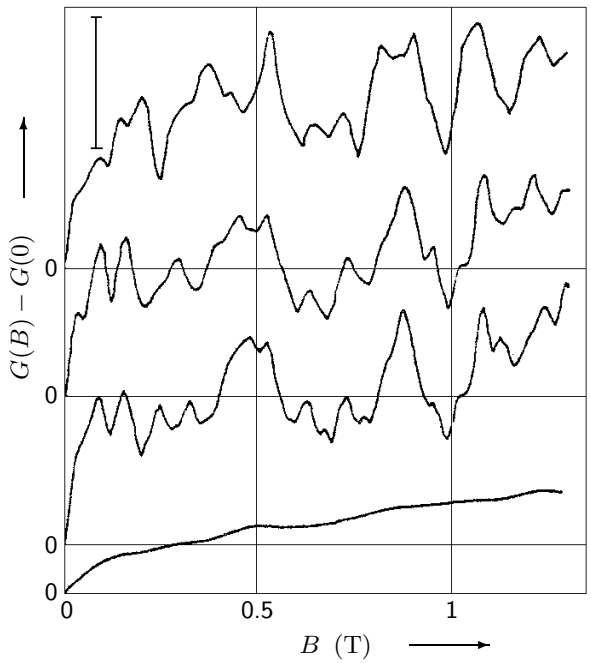

Fig. 181: MC of a wire [87I1] at (top) $T = 1.52\,\mathrm{K}$, 2.92 K, 4.2 K, and 62 K (bottom). The vertical bar denotes an amplitude of e^2/h.

and gate voltages of 6–8 V above threshold. It was $l = 40\,\mathrm{nm}$ and $l_\varphi \approx 1\,\mu\mathrm{m}$. Skocpol et al studied fluctuations of the resistance in the multi–probe devices and found that the amplitude of the fluctuations increased as the square root of the probe spacing for $L > l_\varphi$. At smaller probe spacings, the amplitude remained constant. The fluctuations in the short device were not a locally determined property of the channel between the probes as could be seen from the magnetic field scale of the fluctuations. For a probe spacing of 150 nm, the conductance fluctuations were as large as $20{\cdot}e^2/h$.

Timp et al [87T3] (page 200) measured the MR of wires fabricated on modulation doped GaAs/AlGaAs. AF were observed in R_L and R_H, the amplitude of the conductance fluctuations exceeded e^2/h. The amplitude and the typical spacing of the fluctuations varied with magnetic field.

Thornton et al [87T2] studied split–gate GaAs FETs with a gate separation of 1 μm and a length of 15 μm. They measured MC fluctuations at different temperatures and studied the variance of the fluctuations for different channel widths as a function of temperature (Fig. 185). The temperature dependence of l_φ was deduced. Thornton et al further studied the magnetic correlation field as a function of temperature (Fig. 186) and again deduced $l_\varphi(T)$.

Ishibashi et al [87I2] reported experimental observation of AB oscillations in a small ring of selectively doped GaAs/AlGaAs while a wire fabricated for comparison showed only AF (see page 265).

Taylor et al [88T2] (page 180) measured negative MR and UCF in a GaAs structure. Both, the UCF and the negative MR at low fields varied with the angle between magnetic field and sample–normal.

Simmons et al [88S3] (page 168) performed MR measurements on doubly connected rings and standard Hall bridges made from GaAs/$\mathrm{Al}_x\mathrm{Ga}_{1-x}$As heterostructures. Samples of both geometries showed resistance fluctuations.

Van Houten et al [87vH] (page 195) fabricated GaAs channels and measured the low– and high–field MR. The structure at low fields was attributed to UCF.

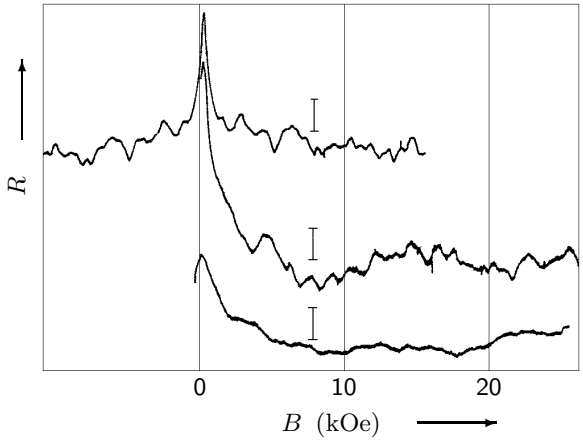

Fig. 182: Change of resistance with magnetic field at T =0.14 K for (top) V_g = 7.97 V, 6.00 V, 4.00 V (bottom) [85L2]. The vertical bars denote amplitudes of (top) 1.12 kΩ, 1.29 kΩ, 14.4 kΩ (bottom). The resistance values at the maxima are (top) 49 kΩ, 85 kΩ, 305 kΩ (bottom).

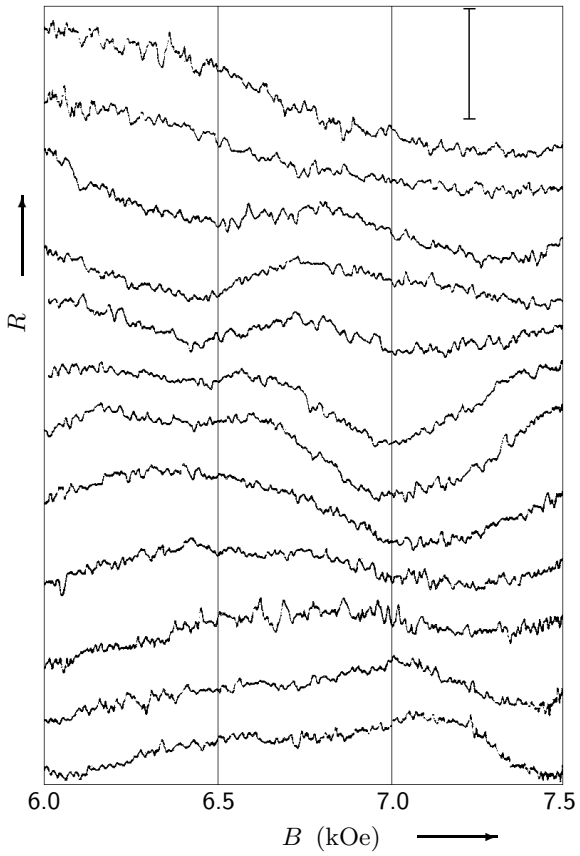

Fig. 183: MR at closely spaced values of V_g: (top) 7.984 V, 8.026 V, 8.067 V, 8.099 V, 8.127 V, 8.161 V, 8.194 V, 8.223 V, 8.256 V, 8.286 V, 8.317 V, 8.350 V (bottom) at T = 0.19 K [85L2]. The Channel resistance was ≈ 50 kΩ. The vertical bar denotes an amplitude of 1 kΩ.

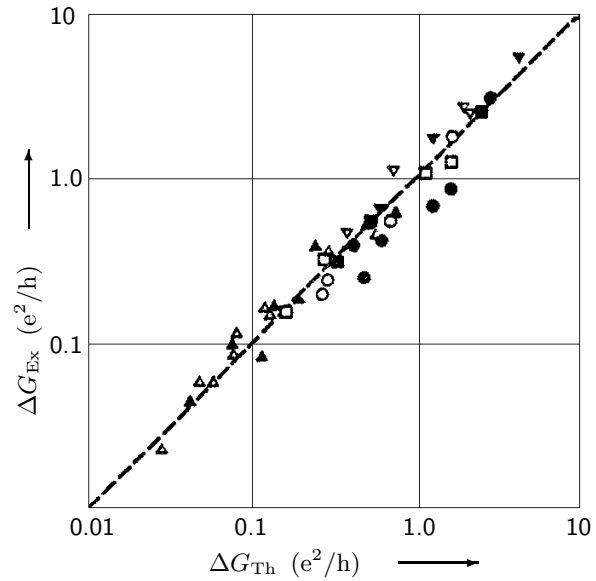

Fig. 184: Measured vs. predicted fluctuation amplitude in units of e^2/h for many data sets with a wide range of experimental parameter values [86S2]. The segments had lengths between 0.15 and 0.75 μm and widths of 0.06 (upright triangles), 0.10 (boxes), 0.25 (downward triangles) and 0.04 μm (circles). Open symbols: 4.2 K; solid ones: 2 K. The inelastic scattering length varied between 0.03 and 0.47 μm.

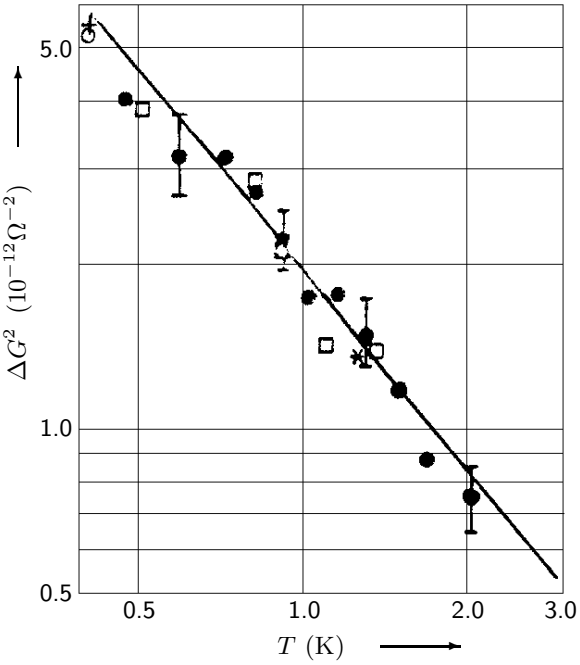

Fig. 185: Variance of the fluctuations for $V_g = -3.010\,V$ (filled circles), $-3.050\,V$ (open squares), $-3.100\,V$ (open circles), $-3.140\,V$ (stars), and $-3.150\,V$ (crosses) vs. temperature on a double logarithmic scale [87T2].

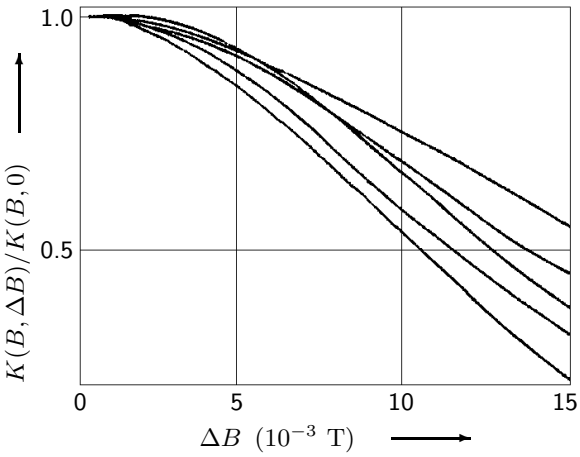

Fig. 186: Temperature dependence of the correlation function $K(B,\Delta B)$ normalized to the variance $\langle \Delta G^2 \rangle = K(B,0)$ [87T2] for (top, right) $T = 1.30\,K$, $0.90\,K$, $0.80\,K$, $0.57\,K$, $0.47\,K$ (bottom,right).

Hiramoto et al [87H1, 88H2] (page 146) fabricated GaAs wires, measured MC and observed AF. The amplitude of the fluctuations depended on the channel width (Fig. 145).

Kastner et al [88K2] (page 169) structured Si wires and measured the MR at several temperatures. UCF were observed at low fields.

Chang et al [88C2] reported MR measurements on ballistic GaAs/$Al_xGa_{1-x}As$ wires patterned by EBL and RIE. The conducting widths were $80 - 200\,nm$, about ten transverse channels carried the current. At $T < 300\,mK$, l_φ exceeded the sample size. Chang et al varied the probe spacing by measuring between different leads. The AF grew in amplitude ($> 30\%$) and shifted in frequency content as the temperature was lowered. They found a nearly zero correlation coefficient between different segments of the sample.

Chang et al [88C1] (page 201) examined narrow GaAs/AlGaAs heterostructures. They measured R_L and R_H as a function of B at $T = 50\,mK$ (Fig. 203). The $\nu = 4$ Hall plateau showed large AF, the R_L minimum showed similar features. The AF in R_H increased with decreasing temperature (Fig. 204).

Mailly et al [89M2] applied a voltage pulse of $0.4\,V$ amplitude and $15\,ms$ duration to a $37\,\mu m$ long and nominally $1\,\mu m$ wide GaAs wire. The resistance increased abruptly, then decreased to its initial value within 15 minutes. Resistance jumps due to the change of the impurity potential occurred. This method was used for sample–averaging. Mailly et al recorded magneto fingerprints, applied a voltage pulse and took MFP again (Fig. 187). The conductance distributions were fitted by Gaussian laws.

Takagaki et al [88T1] (page 207) examined narrow multi–branched electron wave guides made from GaAs/AlGaAs heterostructures, measured MR, and observed AF.

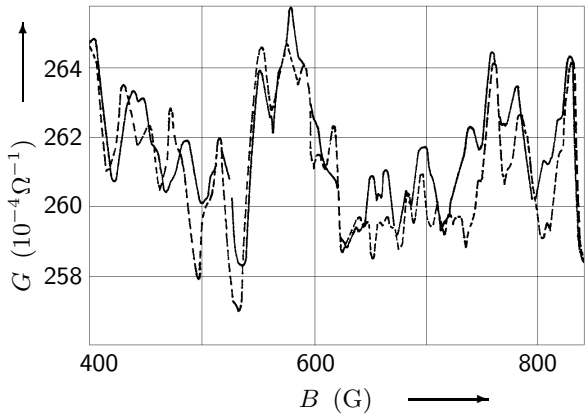

Fig. 187: MFP before voltage pulse (solid line) and MFP 10 h after voltage pulse (dashed line) [89M2].

Mizuno et al [89M4, 90I1] fabricated narrow GaAs wires ($w = 0.7\,\mu$m, $w_{\text{eff}} = 0.4\,\mu$m, $L = 3\,\mu$m, $l \approx 0.1\mu$m) and observed conductance fluctuations in MR curves. The amplitude of the fluctuations was $\approx 0.7 \cdot e^2/h$ below 0.5 K and decreased nearly proportional to $T^{-1/2}$ with increasing T above 0.5 K. In Fourier spectra of the MR data, Mizuno et al found that the high–frequency parts of the spectra were reduced with increasing field (Fig. 188). Fourier spectra in the same field range for different temperatures were almost independent of T.

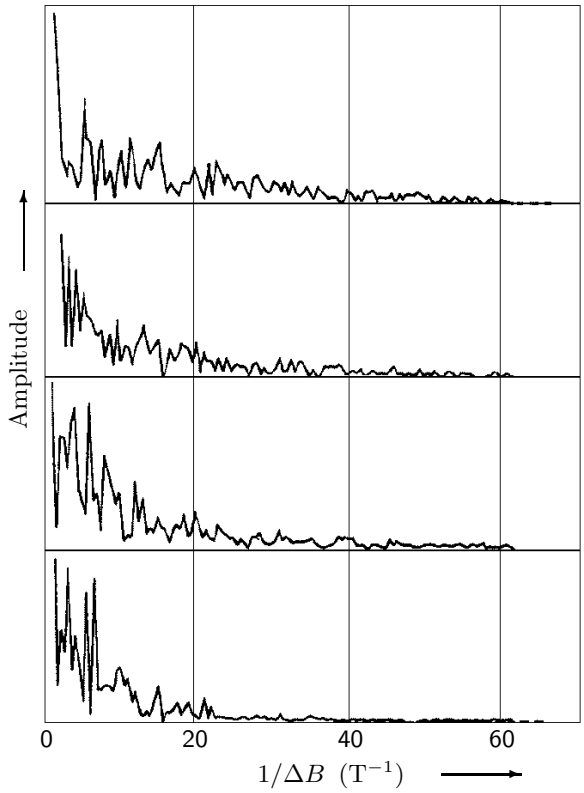

Fig. 188: Fourier spectrum of the MR at 80 mK for (top) $B = 0 - 2.0$ T, $2.1 - 4.1$ T, $4.1 - 6.1$ T, and $6.2 - 8.2$ T (bottom) [89M4].

Taylor et al [89T4] (page 169) fabricated quasi–ballistic GaAs channels, measured the MR at various temperatures and observed UCF.

Mailly et al [90M3] patterned two GaAs wires of different disorder strengths ($w = 1\,\mu$m, $L = 37\,\mu$m and $w = 0.45\,\mu$m, $L = 5\,\mu$m) by ionic etching. They applied voltage pulses to the samples causing the resistance to increase abruptly and then to decrease. The relaxation was followed by resistance jumps due to a redistribution of impurities. They recorded MFP for various disorder

configurations. Completely uncorrelated MFP were obtained after application of a voltage pulse of 1.75 V for 5 s.

Gao et al [89G] examined narrow Si MOSFET's with dimensions $L = 4.3\,\mu$m and $w = 0.14$ or $0.43\,\mu$m. They took low– and high–field MC data and measured the temperature dependence of the conductance. The inelastic diffusion length was extracted as a function of T. Traces of UCF at various temperatures and two different gate voltages were studied. The amplitude of the UCF and the magnetic correlation field as functions of temperature were obtained from the data. The inelastic diffusion length obtained via a different method was examined. For the narrow device, good agreement of all data with UCF theory was found while for the wide device, the temperature dependence of B_c deviated from the theoretical predictions.

Gallagher et al [90G1] (page 143) measured MR in multi–terminal n^+–type GaAs wires and observed AF.

Fukai et al [90F4] (page 140) structured GaAs/AlGaAs on–facet wires and determined the phase coherence length at temperatures down to 50 mK via the conductance fluctuation amplitude and the conductance fluctuation correlation field.

Ochiai et al [90O1, 91I1] (page 170) structured GaAs wires and measured the longitudinal and the Hall resistance. Up to a magnetic field of 2 T, UCF were observed in R_L.

Menschig et al [90M1, 90M2, 91F2] (page 116) patterned $In_{0.53}Ga_{0.47}As$/InP wires and observed UCF at low fields.

Galloway et al [90G2] measured MR of a n^+–GaAs wire ($w = 0.5\,\mu$m, $L = 9\,\mu$m) defined by EBL and dry etching. AF appeared on a background negative MR and coexisted with SdH oscillations at higher fields. An ac voltage source was capacitively coupled to the sample and the dc voltage across the sample was measured as B was increased. Strong oscillations about zero were observed in the rectified voltage. The magnitude of the voltage fluctuations was investigated and compared with theory. When the applied potential was increased, the shape of the traces changed.

Bird et al [90B2] (page 140) observed aperiodic fluctuations in the MR of quasi–ballistic GaAs wires and extracted l_φ by comparison of the data with theory.

Taniguchi et al [90T4] (page 140) fabricated GaAs wires by EBL and two different ion–beam etching techniques and compared the amplitudes of UCF in the wires (Fig. 138).

Bird et al [91B1, 92B2] (page 170) studied the four–terminal MR of a GaAs wire. UCF were observed, they decayed with increasing temperature. At low T, a rapid decay in the high–frequency component of the UCF was found, the noise–like structure at higher fields was quasi–periodic.

Klepper et al [91K3] (page 158) fabricated GaAs wires and studied the MC for different numbers of impurities. By IR illumination of the samples, donors in a Si–doped layer adjacent to the 2DEG were ionised, adding scatterers to the device. Decorrelation of the conductance fluctuation traces was achieved by addition of a sufficiently large number of scatterers, $N_c \approx 30000$ at $T = 2.5$ K.

Ishibashi et al [92I1] (page 147) performed transport measurements in a GaAs wire defined by a split gate. As V_g became increasingly negative, AF became prominent.

Staring et al [92S2] (page 131) examined narrow GaAs wires defined by a split–gate technique. The four–terminal longitudinal conductance exhibited random structure as a function of magnetic field. In the Hall resistance, quasi–periodic oscillations as a function of magnetic field were observed in between the plateaux. Below 2 T, the Hall resistance showed random oscillations.

Taniguchi et al [91T2] (page 140) studied the temperature dependence of the amplitude of UCF in GaAs wires with strong SO scattering.

Haug et al [92H1] (page 180) fabricated narrow channels on the cleaved surface of InAs quantum

well structures and measured the MR in a four–probe configuration. Aperiodic fluctuations were observed. The fluctuations at high fields were consistent with 1D theory. They became weaker for an increasing width of the InAs well.

Gusev et al [92G4] studied two types of GaAs samples: (1) wires fabricated by EBL ($w = 0.1 - 0.2\,\mu$m, $L \approx 1\,\mu$m) and (2) wires fabricated by optical lithography ($w = 0.3 - 0.4\,\mu$m, $L = 2 - 4\,\mu$m). UCF were examined as a function of temperature. In the smaller samples, switching of the resistance was observed, which altered completely $R(B)$ after some time. In samples with a stable resistance, jumps were induced by increasing the voltage. Curves recorded before and after an induced jump corresponded to different realizations of the random potential. Illuminating a sample also changed the potential configuration and a series of measurements was performed in which the sample (type 2) was exposed for a time Δt to light with a fixed intensity.

Geim et al [92G1, 93G1] studied conductance fluctuations in multi–terminal GaAs wires ($w_{\mathrm{eff}} =$ 150, 250, 350, 450 nm, adjacent pairs of probes separated by $1\,\mu$m, $l = 34$ nm, $\omega_c\tau = 1$ at 6 T). In a local geometry, the UCF amplitude was consistent with $l_\varphi = 0.3\,\mu$m. Aperiodic resistance fluctuations were studied in a non–local geometry, the characteristic period increased with magnetic field. The correlation field varied by more than a factor of five over the available field range, the amplitude of the AF depended only weakly on B. This behaviour was inconsistent with the values of l_φ required to fit the measured correlation field. Geim et al concluded that in the regime $\omega_c\tau > 1$ the conductance fluctuations could not be scaled in terms of a single parameter.

Ishibashi et al [92I2] studied conductance fluctuations in quasi–ballistic split–gate GaAs wires ($w = 0.6\,\mu$m, $L = 2$ and $6\,\mu$m, $l = 1\,\mu$m). MR fluctuations superimposed on a negative background due to weak localization were observed at $T = 1.2$ K. The amplitude of the conductance fluctuations was examined as a function of the wire width. It increased with the width in the $2\,\mu$m long sample and eventually approached e^2/h, while it was independent of width in the $6\,\mu$m long wire and smaller than e^2/h. The correlation field was studied as a function of the wire width.

Ochiai et al [93O1] investigated UCF in two types of narrow wire samples ($w = 700$ nm, $w_{\mathrm{eff}} \approx$ 400 nm, $L = 3000$ nm, $l < 150$ nm and $w = 700$ nm, $w_{\mathrm{eff}} \approx 400$ nm, $L = 1700$ nm, $l < 430$ nm) fabricated from GaAs/AlGaAs double and single heterojunctions by EBL and dry etching. The amplitude of the UCF was of the order e^2/h for both samples and depended only weakly on magnetic field. Fourier spectra of the MR were analysed in various ranges of magnetic field. With increasing magnetic field, a reduction of the high–frequency part in the Fourier spectrum was observed which was attributed to a reduction of the effective interference area. Ochiai et al examined the correlation field B_c as a function of magnetic field. In both wires, B_c began to increase around a critical field ($\omega_c\tau = 1$) (Fig. 189). As a function of temperature, the fluctuation amplitude gradually increased with decreasing T, while there was no marked temperature–dependence in B_c. Ochiai et al concluded that the field–dependence of the UCF was inconsistent with single parameter scaling using the inelastic scattering length.

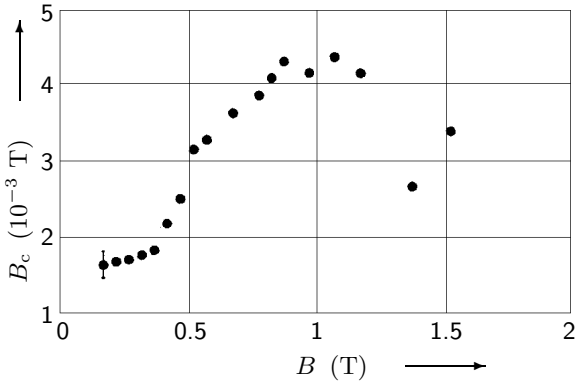

Fig. 189: Magnetic field dependence of the correlation field at $T = 1.2$ K [93O1].

Brown et al [93B2, 93M2] studied UCF in diffusive GaAs wires ($w = 350\,\mathrm{nm}$, $l = 40\,\mathrm{nm}$ and $\omega_c\tau = 3.3$ at $B = 18\,\mathrm{T}$) in a local and a non–local geometry. At low fields, conductance fluctuations of the local longitudinal MR coexisted with a negative MR due to weak localization, and for $B > 8\,\mathrm{T}$ they were superimposed on SdH oscillations. Conductance fluctuations in a Hall geometry, rectification fluctuations, and non–local fluctuations were studied. At low fields, the results were in good agreement with theory. For $\omega_c\tau > 1$, the correlation field B_c increased with increasing magnetic field, but the fluctuation amplitude did not change. In some measurements, B_c did even oscillate as a function of B. Brown et al interpreted their results in terms of two different scaling lengths for $\omega_c\tau > 1$, one responsible for the period of the UCF, the other for the amplitude.

Onishi et al [93O2, 93O3, 94O1] studied MR in split–gate GaAs wires ($w = 0.6\,\mu\mathrm{m}$, $L = 2$ and $6\,\mu\mathrm{m}$, $l = 1\,\mu\mathrm{m}$). In addition to UCF, a negative MR consistent with weak localization was observed. The phase coherence length was extracted from the data, $l_\varphi \approx 1\,\mu\mathrm{m}$ was essentially independent of the effective channel width. The correlation field B_c was smaller in the shorter wires, it increased with decreasing w_{eff}.

Ramon et al [93R] (page 142) patterned narrow GaAs wires, observed UCF, and deduced l_φ from the data.

Dietl et al [93D] reported on n–$Pb_{0.98}Mn_{0.02}Te$ wires patterned by photolithography and dry etching. Reproducible resistance fluctuations had an amplitude greater than expected from UCF theory.

Lettau et al [94L1] (page 173) investigated MR in GaAs wires and observed reproducible AF.

Morgan et al [94M4] investigated UCF in narrow Si MOSFETs ($w = 90\,\mathrm{nm}$, $L = 1.0\,\mu\mathrm{m}$, $l = 0.3\,\mu\mathrm{m}$) patterned by EBL and RIE. The longitudinal resistance (at fixed gate voltage $V_g = 4.95\,\mathrm{V}$) showed reproducible fluctuations. In the asymmetric (with respect to positive and negative B) component of the longitudinal resistance, R_{LA}, SdH oscillations were almost absent. In traces of R_{LA} at a series of gate voltages spaced by 0.1 V, little similarity between adjacent traces was observed, as the correlation scale in V_g was $\approx 20\,\mathrm{mV}$. The correlation field was constant, $B_c = 20\,\mathrm{mT}$ for $B \leq 3\,\mathrm{T}$, yielding $l_\varphi \approx 2\,\mu\mathrm{m}$. For $4\,\mathrm{T} < B < 8\,\mathrm{T}$, B_c increased. For $B > 6\,\mathrm{T}$, B_c started to oscillate (Fig. 190). For $B > 9\,\mathrm{T}$, these oscillations were clearly correlated with the SdH oscillations in the symmetric component of R_{L}.

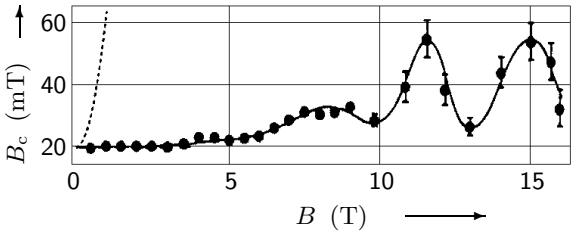

Fig. 190: Dependence of the correlation field B_c on magnetic field, averaged over several gate voltages [94M4]. The error bars indicate the standard deviation where it is larger than the symbol size. The solid line is a guide to the eye, the dotted line is a plot of $B_c(B) = B_c(0)[1 + (\omega_c\tau)^2]^{1/2}$.

Fukai et al [95F2] (page 167) fabricated InGaAs/InAlAs wires, measured UCF and investigated the temperature dependence of the fluctuation amplitude.

Ochiai et al [94O2, 94O3, 95O2] measured UCF in semi–diffusive GaAs wires ($w = 0.7\,\mu\mathrm{m}$, $w_{\mathrm{eff}} = 0.4\,\mu\mathrm{m}$, $L = 3\,\mu\mathrm{m}$, $l = 0.14\,\mu\mathrm{m}$) and investigated the correlation field as a function of B. They studied the field scales at which B_c deviated from its low–field value for different temperatures and discussed the corresponding length scales w_{eff}, l_φ, r_c. The results indicated that the high–field characteristics of the UCF depended strongly on the nature of the interference at zero magnetic field.

Shitara et al [95S] (page 181) prepared GaAs wires by overgrowth on patterned GaAs substrates,

carried out four–terminal MR measurements and observed reproducible resistance fluctuations.

Bird et al [95B2] investigated breakdown of UCF in quasi–ballistic GaAs wires. At low fields, the average amplitude and period of the MR fluctuations were field–independent. When the cyclotron orbit became smaller than the wire width with increasing B, the correlation field and the average amplitude of the fluctuations increased approximately linearly with B (Figs. 191 and 192). The temperature dependence of the average amplitude was independent of magnetic field. The linear increase in the correlation field was attributed to a transition to edge–related transport, and the increase in the average amplitude was assumed to result from a magnetically induced breakdown of correlated diffusion.

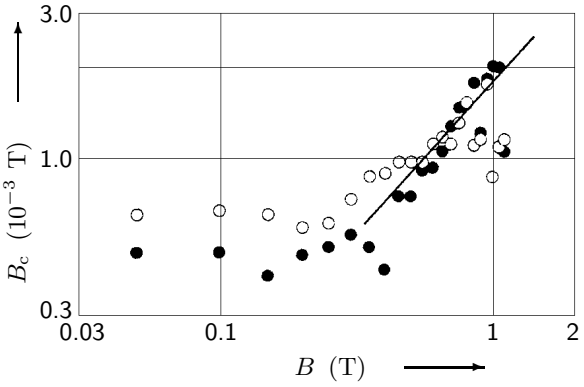

Fig. 191: Magnetic field dependence of the correlation field in a wire of width 0.74 μm at 41 mK (open circles) and 1.22 μm at 58 mK (filled circles) [95B2]. The solid line at high fields indicates the slope $B_c \propto B$.

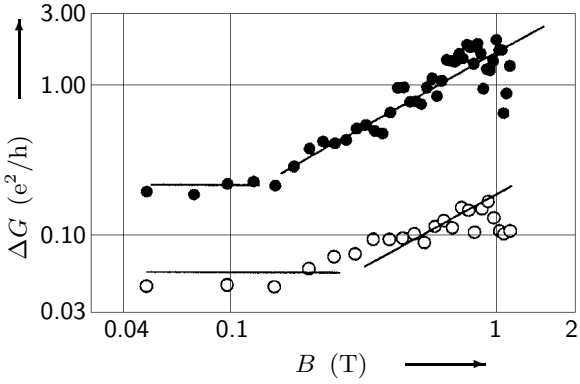

Fig. 192: Magnetic field dependence of the amplitude of the fluctuations in a wire of width 0.74 μm at 41 mK (open circles) and 1.22 μm at 58 mK (filled circles) [95B2]. The solid lines at high magnetic fields indicate the slope $\Delta G \propto B$.

Ochiai et al [95O1] investigated UCF in split–gate wires ($w = 0.6\,\mu$m, $L = 6\,\mu$m, $l = 1\,\mu$m) fabricated on a GaAs/AlGaAs heterostructure. They studied the field dependences of the correlation field B_c and of the average amplitude ΔG and identified magnetic field ranges in which B_c and ΔG exhibited a range–dependent behaviour. They studied the influence of the wire width on $B_c(B)$ and $\Delta G(B)$. Ochiai et al attributed their observations to two kinds of scattering processes affecting the phase breaking of electrons and occurring at low and high magnetic fields, respectively.

Bykov et al [96B4] (page 205) reported observation of quasi–periodic MR oscillations in a GaAs wire in the integer quantum Hall regime. Up to a magnetic field of 1 T, UCF were observed.

Omling et al [95O5] (page 174) observed reproducible aperiodic conductance fluctuations in the MR of a narrow GaAs channel.

Jaroszyński et al [95J, 96D1, 96J2] (page 181) investigated the MR of $Cd_{0.99}Mn_{0.01}Te$ and CdTe wires. The amplitude of AF in $Cd_{0.99}Mn_{0.01}Te$ was independent of magnetic field and increased with decreasing temperature. The correlation field increased with either temperature or magnetic field, a behaviour not observed in non–magnetic wires.

Noguchi et al [96N2] (page 142) measured the MC for $0.4\,\mathrm{K} < T < 30\,\mathrm{K}$ in GaAs wires and observed AF (Fig. 139).

Jaroszyński et al [98J2] studied $Cd_{1-x}M_xTe$ wires ($w = 0.3\,\mu$m) fabricated by EBL and wet etching. They underwent a spin–glass transition at $0.3\,\mathrm{K} \le T_g \le 2.2\,\mathrm{K}$ for $0.07 \le x \le 0.2$. The low–field MR was positive due to spin splitting of the conduction band. The UCF amplitude in low magnetic fields was weakly temperature dependent at $T > 0.3\,\mathrm{K}$, but it increased abruptly below 0.3 K. An increase in the conductance noise was observed in the same temperature range.

The noise was white at $T > T_g$, but behaved as $1/f^\nu$ below T_g, where $\nu = 1.3$ and 1.5 for $x = 0.07$ and 0.2 at 50 mK and $B = 0$ T. Jaroszyński et al further examined history–dependent effects.

Gompertz et al [98G2] (page 156) performed MR measurements on quasi–ballistic GaAs wires in a DQW system. UCF with relative amplitudes close to e^2/h were observed. The UCF were due to electrons tunneling between the layers and disappeared for $B > 10$ T.

Stoddart et al [98S1] (page 156) investigated two parallel GaAs wires in a DQW. For $T < 4$ K and a magnetic field applied perpendicular to the layers, the MR showed conductance fluctuations at low fields. UCF were also found for $B < 8.6$ T when the field was applied parallel to the layers, due to coherent tunneling of electrons between the QWs. The amplitude of the conductance fluctuations decreased with increasing thickness of the barrier between the layers, the correlation field was 70 ± 10 mT for all samples.

Held et al [99H2] (page 175) fabricated GaAs wires by local oxidation using an atomic force microscope. MR traces were measured at 100 mK. UCF at low fields and SdH oscillations at higher fields were observed.

7.7.3.3 Non–local geometry

Takagaki et al [89T2] observed non–local voltage fluctuations in a quasi–ballistic GaAs electron waveguide with two junctions and six leads ($w = 0.6\,\mu$m, $w_{\text{eff}} \approx 0.1\,\mu$m, $L = 1.2\,\mu$m, $l = 2.2\,\mu$m). In a crossed–wire lead configuration, they found AF and a negative average resistance at low magnetic fields. The magnetic field dependence of the resistance showed non–local voltage fluctuations (Figs. 193 and 194) which were reproducible under the same conditions, but changed after thermal cycles, suggesting that the fluctuations were sensitive to the microscopic configuration of elastic scatterers. The fluctuations were completely suppressed above 0.2 T. For a current flowing straight perpendicular to the wire, the fluctuations occurred in a wider field range.

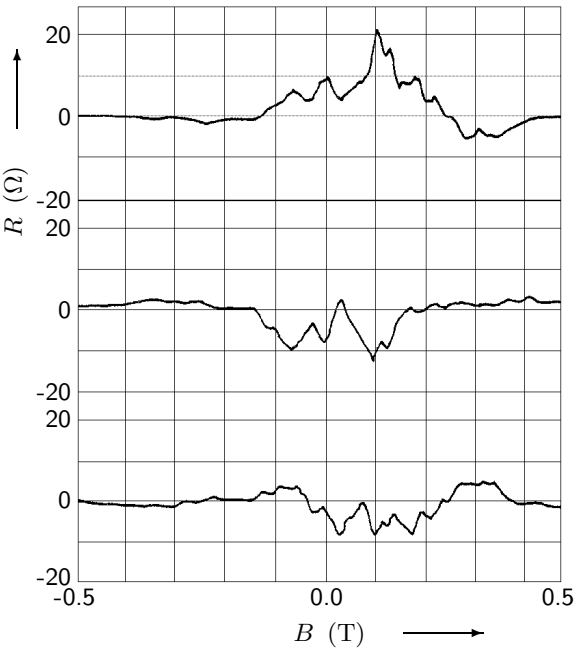

Fig. 193: Non–local voltage fluctuations for different lead configurations: (top) $R_{16,23}$, $R_{16,34}$, $R_{16,42}$ (bottom) [89T2]. Voltage terminals were 1.2 μm apart from the current path.

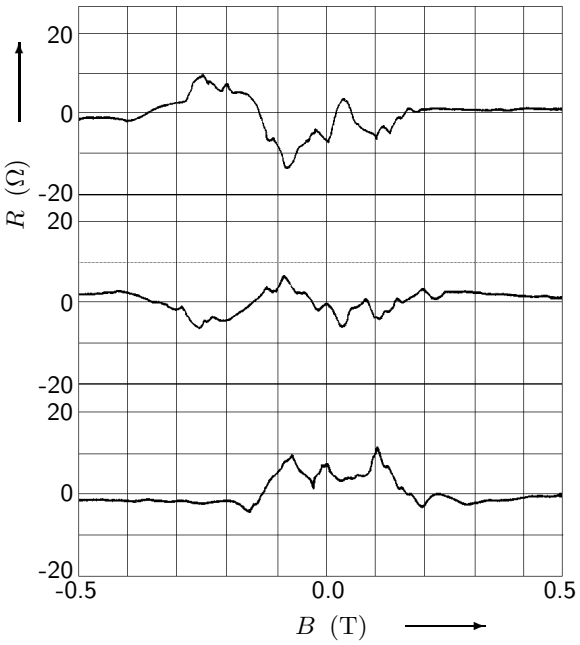

Fig. 194: Non–local voltage fluctuations for different lead configurations: (top) $R_{56,23}$, $R_{56,34}$, $R_{56,42}$ (bottom) [89T2]. Voltage terminals were 1.2 μm apart from the current path.

Takagaki et al [89T3] (page 208) fabricated multi–channel ballistic GaAs wires, performed MR measurements and observed non–local voltage fluctuations.

Takagaki et al [90T1] (page 176) defined multi–terminal narrow GaAs channels and performed four–terminal non–local resistance measurements. At low fields, quasi–periodic fluctuations with a period of 20 mT were observed which disappeared at $B \approx 0.3 - 0.4$ T. The amplitude of the oscillations was studied as a function of ΔL and temperature.

Geim at al [91G, 92G2, 93G1, 93M2] (page 176) fabricated multi–terminal GaAs wires and measured the non–local MR for different temperatures. For $T > 10$ K, the UCF were damped and a new type of oscillations was observed.

Geim et al [92G1, 93G1] (page 190) examined conductance fluctuations in multi–terminal GaAs wires. Aperiodic resistance fluctuations were studied in a non–local geometry, the characteristic period increased with magnetic field. The correlation field varied by more than a factor of five over the available field range, the amplitude of the AF depended only weakly on B.

Brown et al [93B2, 93M2] (page 191) studied UCF in diffusive GaAs wires in a local and a non–local geometry. At low fields, the results were in good agreement with theory. For $\omega_c \tau > 1$, the correlation field B_c increased with increasing magnetic field, but the fluctuation amplitude did not change.

7.7.4 Shubnikov–de–Haas oscillations

At high magnetic fields, the electron density of states splits up into Landau levels. The electron energy is then quantized, the level spacing depends on magnetic field, $\Delta E = \hbar\omega_c$, where $\omega_c = eB/m^*$ is the cyclotron frequency. Changing the magnetic field at a constant Fermi energy pushes the Landau levels through the Fermi level and the longitudinal resistance oscillates periodically in $1/B$, known as *Shubnikov–de–Haas* (SdH) *oscillations*. In a quantum wire, both, 1D geometrical quantization and Landau quantization constitute the electron density of states. At large B, $r_c < w$, the contribution due to the magnetic field dominates and the SdH oscillations are periodic in $1/B$. At lower fields, the contribution due to geometrical quantization shifts the energy levels and thus the magnetic field at which the levels cross the Fermi energy. The oscillations are then not periodic in $1/B$ but move further apart. This effect is called *magnetic depopulation of 1D subbands* (see for example [82A, 90D, 96S2] and references therein).

7.7.4.1 Local geometry

Skocpol et al [84S] (page 125) measured SdH oscillations in a narrow Si channel.

Choi et al [85C, 86C2] (page 168) measured the MR of GaAs devices of different widths. The onset of SdH oscillations occurred at larger B for smaller w.

Skocpol et al [86S1] (page 127) analysed SdH oscillations in quasi 1D Si devices.

Kaplan et al [86K2] performed MC measurements in pinched Si MOSFETs ($L = 10\,\mu$m, see also [82F, 86K3] on pages 125 and 182) at constant magnetic field as a function of V_g and at constant V_g as a function of magnetic field. The high–field oscillations appeared to be spin and valley split. The structures at lower field were evenly spaced in $1/B$, a fan diagram revealed a linear behaviour. The structure in the MC persisted to low gate voltages. Kaplan et al also varied control voltage, source–drain voltage and temperature.

Kaplan et al [86K3] (page 182) studied the MC of narrow Si channels for different angles between the field and the sample–normal (Figs. 177 and 178) and observed SdH oscillations.

Berggren et al [86B2] studied MC in GaAs samples similar to those in [86T] (see page 178)

but with a gate separation of 1.0 μm. The fan diagram in Fig. 195 illustrates the behaviour of the MC as a function of the confining voltage. Reducing the channel width below 250 nm produced a change in the slope and a deviation from the $1/B$ dependence. The MC oscillations then arose from successive magnetic depopulation of the 1D subbands.

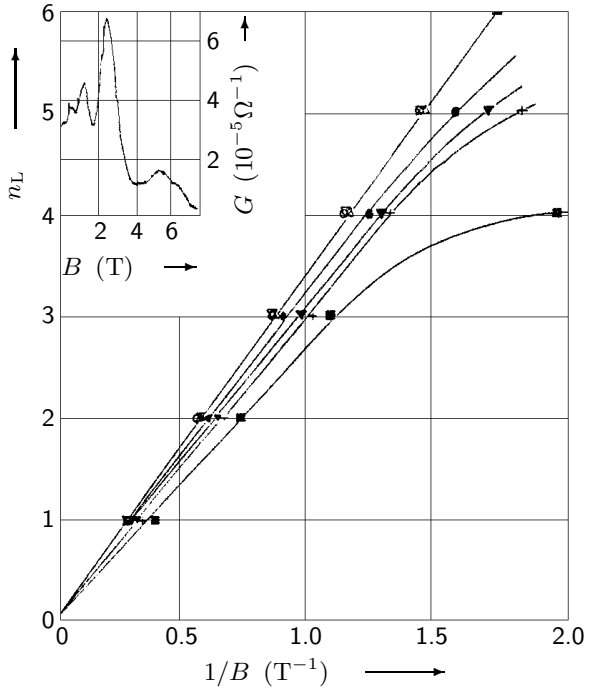

Fig. 195: Fan diagram showing the conductance maxima vs. $1/B$ for various channel widths [86B2]: $V_g = -2.50$ V (open downward triangle), -2.70 V (open upward triangle), -2.80 V (open circle), -2.90 V (times), -3.00 V (closed circle) -3.05 V (closed downward triangle), -3.13 V (cross), -3.20 V (closed box). Inset: MC oscillations for a channel of width 150 ± 20 nm ($V_g = -3.2$ V, $T = 0.35$ K).

Zheng et al [86Z2] (page 145) realized a 1D channel by a split gate and observed an increase in the oscillation period in the SdH oscillations with decreasing V_g, indicating a decreasing electron density.

Van Houten et al [86vH] (page 145) performed SdH measurements in GaAs was wires.

Whittington et al [86W3] (page 182) studied the MR of small n^+GaAs wires and observed SdH oscillations.

Taylor et al [88T2] (page 180) measured negative MR and UCF in GaAs structures and observed SdH oscillations at high fields.

Grassie et al [87G1] studied SdH oscillations in wet–etched GaAs wires ($w \approx 0.4\,\mu$m, $w_{eff} \approx 0.12\,\mu$m). The amplitude of the oscillations was smaller in narrow wires than in wide ones. By comparison with theory, the scattering rate was extracted which was insensitive to temperature in the narrow wires. Grassie et al attributed this to the influence of the sample walls.

Van Houten et al [87vH] fabricated 10 μm long narrow GaAs channels of widths $w = 0.5$, 1.5, and 8 μm using a shallow etch technique and measured the low– and high–field MR. The effective widths of the channels were smaller than the nominal ones due to depletion. A MR trace for the $w = 1.5\,\mu$m wide sample is shown in Fig. 196. The structure at low fields was attributed to UCF, at large fields SdH oscillations appeared. For the two narrower samples, the Landau level index as a function of B^{-1} (Fig. 197) showed deviations from a linear behaviour, indicating depopulation of 1D subbands.

Asai et al [87A3] reported a method of fabricating narrow channels ($w = 4\,\mu$m) on GaAs/AlGaAs sidewall interfaces through selective growth using metal organic chemical vapour deposition. SdH oscillations were measured. The existence of a 2DEG was confirmed from the angular dependence of the SdH oscillations.

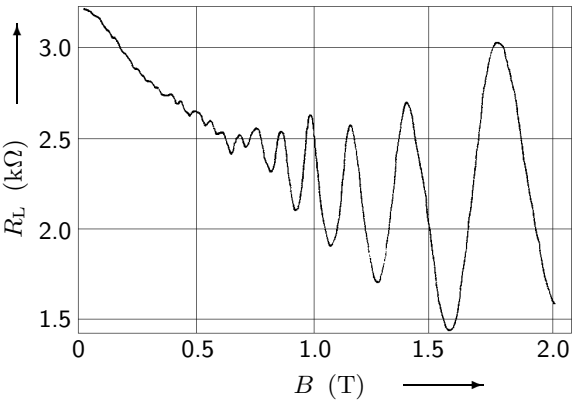

Fig. 196: MR for the 1.5 μm wide sample at $T = 2.4$ K [87vH].

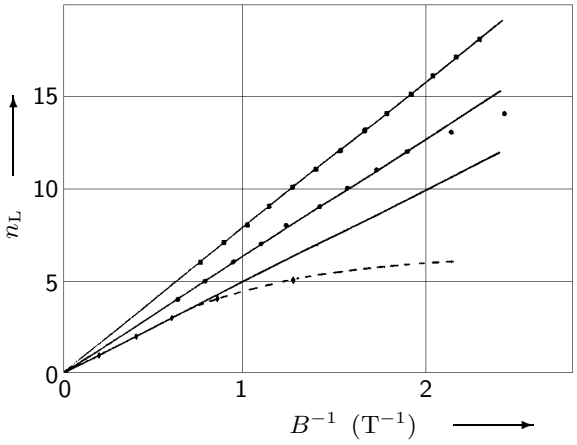

Fig. 197: Landau level index vs. B^{-1} for (top) $w = 8.0\,\mu$m, $1.5\,\mu$m, $0.5\,\mu$m (bottom) at 2.4 K [87vH]. The dashed line represents a fit of the parabolic confinement model.

Timp et al [88T3] (page 207) measured the four–terminal MR of a GaAs electron waveguide. At high magnetic fields, they observed SdH oscillations.

Lakrimi et al [89L2] studied GaAs wires fabricated by wet etching. They measured SdH oscillations and analysed the corresponding Dingle plots. They observed a deviation from linearity at low fields in a number of wires with nominal widths less than 1.0 μm and compared their results with theory.

Takagaki et al [89T3] (page 208) examined multi–channel ballistic GaAs wires and observed SdH oscillations for magnetic fields above 1 T.

Gallagher et al [90G1] (page 143) observed SdH oscillations in multi–terminal n^+–type GaAs wires.

Ochiai et al [90O1, 91I1] (page 170) structured GaAs wires and measured the longitudinal and the Hall resistance. For magnetic fields above 2 T, SdH oscillations occurred. The Landau level index vs. $1/B$ deviated from a straight line for $B^{-1} < 0.4\,\mathrm{T}^{-1}$.

Menschig et al [90M1, 90M2, 91F2] (page 116) measured MR in $In_{0.53}Ga_{0.47}As/InP$ wires. SdH oscillations were periodic in a 310 nm wide wire and non–periodic in a 80 nm wide wire (Fig. 110).

Galloway et al [90G2] (page 189) measured the MR of a n^+–GaAs wire and observed SdH oscillations.

Bird et al [90B2] (page 140) observed 1D subband depopulation and SdH oscillations above 0.4 T in quasi–ballistic GaAs wires.

Bird et al [91B1, 92B2] (page 170) studied the four–terminal MR of a GaAs wire. At large magnetic fields ($r_c < w$) and high T, smooth SdH oscillations were observed.

Nakata et al [91N] (page 147) performed MR measurements on GaAs wires and observed SdH oscillations. A deviation of $1/B$ vs. n_L from a straight line was attributed to magnetic depopulation of 1D subbands.

Ochiai et al [91O1] structured quasi–ballistic four–terminal GaAs wires ($w_{eff} \approx 0.4\,\mu$m, $L = 2\,\mu$m) by EBL and dry etching and studied scattering processes by means of amplitude analysis of SdH oscillations. The amplitudes of the SdH oscillations vs. $1/B$ showed two slopes. The cross over field shifted to higher fields when the effective conduction width was reduced. Ochiai et al

discussed and compared various scattering times and examined size effects.

Feng et al [92F2, 92F1] (page 147) fabricated wires from δ–doped GaAs and inferred from SdH oscillations that the electron density remained constant over the measured range of V_g.

Geim at al [91G, 92G2, 93G1, 93M2] (page 176) fabricated multi–terminal GaAs wires, measured MR and observed SdH oscillations (Fig. 171).

Wróbel et al [92W2] (page 118) prepared a two–terminal GaAs wire, measured the MR, observed SdH oscillations and fitted the level index vs. $1/B$ by 1D theory.

Ishibashi et al [92I1] (page 147) performed transport measurements in a GaAs wire defined by a split gate. The MR showed SdH oscillations at zero gate voltage. As V_g became increasingly negative, the SdH oscillations decayed.

Ochiai et al [91O2, 92O1] (page 171) studied MR in four–terminal GaAs wires fabricated by EBL and dry etching and in two–terminal split–gate wires. An amplitude analysis of SdH oscillations revealed two different scattering times at high and low magnetic fields in the etched wires. In the split–gate system, SdH oscillations became weaker with increasing V_g, only one relaxation time was observed at zero gate voltage, while at $V_g = -1.0\,\mathrm{V}$ again two relaxation times were found.

Haug et al [92H1] (page 180) fabricated narrow channels on the cleaved surface of InAs quantum well structures and measured the MR in a four–probe configuration. In a 80 nm wide channel, SdH oscillations were observed for $B > 5\,\mathrm{T}$.

Blaikie et al [92B3] (page 148) measured the MR of GaAs wires and observed SdH oscillations.

Tang et al [92T2, 93T2] (page 118) performed four–terminal MR measurements on Si MOSFETs. They observed SdH oscillations, investigated the subband index vs. $1/B$ and found deviations from a linear behaviour at high $1/B$.

Hirayama et al [92H2] (page 153) examined four–terminal transport through two in–plane gated parallel GaAs wires coupled by a ballistic window. The longitudinal resistance as a function of magnetic field showed SdH oscillations.

Block et al [93B1] (page 171) studied the MR of wires fabricated from $In_{0.53}Ga_{0.47}As/InP$ heterostructures and observed SdH oscillations (Fig. 167).

Yoh et al [92Y2] fabricated wires ($w = 200 - 800\,\mathrm{nm}$) on InAs/AlGaSb heterostructures by EBL and wet–chemical etching. In the MR of a 350 nm wide wire, spin–splitting of the Landau levels was more pronounced than in the 2DEG. The maximum conductance points coincided in both cases except at low B. Quenching of the Hall resistance was observed. The level index n_L vs. $1/B$ for the 350 nm wide wire deviated from the linear behaviour in the low magnetic field region.

Brown et al [93B2, 93M2] (page 191) studied UCF in diffusive GaAs wires in a local and a non–local geometry. For $B > 8\,\mathrm{T}$, they were superimposed on SdH oscillations.

Main et al [94M2, 94G3] (page 172) studied MR in multi–terminal GaAs wires using local and non–local lead configurations. Strong resistance fluctuations were observed in the SdH oscillations at temperatures of 300 and 600 mK (Fig. 168).

Nakata et al [93N, 94N2] (page 150) measured the MR of buried GaAs wires. The number of SdH oscillations decreased with decreasing wire widths. The Landau level index vs. inverse magnetic field deviated from a linear behaviour for $w < 0.6\,\mu\mathrm{m}$.

Geim et al [94G4] (page 205) examined the quantum Hall effect in three types of GaAs multi–terminal devices: (A) $w \approx 1\,\mu\mathrm{m}$, $L = 10 - 20\,\mu\mathrm{m}$, exposed to bombardment by α particles; (B) $w \approx 1\,\mu\mathrm{m}$, $L = 10 - 20\,\mu\mathrm{m}$; (C) as sample B but with the width of the leads increasing rapidly from ≈ 1 to $10\,\mu\mathrm{m}$. They measured R_L at different temperatures, in sample A the amplitudes of the SdH oscillations above 3T decreased considerably as T decreased. In sample C, the high–field

SdH peaks became narrower at low temperatures, but their amplitudes remained nearly constant. Device B exhibited an intermediate behaviour.

Van der Burgt et al [93vdB] (page 205) investigated the quantum Hall effect in GaAs wires. Traces for R_L and R_H for a 200 nm wide wire showed a plateau–like structure in R_H and SdH oscillations in R_L (at $T = 22 - 25$ K).

Lettau et al [94L1] (page 173) measured MR in GaAs wires. Above 1 T, R_L exhibited oscillations arising from magnetic depopulation of 1D subbands. A Landau plot deviated from a linear $1/B$ behaviour. At sufficiently high B, the period of the SdH oscillations was consistent with a 2D theory.

Morgan et al [94M4] (page 191) investigated UCF in narrow Si MOSFETs. For $B > 9$ T, oscillations in the correlation field as a function of B were correlated with the SdH oscillations.

Honda et al [95H3] (page 120) observed quantized conductance in 2 to 30 μm long GaAs wires (Fig. 117). They determined subband spacings from magnetic depopulation measurements.

Shitara et al [95S] (page 181) prepared GaAs wires by overgrowth on patterned GaAs substrates, carried out four–terminal MR measurements and observed SdH oscillations.

Park et al [95P1, 95P2] (page 176) measured the MR of AlGaAs/GaAs wires. In local probe configurations they observed SdH oscillations which contained small oscillations between the plateaux for $B > 3$ T. In non–local probe configurations, they found fine oscillations superimposed on non–local SdH oscillations.

Bykov et al [96B4] (page 205) observed SdH oscillations in a GaAs wire.

Okada et al [95O3] (page 122) fabricated in–plane gate GaAs wires and observed SdH oscillations at $T = 4.2$ K for several values of V_g. Landau plots showed deviations from a linear behaviour for $V_g = -0.25$ V and $B^{-1} > 0.8\,\mathrm{T}^{-1}$.

Bergmann et al [96B3] (page 154) investigated magneto transport in periodically modulated InGaAs wires and observed SdH oscillations.

Koester et al [96K3] (page 181) observed SdH oscillations in Si wires for $|B| > 1$ T.

Widjaja et al [96W] (page 154) measured MR in wires defined by a split–gate in which one gate included a corrugation that produced a set of coupled quantum dots. They observed SdH oscillations.

Gusev et al [98G3] (page 174) measured MR in a non–uniform magnetic field. For $T = 1.5$ K, fields up to 10 T, and different angles ϕ between the field an the normal substrate plane, they found SdH oscillations. As the field was tilted away from the normal direction, the SdH oscillations shifted to higher fields, their period was not constant on a $1/B$ scale. Gusev et al determined a critical angle ϕ_c at which the SdH oscillations changed their behaviour. Their amplitude decreased when ϕ approached ϕ_c and increased again for $\phi > \phi_c$.

Okada et al [97O] (page 150) measured the MR of in–plane gate GaAs wires and wrap–gate InGaAs wires. Both showed SdH oscillations at $T = 4.2$ K. Landau plots deviated from a linear behaviour at low magnetic fields, indicating 1D transport.

Herfort et al [97H] structured undoped GaAs wires defined by a positively biased narrow top gate ($w = 0.4 - 1.0\,\mu$m). Four–terminal MR measurements were performed at $T = 1.6$ K for different V_g and SdH oscillations were observed. Landau plots deviated from a linear $1/B$ behaviour at weak magnetic fields, indicating 1D quantization. Herfort et al estimated the effective wire widths. At very low B, R_L showed a large positive MR while R_H was quenched.

Stoddart et al [98S1] (page 156) investigated two parallel GaAs wires in a DQW. For $T < 4$ K and a magnetic field applied perpendicular to the layers, the MR showed conductance fluctuations

at low fields followed by SdH oscillations at larger fields.

Held et al [99H2] (page 175) fabricated GaAs wires by local oxidation using an atomic force microscope. MR traces were measured at 100 mK. UCF at low fields and SdH oscillations at higher fields were observed. The sublevel index vs. inverse magnetic field showed a non–linear behaviour indicating quantum confinement.

7.7.4.2 Non–local geometry

Takaoka et al [90T3] fabricated a multi–terminal GaAs wire ($w = 0.4\,\mu$m, $w_{\text{eff}} \approx 0.1 - 0.2\,\mu$m, $L = 0.4 - 3.4\,\mu$m, $l = 0.8\,\mu$m) by EBL and shallow RIE. They measured non–local SdH oscillations (Figs. 198 and 199) for various distances between current and voltage probes, ΔL. The amplitude of the SdH oscillations decreased with increasing ΔL, an exponential decay was assumed. The decay length increased with decreasing Landau indices or increasing magnetic fields. The dependence of the negative transfer resistance on ΔL was investigated.

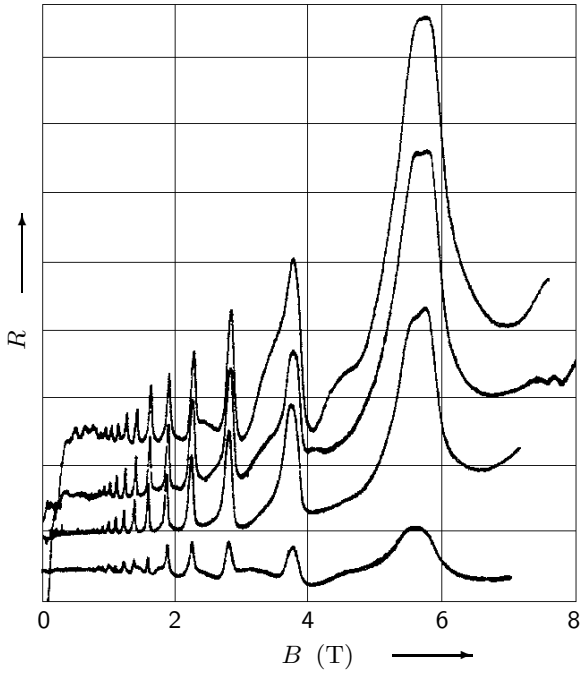

Fig. 198: Non–local SdH oscillations for (top) $\Delta L = 0.4\,\mu$m, $1.1\,\mu$m, $2.9\,\mu$m, and $3.4\,\mu$m (bottom) in the high magnetic field range [90T3]. The curves were shifted vertically for clarity. The horizontal lines have distances of $100\,\Omega$ from each other.

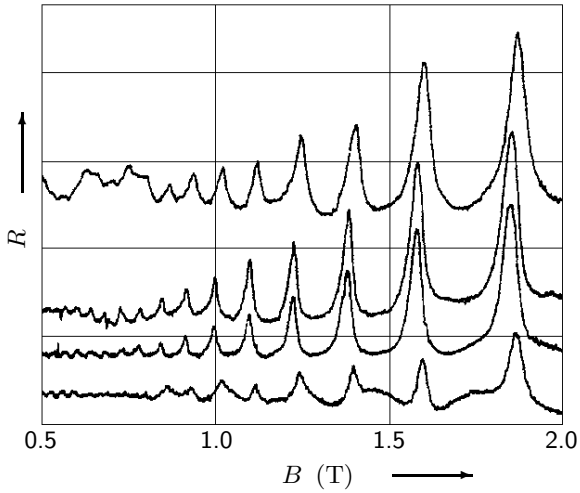

Fig. 199: Non–local SdH oscillations for (top) $\Delta L = 0.4\,\mu$m, $1.1\,\mu$m, $2.9\,\mu$m, and $3.4\,\mu$m (bottom) in the low magnetic field range [90T3]. The curves were shifted vertically for clarity. The horizontal lines have distances of $50\,\Omega$ from each other.

Takaoka et al [91T1, 92T1] measured the non–local MR of macroscopic ($w = 20\,\mu$m, $\Delta L = 0.5$ mm) multi–terminal GaAs wires together with the Hall resistance. The non–local SdH oscillations decreased with increasing current and increased with decreasing temperature from 4.2 K to 1.7 K. The dependence on carrier concentration was examined by generating persistent photo–carriers. The detailed structure of the non–local SdH oscillations varied and the oscillation peaks shifted to higher magnetic fields with increasing carrier concentration. The non–local SdH oscillations were explained by a theory taking into account bulk and edge currents. Influence of the contact resistance on the non–local resistance was examined.

Tsukagoshi et al [91T4, 92T1] (page 176) investigated the non–local resistance in mesoscopic

multi–terminal GaAs wires. The amplitude of non–local SdH oscillations decreased with increasing ΔL (distance between current and voltage probes), it decreased greatly when extra probes were contained between current and voltage probes. In a wide sample, non–local SdH oscillations were observed up to $\Delta L = 1.5\,\mathrm{mm}$.

Tsukagoshi et al [92T3] examined the gate–voltage dependence of the non–local SdH oscillations in high–mobility multi–terminal GaAs wires with a Schottky gate. The gate was positioned across a non–local path. With decreasing V_g (ranging from $+0.2$ to $-0.1\,\mathrm{V}$), the peaks in the SdH oscillations vanished. The peaks due to the up–spin states decreased first, then those due to the down–spin states followed. These features were observed at $T = 0.5$ and $1.7\,\mathrm{K}$. The diminishing of the non–local SdH oscillations (at $-0.1\,\mathrm{V}$) was attributed to the cut–off of the bulk current by the gate voltage (pinch off was at $-0.45\,\mathrm{V}$).

Park et al [95P1, 95P2] (page 176) measured the MR of AlGaAs/GaAs wires. In local probe configurations, they observed SdH oscillations which contained small oscillations between the plateaux for $B > 3\,\mathrm{T}$. In non–local probe configurations, they found fine oscillations superimposed on non–local SdH oscillations. The period of the fine oscillations decreased with increasing magnetic field. Park et al analysed their data in terms of mixing of edge states.

7.7.5 Quantum Hall effect

For an introduction into the Quantum Hall effect [80vK] see for example [86vK, 87A2, 87Y, 92J1, 97F, 97I1, 97J1, 97J2, 98D] and references therein.

At junctions in ballistic conductors, electron collimation takes place, i. e. the longitudinal momentum of the electrons is enhanced at the expense of the perpendicular momentum. The angular distribution of injection is concentrated along the axis of the wire, thus the electrons have a low probability of entering voltage probes at the sides of the wire. Even for a small magnetic field, the Lorentz force is not sufficient to drive the electrons into the probes. The Hall voltage, which rises as $R_\mathrm{H} \propto B$ at small B in large system without collimation, is *quenched* until the magnetic field is large enough to overcome the enhanced direct transmission. Then, the first Hall plateau develops. By structuring mirrors with angles of 45° with respect to the main stream at the junctions, even negative Hall resistances may be obtained, as the carriers are reflected by the mirrors and then enter the wrong voltage probe. Introducing an obstacle in the middle of the junction reduces direct transmission and may enhance the Hall effect above the classical value. These effects can be explained classically using a billiard ball model (see for example [89B1, 92W1, 96S2, 98T2] and references therein).

Zheng et al [86Z1] structured four–terminal GaAs samples by chemical etching and measured the MR of wide ($w = 300\,\mu\mathrm{m}$, $L = 2100\,\mu\mathrm{m}$), short narrow ($w = 1\,\mu\mathrm{m}$, $L = 4.2\,\mu\mathrm{m}$), and long narrow ($w = 1\,\mu\mathrm{m}$, $L = 72\,\mu\mathrm{m}$) devices. Differences in the characteristic features of the QHE were observed. In the long narrow channel, R_L appeared saw–toothed with the peak positions shifted to lower B with respect to the wide sample. In addition, the peak amplitude was reduced by a factor of eight. The Hall plateaux were asymmetric about complete filling of their respective Landau levels. Zheng et al studied the development of these narrow–channel characteristics as a function of channel width. They found that they diminished when the probe spacing was reduced to several micrometers. Comparing a $600\,\mu\mathrm{m}$ wide with a $3\,\mu\mathrm{m}$ wide sample at different temperatures showed that at $4.2\,\mathrm{K}$ the peaks in R_L in the two samples were similar and as T was lowered to 1.2 and $0.6\,\mathrm{K}$, the peak observed in the narrow channel decreased in amplitude and became increasingly saw–toothed.

Timp et al [87T3] measured the MR of wires of lengths from $700\,\mathrm{nm}$ to $4.7\,\mu\mathrm{m}$ and widths from 75 to $220\,\mathrm{nm}$ fabricated on modulation doped GaAs/AlGaAs by EBL and RIE. The width was comparable to λ_F, the distance between the voltage probes was less than l. MR data for R_L

and R_H is shown in Figs. 200 and 201, respectively. The zero–resistance states in R_L and the Hall plateaux in R_H corresponded to the Landau indices 0, 1, and 2. AF were observed both in R_L and R_H, negative dynamic resistances were observed at 35 mK and the amplitude of the conductance fluctuations exceeded e^2/h. The amplitude and the typical spacing of the fluctuations varied with magnetic field.

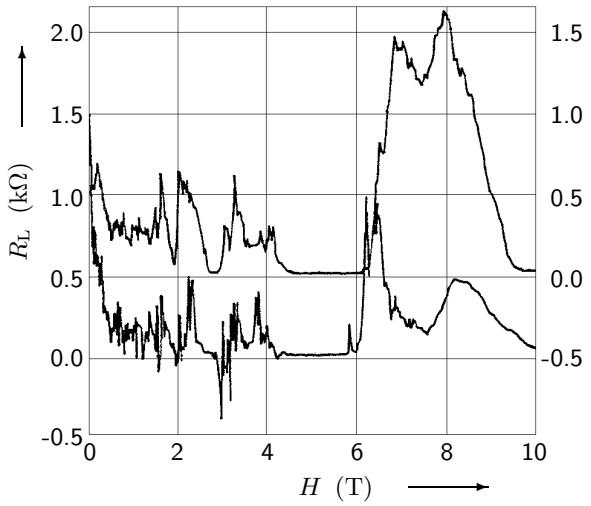

Fig. 200: R_L of a 900 nm long segment for (upper curve, right axis) $T = 400$ mK, (lower curve, left axis) $T = 35$ mK [87T3].

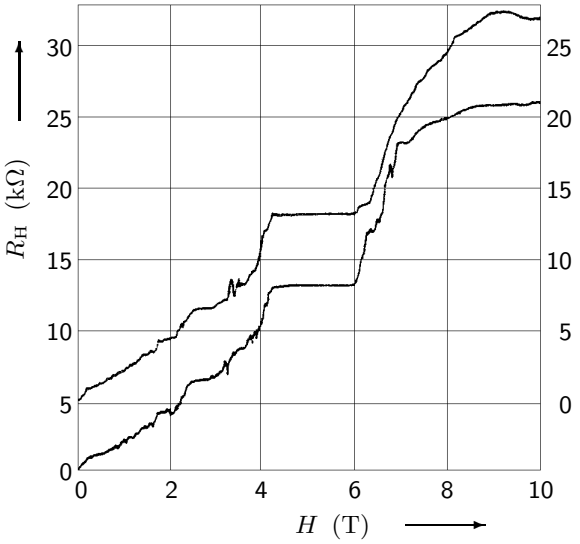

Fig. 201: R_H of a 900 nm long segment for (upper curve, right axis) $T = 400$ mK, (lower curve, left axis) $T = 35$ mK [87T3].

Simmons et al [88S3] (page 168) performed MR measurements on doubly connected rings and standard Hall bridges made from GaAs/Al_xGa_{1-x}As heterostructures. They observed an anomalous step in the Hall resistance at $B \approx 1$ kG in the Hall bridges.

Scherer et al [87S1, 88R] reported the fabrication of conducting channels as narrow as 75 nm by etching only through the thin GaAs cap layer. Sidewall depletion was avoided, carrier density and mobility in the channels were at least as high as in the 2DEG. The MR showed Hall plateaux.

Roukes et al [87R] reported the first quenching of the Hall effect in narrow GaAs channels fabricated by EBL and ion–beam assisted etching. MR data from a 100 nm wide channel is displayed in Fig. 202, showing well–defined integral QH plateaux. The inset of Fig. 202 shows the low–field Hall resistance of a 75 nm wide wire at two different temperatures, demonstrating a quenching of R_H in the case of the smaller temperature. The width dependence of this effect was studied in numerous wires, quenching was observed for $w \leq 200$ nm.

Timp et al [88T3] (page 207) measured the four–terminal MR of a GaAs electron waveguide. At high magnetic fields, they observed the quantized Hall effect.

Chang et al [88C1] examined narrow GaAs/AlGaAs heterostructures of (A) low mobility, $w \approx 200$ nm, $L > 10\,\mu$m, and (B) high mobility, $w \approx 80 - 220$ nm, $L > 6\,\mu$m. By EBL and RIE they structured rings (devices 1 and 2, material A) and a wire (device 3, material B). They measured R_L and R_H in device 1 and R_H in device 2 as a function of B at $T = 50$ mK (Fig. 203). The $\nu = 4$ Hall plateau showed large AF. The R_L minimum showed similar features, a negative resistance was attributed to the non–local nature of the voltage measurement. Deviations of the $\nu = 4$ plateau from its quantized value were found in device 3. The AF in R_H increased with decreasing temperature (Fig. 204). In device 1, the minimum in R_L at $\nu = 2$ showed a stronger temperature dependence than the one at $\nu = 4$. Chang et al discussed finite size quantum percolation effects

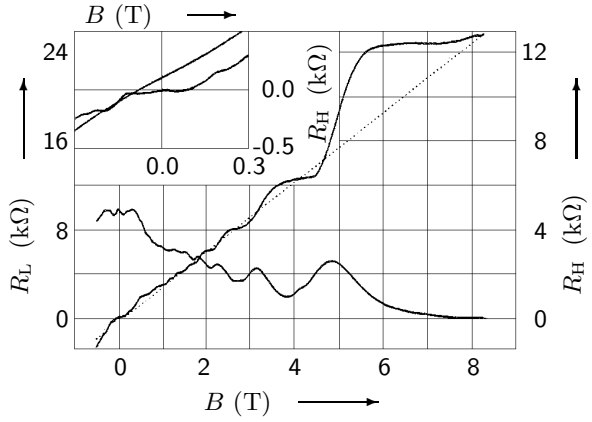

Fig. 202: Longitudinal (left top) and Hall (left bottom) resistance for a 100 nm wide wire at $T = 4.2$ K [87R]. The dotted line is the classical Hall resistance. The inset shows the Hall resistance near $B = 0$ T for a 75 nm wide wire at 4.2 K (curve that is suppressed at $B = 0$ T) and at ≈ 50 K.

and quantum interference effects as possible origins of the deviation of the Hall plateau from its quantized value.

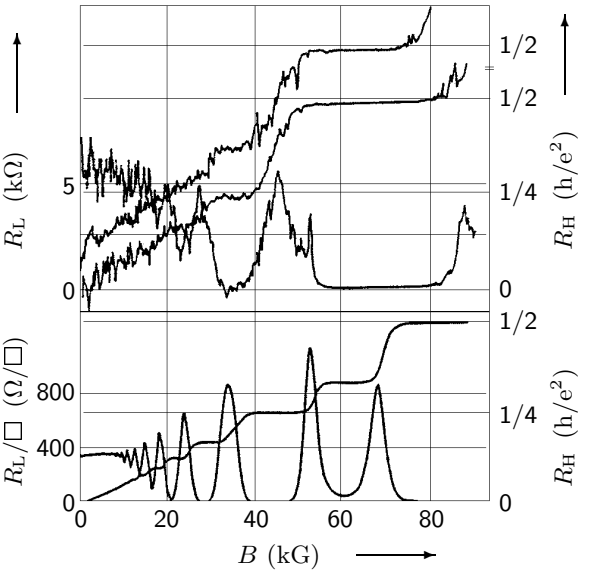

Fig. 203: R_L and R_H vs. B for devices 1 and 2 (top) and results for a wide device made from the same crystal as 1 and 2 (bottom) [88C1]. Top curve in the upper picture is $R_{H,2}$, second curve from the top is $R_{H,1}$, bottom curve is $R_{L,1}$.

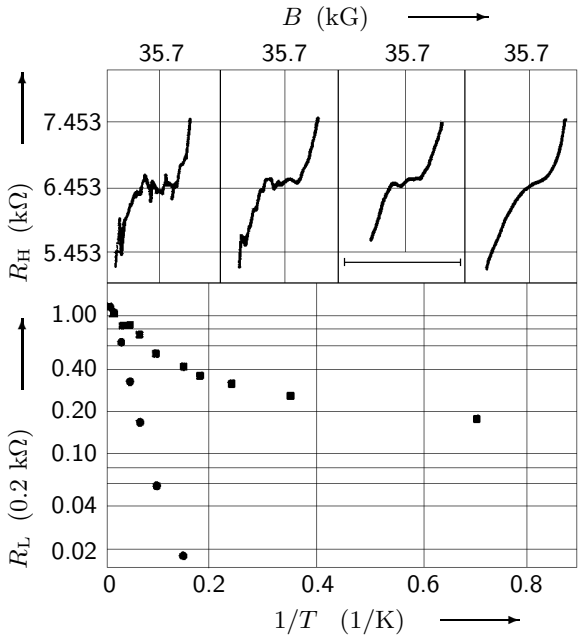

Fig. 204: The $i = 4$ Hall plateau at (upper picture, left) $T = 50$ mK, 0.6 K, 1.5 K, and 4 K (right). The horizontal bar denotes 20 kG. Lower picture is a semilog plot of R_L vs. $1/T$ at the $i = 4$ (boxes) and $i = 2$ (circles) minima in device 1 (bottom) [88C1].

Ford et al [88F2] studied narrow GaAs Hall bars ($w = 1\,\mu$m, $L \approx 3\,\mu$m) defined by a Schottky gate for $V_g \leq -0.6$ V. The effective channel width could be reduced continuously from $0.9\,\mu$m to $\approx 0.1\,\mu$m until pinch off at $V_g \approx -3.25$ V. They studied the Hall voltage as a function of channel width (Fig. 205) and found deviations from the classical behaviour for low B. For $V_g < -2.2$ V, the Hall voltage was quenched at low magnetic fields and fluctuated reproducibly about zero. The quenched region of the Hall resistance was studied for a large number of gate voltages.

Washburn et al [88W3] studied the effect of narrow barriers on transport in GaAs/$Al_xGa_{1-x}As$

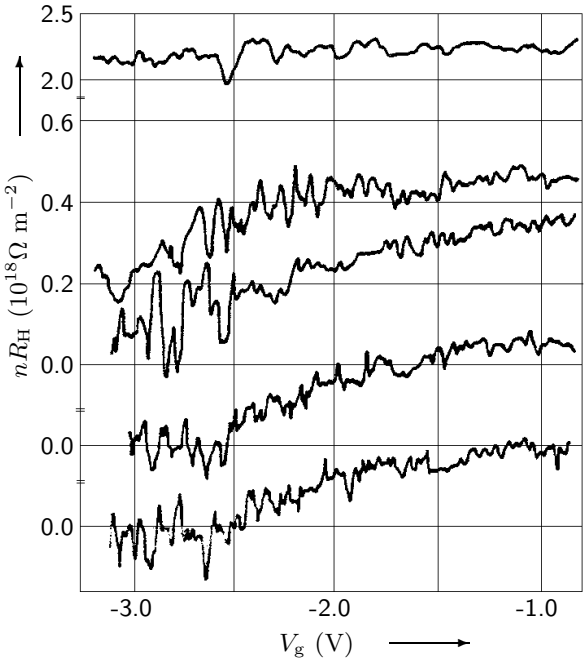

Fig. 205: Product of R_H and n (carrier concentration) vs. V_g for (top) $B = 0.380$ T, 0.078 T, 0.062 T, 0.047 T, and 0.039 T (bottom) [88F2]. The origins of the lower two curves have been offset, the scale for the uppermost curve has been reduced by a factor of 3.

samples with $w = 2\,\mu$m, $L = 10\,\mu$m, $l_\varphi \approx L$. They measured $R_{12,43}$ and $R_{13,42}$ as functions of magnetic field at $V_g = 0$ V (Fig. 206). They varied V_g at constant $B = 5.16$ T (Fig. 207) and found plateaux in $R_{12,43}$ and $R_{13,42}$ quantized at $h/4e^2$ and $h/2e^2$ for $-0.32\,\text{V} < V_g < -0.25\,\text{V}$. The difference $R_{13,42} - R_{12,43}$ varied around $h/4e^2$. For $1\,\text{T} < B < 3\,\text{T}$, no quantized plateaux were found. Measuring $R_{13,42}$ vs. V_g at several values for B, the locations of the plateaux were observed to depend smoothly on B.

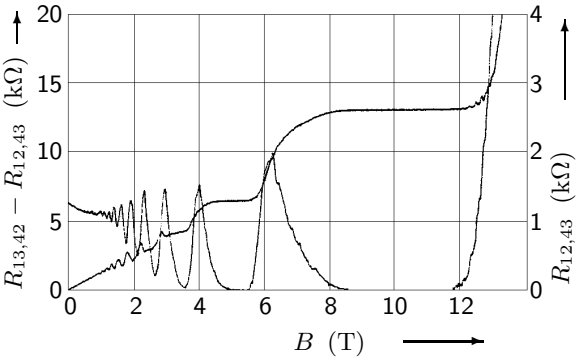

Fig. 206: Resistances $R_{12,34}$ (oscillating curve, right axis) and $R_{13,42} - R_{12,43}$ (step–like curve, left axis) at $V_g = 0$ V and $T = 0.9$ K vs. magnetic field [88W3].

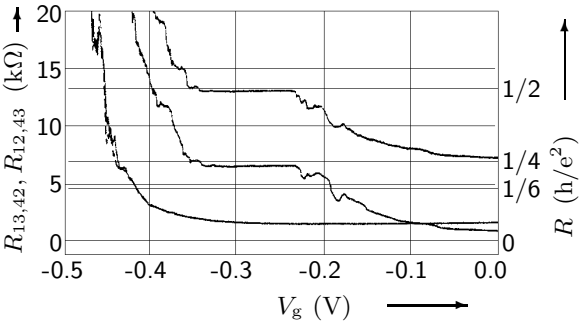

Fig. 207: Resistances $R_{12,43}$ and $R_{13,42}$ (two upper solid curves) as functions of gate voltage at $B = 5.16$ T and $T = 0.9$ K [88W3]. For reference, the behaviours of $R_{12,43}$ (lower solid curve) and $R_{13,42}$ (dashed curve) at $B = 0$ T are displayed as well.

Ford et al [89F2] (page 151) studied different ballistic GaAs samples with two cross regions 6 μm apart, joined by a straight narrow channel of constant width. The Hall resistance vs. B is shown in Figs. 150, 151, and 152. The quenching disappeared for $T \geq 10$ K, the negative R_H survived up to 20 K.

Takagaki et al [89T3] (page 208) fabricated multi–channel ballistic GaAs wires, performed MR measurements and and compared the longitudinal resistance, the bend resistance, and the Hall

resistance.

Ford et al [90F3] (page 208) extended previous studies (see [89F2] on page 151) on how the geometry of a cross region affected the Hall resistance.

Simmons et al [89S3, 91S1] structured a narrow multi–terminal GaAs Hall bar ($w = 2$ and $2.5\,\mu$m) by photolithography and wet–etching techniques. They measured R_L and R_H around $\nu = 2$ and found: (1) high–frequency fluctuations of period ≈ 0.016 T were present on the shoulders of the minimum in R_L; (2) further from the minimum, the fluctuations shifted to a period of $\approx 0.05 - 0.10$ T; (3) the fluctuations dropped below resolution for a broad B range in the centre of the minimum; (4) as T was raised, the low–frequency resistance peaks remained relatively unchanged, while the high–frequency peaks diminished rapidly. This general behaviour was also observed near the R_L minima for other integer ν. At the high–B side of $\nu = 1/3$, high–frequency fluctuations were present near the minimum, no fluctuations were present for a broad B range in the centre. The period was $0.05\,\mathrm{T} \pm 25\%$. When cycling the sample to 300 K and back to 25 mK, the particular pattern of fluctuations changed, but not the period. For other probe combinations, the resistance fluctuations near the minima in R_L were similar to those already observed. The typical amplitudes of the fluctuations were $\approx 25\,\Omega$ near $\nu = 3$ and 4; $\approx 100 - 200\,\Omega$ near $\nu = 2$; $\approx 50\,\Omega$ near $\nu = 1$, and $\approx 100 - 200\,\Omega$ near $\nu = 1/3$. Simmons et al also investigated the correlation between fluctuation patterns from various probe configurations. They investigated the dependence of the fluctuations on temperature and on current. Finally, they discussed their results in terms of a model of inter–edge–state tunneling via disorder–induced magnetically bound states. They interpreted the difference in fluctuation periods for integer ν and $\nu = 1/3$ as a manifestation of the fractional charge $e/3$

Ochiai et al [90O1, 91I1] (page 170) structured GaAs wires and measured the longitudinal and the Hall resistance. The latter did not show perfect plateaux.

Takagaki et al [90T2] (page 208) fabricated narrow crossed GaAs wire junctions and studied the bend resistance and the Hall resistance. The observed quenching of the Hall resistance.

Kakuta et al [91K2, 92K2] (page 208) fabricated a cross–shaped GaAs junction with four side gates. The corners of each wire were rounded. The average slope of the Hall resistance was almost zero at $V_g = 0$ V and became negative with increasing V_g. The average slope of the negative R_H as a function of V_g was studied. Around $B = 0.1$ T, a positive peak in R_H appeared, at that field r_c coincided with the curvature radius of the widened cross.

Staring et al [92S2] (page 131) examined narrow GaAs wires defined by a split–gate technique. In the Hall resistance, quasi–periodic oscillations as a function of magnetic field were observed in between the plateaux while the Hall resistance showed random oscillations below 2 T.

Blaikie et al [92B3] (page 148) measured the MR of GaAs wires and observed quantized plateaux in R_H.

Alphenaar et al [92A2] fabricated a standard Hall bar and formed a narrow channel near the centre of the Hall bar by applying a gate voltage $V_g < -0.3$ V on a split gate ($w = 0.5 - 1.5\,\mu$m, $L = 8.5\,\mu$m). In the fractional quantum Hall regime ($\nu = 1/3$), a four–terminal conductance measurement as a function of gate voltage showed a series of conductance fluctuations for $V_g \leq -0.40$ V until the constriction shut off at $V_g \approx -0.60$ V. As temperature decreased, most peaks approached the conductance ($e^2/3h$). One peak, however, approached (e^2/h) at 45 mK. The height of this peak depended strongly on temperature and dropped below ($e^2/3h$) at $T \approx 120$ mK. Alphenaar et al investigated G vs. V_g at different magnetic fields and for different temperatures between 45 and 700 mK. With increasing B, the onset of the fluctuations shifted to less negative V_g, the fluctuation pattern hardly varied with B.

Hirayama et al [92H2] (page 153) examined four–terminal transport through two in–plane gated parallel GaAs wires coupled by a ballistic window. The Hall resistance showed quantized plateaux.

Yoh et al [92Y2] (page 197) examined InAs/AlGaSb wires and observed quenching of the Hall resistance.

Hwang et al [94H1, 94H2] (page 172) reported systematic experimental study on transport in a low–disorder, low–density GaAs wire defined by a split gate. For $V_g > -2.2\,V$, the IQHE was found. The FQHE was observed for $V_g > -1.9\,V$, the development of the 1/3 FQHE state was investigated as a function of V_g. As B increased beyond the 1/3 FQHE state, the channel became an insulator.

Wendel et al [93W1] investigated narrow GaAs wires ($w = 100 - 153\,nm$, $L = 15\,\mu m$), the samples had the form of two perpendicularly intersecting Hall bars. At filling factors $\nu = 4$ and 6, the minima in R_L were not very deep and their positions did not coincide with the positions of the plateaux in R_H. The resistance values on the plateaux deviated from those expected for quantum Hall states. Wendel et al interpreted their data in terms of scattering between the edge channels.

Geim et al [94G4] examined the quantum Hall effect in three types of multi–terminal devices fabricated from a GaAs/AlGaAs heterostructure: (A) $w \approx 1\,\mu m$, $L = 10 - 20\,\mu m$, exposed to bombardment by α particles; (B) $w \approx 1\,\mu m$, $L = 10 - 20\,\mu m$; (C) as sample B but with the width of the leads increasing rapidly from ≈ 1 to $10\,\mu m$. They measured R_L at different temperatures. In samples A, the amplitudes of the SdH oscillations above 3T decreased considerably as T decreased. In samples C, the high–field SdH peaks became narrower at low temperatures but their amplitudes remained nearly constant. Device B exhibited an intermediate behaviour. The plateaux in R_H in sample A were widest at 5 K and decreased at both higher and lower temperature. In device C, the plateaux were always wider at lower T. Sample B exhibited a slight shrinking of the plateau at $\nu = 2$ at low T. Geim et al attributed their observations to the fact that the presence of scattering in the contact region yielded unequal populations of different in–going and out–going electron channels and (at sufficiently low temperatures) this may lead to decoupling of a channel from the effective thermal reservoir.

Van der Burgt et al [93vdB] investigated the quantum Hall effect in GaAs wires ($w_{eff} = 200$ and 800 nm, probes separated by 2, 5, 50, and $100\,\mu m$, $l = 40\,nm$) fabricated by EBL and dry etching. Traces for R_L and R_H for a 200 nm wide wire showed a plateau–like structure in R_H and SdH oscillations in R_L (at $T = 22 - 25\,K$). The resistance values at the Hall plateaux differed from the quantized values h/Ne^2 by $10 - 15\%$. Not all of the expected plateaux were observed. Different pairs of Hall probes gave plateaux at different N. In the 800 nm wide sample, R_H was a straight line at $T = 17\,K$ while for $T = 6 - 8\,K$, plateaux appeared.

Lettau et al [94L1] (page 173) investigated MR in GaAs wires, the low–field ($B < 1\,T$) Hall resistance was quenched. In addition, it exhibited a series of plateau–like features which were independent of temperature.

Blaikie et al [95B1] (page 173) performed MR measurements on quasi–ballistic multi–terminal GaAs wires defined by implanted p–type gates and observed quenching of the Hall resistance. Samples with voltage probes joining the wire at angles $\neq 90°$ were structured and the Hall resistance was again non–linear although quenching around $B = 0\,T$ was not strong.

Park et al [95P1, 95P2] (page 176) measured the MR of AlGaAs/GaAs wires and observed typical quantum Hall plateaux.

Bykov et al [96B4] reported observation of quasi–periodic MR oscillations in a GaAs wire ($w = 0.3\,\mu m$, $w_{eff} \approx 0.1 - 0.2\,\mu m$, $L = 1.5\,\mu m$) in the integer quantum Hall regime. They performed four–terminal measurements at $T \approx 20\,mK$. Up to a magnetic field of 1 T, UCF were observed. At higher fields, SdH oscillations appeared and at $\approx 3\,T$ the IQHE regime was reached. At $\nu = 6$ and $\nu = 8$, resistance fluctuations were observed around the minima in R_L (Figs. 208 and 209). Fourier spectra revealed that the fluctuations contained components periodic in magnetic field (Figs. 210 and 211). The average fluctuation period was smaller on the low B side of a MR minimum than

on the high B side. Bykov et al analysed their data within the framework of magnetic edge states.

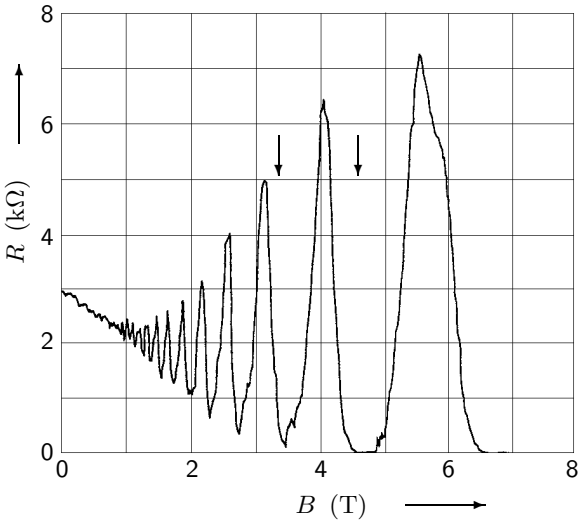

Fig. 208: MR of a wire over the whole magnetic field range [96B4]. Arrows denote the (left) $\nu = 8$ and the (right) $\nu = 6$ minimum.

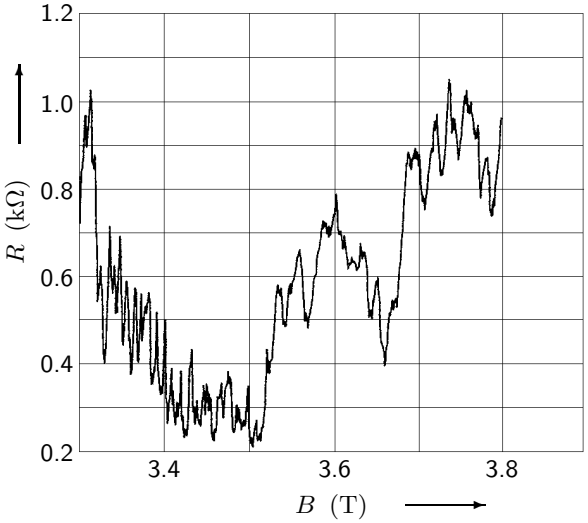

Fig. 209: MR of the wire of fig. 208 in the vicinity of the minimum at $\nu = 8$ [96B4].

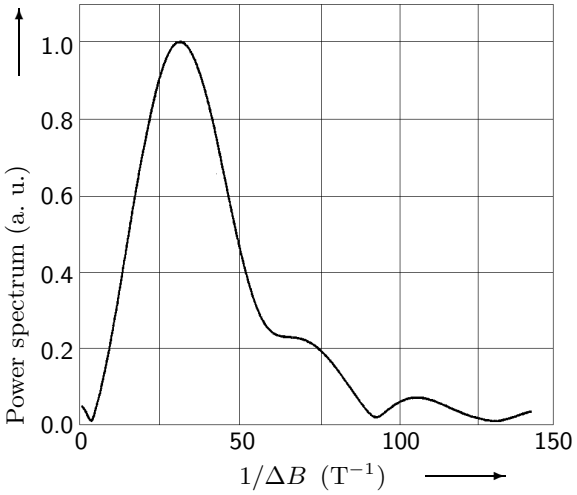

Fig. 210: Fourier spectra of the fluctuations to the right of the $\nu = 8$ MR minimum of Fig. 208 [96B4].

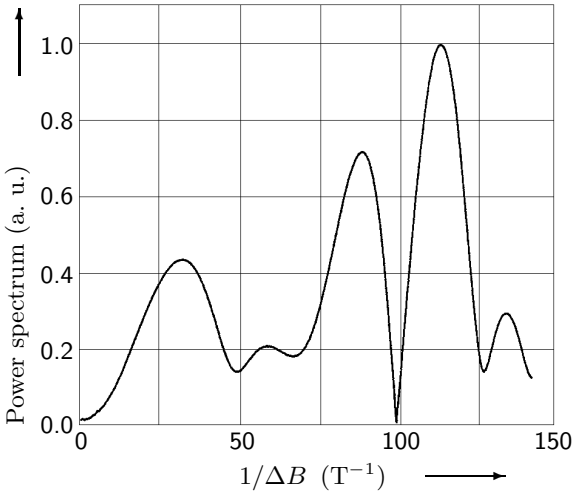

Fig. 211: Fourier spectra of the fluctuations to the left of the $\nu = 8$ MR minimum of Fig. 208 [96B4].

Herfort et al [97H] (page 198) investigated undoped GaAs wires defined by a positively biased narrow top gate. At very low B, R_H was quenched.

7.7.6 Bend resistance

Another consequence of electron collimation at junctions in ballistic conductors (see Section 7.7.5 on page 200) is the *negative bend resistance*. A resistance is called *bend resistance* when the classical current flows around a bend on its way from source to drain. In a four–probe geometry, source and drain of the current injection are located at two adjacent probes and the voltage is measured across

the other two adjacent probes. The collimated electrons enter the voltage probe lying straight ahead instead of flowing around the bend into the current drain due to enhanced forward transmission. This causes an increase of resistance in a two–terminal measurement and a negative resistance at zero magnetic field in a four–terminal measurement (see for example [92W1, 97F, 98T2] and references therein).

Timp et al [88T3] measured the four–terminal MR of a GaAs electron waveguide ($w_{\text{eff}} = 100-200\,\text{nm}$). At high magnetic fields, they observed the quantized Hall effect and SdH oscillations. The MR at low fields was asymmetric around $B = 0\,\text{T}$, but became approximately symmetric when the current and voltage leads were interchanged. The MR consisted of fluctuating symmetric and asymmetric components. The average symmetric MR changed dramatically when the current path bent through a junction at the voltage terminals or beyond, which was attributed to differences in the transmission coefficients.

Takagaki et al [88T1] examined multi–branched electron waveguides made from GaAs/AlGaAs heterostructures. By EBL and ion beam etching a crossed–wires shape was structured from a low mobility wafer ($w_{\text{eff}} = 0.2-0.4\,\mu\text{m}$, $l = 0.22\,\mu\text{m}$, number of occupied 1D channels $\approx 20-40$) and a multi–probe wire geometry was structured from a high mobility wafer ($w_{\text{eff}} = 0.1\,\mu\text{m}$, $l = 2.2\,\mu\text{m}$, number of occupied 1D channels ≈ 4). In the crossed wire geometry, the current flowed diffusively between adjacent probes, the transverse MR was measured. It was asymmetric and showed AF, the average resistance was positive. In the high mobility device, electron transport was ballistic, two traces of MR are shown in Fig. 212. In the configuration, in which the current had to flow around a bend, an increase of the average resistance was observed. For a measurement with a similar lead configuration as in the crossed-wires shape, the average resistance was negative (Fig. 213).

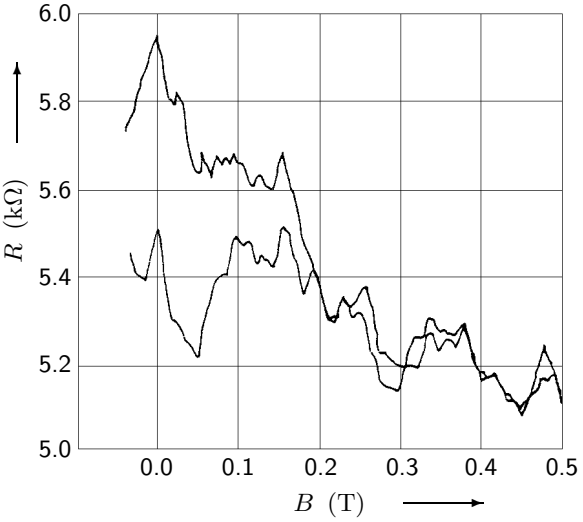

Fig. 212: MR of a $1.4\,\mu\text{m}$ long wire with six narrow branches made from a high mobility wafer [88T1]. The voltage difference is measured between the same leads in both curves, while the current is injected in two different ways: it flows in a straight channel for $R_{63,12}$ (lower curve), it flows around a corner for $R_{64,12}$ (upper curve).

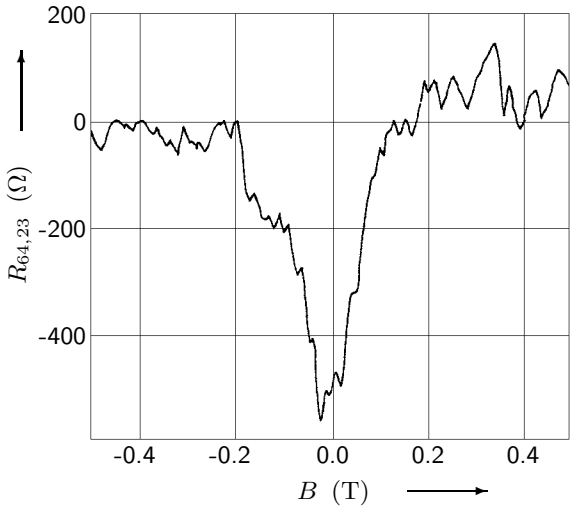

Fig. 213: MR of cross–wires in the multi–terminal device, $R_{64,23}$ [88T1]. The four–terminal resistance is negative at zero magnetic field and decays to zero at 0.2 T.

Takagaki et al [89T1] revisited the four–terminal negative resistance found previously (see [88T1] on page 207) and studied the magnetic field and temperature dependences of the effect. In a cross wire, the resistance was negative at $B = 0\,\text{T}$ and approached the classical value $R_0 \approx$

40 Ω with increasing field but showed a maximum around $B = 0.3$ T (Fig. 214). With increasing temperature, the zero field resistance increased while the resistance around $B = 0.3$ T decreased. Takagaki et al discussed the observed behaviour in terms of the Landauer–Büttiker resistance formula.

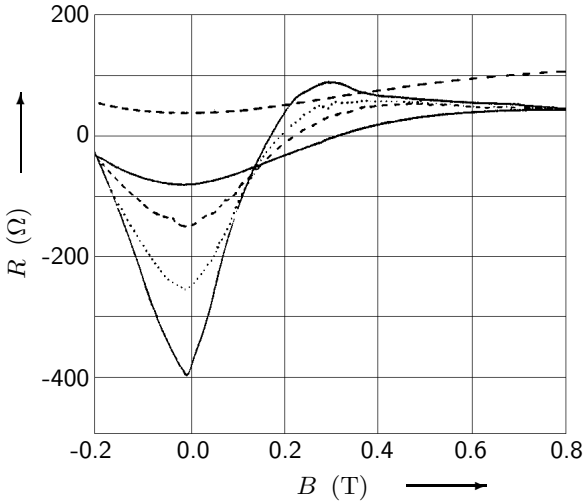

Fig. 214: Magnetic field dependence of a negative resistance for (bottom at negative peak) $T = 1.4$, 20, 40, 80, and 140 K (top) [89T1].

Takagaki et al [89T3] fabricated multi–channel ballistic GaAs wires ($w = 0.5 - 0.6\,\mu$m, $w_{\text{eff}} = 0.1 - 0.2\,\mu$m, $L = 1.2\,\mu$m, $l = 2.2\,\mu$m) by EBL and shallow ion etching. They performed MR measurements and found an increase in the resistance due to a bend in the current path and four–terminal negative resistance at a crossed wire junction. They observed SdH oscillations above 1 T. The longitudinal resistance, the bend resistance, and the Hall resistance were compared and all showed a characteristic feature at 0.2 T where the cyclotron radius became equal to the channel width. Non–local voltage fluctuations were observed. Further, a side–gate transistor was described.

Ford et al [90F3] extended previous studies (see [89F2] on page 151) on how the geometry of a cross region affected the Hall resistance and measured the bend resistance.

Takagaki et al [90T2] fabricated narrow crossed GaAs wire junctions and studied the bend resistance and the Hall resistance. They observed a negative bend resistance at zero field and quenching of the Hall resistance. The temperature dependence of the amplitude of the negative bend resistance was examined. The suppression of the amplitude with rising T was attributed to the population of higher subbands.

Kakuta et al [91K2, 92K2] fabricated a cross–shaped GaAs junction with four side gates by EBL and ion–beam damaging ($l = 13\,\mu$m). The corners of each wire were rounded, the wires became wider over a distance of $0.7\,\mu$m towards the cross ($w = 0.5\,\mu$m). The bend resistance vs. B was studied for several V_{g}. The negative resistance was enhanced with decreasing V_{g}, oscillations of R_{B} with varying V_{g} were observed. The average slope of the Hall resistance was almost zero at $V_{\text{g}} = 0$ V and became negative with increasing V_{g}. The average slope of the negative R_{H} as a function of V_{g} was studied. Around $B = 0.1$ T, a positive peak in R_{H} appeared, at that field r_{c} coincided with the curvature radius of the widened cross. At lower V_{g}, irregular fluctuations appeared.

Cumming et al [93C3] fabricated a multi–terminal split–gate GaAs wire ($w = 2.5\,\mu$m, $L = 8\,\mu$m, $l = 30\,\mu$m) with voltage probes connected at angles of 45°. The voltage probes were shadowed from the adjacent current probes. The longitudinal resistance as a function of magnetic field showed a zero–field resistance of $-5\,\Omega$ and a negative peak of $-30\,\Omega$ at ± 0.11 T. The bend resistance had its minimum not a $B = 0$ T, but at $B = -0.11$ T (Fig. 215). The negative value of R_{B} was much greater than that of R_{L}. The data was compared with simulations based upon a semi–classical

billiard model.

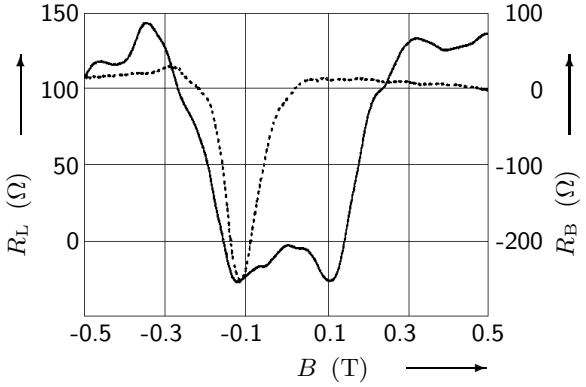

Fig. 215: R_L (solid curve, left axis) and R_B (dotted curve, right axis) as a function of magnetic field [93C3].

Blaikie et al [95B1] (page 173) performed MR measurements on quasi–ballistic multi–terminal GaAs wires defined by implanted p–type gates. A negative bend resistance at $B = 0\,\mathrm{T}$ was observed. Samples with voltage probes joining the wire at angles $\neq 90°$ were structured, the bend resistance was negative at $B \neq 0\,\mathrm{T}$.

7.8 Electron spin

The electron spin leads to Zeeman spin splitting of energy levels which can for example be observed in Shubnikov–de–Haas oscillations (see Section 7.7.4 on page 194). The interaction of the electron spin with the electron angular momentum leads to spin–orbit scattering (see Section 7.6.3 on page 167). In samples containing magnetic impurities, spin–flip scattering destroys phase coherence of the electron wavefunction (see for example [82A, 84B2, 86C1] and references therein).

Wainer et al [88W1] (page 129) measured MC fluctuations in narrow Si MOSFETs for a range of gate voltages. The peaks shifted for an increasing magnetic field to lower or higher V_g. At high fields, the density of peaks was reduced. The observed effects were attributed to Zeeman spin splitting of energy levels.

Fukai et al [90F4] (page 140) structured GaAs/AlGaAs on–facet wires and determined the phase coherence length from weak localization. The MR was positive at low field for $T \leq 0.08\,\mathrm{K}$, indicating the presence of SO interaction.

Taniguchi et al [91T2] (page 140) studied the phase breaking time τ_φ and the SO scattering time τ_{SO} in Si δ–doped GaAs wires. They investigated the temperature dependence of τ_φ and τ_{SO} and found saturation of τ_φ when τ_φ became comparable to τ_{SO}. The temperature dependence of the amplitude of UCF in wires with strong SO scattering was examined.

Yoh et al [92Y2] (page 197) investigated wires on InAs/AlGaSb heterostructures fabricated by EBL and wet–chemical etching. In the MR of a 350 nm wide wire, spin–splitting of the Landau levels was more pronounced than in the 2DEG.

Fukai et al [95F2] (page 167) examined InGaAs/InAlAs wires fabricated by Ga FIB implantation. The decrease of resistance below 1.6 K was interpreted as anti–localization in the presence of strong SO scattering.

Jaroszyński et al [95J, 96D1, 96J2] (page 181) investigated the MR of $Cd_{0.99}Mn_{0.01}Te$ and CdTe wires. The positive low–field MR in n^+–$Cd_{0.99}Mn_{0.01}Te$ was attributed to the effect of the giant exchange spin splitting upon electron–electron interaction.

Noguchi et al [96N2] (page 142) investigated the phase breaking time of GaAs wires. They

measured the MC for $0.4\,\mathrm{K} < T < 30\,\mathrm{K}$ and observed weak localization and AF (Fig. 139). From theoretical fits, τ_φ vs. T was obtained. Noguchi et al ascribed the saturation of τ_φ to spin–flip scattering by paramagnetic electron–trapped donors.

7.9 Non–linear effects

The current–voltage characteristic of a small disordered conductor is in general neither linear nor does it exhibit inversion symmetry as a classical conductor does. The transmission coefficient of a random potential does not rise monotonically with the applied voltage bias and thus the current is not a monotonic function of the source–drain voltage. Further, as the random potential does not exhibit inversion symmetry, the current does not and $R(I) \neq R(-I)$ (see for example [88K1, 90D, 91W2, 92W1] and references therein). Another possible origin of a non–linear I–V characteristic is a pinned CDW or WC (see Section 7.2.2 on page 130). In the localized regime, the current may depend exponentially on the driving voltage. In conductors with a non–linear current–voltage characteristic, increasing the voltage bias may decrease the current, leading to a negative differential conductance. Further, when an ac bias is applied, higher harmonics are generated. Finally, in the case of an asymmetric I–V characteristic, rectification takes place.

Kwasnick et al [84K2] (page 125) studied Si MOSFETs with $\approx 70\,\mathrm{nm}$ wide inversion layers. The current increased exponentially with the driving voltage (Fig. 125).

Webb et al [85W, 86W2, 88F3] (page 127) measured I–V characteristics of Si MOSFETs for several temperatures (Fig. 128). A second harmonic signal was observed.

Kastner et al [87K1] (page 129) examined the conductance of narrow Si MOSFETs. The current depended exponentially on the source–drain voltage over a certain range of V_{SD}. A crossover from exponential to linear behaviour was observed for small V_{SD}.

Kastner et al [88K2] (page 169) structured Si wires, studied the current as a function of source–drain voltage and observed a small negative differential resistance (Fig. 166).

De Vegvar et al [88dV] studied second harmonic generation in small rings and wires fabricated from GaAs/$\mathrm{Al}_x\mathrm{Ga}_{1-x}$As heterostructures (see page 273).

Scott–Thomas et al [89S2] (page 130) created narrow Si inversion layers, studied the dependence of the differential conductance on V_{SD}, and found an increase by orders of magnitude as V_{SD} changed from 0 meV to 0.2 meV. Above 0.2 meV, the differential conductance overshot and approached its high–temperature value.

Meirav et al [89M3] (page 130) patterned $1.0\,\mu$m wide and 2 and $8\,\mu$m long GaAs channels and found a non–linear dependence of G on an applied dc bias.

Field et al [90F2] (page 131) studied Si MOSFETs and narrow channels in GaAs/$\mathrm{Al}_x\mathrm{Ga}_{1-x}$As. For small V_{SD}, the current obeyed Ohm's law while at higher V_{SD}, the I–V characteristic was non–linear.

Galloway et al [90G2] (page 189) coupled an ac voltage source to a GaAs sample and measured the dc voltage across the sample as B was increased. Strong oscillations about zero were observed in the rectified voltage.

Tarucha et al [93T3] (page 148) investigated transport in ballistic GaAs channels. The differential resistance vs. voltage for $2\,\mu$m wide channels showed a minimum at a voltage of several mV.

Hwang et al [94H1, 94H2] (page 172) reported systematic experimental study on transport in a low–disorder low–density GaAs wire defined by a split gate. As a function of the electron density,

conductance oscillations were observed in a B–induced insulating phase. The I–V characteristics at a maximum and a minimum of the conductance oscillations were non–linear.

Chandrasekhar et al [94C1] (see page 275) investigated In_2O_{3-x} wires and rings and observed a non–linear I–V characteristic.

Wada et al [94W] studied transport phenomena in a poly–Si slit nanowire ($w = 5 - 8\,\mathrm{nm}$, $L = 3\,\mu\mathrm{m}$, grain length $\approx 100\,\mathrm{nm}$). In the I–V characteristics two distinct features were observed: (1) the resistance of the slit nanowire increased with decreasing temperature ($4.2\,\mathrm{K} < T < 300\,\mathrm{K}$), and (2) the conductance exhibited a dip of $\approx 30\,\mathrm{mV}$ for $T \leq 10\,\mathrm{K}$. The resistance as a function of temperature was also measured ($10\,\mathrm{K} < T < 300\,\mathrm{K}$).

Okada et al [95O3] (page 122) fabricated in–plane gate GaAs wires, measured I–V characteristics and found complete pinch–off and saturation at 3.8 K. The saturation current depended linearly on gate voltage.

Okada et al [95O4] fabricated in–plane gate GaAs wires using direct Schottky gates at the quantum well edges ($w = 1.4\,\mu\mathrm{m}$, $L = 11\,\mu\mathrm{m}$). They measured I–V characteristics at room temperatures (Fig. 216).

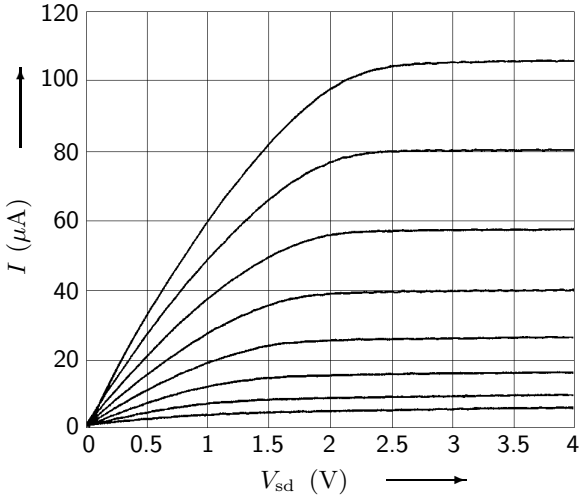

Fig. 216: Typical I–V characteristics at room temperature for (top) $V_g = 1\,\mathrm{V}$, $0\,\mathrm{V}$, $-1\,\mathrm{V}$, $-2\,\mathrm{V}$, $-3\,\mathrm{V}$, $-4\,\mathrm{V}$, $-5\,\mathrm{V}$, and $-6\,\mathrm{V}$ (bottom) [95O4].

Smith et al [97S3] observed strongly non–ohmic behaviour in Si wires ((A) $w \approx 60 \pm 5\,\mathrm{nm}$, $L = 4\,\mu\mathrm{m}$; (B) $w \approx 70 \pm 1\,\mathrm{nm}$, $L = 6\,\mu\mathrm{m}$) defined by side gates. Measurements carried out at room temperature showed ohmic behaviour. At 2.0 K, the current as a function of source–drain voltage in sample A was zero in a 80 mV wide region. Outside this region, the conductance increased first sharply and then more gradually. Several equally spaced peaks were superimposed on the curves. A voltage applied on one gate influenced the width of the blockade region and the slope of the abrupt rise. Sample B showed a similar behaviour, a clear Coulomb blockade staircase in the differential conductance was observed. The features of the staircase changed with V_g. The current as a function of gate voltage showed fine scale current oscillations. Further, the samples showed resistance switching due to single electron trapping. The step size was $\approx 50\%$ of the current value. With increasing temperature, the non–linearity became less pronounced. At 46 K, the wire had a linear I–V characteristic. Smith et al discussed their results in terms of the Coulomb blockade effect.

Yacoby et al [96Y1, 97Y1] (page 122) fabricated GaAs wires by cleaved edge overgrowth and observed quantized steps in the linear response conductance. In the non–linear differential conductance, the plateaux rose with increasing dc bias, even exceeding $N(2 \cdot e^2/h)$.

Linke et al [97L] (page 164) investigated the dephasing rate of electrons not in equilibrium in

the diffusive regime. For zero magnetic field, the conductance as a function of dc bias showed a pronounced minimum with a half–width of 1 mV, symmetric around zero bias voltage.

Hashizume et al [96H1] (page 123) fabricated in–plane gate GaAs wires, measured I–V characteristics at $T = 2\,\mathrm{K}$ for different V_g and found a non–linear behaviour.

Koester et al [97K1] observed a negative differential conductance in Si wires ($w = 0.27\,\mu\mathrm{m}$, $L = 15\,\mu\mathrm{m}$) which persisted up to temperatures of $T = 83\,\mathrm{K}$. They determined the electric field distribution along the wire by structuring a wire with probes along the channel and found that the onset of a negative differential conductance corresponded to the development of a high–field region at the drain end of the wire.

Fujii et al [98F2] fabricated Si wires ($w = 20\,\mathrm{nm}$, $L = 150\,\mathrm{nm}$) by EBL, RIE and subsequent thermal oxidation at 900 °C. The wire was separated from the Si substrate by an air gap. The I–V characteristic was measured at room temperature. The resistance was estimated to be $60\,\mathrm{M\Omega}$ under illumination. The current saturated around 20 nA and showed fluctuations.

7.10 Localization

In disordered samples, electron wavefunctions may be completely localized in space. The wave function amplitude decays as $e^{-x/\xi}$, where ξ is the localization length. When $L \gg \xi$, the sample is an insulator, $G \ll e^2/h$. Transport proceeds by hopping among or tunneling through the isolated states. The resistance increases exponentially with increasing sample length or decreasing temperature (see for example [82G, 85E, 85G, 85L1, 85K, 85P, 91P1, 91W2, 92W1, 93K, 97I1, 98J1] and references therein).

Dean et al [84D] examined Si MOSFETs with channel widths of $\approx 1\,\mu\mathrm{m}$ (see [82D] on page 132). The conductance as a function of temperature exhibited drastic changes, indicating 1D localization. A drop in the conductivity with increasing magnetic field was assumed to be due to electron–electron interaction effects. They performed electron heating measurements and studied electron–phonon scattering. Further, they searched for an indication of a 1D density of states in the conductance as a function of gate voltage.

Webb et al [85W, 86W2, 88F3] (page 127) studied Si MOSFETs with channel lengths of $10\,\mu\mathrm{m}$ and widths less than 30 nm. The conductance vs. gate voltage for several temperatures is shown in Fig. 126 (page 128). The temperature dependence of the four largest peaks agreed with variable–range hopping above 200 mK (Fig. 127 on page 128).

Kastner et al [87K1] (page 129) investigated transport in narrow Si MOSFETs. Their data indicated a transition from localized to extended states at $G = 10^{-6}\,\Omega^{-1}$.

Wainer et al [88W1] (page 129) measured MC fluctuations in narrow Si MOSFETs in the strongly localized regime.

Ohata et al [92O2] fabricated narrow Si channels ($w < 0.1\,\mu\mathrm{m}$, $L = 8\,\mu\mathrm{m}$) and measured conductance vs. gate voltage at various temperatures. AF near the turn–on voltage were completely reproducible, even after the sample was once warmed up to room temperature. As temperature was lowered, the fluctuations became gradually accentuated. The peak positions were insensitive to temperature or magnetic field. Peak conductance and peak width showed strong temperature dependence. The observations were explained in terms of hopping conduction in the strongly localized regime. Ohata et al also measured the MC at different gate voltages. A large positive MC was observed in the hopping regime around 3 T using a perpendicular field. The MC changed for a variation of V_g. For a parallel magnetic field, the MC was negative.

Iwano et al [93I] (page 133) fabricated p–type Si wires using FIB doping with Ga ions. Two kinds of samples with different impurity concentrations (A: $N_\mathrm{Ga} \approx 5.1 \times 10^7\,\mathrm{cm}^{-1}$; B: $N_\mathrm{Ga} \approx$

$5.1 \times 10^9\,\mathrm{cm}^{-1}$) were prepared. The conductance of sample A had an activation–type temperature dependence while sample B showed a strong and a weak temperature–dependent region (Fig. 134) attributed to a competition between band conduction and 1D hopping conduction.

Iwano et al [94I3] (page 133) fabricated Si wires by FIB implantation of Ga^+ ions and studied the electrical conductance for different ion doses and annealing temperatures. They found VRH and NNH conductance. The MR was measured and a positive MR was interpreted as a reduction of the localization length.

Hughes et al [96H2] examined variable range hopping conductance fluctuations in Si wires ($w = 0.5 - 2.0\,\mu$m, $L = 5 - 20\,\mu$m) and GaAs wires ($w_{\mathrm{eff}} \approx 0.2\,\mu$m, $L = 1.8\,\mu$m). In a two–terminal measurement, $\ln(G)$ was determined as a function of gate voltage at different temperatures. The temperature dependence of the fluctuation amplitude was studied. The data was analysed by means of its distribution function. The influence of a magnetic field was also investigated.

Iwano et al [98I2] fabricated Si wires by FIB doping and investigated the localization length and the hopping distance in the 1D VRH regime. The temperature dependence of the conductivity showed an activation type behaviour for $T > 50\,\mathrm{K}$ and a VRH type behaviour for $T < 50\,\mathrm{K}$. They estimated $a\rho_{\mathrm{F}}$ from the data, where a was the localization length and ρ_{F} the density of localized states at the Fermi level. Iwano et al further measured MR and found both, negative and positive MR at low fields in different samples. They extracted $a = 2\,\mathrm{nm}$, a hopping distance $r = 8 - 9\,\mathrm{nm}$, and $\rho_{\mathrm{F}} = 10^9\,\mathrm{cm}^{-1}\mathrm{eV}^{-1}$. The localization lengths were close to the effective Bohr radii of light and heavy holes bounded by Ga impurities while the hopping distance was comparable to the distance between activated Ga atoms. The authors suggested that the diameter of the conductive regions in their wires was less than a few tens of nanometres.

7.11 References for Section 7

[62S] Schmidt–Tiedemann, K.J.: Festkörperprobleme 1, edited by Sauter, F. (Friedr. Vieweg & Sohn 1962.)

[79B] Berlinsky, A.J.: Rep. Prog. Phys. **42** (1979) 1243.

[79E] Emery, V.J.: Highly Conducting One–Dimensional Solids, edited by Devreese, J.T., Evrard, R.P., van Doren, V.E. (Plenum Press, 1979).

[79L1] Lee, P.A., Rice, T.M.: Phys. Rev. B **19** (1979) 3970.

[79S] Sólyom, J.: Adv. Phys. **28** (1979) 201.

[80vK] von Klitzing, K., Dorda, G., Pepper, M.: Phys. Rev. Lett. **45** (1980) 494.

[82A] Ando, T., Fowler, A.B., Stern, F.: Rev. Mod. Phys. **54** (1982) 437.

[82D] Dean, C.C., Pepper, M.: J. Phys. C: Solid State Phys. **15** (1982) L1287.

[82F] Fowler, A.B., Hartstein, A., Webb, R.A.: Phys. Rev. Lett. **48** (1982) 196.

[82G] Gogolin, A.A.: Phys. Rep. **86** (1982) 1.

[82H] Houghton, A., Senna, J.R., Ying, S.C.: Phys. Rev. B **25** (1982) 2196.

[82W] Wheeler, R.G., Choi, K.K., Goel, A., Wisnieff, R., Prober, D.E.: Phys. Rev. Lett. **49** (1982) 1674.

[83F] Fowler, A.B., Hartstein, A., Webb, R.A.: Physica **117B & 118B** (1983) 661.

[84A1] Al'tshuler, B.L., Aronov, A.G., Khmel'nitskii, D.E., Larkin, A.I.: Quantum Theory of Solids, edited by Lifshits, I.M. (MIR Publishers, 1984).

[84B2] Bergmann, G.: Phys. Rep. **107** (1984) 1.

[84D] Dean, C.C., Pepper, M.: J. Phys. C: Solid State Phys. **17** (1984) 5663.

[84H] Hartstein, A., Webb, R.A., Fowler, A.B., Wainer, J.J.: Surf. Sci. **142** (1984) 1.

[84K1] Kaveh, M., Wiser, N.: Adv. Phys. **33** (1984) 257

[84K2] Kwasnick, R.F., Kastner, M.A., Melngailis, J., Lee, P.A.: Phys. Rev. Lett. **52** (1984) 224.

[84S] Skocpol, W.J., Jackel, L.D., Howard, R.E., Craighead, H.G., Fetter, L.A., Mankiewich, P.M., Grabbe, P., Tennant, D.M.: Surf. Sci. **142** (1984) 14.

[84W] Wheeler, R.G., Choi, K.K., Wisnieff, R.: Surf. Sci. **142** (1984) 19.

[85A1] Al'tshuler, B.L., Aronov, A.G.: Electron–Electron Interaction in Disordered Conductors, edited Efros, A.L. and Pollak, M. (Elsevier Science Publishers, 1985).

[85C] Choi, K.K., Tsui, D.C., Palmateer, S.C.: Phys. Rev. B **32** (1985) 5540.

[85E] Efros, A.L., Shklovskii, B.I.: Electron–Electron Interaction in Disordered Conductors, edited Efros, A.L. and Pollak, M. (Elsevier Science Publishers, 1985).

[85F] Fukuyama, H.: Electron–Electron Interaction in Disordered Conductors, edited Efros, A.L. and Pollak, M. (Elsevier Science Publishers, 1985).

[85G] Gor'kov, L.P.: Electron–Electron Interaction in Disordered Conductors, edited Efros, A.L. and Pollak, M. (Elsevier Science Publishers, 1985).

[85K] Kamimura, H.: Electron–Electron Interaction in Disordered Conductors, edited Efros, A.L. and Pollak, M. (Elsevier Science Publishers, 1985).

[85L1] Lee, P.A., Ramakrishnan, T.V.: Rev. Mod. Phys. **57** (1985) 287.

[85L2] Licini, J.C., Bishop, D.J., Kastner, M.A., Melngailis, J.: Phys. Rev. Lett. **55** (1985) 2987.

[85P] Pollak, M., Ortuño, M.: Electron–Electron Interaction in Disordered Conductors, edited Efros, A.L. and Pollak, M. (Elsevier Science Publishers, 1985).

[85W] Webb, R.A., Hartstein, A., Wainer, J.J., Fowler, A.B.: Phys. Rev. Lett. **54** (1985) 1577.

[86B2] Berggren, K.-F., Thornton, T.J., Newson, D.J., Pepper, M.: Phys. Rev. Lett. **57** (1986) 1769

[86C1] Chakravarty, S., Schmid, A.: Phys. Rep. **140** (86) 193.

[86C2] Choi, K.K., Tsui, D.C., Palmateer, S.C.: Phys. Rev. B **33** (1986) 8216.

[86K2] Kaplan, S.B., Hartstein, A.: Phys. Rev. B **33** (1986) 2909.

[86K3] Kaplan, S.B., Hartstein, A.: Phys. Rev. Lett. **56** (1986) 2403.

[86L] Landauer, R.: Philos. Mag. **21** (1970) 1761.

[86S1] Skocpol, W.J., Jackel, L.D., Howard, R.E., Mankiewich, P.M., Tennant, D.M., White, A.E., Dynes, R.C.: Surf. Sci. **170** (1986) 1.

[86S2] Skocpol, W.J., Mankiewich, P.M., Howard, R.E., Jackel, L.D., Tennant, D.M., Stone, A.D.: Phys. Rev. Lett. **56** (1986) 2865.

[86T] Thornton, T.J., Pepper, M., Ahmed, H., Andrews, D., Davies, G.J.: Phys. Rev. Lett. **56** (1986) 1198.

[86vH] van Houten, H., van Wees, B.J., Heijman, M.G.J., André, J.P.: Appl. Phys. Lett. **49** (1986) 1781.

[86vK] von Klitzing, K.: Rev. Mod. Phys. **58** (1986) 519

[86W1] Washburn, S., Webb, R.A.: Adv. Phys. **35** (1986) 375.

[86W2] Webb, R.A., Fowler, A.B., Hartstein, A., Wainer, J.J.: Surf. Sci. **170** (1986) 14.

[86W3] Whittington, G.P., Main, P.C., Eaves, L., Taylor, R.P., Thoms, S., Beaumont, S.P., Wilkinson, C.D.W., Stanley, C.R., Frost, J.: Superlatt. Microstruct. **2** (1986) 381.

[86Z1] Zheng, H.Z., Choi, K.K., Tsui, D.C., Weimann, G.: Surf. Sci. **170** (1986) 209.

[86Z2] Zheng, H.Z., Wei, H.P., Tsui, D.C., Weimann, G.: Phys. Rev. B **34** (1986) 5635.

[87A1] Anisovich, A.V., Al'tshuler, B.L., Aronov, A.G., Zyuzin, A.Yu.: JETP Lett. **45** (1987) 295.

[87A2] Aoki, H.: Rep. Prog. Phys. **50** (1987) 655.

[87A3] Asai, H., Yamada, S., Fukui, T.: Appl. Phys. Lett. **51** (1987) 1518.

[87C1] Choi, K.K., Tsui, D.C., Alavi, K.: Appl. Phys. Lett. **50** (1987) 110.

[87C2] Choi, K.K., Tsui, D.C., Alavi, K.: Phys. Rev. B **36** (1987) 7751.

[87E] Esposito, F.P., Goodman, B., Ma, M.: Phys. Rev. B **36** (1987) 4507.

[87G1] Grassie, A.D.C., Hutchings, K.M., Lakrimi, M., Foxon, C.T., Harris, J.J.: Phys. Rev. B **36** (1987) 4551.

[87H1] Hiramoto, T., Hirakawa, K., Iye, Y., Ikoma, T.: Appl. Phys. Lett. **51** (1987) 1620.

[87I1] Ishibashi, K., Nagata, K., Gamo, K., Namba, S., Ishida, S., Murase, K., Kawabe, M., Aoyagi, Y.: Sol. St. Commun. **61** (1987) 385.

[87I2] Ishibashi, K., Takagaki, Y., Gamo, K., Namba, S., Ishida, S., Murase, K., Aoyagi, Y., Kawabe, M.: Sol. St. Commun. **64** (1987) 573.

[87K1] Kastner, M.A., Kwasnick, R.F., Licini, J.C., Bishop, D.J.: Phys. Rev. B **36** (1987) 8015.

[87L2] Lee, P.A., Stone, A.D., Fukuyama, H.: Phys. Rev. B **35** (1987) 1039.

[87R] Roukes, M.L., Scherer, A., Allen Jr., S.J., Craighead, H.G., Ruthen, R.M., Beebe, E.D., Harbison, J.P.: Phys. Rev. Lett. **59** (1987) 3011.

[87S1] Scherer, A., Roukes, M.L., Craighead, H.G., Ruthen, R.M., Beebe, E.D., Harbison, J.P.: Appl. Phys. Lett. **51** (1987) 2133.

[87S2] Skocpol, W.J., Mankiewich, P.M., Howard, R.E., Jackel, L.D., Tennant, D.N., Stone, A.D.: Phys. Rev. Lett. **58** (1987) 2347.

[87T2] Thornton, T.J., Pepper, M., Ahmed, H., Davies, G.J., Andrews, D.: Phys. Rev. B **36** (1987) 4514.

[87T3] Timp, G., Chang, A.M., Mankiewich, P., Behringer, R., Cunningham, J.E., Chang, T.Y., Howard, R.E.: Phys. Rev. Lett. **59** (1987) 732.

[87vH] van Houten, H., van Wees, B.J., Mooij, J.E., Roos, G., Berggren, K.-F.: Superlatt. Microstruct. **3** (1987) 497.

[87Y] Yennie, D.R.: Rev. Mod. Phys. **59** (1987) 781.

[88B2] Büttiker, M.: IBM J. Res. Develop. **32** (1988) 317.

[88C1] Chang, A.M., Timp, G., Chang, T.Y., Cunningham, J.E., Mankiewich, P.M., Behringer, R.E., Howard, R.E.: Sol. St. Commun. **67** (1988) 769.

[88C2] Chang, A.M., Timp, G., Cunningham, J.E., Mankiewich, P.M., Behringer, R.E., Howard, R.E., Baranger, H.U.: Phys. Rev. B **37** (1988) 2745.

[88C3] Cheeks, T.L., Roukes, M.L., Scherer, A., Craighead, H.G.: Appl. Phys. Lett. **53** (1988) 1964.

[88dV] de Vegvar, P.G.N., Timp, G., Mankiewich, P.M., Cunningham, J.E., Behringer, R., Howard, R.E.: Phys. Rev. B **38** (1988) 4326.

[88F2] Ford, C.J.B., Thornton, T.J., Newbury, R., Pepper, M., Ahmed, H., Peacock, D.C., Ritchie, D.A., Frost, J.E.F., Jones, G.A.C.: Phys. Rev. B **38** (1988) 8518.

[88F3] Fowler, A.B., Wainer, J.J., Webb, R.A.: IBM J. Res. Develop. **32** (1988) 372.

[88H2] Hiramoto, T., Hirakawa, K., Ikoma, T.: J. Vac. Sci. Technol. B **6** (1988) 1014.

[88K1] Kaplan, S.B., Hartstein, A.: IBM J. Res. Develop. **32** (1988) 347.

[88K2] Kastner, M.A., Field, S.B., Licini, J.C., Park, S.L.: Phys. Rev. Lett. **60** (1988) 2535.

[88R] Roukes, M.L., Scherer, A., Craighead, H.G., Allen Jr., S.J., Ruthen, R.M., Beebe, E.D., Harbison, J.P.: Surf. Sci. **196** (1988) 79.

[88S1] Scott–Thomas, J.H.F., Kastner, M.A., Antoniadis, D.A., Smith, H.I., Field, S.: J. Vac. Sci. Technol. **B6** (1988) 1841.

[88S2] Serota, R.A., Ma, M., Goodman, B.: Phys. Rev. B **37** (1988) 6540.

[88S3] Simmons, J.A., Tsui, D.C., Weimann, G.: Surf. Sci. **196** (1988) 81.

[88T1] Takagaki, Y., Gamo, K., Namba, S., Ishida, S., Takaoka, S., Murase, K., Ishibashi, K., Aoyagi, Y.: Sol. St. Commun. **68** (1988) 1051.

[88T2] Taylor, R.P., Leadbeater, M.L., Whittington, G.P., Main, P.C., Eaves, L., Beaumont, S.P., McIntyre, I., Thoms, S., Wilkinson, C.D.W.: Surf. Sci. **196** (1988) 52.

[88T3] Timp, G., Baranger, H.U., de Vegvar, P., Cunningham, J.E., Howard, R.E., Behringer, R., Mankiewich, P.M.: Phys. Rev. Lett. **60** (1988) 2081.

[88vH] van Houten, H., Beenakker, C.W.J., van Wees, B.J., Mooij, J.E.: Surf. Sci. **196** (1988) 144.

[88vW] van Wees, B.J., van Houten, H., Beenakker, C.W.J., Williamson, J.G., Kouwenhoven, L.P., van der Marel, D., Foxon, C.T.: Phys. Rev. Lett. **60** (1988) 848.

[88W1] Wainer, J.J., Fowler, A.B., Webb, R.A.: Surf. Sci. **196** (1988) 134.

[88W2] Washburn, S.: IBM J. Res. Develop. **32** (1988) 335.

[88W3] Washburn, S., Fowler, A.B., Schmid, H., Kern, D.: Phys. Rev. Lett. **61** (1988) 2801.

[88W4] Wharam, D.A., Thornton, T.J., Newbury, R., Pepper, M., Ahmed, H., Frost, J.E.F., Hasko, D.G., Peacock, D.C., Ritchie, D.A., Jones, G.A.C.: J. Phys. C: Solid State Phys. **21** (1988) L209.

[89B1] Beenakker, C.W.J., van Houten, H., van Wees, B.J.: Advances in Solid State Physics, Volume 29, edited by Rössler, U. (Friedr. Vieweg & Sohn, 1989).

[89B2] Behringer, R.E., Mankiewich, P.M., Timp, G., Howard, R.E., Baranger, H.U., Cunningham, J., Sampere, S.: J. Vac. Sci. Technol. B **7** (1989) 2039.

[89F2] Ford, C.J.B., Washburn, S., Büttiker, M., Knoedler, C.M., Hong, J.M.: Phys. Rev. Lett. **62** (1989) 2724.

[89G] Gao, J.R., Caro, J., Verbruggen, A.H., Radelaar, S., Middelhoek, J.: Phys. Rev. B **40** (1989) 11676.

[89H] Hiramoto, T., Hirakawa, K., Iye, Y., Ikoma, T.: Appl. Phys. Lett. **54** (1989) 2103.

[89L2] Lakrimi, M., Grassie, A.D.C., Hutchings, K.M., Harris, J.J., Foxon, C.T.: Semicond. Sci. Technol. **4** (1989) 313.

[89M2] Mailly, D., Sanquer, M., Pichard, J.-L., Pari, P.: Europhys. Lett. **8** (1989) 471.

[89M3] Meirav, U., Kastner, M.A., Heiblum, M., Wind, S.J.: Phys. Rev. B **40** (1989) 5871.

[89M4] Mizuno, M., Ishibashi, K., Noh, S.K., Ochiai, Y., Aoyagi, Y., Gamo, K., Kawabe, M., Namba, S.: Jpn. J. Appl. Phys. **28** (1989) L1025.

[89P] Pooke, D.M., Paquin, N., Pepper, M., Gundlach, A.: J. Phys.: Condens. Matter **1** (1989) 3289.

[89S1] Scherer, A., Roukes, M.L.: Appl. Phys. Lett. **55** (1989) 377.

[89S2] Scott–Thomas, J.H.F., Field, S.B., Kastner, M.A., Smith, H.I., Antoniadis, D.A.: Phys. Rev. Lett. **62** (1989) 583.

[89S3] Simmons, J.A., Wei, H.P., Engel, L.W., Tsui, D.C., Shayegan, M.: Phys. Rev. Lett. **63** (1989) 1731.

[89T1] Takagaki, Y., Gamo, K., Namba, S., Takaoka, S., Murase, K., Ishida, S.: Sol. St. Commun. **71** (1989) 809.

[89T2] Takagaki, Y., Gamo, K., Namba, S., Takaoka, S., Murase, K., Ishida, S., Ishibashi, K., Aoyagi, Y.: Sol. St. Commun. **69** (1989) 811.

[89T3] Takagaki, Y., Wakaya, F., Takaoka, S., Gamo, K., Murase, K., Namba, S.: Jpn. J. Appl. Phys. **28** (1989) 2188.

[89T4] Taylor, R.P., Main, P.C., Eaves, L., Beaumont, S.P., McIntyre, I., Thoms, S., Wilkinson, C.D.W.: J. Phys.: Condens. Matter **1** (1989) 10413.

[89T5] Thornton, T.J., Roukes, M.L., Scherer, A., van de Gaag, B.P.: Phys. Rev. Lett. **63** (1989) 2128.

[89vH] van Houten, H., Beenakker, C.W.J.: Phys. Rev. Lett. **63** (1989) 1893

[89W1] Washburn, S.: Am. J. Phys. **57** (1989) 1069.

[89Y] Yamada, S., Asai, H., Fukai, Y.K., Fukui, T.: Phys. Rev. B **39** (1989) 11199.

[90B2] Bird, J.P., Grassie, A.D.C., Lakrimi, M., Hutchings, K.M., Harris, J.J., Foxon, C.T.: J. Phys.: Condens. Matter **2** (1990) 7847.

[90D] Datta, S., McLennan, M.J.: Rep. Prog. Phys. **53** (1990) 1003.

[90E] Eugster, C.C., del Alamo, J.A., Rooks, M.J.: Jpn. J. Appl. Phys. **29** (1990) L2257.

[90F2] Field, S.B., Kastner, M.A., Meirav, U., Scott–Thomas, J.H.F., Antoniadis, D.A., Smith, H.I., Wind, S.J.: Phys. Rev. B **42** (1990) 3523.

[90F3] Ford, C.J.B., Washburn, S., Büttiker, M., Knoedler, C.M., Hong, J.M.: Surf. Sci. **229** (1990) 298.

[90F4] Fukai, Y.K., Yamada, S., Nakano, H.: Appl. Phys. Lett. **56** (1990) 2123.

[90G1] Gallagher, B.L., Galloway, T., Beton, P., Oxley, J.P., Beaumont, S.P., Thoms, S., Wilkinson, C.D.W.: Phys. Rev. Lett. **64** (1990) 2058.

[90G2] Galloway, T., Gallagher, B.L., Beton, P.H., Oxley, J.P., Beaumont, S.P., Thoms, S., Wilkinson, C.D.W.: J. Phys.: Condens. Matter **2** (1990) 5641.

[90I1] Ishibashi, K., Noh, S.K., Aoyagi, Y., Namba, S., Mizuno, M., Ochiai, Y., Kawabe, M., Gamo, K.: Surf. Sci. **228** (1990) 286.

[90M1] Menschig, A., Forchel, A., Roos, B., Germann, R., Pressel, K., Heuring, W., Grützmacher, D.: Appl. Phys. Lett. **57** (1990) 1757.

[90M2] Menschig, A., Roos, B., Germann, R., Forchel, A., Pressel, K., Heuring, W., Grützmacher, D.: J. Vac. Sci. Technol. B **8** (1990) 1353.

[90M3] Mailly, D., Sanquer, M.: Surf. Sci. **229** (1990) 260.

[90O1] Ochiai, Y., Mizuno, M., Kawabe, M., Ishibashi,K., Aoyagi, Y., Gamo, K., Namba, S.: Jpn. J. Appl. Phys. **29** (1990) L739.

[90P1] Pfeiffer, L., West, K.W., Stormer, H.L., Eisenstein, J.P., Baldwin, K.W., Gershoni, D., Spector, J.: Appl. Phys. Lett. **56** (1990) 1697.

[90T1] Takagaki, Y., Gamo, K., Namba, S., Takaoka, S., Murase, K.: Sol. St. Commun. **75** (1990) 873.

[90T2] Takagaki, Y., Kusumi, Y., Takaoka, S., Gamo, K., Murase, K., Namba, S.: Jpn. J. Appl. Phys. **29** (1990) 2824.

[90T3] Takaoka, S., Kubota, H., Murase, K., Takagaki, Y., Gamo, K., Namba, S.: Sol. St. Commun. **75** (1990) 293.

[90T4] Taniguchi, H., Nagoya, T., Takagaki, Y., Yuba, Y., Takaoka, S., Gamo, K., Murase, K., Namba, S.: Jpn. J. Appl. Phys. **29** (1990) 2321.

[91A1] Al'tshuler, B.L., Kravtsov, V.E., Lerner, I.V.: Mesoscopic Phenomena in Solids, edited by Al'tshuler, B.L., Lee, P.A., and Webb, R.A. (Elsevier Science Publishers, 1991).

[91A2] Averin, D.V., Likharev, K.K.: Mesoscopic Phenomena in Solids, edited by Al'tshuler, B.L., Lee, P.A., and Webb, R.A. (Elsevier Science Publishers, 1991).

[91B1] Bird, J.P., Grassie, A.D.C., Lakrimi, M., Hutchings, K.M., Meeson, P., Harris, J.J., Foxon, C.T.: J. Phys.: Condens. Matter **3** (1991) 2897.

[91E] Eugster, C.C., del Alamo, J.A., Belk, P.A., Rooks, J.M.: Appl. Phys. Lett. **58** (1991) 2966.

[91F2] Forchel, A., Menschig, A., Maile, B.E., Leier, H., Germann, R.: J. Vac. Sci. Technol. B **9** (1991) 444.

[91G] Geim, A.K., Main, P.C., Beton, P.H., Streda, P., Eaves, L., Wilkinson, C.D.W., Beaumont, S.P.: Phys. Rev. Lett. **67** (1991) 3014.

[91I1] Ishibashi, K., Aoyagi, Y., Namba, S., Ochiai, Y., Kawabe, M., Gamo, K.: Superlatt. Microstruct. **9** (1991) 457.

[91I2] Ismail, K., Washburn, S., Lee, K.Y.: Appl. Phys. Lett. **59** (1991) 1998.

[91K2] Kakuta, T., Takagaki, Y., Gamo, K., Namba, S., Takaoka, S., Murase, K.: Phys. Rev. B **43** (1991) 14321.

[91K3] Klepper, S.J., Millo, O., Keller, M.W., Prober, D.E., Sacks, R.N.: Phys. Rev. B **44** (1991) 8380.

[91L1] Lee, K.Y., Kern, D.P., Ismail, K., Washburn, S.: J. Vac. Sci. Technol. B **9** (1991) 2834.

[91N] Nakata, S., Hirayama, Y., Tarucha, S., Horikoshi, Y.: J. Appl. Phys. **69** (1991) 3633.

[91O1] Ochiai, Y., Abe, S., Kawabe, M., Ishibashi, K., Aoyagi, Y., Gamo, K., Namba, S.: Phys. Rev. B **43** (1991) 14750.

[91O2] Ochiai, Y., Onishi, T., Bird, J.P., Kawabe, M., Ishibashi, K., Aoyagi, Y., Namba, S.: Jpn. J. Appl. Phys. **30** (1991) 3859.

[91O3] Okiji, A., Kasai, H., Nakamura, A.: Prog. Theor. Phys. Suppl. **106** (1991) 209.

[91P1] Hopping Transport in Solids, edited by Pollak, M., Shklovskii, B. (Elsevier Science Publishers, 1991).

[91R1] Ridley, B.K.: Rep. Prog. Phys. **54** (1991) 169.

[91R2] Rössler, U.: Quantum Coherence in Mesoscopic Systems, NATO ASI Series B: Physics Vol. 254, edited by Kramer, B (Plenum Press 1991.)

[91S1] Simmons, J.A., Hwang, S.W., Tsui, D.C., Wei, H.P., Engel, L.W., Shayegan, M.: Phys. Rev. B **44** (1991) 12933.

[91T1] Takaoka, S., Sawasaki, T., Tsukagoshi, K., Oto, K., Murase, K., Gamo, K., Namba, S.: Sol. St. Commun. **80** (1991) 571.

[91T2] Taniguchi, H., Takahara, J., Takagaki, Y., Gamo, K., Namba, S., Takaoka, S., Murase, K.: Jpn. J. Appl. Phys. **30** (1991) 2808.

[91T3] Timp, G.: Mesoscopic Phenomena in Solids, edited by Al'tshuler, B.L., Lee, P.A., and Webb, R.A. (Elsevier Science Publishers, 1991).

[91T4] Tsukagoshi, K., Oto, K., Takaoka, S., Murase, K., Takagaki, Y., Gamo, K., Namba, S.: Sol. St. Commun. **80** (1991) 797.

[91W2] Washburn, S.: Mesoscopic Phenomena in Solids, edited by Al'tshuler, B.L., Lee, P.A., and Webb, R.A. (Elsevier Science Publishers 1991).

[92A1] Aihara, K., Yamamoto, M., Mizutani, T.: Jpn. J. Appl. Phys. **31** (1992) L916.

[92A2] Alphenaar, B.W., Williamson, J.G., van Houten, H., Beenakker, C.W.J., Foxon, C.T.: Phys. Rev. B **45** (1992) 3890.

[92B2] Bird, J.P., Grassie, A.D.C., Lakrimi, M., Hutchings, K.M., Meeson, P., Harris, J.J., Foxon, C.T.: Surf. Sci. **267** (1992) 277.

[92B3] Blaikie, R.J., Cleaver, J.R.A., Ahmed, H., Nakazato, K.: Appl. Phys. Lett. **60** (1992) 1618.

[92C] Chou, S.Y., Wang, Y.: Appl. Phys. Lett. **61** (1992) 1591.

[92F1] Feng, Y., Thornton, Green, M., T.J., Harris, J.J.: Superlatt. Microstruct. **11** (1992) 281.

[92F2] Feng, Y., Thornton, T.J., Harris, J.J., Williams, D.: Appl. Phys. Lett. **60** (1992) 94.

[92G1] Geim, A.K., Main, P.C., Beton, P.H., Eaves, L., Beaumont, S.P., Wilkinson, C.D.W.: Phys. Rev. Lett. **69** (1992) 1248.

[92G2] Geim, A.K., Main, P.C., Beton, P.H., Streda, P., Eaves, L., Wilkinson, C.D.W., Beaumont, S.P.: Surf. Sci. **263** (1992) 298.

[92G3] Single Charge Tunneling, Coulomb Blockade Phenomena in Nanostructures, NATO ASI Series B, Physics Vol. 294, edited by Grabert, H., Devoret, M.H. (Plenum Press, 1992).

[92G4] Gusev, G.M., Kyon, Z.D., Ol'shanetskii, E.B.: Sov. Phys. JETP **74** (1992) 735.

[92H1] Haug, R.J., Munekata, H., Chang, L.L.: Jpn. J. Appl. Phys. **31** (1992) L127.

[92H2] Hirayama, Y., Wieck, A.D., Bever, T., von Klitzing, K., Ploog, K.: Phys. Rev. B **46** (1992) 4035.

[92H3] Hirayama, Y., Wieck, A.D., Ploog, K.: J. Appl. Phys. **72** (1992) 3022.

[92I1] Ishibashi, K., Aoyagi, Y., Namba, S., Ochiai, Y., Bird, J.P., Kawabe, M.: Surf. Sci. **263** (1992) 378.

[92I2] Ishibashi, K., Bird, J.P., Sugano, T., Aoyagi, Y., Ochiai, Y., Onishi, T., Kawabe, M.: Jpn. J. Appl. Phys. **31** (1992) 4504.

[92J1] Jain, J.K.: Adv. Phys. **41** (1992) 105.

[92J2] Jin, G., Tang, Y.S., Thoms, S., Wilkinson, C.D.W., Gundlach, A.M.: J. Vac. Sci. Technol. B **10** (1992) 2873.

[92K2] Kakuta, T., Takagaki, Y., Gamo, K., Namba, S., Takaoka, S., Murase, K.: Superlatt. Microstruct. **11** (1992) 185.

[92K3] Kastner, M.A.: Rev. Mod. Phys. **64** (1992) 849.

[92O1] Ochiai, Y., Onishi, T., Bird, J.P., Kawabe, M., Ishibashi, K., Aoyagi, Y., Namba, S.: Surf. Sci. **263** (1992) 388.

[92O2] Ohata, A., Toriumi, A.: Surf. Sci. **263** (1992) 157.

[92S2] Staring, A.A.M., van Houten, H., Beenakker, C.W.J., Foxon, C.T.: Phys. Rev. B **45** (1992) 9222.

[92T1] Takaoka, S., Tsukagoshi, K., Oto, K., Sawasaki, T., Murase, K., Takagaki, Y., Gamo, K., Namba, S.: Surf. Sci. **267** (1992) 282.

[92T2] Tang, Y.S., Jin, G., Davies, J.H., Williamson, J.G., Wilkinson, C.D.W.: Phys. Rev. B **45** (1992) 13799.

[92T3] Tsukagoshi, K., Takaoka, S., Oto, K., Murase, K., Takagaki, Y., Gamo, K., Namba, S.: Phys. Rev. B **46** (1992) 5016.

[92W1] Washburn, S., Webb, R.A.: Rep. Prog. Phys. **55** (1992) 1311.

[92W2] Wróbel, J., Kuchar, F., Ismail, K., Lee, K.Y., Nickel, H., Schlapp, W.: Surf. Sci. **263** (1992) 261.

[92Y1] Yamada, M., Hirakawa, K., Odagiri, T., Thornton, T.J., Ikoma, T.: Superlatt. Microstruct. **11** (1992) 261.

[92Y2] Yoh, K., Taniguchi, H., Kiyomi, K., Sakamoto, R., Inoue, M.: Semicond. Sci. Technol. **7** (1992) B295.

[93B1] Block, S., Suhrke, M., Wilke, S., Menschig, A., Schweizer, H., Grützmacher, D.: Phys. Rev. B **47** (1993) 6524.

[93B2] Brown, C.V., Geim, A.K., Foster, T.J., Langerak, C.J.G.M., Main, P.C.: Phys. Rev. B **47** (1993) 10935.

[93B3] Buot, F.A.: Phys. Rep. **234** (1993) 73.

[93C2] Chou, S.Y., Wang, Y.: Appl. Phys. Lett. **63** (1993) 788.

[93C3] Cumming, D.R.S., Blaikie, R.J., Ahmed, H.: Appl. Phys. Lett. **62** (1993) 870.

[93D] Dietl, T., Grabecki, G., Jaroszyński, J.: Semicond. Sci. Technol. **8** (1993) S141.

[93F] Feng, Y., Sachrajda, A.S., Taylor, R.P., Adams, J.A., Davies, M., Zawadzki, P., Coleridge, P.T., Landheer, D., Marshall, P.A., Barber, R.: Appl. Phys. Lett. **63** (1993) 1666.

[93G1] Geim, A.K., Main, P.C., Eaves, L., Beton, P.H.: Superlatt. Microstruct. **13** (1993) 11.

[93H1] Hirayama, Y., Tokura, Y., Wieck, A.D., Koch, S., Haug, R.J., von Klitzing, K., Ploog, K.: Phys. Rev. B **48** (1993) 7991.

[93I] Iwano, H., Zaima, S., Koide, Y., Yasuda, Y.: J. Vac. Sci. Technol. B **11** (1993) 61.

[93K] Kramer, B., MacKinnon, A.: Rep. Prog. Phys. **56** (1993) 1469.

[93L1] Phonons in Semiconductor Nanostructures, NATO ASI Series E: Applied Sciences Vol. 236, edited by Leburton, J.-P., Pascual, J., Sotomayor Torres, C. (Kluwer Academic Publishers, 1993).

[93M2] Main, P.C., Geim, A.K., Beton, P.H., Eaves, L.: Physica B **184** (1993) 341.

[93N] Nakata, S., Ikuta, K., Yamamoto, M., Mizutani, T.: Jpn. J. Appl. Phys. **32** (1993) 6258.

[93O1] Ochiai, Y., Onishi, T., Kawabe, M., Ishibashi, K., Bird, J.P., Aoyagi, Y., Sugano, T.: Jpn. J. Appl. Phys. **32** (1993) 528.

[93O2] Onishi, T., Kawabe, M., Ishibashi, K., Bird, J.P., Aoyagi, Y., Sugano, T., Ochiai, Y.: Phys. Rev. B **48** (1993) 12353.

[93O3] Onishi, T., Ochiai, Y., Kawabe, M., Ishibashi, K., Bird, J.P., Aoyagi, Y., Sugano, T.: Physica B **184** (1993) 351.

[93R] Ramon, A., Heiblum, M., Shtrikman, H.: Semicond. Sci. Technol. **8** (1993) 2176.

[93T1] Tang, Y.S., Jin, G., Wilkinson, C.D.W.: Appl. Phys. Lett. **62** (1993) 2530.

[93T2] Tang, Y.S., Jin, G., Wilkinson, C.D.W.: Sol. St. Commun. **85** (1993) 189.

[93T3] Tarucha, S., Saku, T., Tokura, Y., Hirayama, Y.: Phys. Rev. B **47** (1993) 4064.

[93T4] Taylor, R.P., Adams, J.A., Davies, M., Marshall, P.A., Barber, R.: J. Vac. Sci. Technol. B **11** (1993) 628.

[93vdB] van der Burgt, M., Geim, A.K., van Bockstal, L., Dubonos, S.V., Herlach, F.: Physica B **184** (1993) 369.

[93W1] Wendel, M., Lettau, C., Hansen, W., Dolgopolov, V., Böhm, G., Weimann, G.: Sol. St. Commun. **87** (1993) 1101.

[93Y] Yamada, S., Yamamoto, M., Aihara, K.: Sol. St. Commun. **85** (1993) 573.

[94C1] Chandrasekhar, V., Webb, R.A.: J. Low Temp. Phys. **97** (1994) 9.

[94G3] Geim, A.K., Main, P.C., Brown, C.V., Taboryski, R., Carmona, H., Foster, T.J., Lindelof, P.E., Eaves, L.: Surf. Sci. **305** (1994) 624.

[94G4] Geim, A.K., Main, P.C., Taboryski, R., Veje, E., Carmona, H.A., Brown, C.V., Foster, T.J., Eaves, L.: Phys. Rev. B **49** (1994) 2265.

[94G5] Gogolin, A.O.: Ann. Phys. Fr. **19** (1994) 411.

[94H1] Hwang, S.W., Tsui, D.C., Shayegan, M.: Phys. Rev. B **49** (1994) 16441.

[94H2] Hwang, S.W., Tsui, D.C., Shayegan, M.: Surf. Sci. **305** (1994) 629.

[94I2] Inoue, M., Yoh, K., Nishida, A.: Semicond. Sci. Technol. **9** (1994) 966.

[94I3] Iwano, H., Zaima, S., Kimura, T., Matsuo, K., Yasuda, Y.,: Jpn. J. Appl. Phys. **33** (1994) 7190.

[94K2] Kirczenow, G., Sachrajda, A.S., Feng, Y., Taylor, R.P., Henning, L., Wang, J., Zawadzki, P., Coleridge, P.T.: Phys. Rev. Lett. **72** (1994) 2069.

[94L1] Lettau, C., Wendel, M., Schmeller, A., Hansen, W., Kotthaus, J.P., Klein, W., Böhm, G., Tränkle, G., Weimann, G., Holland, M.: Phys. Rev. B **50** (1994) 2432.

[94M2] Main, P.C., Geim, A.K., Carmona, H.A., Brown, C.V., Foster, T.J., Taboryski, R., Lindelof, P.E.: Phys. Rev. B **50** (1994) 4450.

[94M3] Molenkamp, L.W., de Jong, M.J.M.: Phys. Rev. B **49** (1994) 5038.

[94M4] Morgan, A., Cobden, D.H., Pepper, M., Jin, G., Tang, Y.S., Wilkinson, C.D.W.: Phys. Rev. B **50** (1994) 12187.

[94N1] Nakajima, Y., Takahashi, Y., Horiguchi, S., Iwadate, K., Namatsu, H., Kurihara, K., Tabe, M.: Appl. Phys. Lett. **65** (1994) 2833.

[94N2] Nakata, S., Tomizawa, M., Yamamoto, M., Ikuta, K., Mizutani, T.: J. Appl. Phys. **76** (1994) 2330.

[94O1] Ochiai, Y., Yamamoto, K., Onishi, T., Ishibashi, K., Bird, J.P., Aoyagi, Y., Sugano, T.: Superlatt. Microstruct. **16** (1994) 179.

[94O2] Ochiai, Y., Yamamoto, K., Onishi, T., Ishibashi, K., Bird, J.P., Aoyagi, Y., Sugano, T., Ferry, D.K.: Physica B **201** (1994) 357.

[94O3] Ochiai, Y., Yamamoto, K., Onishi, T., Kawabe, M., Ishibashi, K., Bird, J.P., Aoyagi, Y., Sugano, T.: Physica B **194-196** (1994) 1139.

[94T] Thornton, T.J.: Rep. Prog. Phys. **57** (1994) 311.

[94W] Wada, Y., Suga, M., Kure, T., Yoshimura, T., Sudo, Y., Kobayashi, T., Goto, Y., Kondo, S.: Appl. Phys. Lett. **65** (1994) 624.

[94Y] Yoh, K., Nishida, A., Kawahara, H., Izumiya, S., Inoue, M.: Semicond. Sci. Technol. **9** (1994) 961.

[95B1] Blaikie, R.J., Cumming, D.R.S., Cleaver, J.R.A., Ahmed, H., Nakazato, K.: J. Appl. Phys. **78** (1995) 330.

[95B2] Bird, J.P., Ishibashi, K., Ochiai, Y., Lakrimi, M., Grassie, A.D.C., Hutchings, K.M., Aoyagi, Y., Sugano, T.: Phys. Rev. B **52** (1995) 1793.

[95dJ] de Jong, M.J.M., Molenkamp, L.W.: Phys. Rev. B **51** (1995) 13389.

[95F2] Fukai, Y.K., Nakano, H., Nakata, S., Tarucha, S., Arai, K.: Sol. St. Commun. **94** (1995) 757.

[95H1] Hasegawa, H., Hashizume, T., Okada, H., Jinushi, K.: J. Vac. Sci. Technol. **13** (1995) 1744.

[95H2] Hashizume, T., Okada, H., Jinushi, K., Hasegawa, H.: Jpn. J. Appl. Phys. **34** (1995) L635.

[95H3] Honda, T., Tarucha, S., Saku, T., Tokura, Y.: Jpn. J. Appl. Phys. **34** (1995) L72.

[95J] Jaroszyński, J., Wróbel, J., Sawicki, M., Kamińska, E., Skośkiewicz, T., Karczewski, G., Wojtowicz, T., Piotrowska, A., Kossut, J., Dietl, T.: Phys. Rev. Lett. **75** (1995) 3170.

[95M1] Meirav, U., Foxman, E.B.: Semicond. Sci. Technol. **10** (1995) 255.

[95N1] Nakajima, Y., Takahashi, Y., Horiguchi, S., Iwadate, K., Namatsu, H., Kurihara, K., Tabe, M.: Jpn. J. Appl. Phys. **34** (1995) 1309.

[95N2] Namatsu, H., Takahashi, Y., Nagase, M., Murase, K.: J. Vac. Sci. Technol. **13** (1995) 2166.

[95O1] Ochiai, Y., Yamamoto, K., Ishibashi, K., Bird, J.P., Aoyagi, Y., Sugano, T., Ferry, D.K.: Jpn. J. Appl. Phys. **34** (1995) 4345.

[95O2] Ochiai, Y., Yamamoto, K., Onishi, T., Kawabe, M., Ishibashi, K., Bird, J.P., Aoyagi, Y., Sugano, T., Ferry, D.K.: Jpn. J. Appl. Phys. **34** (1995) 1339.

[95O3] Okada, H., Hashizume, T., Hasegawa, H.: Jpn. J. Appl. Phys. **34** (1995) 6971.

[95O4] Okada, H., Jinushi, K., Wu, N.-J., Hashizume, T., Hasegawa, H.: Jpn. J. Appl. Phys. **34** (1995) 1315.

[95O5] Omling, P., Linke, H., Deppert, K., Samuelson, L., Hansen, L.T., Lindelof, P.E.: Jpn. J. Appl. Phys. **34** (1995) 4575.

[95P1] Park, K.W., Lee, S., Shin, M., Kwon, H., Lee, E.-H.: Jpn. J. Appl. Phys. **34** (1995) 4357.

[95P2] Park, K.W., Lee, S., Shin, M., Lee, E.-H., Kwon, H.: Sol. St. Commun. **95** (1995) 717.

[95S] Shitara, T., Tornow, M., Kurtenbach, A., Weiss, D., Eberl, K., von Klitzing, K.: Appl. Phys. Lett. **66** (1995) 2385.

[95T] Tarucha, S., Honda, T., Saku, T.: Sol. St. Commun. **94** (1995) 413.

[95V] Voit, J.: Rep. Prog. Phys. **58** (1995) 977.

[95W] Wróbel, J., Brandes, T., Kuchar, F., Kramer, B., Ismail, K., Lee, K.Y., Hillmer, H., Schlapp, W., Dietl, T.: Europhys. Lett. **29** (1995) 481.

[95Y1] Yano, K., Ishii, T., Hashimoto, T., Kobayashi, T., Murai, F., Seki, K.: Appl. Phys. Lett. **67** (1995) 828.

[96B3] Bergmann, R., Schweizer, H., Härle, V., Scholz, F.: Appl. Phys. Lett. **68** (1996) 2267.

[96B4] Bykov, A.A., Kvon, Z.D., Ol'shanetskii, E.B., Litvin, L.V., Moshchenko, S.P.: Phys. Rev. B **54** (1996) 4464.

[96D1] Dietl, T., Jaroszyński, J., Grabecki, G., Wróbel, J., Sawicki, M., Skośkiewicz, T., Kamińska, E., Piotrowska, A., Karczewski, G., Wojtowicz, T., Kossut, J.: Semicond. Sci. Technol. **11** (1996) 1618.

[96H1] Hashizume, T., Okada, H., Hasegawa, H.: Physica B **227** (1996) 42.

[96H2] Hughes, R.J.F., Savchenko, A.K., Frost, J.E.F., Linfield, E.H., Nicholls, J.T., Pepper, M., Kogan, E., Kaveh, M.: Phys. Rev. B **54** (1996) 2091.

[96J2] Jaroszyński, J., Wróbel, J., Sawicki, M., Skośkiewicz, T., Karczewski, G., Wojtowicz, T., Kossut, J., Dietl, T., Kamińska, E., Papis, E., Piotrowska, A.: Surf. Sci. **361/362** (1996) 718.

[96J3] Jaskólski, W.: Phys. Rep. **271** (1996) 1.

[96K2] Kikutani, T., Aoki, N., Oki, A., Hong, C., Hori, H., Yamada, S.: Jpn. J. Appl. Phys. **35** (1996) 6659.

[96K3] Koester, S.J., Ismail, K., Lee, K.Y., Chu, J.O.: Phys. Rev. B **54** (1996) 10604.

[96N1] Naylor, A.J., Strickland, K.R., Kent, A.J., Henini, M.: Surf. Sci. **361/362** (1996) 660.

[96N2] Noguchi, M., Ikoma, T., Odagiri, T., Sakakibara, H., Wang, S.N.: J. Appl. Phys. **80** (1996) 5138.

[96S2] Smith, C.G.: Rep. Prog. Phys. **59** (1996) 235.

[96S3] Sassetti, M.: Quantum Transport in Semiconductor Submicron Structures, NATO ASI Series E: Applied Sciences Vol. 326, edited by Kramer, B. (Kluwer Academic Publishers, 1996).

[96W] Widjaja, A.W., Sasaki, N., Yamamoto, K., Ochiai, Y., Ishibashi, K., Bird, J.P., Aoyagi, Y., Sugano, T., Ferry, D.K.: Superlatt. Microstruct. **20** (1996) 317.

[96Y1] Yacoby, A., Stormer, H.L., Wingreen, N.S., Pfeiffer, L.N., Baldwin, K.W., West, K.W.: Phys. Rev. Lett. **77** (1996) 4612.

[96Y2] Yamada, S., Yamamoto, M.: J. Appl. Phys. **79** (1996) 8391.

[97A2] Aoki, N., Kikutani, T., Oki, A., Hori, H., Yamada, S.: Superlatt. Microstruct. **22** (1997) 229.

[97F] Ferry, D.K., Goodnick, S.M.: Transport in Nanostructures (Cambridge University Press, 1997).

[97G1] Geim, A.K., Dubonos, S.V., Lok, J.G.S., Grigorieva, I.V., Maan, J.C., Hansen, L.T., Lindelof, P.E.: Appl. Phys. Lett. **71** (1997) 2379.

[97H] Herfort, J., Austing, D.G., Hirayama, Y.: J. Appl. Phys. **82** (1997) 4384.

[97I1] Imry, Y.: Introduction to Mesoscopic Physics (Oxford University Press, 1997).

[97I2] Inoue, M., Sugihara, T., Maemoto, T., Sasa, S., Dobashi, H., Izumiya, S.: Superlatt. Microstruct. **21** (1997) 69.

[97J1] Janssen, M., Viehweger, O., Fastenrath, U., Hajdu, J.: Introduction to the Theory of the Integer Quantum Hall Effect (VCH Verlag, 1994.)

[97J2] Johnson, B.L., Kirczenow, G.: Rep. Prog. Phys. **60** (1997) 889.

[97K1] Koester, S.J., Ismail, K., Lee, K.Y., Chu, J.O.: Appl. Phys. Lett. **71** (1997) 1528.

[97L] Linke, H., Omling, P., , Xu, H., Lindelof, P.E.: Phys. Rev. B **55** (1997) 4061.

[97M] Maemoto, T., Yamamoto, H., Konami, M., Kajiuchi, A., Ikeda, T., Sasa, A., Inoue, M.: phys. stat. sol. b **204** (1997) 255.

[97O] Okada, H., Kasai, S., Fujikura, H., Hashizume, T., Hasegawa, H.: Jpn. J. Appl. Phys. **36** (1997) 4156.

[97S3] Smith, R.A., Ahmed, H.: J. Appl. Phys. **81** (1997) 2699.

[97Y1] Yacoby, A., Stormer, H.L., Baldwin, K.W., Pfeiffer, L.N., West, K.W.: Sol. St. Commun. **101** (1997) 77.

[97Y2] Yoh, K., Takabayashi, S.: phys. stat. sol. b **204** (1997) 259.

[98C1] Castleton, I.M., Davies, A.G., Hamilton, A.R., Frost, J.E.F., Simmons, M.Y., Ritchie, D.A., Pepper, M.: Physica B **249-251** (1998) 157.

[98D] Dittrich, T., Hänggi, P., Ingold, G.-L., Kramer, B., Schön, G., Zwerger, W.: Quantum Transport and Dissipation. (Wiley-VCH, 1998)

[98F1] Ford, E.M., Ahmed, H.: J. Vac. Sci. Technol. B **16** (1998) 3800.

[98F2] Fujii, H., Kanemaru, S., Matsukawa, T., Hiroshima, H., Yokoyama, H., Itoh, J.: Jpn. J. Apll. Phys. **37** (1998) 7182.

[98G2] Gompertz, M.J., Ihn, T., Main, P.C., Nogaret, A., Eaves, L., Henini, M., Beaumont, S.P.: Physica B **249-251** (1998) 162.

[98G3] Gusev, G.M., La Scala Jr., N., Lubyshev, D.I., González–Borrero, P.P., da Silva, M.A.P., Basmaji, P., Rossi, J.C., Portal, J.C.: Superlatt. Microstruct. **24** (1998) 197.

[98I1] Irvine, A.C., Durrani, Z.A.K., Ahmed, H., Biesemans, S.: Appl. Phys. Lett. **73** (1998) 1113.

[98I2] Iwano, H., Zaima, S., Yasuda, Y.: J. Vac. Sci. Technol. B **16** (1998) 2551.

[98J1] Janssen, M.: Phys. Rep. **295** (1998) 1.

[98J2] Jaroszyński, J., Wróbel, J., Karczewski, G., Wojtowicz, T., Dietl, T.: Phys. Rev. Lett. **80** (1998) 5635.

[98K1] Kane, B.E., Facer, G.R., Dzurak, A.S., Lumpkin, N.E., Clark, R.G., Pfeiffer, L.N., West, K.W.: Appl. Phys. Lett. **72** (1998) 3506.

[98K2] Kikutani, T., Aoki, N., Hong, C.U., Hori, H., Yamada, S.: Physica B **249-251** (1998) 513.

[98N1] Ng, V., Ahmed, H., Shimada, T.: Appl. Phys. Lett. **73** (1998) 972.

[98P1] Park, K.W., Lee, S., Shin, M., Yuk, J.S., Lee, E.-H., Kwon, H.C.: Phys. Rev. B **58** (1998) 3557.

[98S1] Stoddart, S.T., Main, P.C., Gompertz, M.J., Nogaret, A., Eaves, L., Henini, M., Beaumont, S.P.: Physica B **256-258** (1998) 413.

[98T2] Thornton, T.J.: Superlatt. Microstruct. **23** (1998) 601.

[98Y] Yamada, S., Kikutani, T., Aoki, N., Hori, H., Tatara, G.: Phys. Rev. Lett. **81** (1998) 5422.

[99F1] Fujii, H., Kanemaru, S., Matsukawa, T., Itoh, J.: Appl. Phys. Lett. **75** (1999) 3986.

[99H1] Harrell, R.H., Pyshkin, K.S., Simmons, M.Y., Ritchie, D.A., Ford, C.J.B., Jones, G.A.C., Pepper, M.: Appl. Phys. Lett. **74** (1999) 2328.

[99H2] Held, R., Lüscher, S., Heinzel, T., Ensslin, K., Wegscheider, W.: Appl. Phys. Lett. **75** (1999) 1134.

[99K] Kaufman, D., Berk, Y., Dwir, B., Rudra, A., Palevski, A., Kapon, E.: Phys. Rev. B **59** (1999) R10433.

[99L] Liang, C.T., Simmons, M.Y., Smith, C.G., Ritchie, D.A., Pepper, M.: Appl. Phys. Lett. **75** (1999) 2975.

[99M] Moon, J.S., Blount, M.A., Simmons, J.A., Wendt, J.R., Lyo, S.K., Reno, J.L.: Phys. Rev. B **60** (1999) 11530.

[99T] Thomas, K.J., Nicholls, J.T., Simmons, M.Y., Tribe, W.R., Davies, A.G., Pepper, M.: Phys. Rev. B **59** (1999) 12252.

[00A] Auslaender, O.M., Yacoby, A., de Picciotto, R., Baldwin, K.W., Pfeiffer, L.N., West, K.W.: Phys. Rev. Lett. **84** (2000) 1764.